AD-A092 547 AIR FORCE INST OF TECH WRIGHT-PATTERSON AFB OH F/G 22/2
OPTIMAL REGULATION WITHIN SPATIAL CONSTRAINTS. AN APPLICATION T--ETC(U)
AUG 80 E G TAYLOR
UNCLASSIFIED AFIT-CI-80-46D NL

1 OF 4
AD A092547

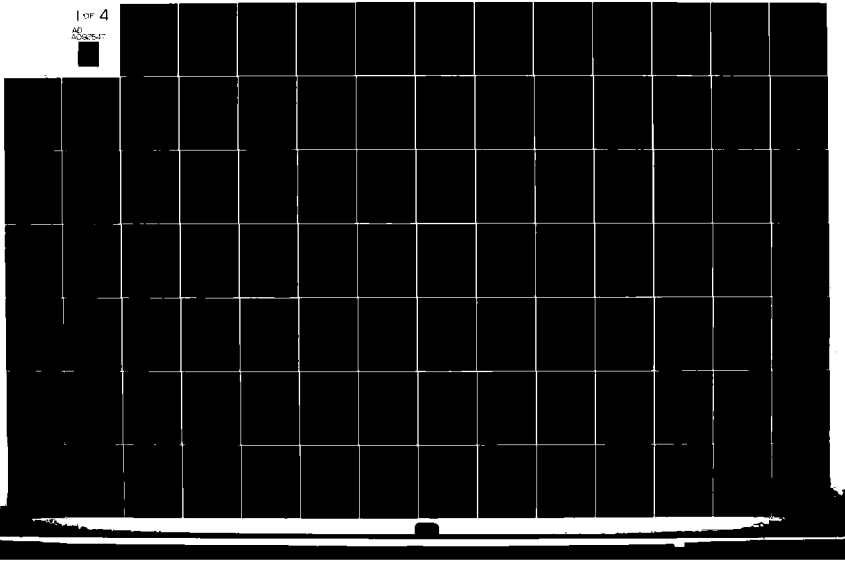

UNCLASS

SECURITY CLASSIFICATION OF THIS PAGE (When Data Entered)

LEVEL II

REPORT DOCUMENTATION PAGE

READ INSTRUCTIONS BEFORE COMPLETING FORM

1. REPORT NUMBER	2. GOVT ACCESSION NO	3. RECIPIENT'S CATALOG NUMBER
80-46D	AD-A092 547	

4. TITLE (and Subtitle)	5. TYPE OF REPORT & PERIOD COVERED
Optimal Regulation Within Spatial Constraints - An Application To Flexible Structures	THESIS/DISSERTATION
	6. PERFORMING ORG. REPORT NUMBER
7. AUTHOR(s)	8. CONTRACT OR GRANT NUMBER(s)
Capt Edward G. Taylor	
9. PERFORMING ORGANIZATION NAME AND ADDRESS	10. PROGRAM ELEMENT, PROJECT, TASK AREA & WORK UNIT NUMBERS
AFIT STUDENT AT: Massachusetts Institute of Technology	
11. CONTROLLING OFFICE NAME AND ADDRESS	12. REPORT DATE
AFIT/NR WPAFB OH 45433	Aug 1980
	13. NUMBER OF PAGES 302
14. MONITORING AGENCY NAME & ADDRESS(if different from Controlling Office)	15. SECURITY CLASS. (of this report) UNCLASS
	15a. DECLASSIFICATION DOWNGRADING SCHEDULE

16. DISTRIBUTION STATEMENT (of this Report)

APPROVED FOR PUBLIC RELEASE; DISTRIBUTION UNLIMITED

DTIC ELECTE DEC 0 8 1980 S D E

17. DISTRIBUTION STATEMENT (of the abstract entered in Block 20, if different from Report)

18. SUPPLEMENTARY NOTES

APPROVED FOR PUBLIC RELEASE: IAW AFR 190-17

Air Force Institute of Technology (ATC)
Wright-Patterson AFB, OH 45433

FREDRIC C. LYNCH, Major, USAF
Director of Public Affairs

19. KEY WORDS (Continue on reverse side if necessary and identify by block number)

20. ABSTRACT (Continue on reverse side if necessary and identify by block number)

ATTACHED

DD FORM 1 JAN 73 1473 EDITION OF 1 NOV 65 IS OBSOLETE

UNCLASS

SECURITY CLASSIFICATION OF THIS PAGE (When Data Entered)

AD A092547

DTIC FILE COPY

OPTIMAL REGULATION WITHIN SPATIAL CONSTRAINTS: AN APPLICATION TO FLEXIBLE STRUCTURES

by

Edward Gregory Taylor

B.S., Illinois Institute of Technology
(1972)

M.S., Air Force Institute of Technology
(1974)

SUBMITTED IN PARTIAL FULFILLMENT
OF THE REQUIREMENT FOR
DEGREE OF
DOCTOR OF PHILOSOPHY

at the
Massachusetts Institute of Technology

AUGUST 1980

Signature of Author Edward G Taylor
Department of Aeronautics and Astronautics
August 1980

Approved by _____
Chairman of the Thesis Committee

Approved by _____
Thesis Advisor

Approved by _____
Thesis Advisor

Approved by _____
Thesis Advisor

Accepted by _____
Chairman, Department Graduate Committee

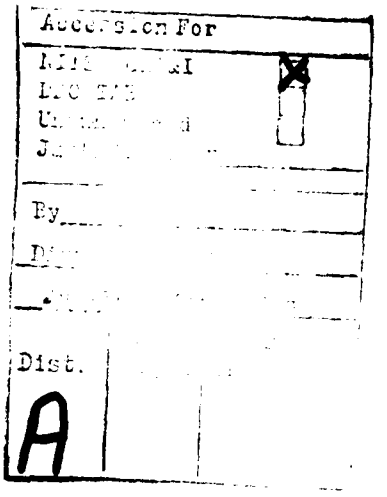

OPTIMAL REGULATION WITHIN SPATIAL CONSTRAINTS— AN APPLICATION TO FLEXIBLE STRUCTURES

by

Capt. Edward G. Taylor

Submitted to the Department of

Aeronautics and Astronautics on September 2, 1980

in partial fulfillment of the requirements for

the degree of Doctor of Science

ABSTRACT

The contribution of this research is a candidate controller architecture for application to lightly damped, flexible vehicles, where stiffness and mass are distributed parameters. The architecture acknowledges that a reduced order controller is required. Singular perturbation theory and the spatial shaping of control inputs and observation residuals are then coupled to derive an appropriate, asymptotically correct, low frequency plant representation, and a cascaded estimator/optimal regulator is used to construct a linear feedback law based on this low order model. The primary benefit of this approach is the capability to rigorously construct control laws for systems where the dimensions of the control vector, output vector, and the plant dynamics are high. Design examples are given which illustrate that the reduced order designs compare favorably to the optimal fullstate regulator.

Thesis Supervisor: H. Phillip Whitaker
Title: Professor of Aeronautics and Astronautics

Thesis Supervisor: Richard H. Battin
Title: Professor of Aeronautics and Astronautics
Assoc. Dept. Head, CSDL

Thesis Supervisor: William S. Widnall
Title: Associate Professor of Aeronautics and Astronautics

Thesis Supervisor: Kevin Daly, CSDL

ACKNOWLEDGMENT

The formulation and completion of this thesis, and indeed the richness of my doctoral program, owe much to the unique combination of resources and individuals I have found in the MIT/Draper Laboratory environment. A single page in a preface cannot properly acknowledge the benefits I have received from both institutions, nor can it express my respect for the people involved. I am privileged to have been here.

Stark Draper, Robert Duffy, William Manlove, and John Sinkiewicz not only extended to me the resources of Draper Lab, but also took time from their work to encourage me in mine. Robert Strunce (computer software), Tim Henderson (satellite structural design), and Rudrapatna Ramnath (singular perturbation theory), all of Draper, supplied technical help which was invaluable in the completion of my thesis. To Jane Carmody, also of Draper, I owe the careful preparation of this text.

My debt to Prof. H. Phillip Whitaker, Prof. Richard Battin, Prof. William Widnall, and Dr. Kevin Daly goes much beyond my gratitude for their work on my doctoral committee. It was my good fortune to take course work from Dr. Battin, who showed me the elegance of celestial mechanics, and from Professors Whitaker and Widnall, whose teaching reflects their eminence in the fields of classical and modern control. Dr. Daly was the direct supervisor of my thesis, and I wish to thank him for the endless time and energy he put in. It was always a pleasure to discuss my research with Kevin because he has both a broad perspective and a quick appreciation of subtle points and problems.

Finally, I would like to thank Robert Calico of the Air Force Institute of Technology, a member of my masters committee, whose helpful critical comments led to the initial formulation of this thesis topic. Those I must thank for its completion include many teachers, colleagues and friends not mentioned above; in particular, Professors Baron and VanderVelde, Robert Fraser, James Kidder, Robert Copper, Susan Fennelly, my brother Stephen, and my sister Marie. Their moral support and valuable insights, criticisms, and corrections are directly responsible for my completion of this thesis.

This thesis is dedicated to Bill Manlove, for whom I have more respect than I can say; to D.B., whose avid interest in sailing allowed me to spend my weekends studying; and to Major General G.E. Cook of USAF/ATC, who provided the support for this research.

TABLE OF CONTENTS

TABLE OF CONTENTS (Cont.)

CHAPTER 1

INTRODUCTION

In his article "Two Decades of Spacecraft Attitude Control"[1]* Roberson expresses the judgment that attitude controller design has become "conventional engineering practice". In some areas, like gyroscopic or field stabilization, this judgment is doubtless correct. One exception is the design of controllers for flexible, lightly damped spacecraft, where in including the flexibility effects, one must also acknowledge the distributed nature of vibration energy. This implies that finite dimension spacecraft models, including state space representations, will have errors which become large at higher frequencies. The control of distributed parameter systems is not a new area. Aircraft and missile structural effects have been successfully dealt with in the past. Notch filters and/or gain stabilization were used, depending on the bandwidth and the frequency spectrum. Difficulties arise in the spacecraft context for the following reasons.

(1) The system is multivariable and too large in scale for a full order controller to be feasible.

(2) Pointing accuracy and dynamic response requirements demand a high bandwidth.

(3) Structural frequencies are extremely low.

---

*Superscript numerals refer to similarly numbered items in the List of References.

(4) Damping ratios are no larger than several percent of critical damping.

(5) The spectrum of modes which must be controlled may overlap the spectrum of modes which need not be controlled.

Noting these spacecraft characteristics, Croopnick[2] in A Survey of Automatic Control Techniques for Large Space Structures, states: "It is nontrivial to design a robust controller for a distributed parameter system with modeling errors and parameter variations, which simultaneously guarantees stability and meets performance requirements."

Classical techniques are powerful enough to address the flexible spacecraft issues. Successful controllers have been designed and deployed; a current example is the Galileo spacecraft, where four structural modes were within the stator control bandwidth. These controllers, however, are generally single-input/single-output. For multivariable systems, particularly of high-dimension, state space techniques are increasingly attractive. Unfortunately, current modern control approaches, including pole placement and LQG regulators, are very sensitive to plant/model mismatch. In applications, Harris[3], Ginter[4], and others have demonstrated that instability can occur even for simple systems, if truncated structural representations are used. Alternate approaches have been suggested, as will be detailed below, but in all of them, stability, robustness, and model-sensitivity issues exist.

The intent of the research discussed in this thesis is to demonstrate a control architecture which is specifically applicable to flexible, lightly damped satellites. Knowledge of the satellite structural response characteristics, and insights from linear algebra and singular perturbation theory are exploited to derive a reduced-order controller that is stable and which meets dynamic performance requirements.

To motivate and provide a context for the presentation of specific thesis results, this introduction starts with a general discussion of flexible spacecraft structural characteristics and control requirements.

This is followed by a survey of available control design theories, and a discussion of the drawbacks of these theories in a flexible spacecraft context. The thesis results are then outlined.

1.1 Flexible Spacecraft Response Characteristics

The development of the Space Transportation System (STS) will have a significant effect on future generations of spacecraft. One can envision that two distinct classes of vehicles will result. Clearly, there will be large structures erected in space to serve as antennas, manufacturing or research platforms, or solar power collectors. Such structures will, by nature, be multiple-input/multiple-output distributed parameter systems characterized by low natural frequencies and little damping. Control requirements will consist of slewing or station keeping commands, control of vibration in the presence of disturbances, and control of those modes which significantly affect shape. A second class of vehicles is also consistent with the STS capability and future missions. Such vehicles will be much smaller and may consist of a rigid central portion and flexible appendages to mount sensors, solar panels, and communications devices. These satellites will share many of the structural response characteristics of the large space structures and may be more prone to two added complications: changing of configuration with appendage movement, and a possibility of having noncollocated sensors and activators.

1.1.1 Structural Modeling

The dynamics of flexible damped systems are typically described by a partial differential equation in spatial variables and time. In general, this equation is separable into ordinary differential equations by the assumption

$$q[\underline{Y},t] = Y[\underline{Y}]T[t] \qquad (1)$$

where

q = elastic deformation vector

$\underline{Y}$ = a set of continuous spatial variables such as x, y, z

Solutions are found in terms of an infinite semibounded set of complex eigenvalues λ_i; the associated vector valued eigenfunctions $\phi_i[\underline{Y}]$, and time functions $\zeta_i[t]$. The forced response at any point [x,y,z] is given in terms of an infinite series

$$q[x,y,z,t] = \sum_{i=1}^{\infty} \phi_i[x,y,z]\ \xi_i[t] \tag{2}$$

where

$$M_i\ \ddot{\xi}_i + M_i\ \zeta_i\ \omega_i\ \dot{\xi}_i + M_i\ \omega_i^2\ \xi_i = \Xi_i$$

$$M_i = \int_V |\phi_i|^2\ \rho\ dV$$

$$\Xi_i = \int_S [F \cdot \phi_i]\ dS$$

Finite-element methods describe q[Y,t] with a finite number of points [n], and truncate the series description at each point after n terms. This results in a set of second-order ordinary differential equations in terms of physical translation and rotation, which can be diagonalized and put into the form

$$\begin{aligned} \dot{\underline{x}} &= A\underline{x} + B\underline{u} \\ \underline{y} &= C\underline{x} \end{aligned} \tag{3}$$

The matrix A is block diagonal

$$A = \begin{bmatrix} A_1 & & & \\ & A_2 & & \\ & & \ddots & \\ & & & A_\ell \end{bmatrix}$$

The individual blocks may take the form

$$A_i = \begin{bmatrix} 0 & 1 \\ -\omega_i^2 & -2\zeta_i\omega_i \end{bmatrix}, \text{ or } \begin{bmatrix} \lambda_i & \\ & \lambda_i^* \end{bmatrix}, \text{ or } \begin{bmatrix} \alpha_i & \beta_i \\ -\beta_i & \alpha_i \end{bmatrix}$$

where

$\lambda_i = \alpha_i + j\beta_i$ the complex eigenvalue of the mode

$\lambda_i^* = \alpha_i - j\beta_i$ the conjugate of λ_i

$\omega_i^2 = \alpha_i^2 + \beta_i^2$ the natural frequency

$\zeta_i = \alpha_i/\omega_i$ the damping ratio

The B and C matrices depend on the mode shapes evaluated at the actuator or sensor locations.

The derivation of Eq. (3) is presented in Appendix F. There are two points of interest here. The first is that Eq. (3) introduces a discrete representation of Y[$\underline{Y}$], which, in fact, ignores the high-frequency modes. The second point is that control systems commonly work in the time or frequency domain, and therefore seek to control q[x,y...t] by controlling the magnitude of $\xi_i[t]$, $i = 1,\infty$.

1.1.2 Frequency Characteristics

The frequency spectrum (see Figure 1) for a continuous structure is directly related to the semibounded infinite set of eigenvalues. In this context, the following definitions can be made.[2]

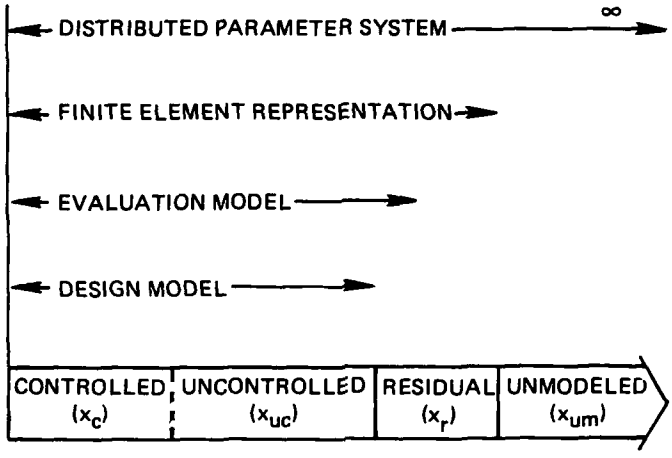

Figure 1. Frequency spectrum.

(1) Controlled modes, x_c, are the modes of the design model which are explicitly controlled in order to achieve system performance requirements.

(2) Uncontrolled modes, x_{uc}, are the modes of the design model which are included in the controller design process, but are not explicitly controlled.

(3) Residual modes, x_r, are those modes which appear in the large dimensional finite-element model, but are excluded from the design model.

(4) Unmodeled modes, x_{um}, are those modes which are assumed to exist, yet remain unmodeled.

(5) The evaluation model consists of the controlled modes, the uncontrolled modes, and some subset of the residual modes. The size of the subset is typically constrained by the dimension of available computer analysis tools. It is assumed that testing control alternatives against the evaluation model will be representative of testing these alternatives against the actual distributed parameter plant.

(6) Observation spillover is that portion of the measurement which is contaminated by modes (i.e., x_{uc}, x_r, x_{um}) not explicitly controlled.

(7) Control spillover is that feedback control which excites those modes (i.e., x_{uc}, x_r, x_{um}) not explicitly controlled.

Note that the above definitions do not restrict eigenvalue multiplicity, mode frequency separation, or frequency interleaving of controlled, uncontrolled, and residual modes.

If a state space model of the system is used, then two states are required to model the dynamics of each mode. For discussions in this thesis the following designations are made.

(1) $\underline{x}_1$ states correspond to x_c modes.

(2) $\underline{x}_2$ states describe those x_{uc} modes which are frequency interleaved with the x_c modes.

(3) $\underline{x}_3$ and $\underline{x}_4$ states are associated with the remaining x_{uc} modes. The distinction between $\underline{x}_3$ and $\underline{x}_4$ will be made later in the text.

(4) $\underline{x}_5$ models the residual (x_r) modes.

1.1.3 Control Requirements[2]

An attitude controller may be required to meet objectives in three functional categories: pointing control, vibration control, and figure or shape control.

Pointing control refers to the static and dynamic errors involved in following system pointing commands. Traditional designs have focused on controlling the rigid-body modes and use gain stabilization or an alternate frequency separation technique to minimize system response at frequencies above the control system bandwidth. For a flexible satellite, the low natural frequencies imply that some of the vibration modes will affect system pointing and, therefore, the dynamics of these modes must also be controlled. Additionally, frequency separation techniques are often invalid because of the low damping ratios and the lack of a defined frequency separation.

Vibration control is implemented to damp the vibrational energy in the structure. Sources of vibration excitation include the pointing controller, internal mechanisms like vibrating or scanning sensors, and external impulses. The spectrum of these disturbances is sketched in Figure 2, and may include a broadband low-frequency component, narrowband components at discrete higher frequencies, and a white noise representation of impulsive loads. Shape control implies maintaining a portion or all of the structures contour close to a specified configuration. Here, it is assumed that the shape reference is an equilibrium configuration, and that shape control will require that certain modes be constrained.

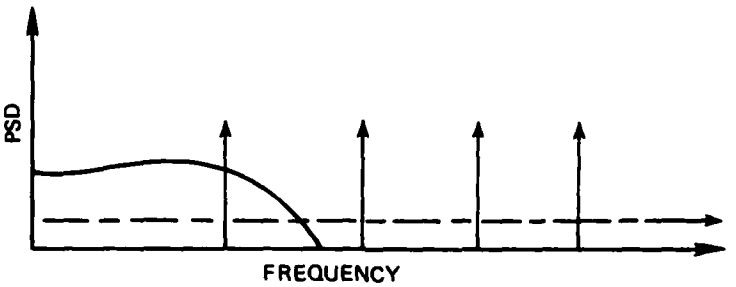

Figure 2. Vibration disturbance spectrum.

As noted previously, the pointing, vibration, and figure control requirements may result in frequency interleaving of controlled, uncontrolled, and residual modes. The objective of flexible spacecraft control designs is to meet these requirements, and the response times associated with them, without increasing the dimension of the controller unduly. Additionally, the controller must have good robustness properties, be economical of flight computer resources, and be tolerant of external disturbances.

1.2 Controller Approaches

The difficulties in flexible satellite control stem from three sources. The first is that the plant is flexible, lightly damped, and has distributed mass and stiffness. This implies that plant magnitude drops off very slowly with frequency and that an accurate discrete representation could require an infinite number of states. A second difficulty is that design requirements dictate that the bandwidth contain some of the structural modes, and the case where the controlled and the uncontrolled modes are frequency interleaved may exist. (see Figure 3). Finally, the space structure can be expected to be a multiple input-multiple output system.

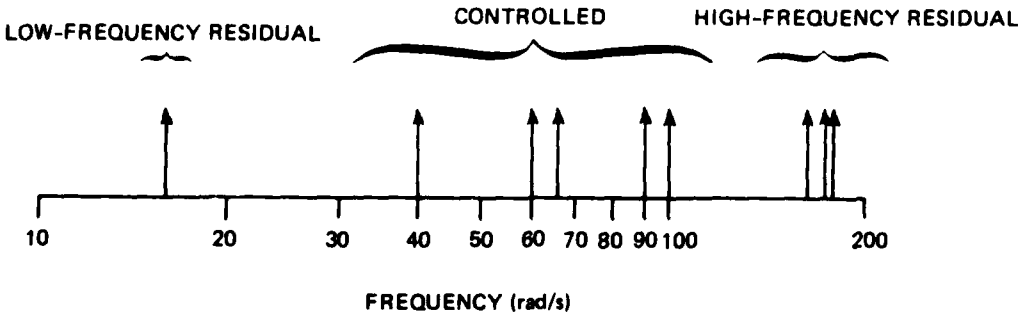

Figure 3. Controller approaches.[5]

Classical designs, employing notch filters and gain stabilization, are possible, and successful examples are deployed today.[20] The strongest deficiency of these techniques is their sensitivity to dimension. When the dimension of the input or the output becomes large, implementation becomes difficult. Because of this, state space techniques have been examined as an alternate design methodology. Two approaches have been taken. One course focuses on the optimal regulator and trying to implement it. Difficulties arise here because of the distributed nature of the plant. As another option, direct output feedback techniques are being looked at. The challenge in applying output feedback is simultaneously achieving stability, robustness, and the capability to meet dynamic requirements.

1.2.1 The Optimal Regulator

The optimal state feedback regulator is attractive for a number of reasons. It is an efficient technique for multivariable problems, it guarantees a stable closed-loop system if well defined conditions are met,[6] it can meet dynamic response requirements, and it has impressive gain and phase margins.[7] Moreover, it is simple to implement in the sense that it requires only a set of constant gains.

An initial drawback to using a regulator is that it requires full-state feedback. Extensions to theory have included the separation theorem,[6] which under appropriate conditions guarantees stability and good dynamic performance even if a reconstructed or estimated state is used in the feedback loop. In addition, Doyle and Stein [8] have shown that full-state robustness properties can be retained if observer gains are properly chosen.

A more serious drawback to use in spacecraft control design occurs because the regulator theory, including the robustness theorems, assumes an accurate plant model. States must be represented adequately, and all important states must be modeled. Neglecting higher order states may be justified if the plant is strongly damped, though this must be done carefully because, above the bandwidth, the regulator falls off only as $1/\omega$.

In the flexible satellite case neglecting higher order states may not be possible. Harris,[3] Ginter,[4] and others have demonstrated that using a truncated structural model in regulator design will produce instability or undesirable dynamics. Current research in regulator application includes three approaches to reducing regulator sensitivity to unmodeled modes; defining the region where neglecting the unmodeled modes is valid, modifying the regulator to decrease its sensitivity, and estimating the unmodeled modes by a set of error functions.

Research that rigorously defines the conditions where truncated models are valid, is clearly of interest. Results are available in terms of system eigenvalues [A matrix], and in terms of actuator/sensor locations [B and C matrices]. Singular perturbation theory, which is valid if the plant has identifiable slow and fast modes, will allow a controller to be designed for the slow modes; and if the open-loop system is stable, it will guarantee stability for the fast modes.[9] The basic theorems in this area have been extended to the case where an observer is used to reconstruct some of the slow modes.[10] Investigations into applying singular perturbation control formulations to the flexible spacecraft problem,[11,12] despite the fact that the slow/fast condition was not strictly met, have produced nonrobust controllers.[12,13]

Balas[14] represents an alternate set of conditions which also allow a truncated controller. The flexible spacecraft model can be diagrammed as shown in Figure 4, where the modeled dynamics contain both controlled and uncontrolled modes. Note that there is not dynamic coupling between modes, a result of the block diagonal A matrix. If $C_5 = 0$, the poles of the residual dynamics will not be shifted, so if the open-loop residual dynamics were stable the closed-loop residual dynamics will also be stable. If $B_5 = 0$, there will be no excitation of the residual modes. To the extent that the control designer has control over the configuration, B_5 and C_5 can be minimized and valid designs implemented.[14]

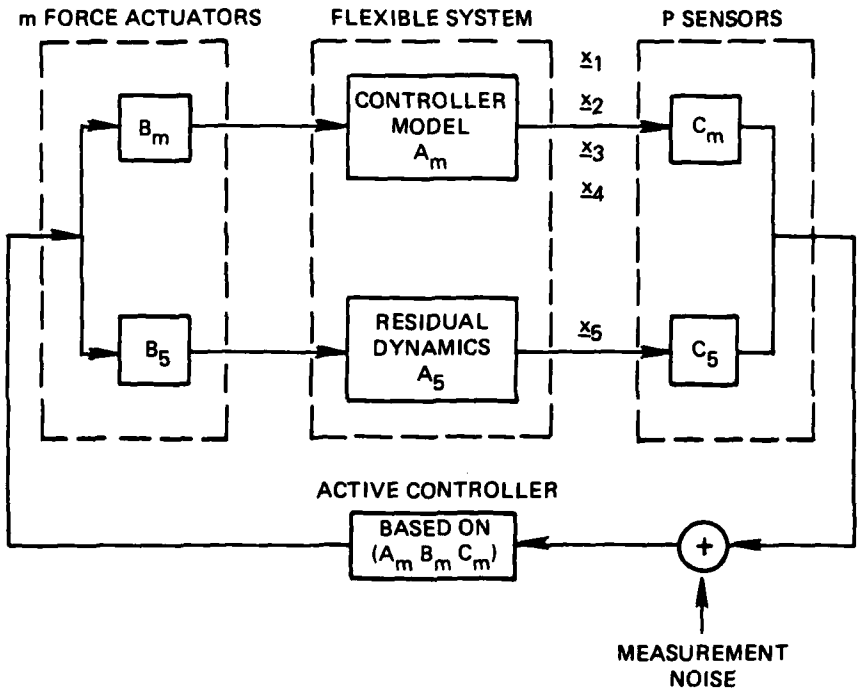

Figure 4. Flexible spacecraft model.

Gupta[15] has actively modified regulator theory to reduce the sensitivity to modeling errors. He introduces frequency-dependent weights in the cost function and obtains a greater than $1/\omega$ rolloff outside the bandwidth, at the expense of adding dynamics in the feedback loop. The feasibility of this concept for application to spacecraft has not yet been demonstrated.

As a third alternative, Skelton designs a reduced-order controller, but accounts for the neglected modes with an orthogonal function approximation.[16] In their assessment of this method, Joshi and Groom[17] note that it offers "no advantage in the example considered, although spillover estimates appear to be acceptable."

1.2.2 Output Feedback

Application of the regulator to distributed parameter problems is limited because of sensitivity to plant/model mismatch, particularly in dimension. An alternative which is being explored is output feedback. without feedback loop dynamics. Output feedback controller laws are of the form

$$\underline{u} = K\underline{y} \tag{4}$$

where y is the system output. There is a body of theory available for selecting the elements of the K matrix. If a finite plant model of dimension n is used, and m actuators and p sensors are available, then K can be chosen to place m + p - 1 closed-loop poles. If m + p - 1 > n, then eigenvectors can also be selected.[18] The applicability of these techniques to spacecraft design is limited for the same reason as the regulator (i.e., spillover). Because the controller interacts with residual modes, definitive statements about closed-loop system stability are not generally possible.

Although one cannot ensure stability in general, results are available for special forms of the matrix K. In particular, Canavin[19] establishes that if feedback consists only of velocity measurements, even if limited in number, and each sensor output is fed back only to a co-located actuator, then stability of the closed-loop system can be guaranteed. There is a restricted capability, however, to meet system dynamic requirements, and the stability results are not strictly valid if actuator or sensor dynamics are acknowledged.

1.2.3 Summary

State space techniques are attractive because they make the design of controllers for multiple-sensor/multiple-actuator systems tractable. However, when these techniques have been applied to the flexible-spacecraft

problem, they have produced designs which are not totally satisfactory. For purposes of this thesis, a satisfactory design meets four criteria:

(1) Insensitivity to the process which converts the distributed parameter structural description to a finite dimensional controller design model.

(2) Insensitivity to parameter variations within the design model.

(3) Acceptable closed-loop dynamics.

(4) Guaranteed stability.

The fundamental difficulty seems to be in satisfying the first of these criteria.

1.3 Thesis Overview

1.3.1 Discussion of Results

The research detailed in this thesis develops a methodology for designing flexible-spacecraft controllers. This methodology uses a low-order regulator/observer as the key controller element, but represents a departure from previous applications for two reasons.

(1) The controller input and output are constrained in the spatial domain.

(2) Residual modes are explicitly accounted for in the controller.

The philosophy that motivated these modifications is based on four postulates:

(1) The fact that modes can be placed in categories (x_c, x_{uc}, x_r) represents valuable information. One of the strengths of the classical control approach is that it permits modes

to be phase-stabilized, notch-filtered, or gain-stabilized depending on mode characteristics. State space techniques do not permit this flexibility.

(2) The spatial content of control inputs and observed outputs is important. The focus of traditional state space controller designs is in the time or frequency domain; and spatial information is typically not fully exploited or acknowledged. However, spatial concepts are of interest, particularly in the case of flexible satellites. In the time domain, a system input, $f[t] = f_o \cdot \sin[\omega t]$, is a narrowband input, while a discrete inpulse, $f[t] = f_o\, \delta[t - t_1]$, is wideband. Similarly, in the spatial domain, an input of the form $F[\underline{y}, t] = \phi_i[\underline{y}]\, f[t]$ is narrowband, and will (for a self-adjoint system) excite only the i^{th} mode. A point actuator is spatially wideband and will excite all modes except those where $\phi_K[\underline{y}_a] = 0$ ($\underline{y}_a$ is the actuator location).

(3) A truncated controller design model that ignores higher order modes is not asymptotically valid. The characteristic values of the truncated dynamical matrix will not approach the true eigenvalues even in the limit where neglected frequencies become infinite.[21]

(4) A reduced-order controller is required. In the spacecraft environment, computer computation and memory resources are limited, and while dynamics are allowed in the feedback loop, it is desirable to keep controller dimensions small.

A block diagram represenation of the proposed controller architecture is shown in Figure 5. Transformations T_2 and T_3 are introduced in the feedback path and serve to constrain the spatial content of $\bar{\underline{y}}$ and $\underline{u}$. The term $C_4 A_4^{-1} B_4\, \underline{u}$ in the observer estimate of the system

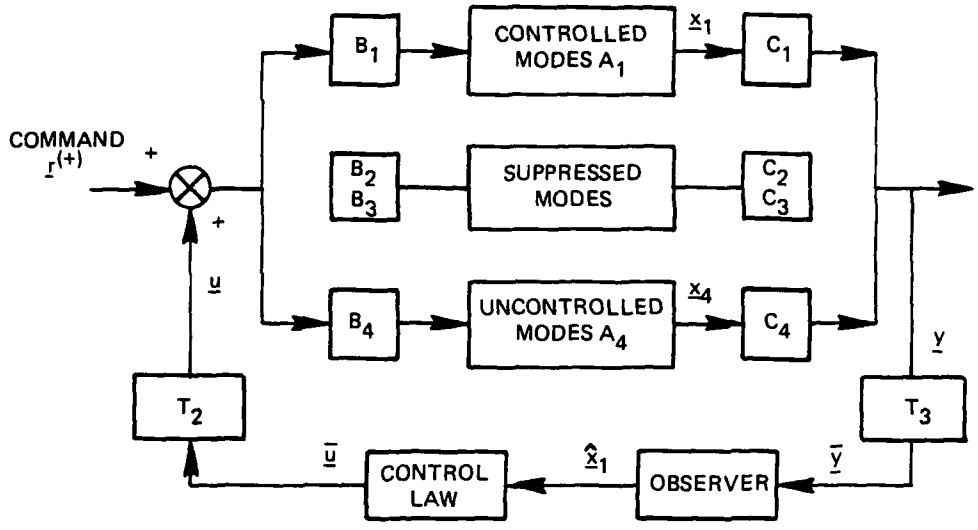

- CONTROL LAW $\bar{u} = \bar{K}\hat{x}_1$
- OBSERVER $\dot{\hat{x}}_1 = A_1\hat{x}_1 + B_1 u + GT_3[y - \hat{y}]$

$$\hat{y} = C_1\hat{x}_1 + C_4A_4^{-1}B_4 u$$

Figure 5. Reduced-order controller.

output represents a dc correction for residual state effects. The operation of this controller is perhaps best described in the frequency domain (see Figure 6). A reduced-order regulator (dimension $[x_1]$) is designed to give the x_1 states adequate dynamic response, but constrained to choose control laws of the form $u = T_2K\hat{x}_1$. If T_2 is chosen so that

$$B_2T_2 = 0$$

and (5)

$$B_3T_2 = 0$$

then, u will not spill over into x_2 or x_3. Similarly, the output residual which drives the observer is constrained to be of the form $GT_3[y - \hat{y}]$

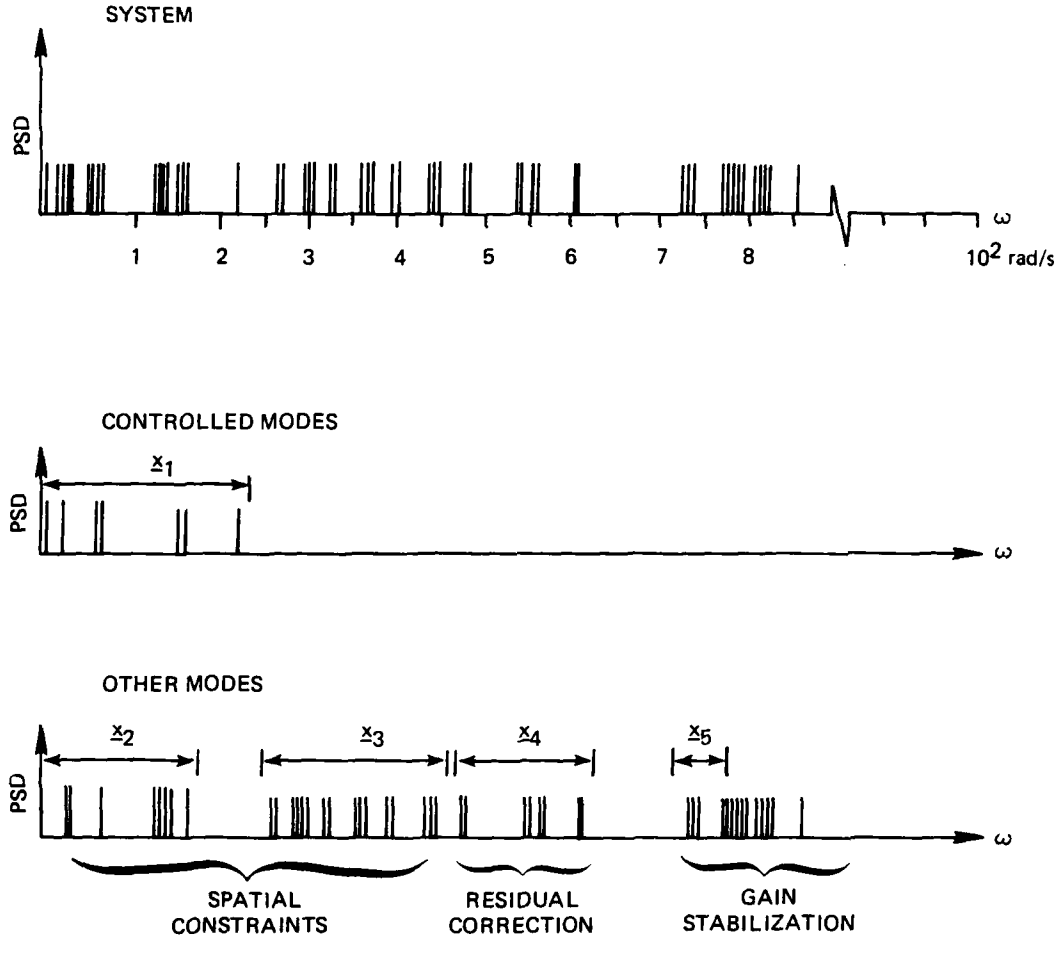

Figure 6. System mode categories.

where $\hat{y}$ is the observer estimate of the output. If T_3 is chosen so that

$$T_3 C_2 = 0$$

and (6)

$$T_3 C_3 = 0$$

then, the observation residual will not contain $\underline{x}_2$ or $\underline{x}_3$ information. If T_2 and T_3 are chosen to satisfy equations (5) and (6) then the spectral content of the $\underline{u}$ to $\underline{\bar{y}}$ signal path exhibits an identifiable frequency separation (see Figure 7). A subset ($\underline{x}_4$) of the higher order modes can then be acknowledged in the controller by a singular pertubation correction term.

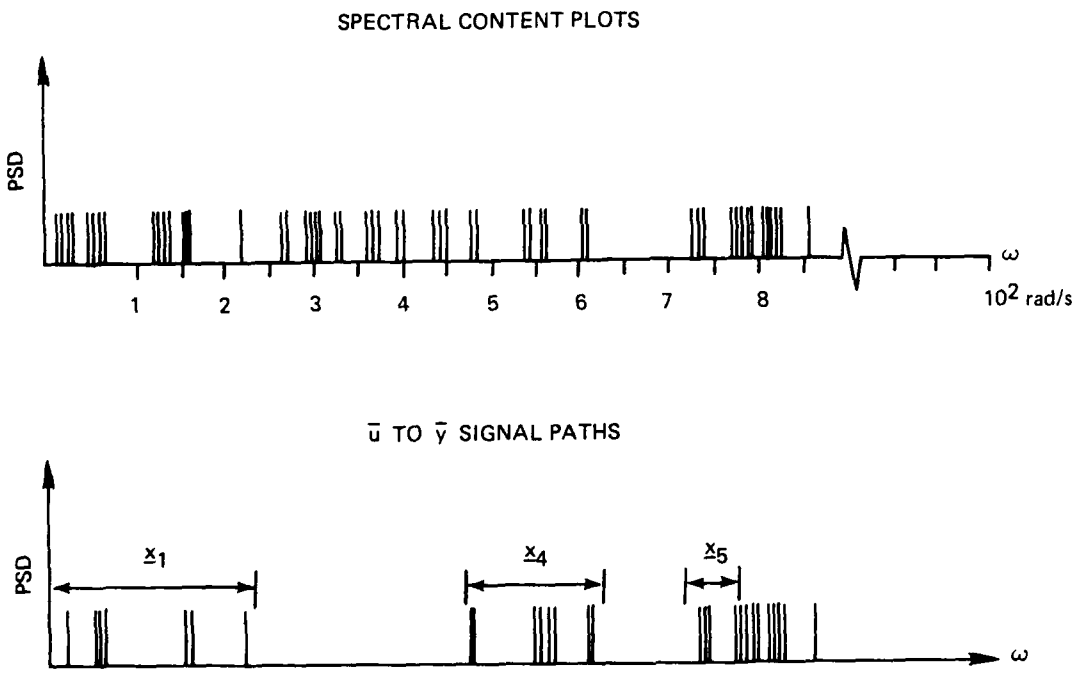

Figure 7. Spectral content plots: System, $\bar{u}$ to $\bar{y}$.

For the class of problem addressed here, this correction term is shown to be of a simple form: the observer estimate of state output is modified by a dc approximation of $\underline{x}_4$ dynamics.

$$\hat{\underline{y}} = C_1 x_1 + C_4 A_4^{-1} B_4 \underline{u} \tag{7}$$

The term $C_4 A_4^{-1} B_4$ is bounded even if the dimension of $\underline{x}_4$ is increased without limit. It represents the steady-state structural deflections of the x_y modes at the sensor locations due to unit loads at the actuator locations. The $\underline{x}_5$ states model the residual modes. It is assumed here that if the controller previously discussed is implemented, and the dimensions of $\underline{x}_3$ and $\underline{x}_4$ are big enough, then the $\underline{x}_5$ states will be gain-stabilized.

1.3.2 Specific Contents

The intent of this thesis is to theoretically justify and illustrate the controller architecture which is discussed in the previous section. To this end, five chapters and eight supporting appendices are presented:

Chapter 1	Introduction
Chapter 2	M2V2 Satellite Description
Chapter 3	Controller Alternatives
Chapter 4	Summary and Suggestions for Future Research
Chapter 5	Conclusions
Appendices	A Transform Methodology
	B Effect of Filtering a Control Input
	C Adaptive Transforms
	D Poles and Zeros of Multivariable Systems
	E Singular Perturbation Theory
	F Equations of Motion
	G Eigensystem Perturbation Theory
	H Implementation Issues

This organization of information treats the controller problem on two levels. The main body of the text investigates the system's implications of alternate controller architectures. A representative satellite design, the CSDL M2V2 spacecraft, is introduced in Chapter 2. The state space structural response model of this system is used to help fix ideas and to illustrate key technical points. Specifically, results are presented in Chapter 3 which compare the performance of a full-order optimal regulator with various reduced-order controller options. In contrast to the text, the appendices present detailed theoretical developments; developments needed to motivate and justify the controller designs of Chapter 3. Of particular interest are Appendix A, where it is shown that satisfying Eq. (5) and (6) is equivalent to

(1) Placing zeros at the same locations in the complex frequency plane as the poles of A_2 and A_3 for all $\underline{u}$ to $\underline{y}$ signal paths.

(2) Nulling control and observation spillover for $\underline{x}_2$ and $\underline{x}_3$.

(3) Making $\underline{x}_2$ and $\underline{x}_3$ unobservable and uncontrollable.

(4) Placing $\bar{u}$ in the row null space of $\begin{bmatrix} B_2 \\ B_3 \end{bmatrix}$ and $\bar{y}$ in the column null space of $[C_2 C_3]$.

and Appendix E, where the details of constructing an appropriate, asymptotically correct, low-order dynamic control design model are presented.

CHAPTER 2

M2V2 SPACECRAFT

This chapter summarizes the configuration and structural response characteristics of the CSDL M2V2 spaceborne optical system. Controller requirements are then discussed within this context. The M2V2 is a preliminary prototype design due to Henderson.[22] It is used in this thesis to illustrate the implications of various controller designs. No attempt is made to address the many implementation issues associated with actually deploying a satellite of this class.

2.1 Configuration

The optical system under discussion here is a larger scale version of the Space Telescope. It consists of two space-grade mirrors (a concave primary and an convex secondary) in a Cassegrain configuration (see Figure 8). The image reflects off the primary mirror onto the secondary, where it is then directed to the focal plane. In the design used here, key dimensions include

18 m base length

1.5 m secondary-mirror diameter

5.5 m primary-mirror diameter

The size of the secondary mirror represents a tradeoff between obscuration and field of view.

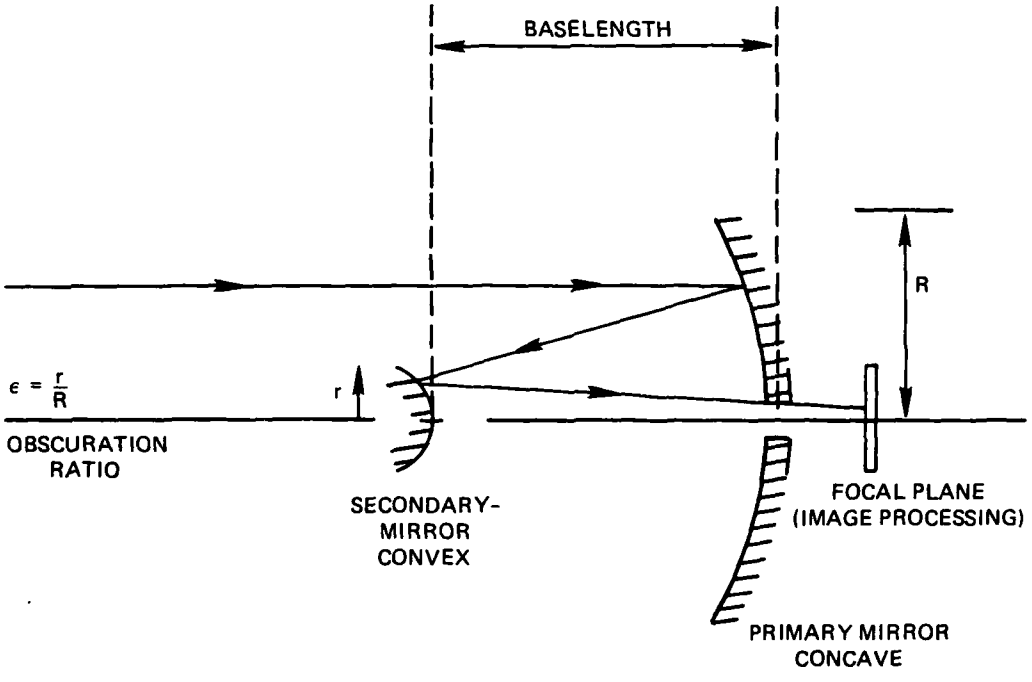

Figure 8. Cassegrain configuration.

The M2V2 satellite consists of the optics described above, a support structure, processing equipment, a power system, and a sensor/actuator package. These components are discussed only to the degree necessary to explain their interaction with the control system.

(1) The support structure is constructed of low-thermal-expansion graphite-epoxy tubing, and consists of a rigid base and a metering truss to hold the secondary mirror (see Figures 9 and 10).

(2) The processing equipment includes cooled focal plane sensors, recorders, and communication devices. For purposes of controller design, this equipment is modeled as a wideband disturbance in the base section.

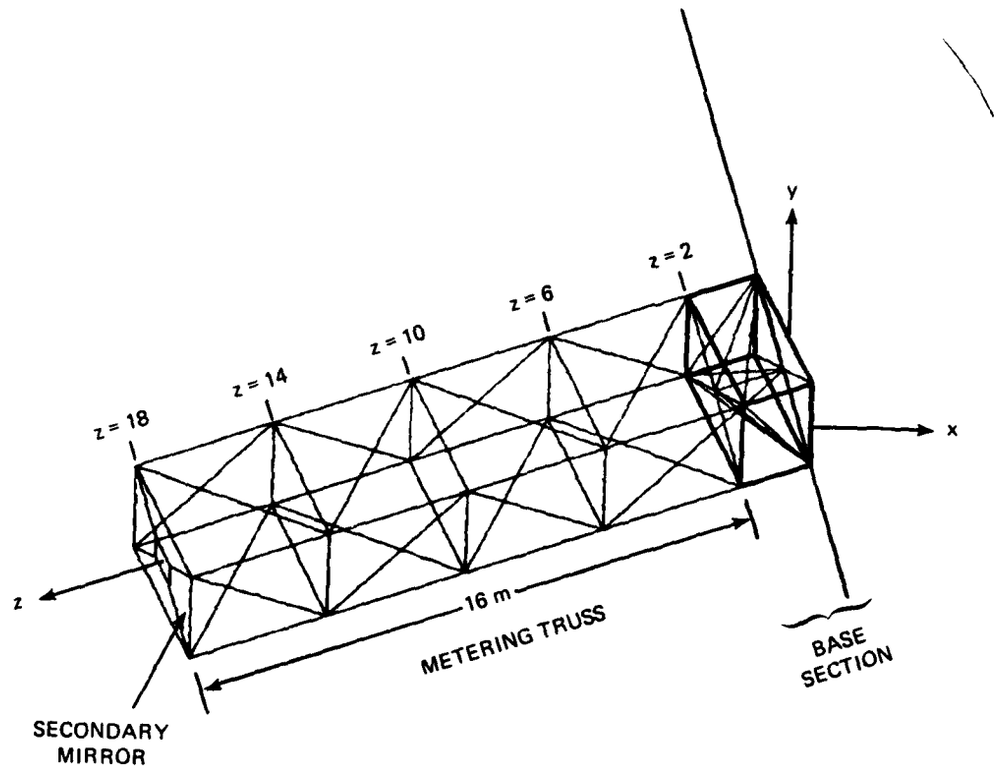

Figure 9. Support structure with rigid base and metering truss.

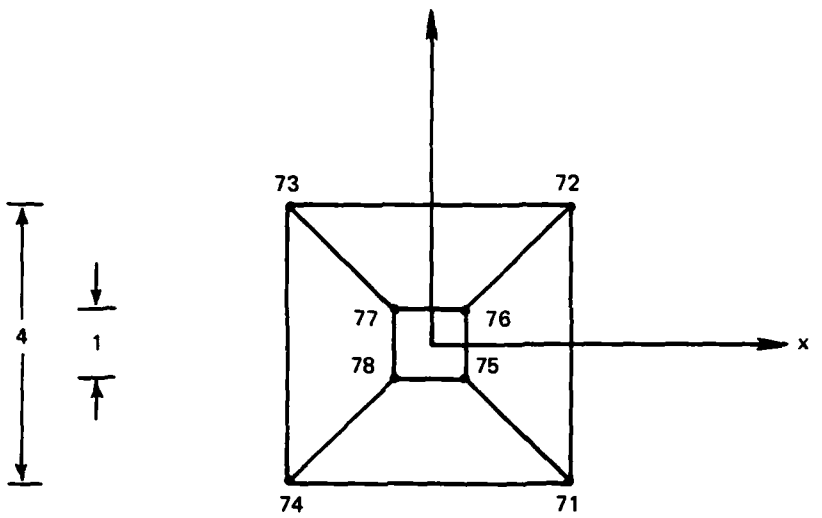

TELESCOPE SECTION

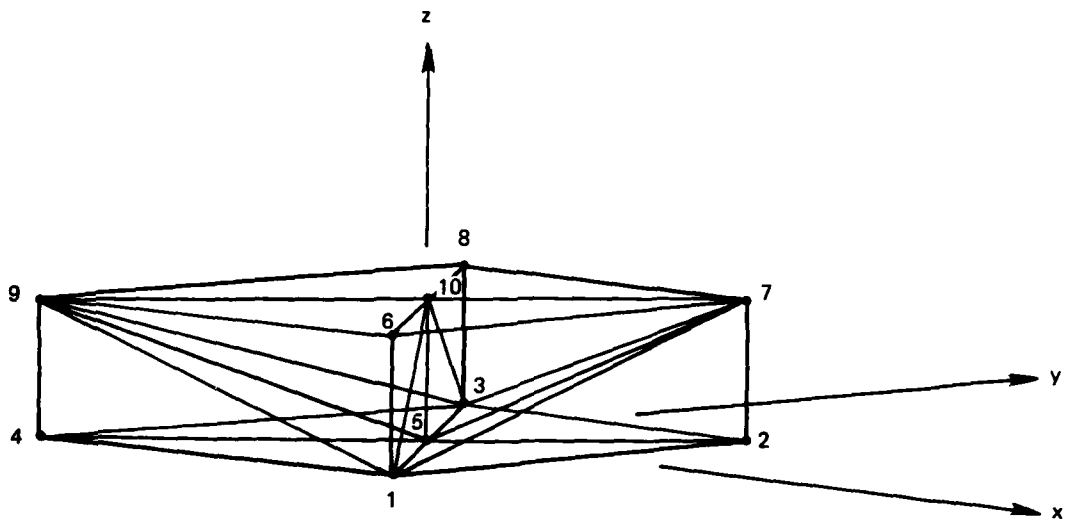

BASE SECTION

Figure 10. Support structure: telescope and base sections

(3) The power system converts and stores solar energy for use by mission equipment. The components of interest to the controller are the two flexible solar panels which are rigidly mounted to the base section.

(4) In general, a satellite sensor/actuator package provides the control authority and the information necessary to perform station-keeping, pointing, and vibration control tasks. In this thesis, attention is limited to motions about the center of mass. The specific sensors and actuators that are used are summarized in Figure 11. Measurements 14, 15, and 16 are local angle measurements from an inertial system. The remaining measurements are displacements from piezo-electric sensors.

Appendix F models the satellite structure, develops the equations of motion, and discusses the dynamic response modes. Details of mass distribution and member sizing are also given.

2.2 Structural Response Characteristics

The dynamic response of the M2V2 system can be characterized in terms of eigenfrequencies and mode shapes. The details of this characterization are given in Appendix F. There are, however, some general comments of interest here. Figure 12 gives the spectral distribution of the satellite response. There is a dense distribution of modes with occasions where the eigenvalue multiplicty reaches 4. This spectra is typical of the distributed parameter system discussed in Chapter 1. Key points to be noted include the following.

(1) There is no evident frequency separation between a set of high- and low-frequency modes.

(2) When several modes have the same or nearly the same natural frequency it is very difficult to distinguish them in the frequency domain. Spatial characteristics however, may permit separation of effects (see Figure 13).

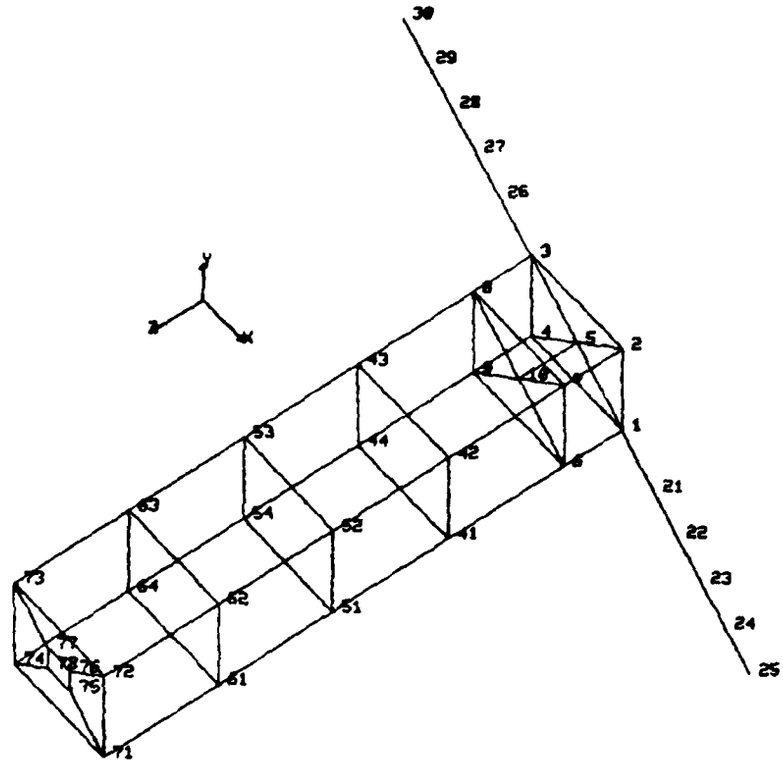

ACTUATOR LOCATIONS		
PIEZO ELECTRIC MEMBER ACTUATORS		
ACTUATOR	NODE 1	NODE 2
1	5	10
2	51	64
3	52	61
4	53	62
5	54	63
6	64	71
7	61	72
8	62	73
9	63	74
10	6	41
11	7	42
12	8	43
13	9	44
CONTROL MOMENT GYROS		
ACTUATOR	AXIS	
14	x	
15	y	
16	z	

SENSOR LOCATIONS		
SENSOR	NODE	DIRECTION
1-16	SENSORS & ACTUATORS COLOCATED	
17	1	+x +y
18	21	+x +y
19	21	z
20	22	+x +y
21	22	z
22	23	+x +y
23	23	z
24	24	+x +y
24	24	z
26	25	+x +y
27	25	z
28	3	+x +y
29	26	+x +y
30	26	z
31	27	+x +y
32	27	z
33	28	+x +y
34	28	z
35	29	+x +y
36	29	z
37	30	+x +y
38	30	z

Figure 11. Summary of actuators and sensors.

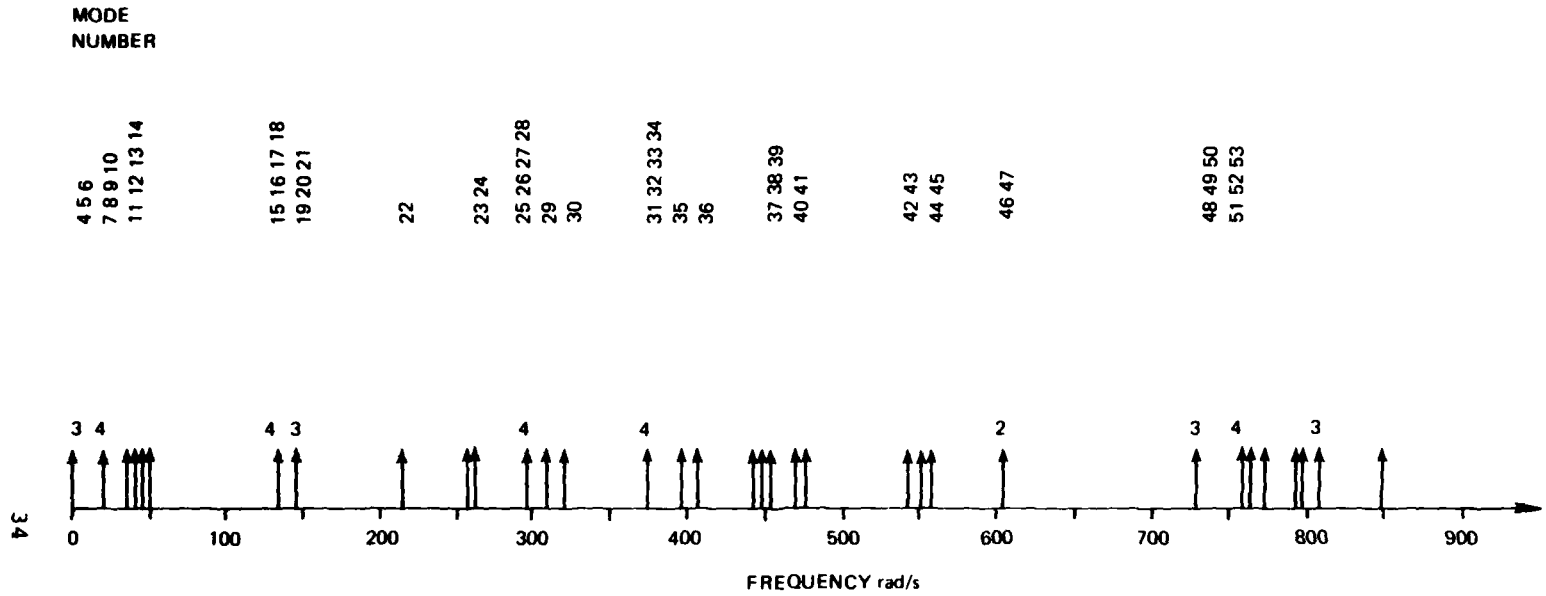

Figure 12. Spectral distribution of the satellite response.

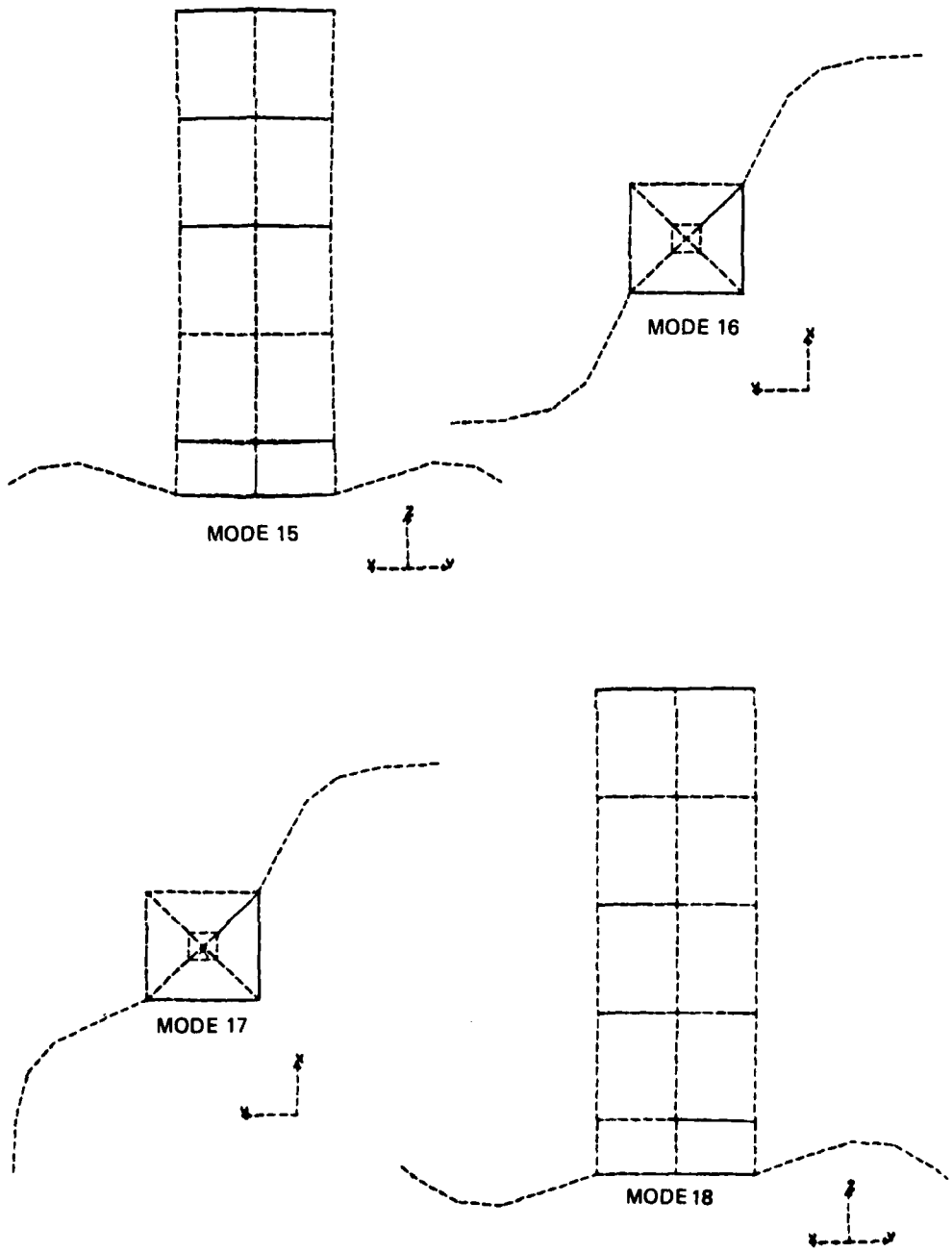

Figure 13. Separation of effects, λ = 137 Hz.

2.3 Performance Index and Control Requirements

The performance of the optical system is degraded if the baseline geometric relationships are not maintained. In particular, the following quantities are of interest.

(1) The change in baselength (z spacing between mirrors) which affects the focus.

(2) The differential displacements between the mirrors in the x and y directions, which affect the line of sight.

(3) The differential rotations of the mirrors around either the x or the y axis, which affect the location of the image on the focal plane.

These five quantities can be defined in modal coordinates; the specific relationships are given in Table 1. The notation ... refers to higher frequency modes which are not included in the truncated discrete model. From these relationships a scalar cost function in

Table 1. Performance relationships in modal coordinates.

Focal length change (m)

$$\Delta_f = 0.01315\,\xi_{11} - 0.01207\,\xi_{22} + 0.00239\,\xi_{28} + 0.00488\,\xi_{29} + \ldots$$

Line-of-Sight Deviations (m)

$$\Delta_x = -0.001130\,\xi_7 + 0.002036\,\xi_{12} + 0.001956\,\xi_{13} + 0.005727\,\xi_{23} - 0.001142\,\xi_{26} + 0.004582\,\xi_{30} + \ldots$$

$$\Delta_y = -0.001127\,\xi_7 + 0.002047\,\xi_{12} - 0.001934\,\xi_{13} + 0.005733\,\xi_{23} - 0.009312\,\xi_{26} - 0.004582\,\xi_{30} + \ldots$$

Deviations of Mirrors from Parallel (rad)

$$\theta_x = -0.019368\,\xi_{20} + 0.007237\,\xi_{21} + \ldots$$

$$\theta_y = 0.007265\,\xi_{20} + 0.019353\,\xi_{21} + \ldots$$

terms of modal displacements can be constructed. This particular approach is not taken in this thesis. An alternate philosophy is adopted which focuses on the following three objectives.

(1) Achieving adequate rigid-body rotation response.

(2) Adding damping to performance-related modes to improve disturbance suppression.

(3) Ensuring closed-loop stability.

These objectives translate into the following controller requirements.

(1) A rigid-body bandwidth of less than 1 radian/second.

(2) A 10 percent damping for modes 7, 11, 12, 13, 20, 21, 22.

(3) The isolation of modes 23, 26, 28, 29, 30 from controller influences.

(4) Adequate stability margins.

Table 2 details the modes which are to be controlled and those which are to be isolated from the controller. Both sets influence the optical performance. The intent is to add damping to the first set to improve time response and to reduce resonance amplification due to disturbances from either the controller or from the processing equipment. The second set of modes is of higher frequency (see Figure 14). The time response of these modes is adequate, and it is likely that they are above the bandwidth of the equipment disturbances. The potential for being excited by the controller remains, however, and isolation from control influences is desirable.

2.4 Summary

The focus of this thesis is on the design of controllers for large-scale, lightly damped, multiple-input/multiple-output systems where the stiffness and mass are distributed parameters. The M2V2

Table 2. Controller requirements.

Controlled Modes (see Figure 14, sheets 1 and 2)

Mode	Effect
4, 5, 6	rigid-body rotations
7	line of sight
11	focus
12, 13	line of sight
20, 21	mirror rotation
22	focus

Modes To Be Decoupled From Controller Actions (see Figure 14, sheets 3 and 4)

Mode	Effect
23, 26	line of sight
28, 29	focus
30	line of sight

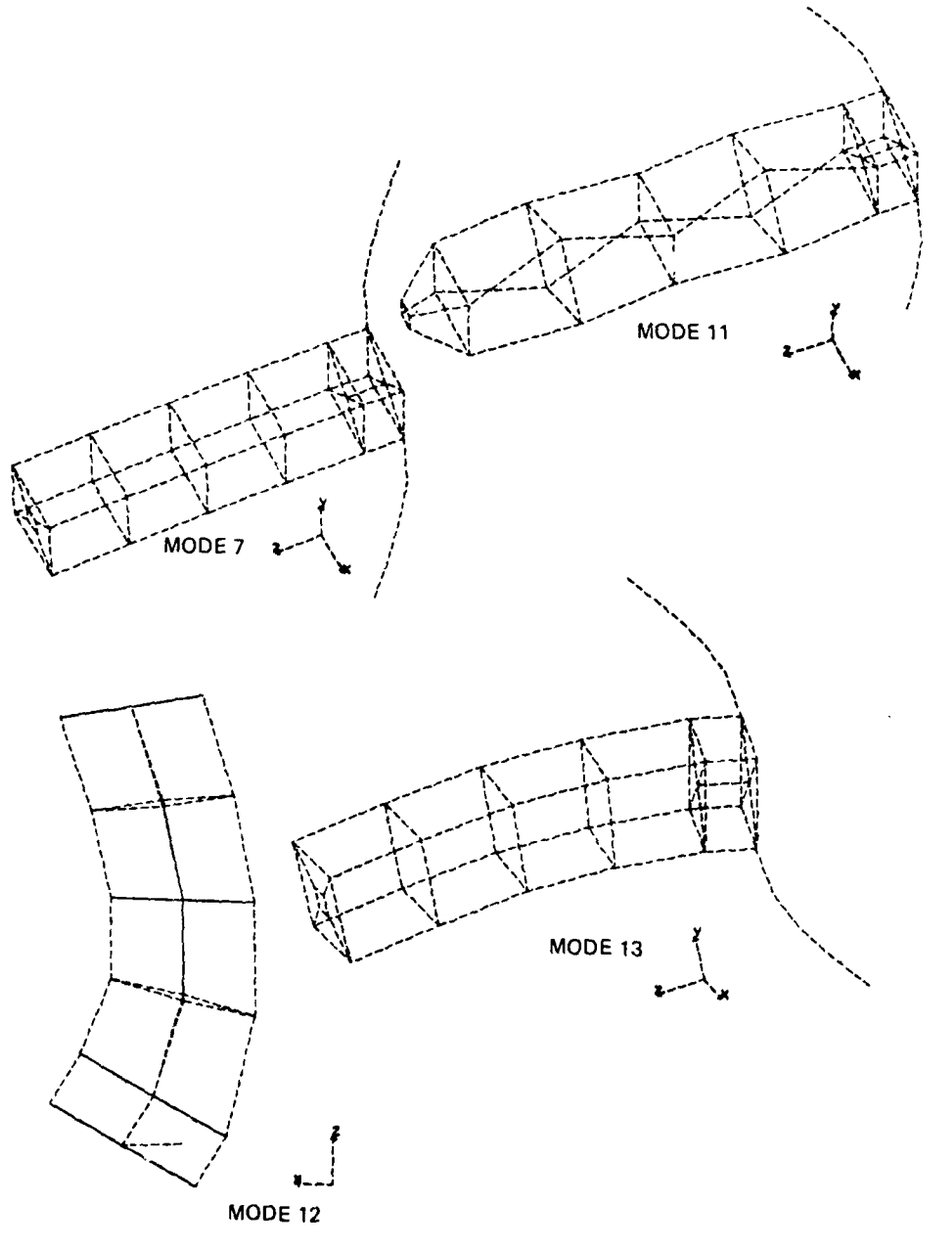

Figure 14. Controller requirements (sheet 1 of 4).

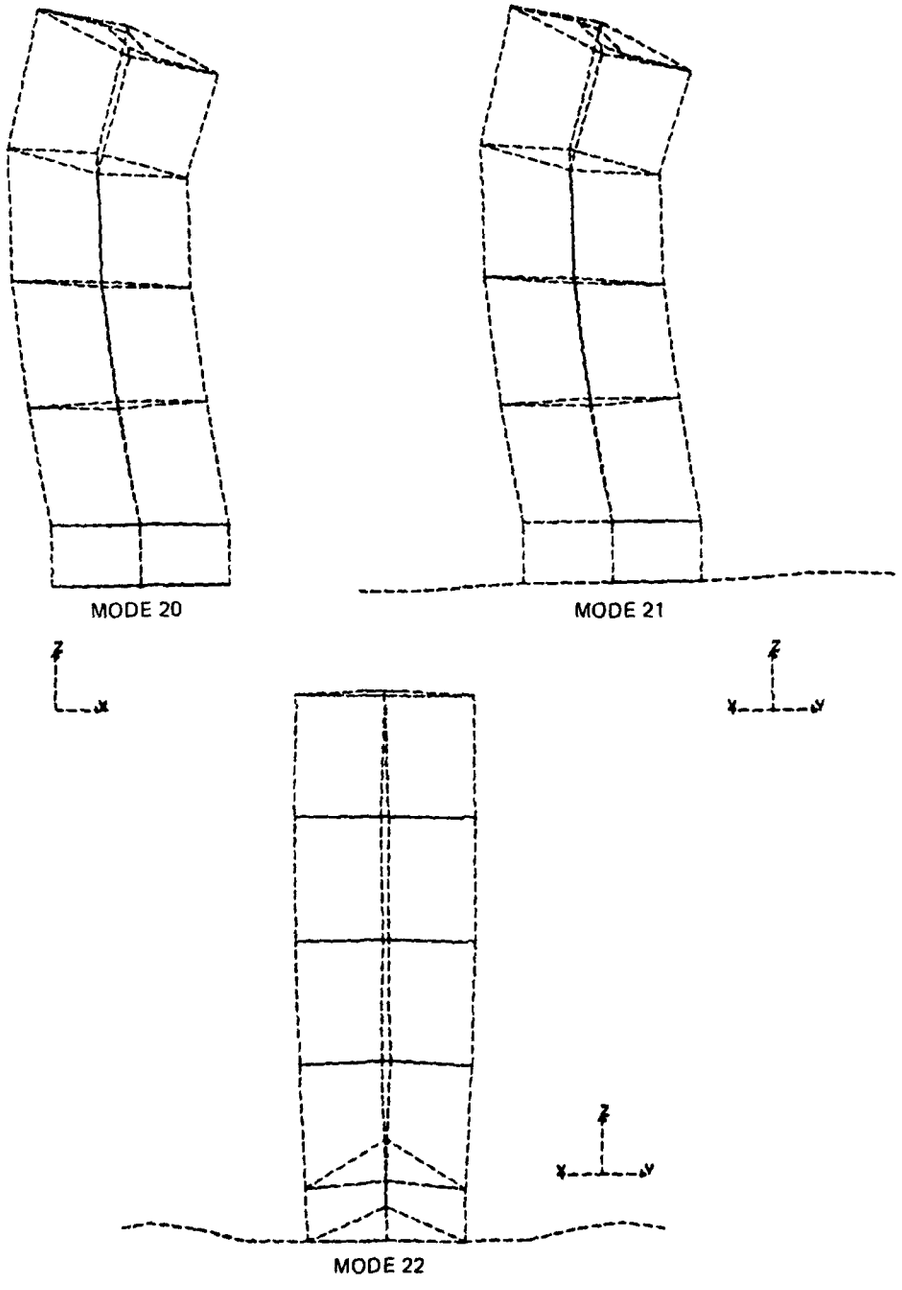

Figure 14. Controller requirements (sheet 2 of 4).

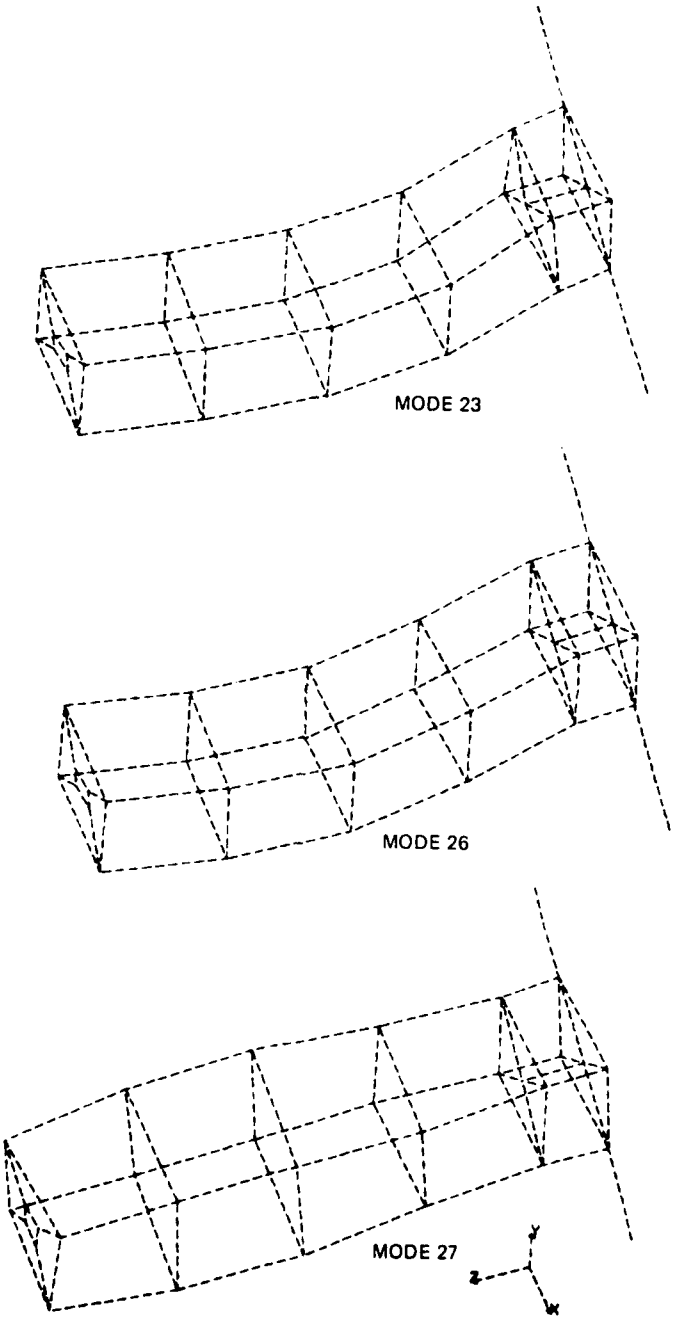

Figure 14. Controller requirements (sheet 3 of 4).

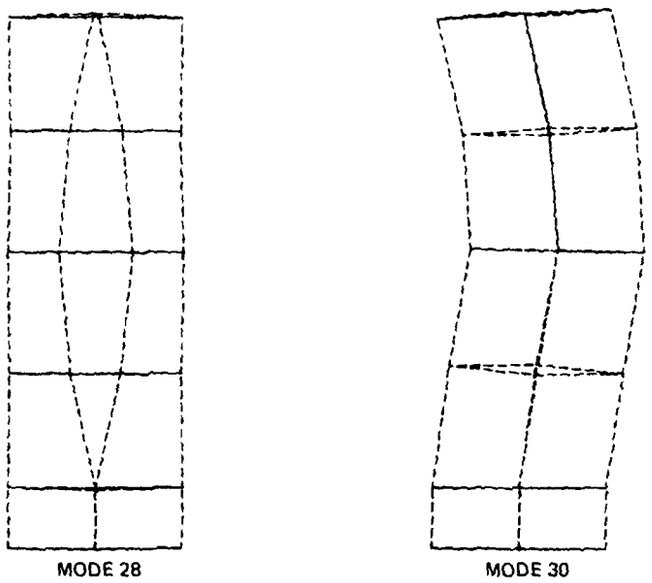

Figure 14. Controller requirements (sheet 4 of 4).

optical satellite is a well characterized design which is representative of this class of system. This chapter describes this satellite with the express intent of using it to illustrate controller options in Chapter 3.

It is interesting to note, by way of a side comment, that while the introduction makes the distinction between discrete and distributed parameter systems, each of these concepts is an idealization. Real structures will fall somewhere in between. The M2V2 has distributed stiffness and mass, but there are also the following discretizing influences.

(1) Large concentrated optical and equipment masses.

(2) Low moment capacity joints.

(3) Members and components with individual frequencies which are much higher than the truss frequencies.

(4) Stiff subunit structures like the base section.

The effect of these influences it to produce readily definable truss and member modes. The point which is of particular interest here is that the structural designer does have substantial control over the spectral pattern of the system. Although this thesis does not address the subject, there appears to be a potential for configuring the truss and sizing the structural members so that significant frequency separation occurs between high- and low-frequency modes.

CHAPTER 3

CONTROLLER OPTIONS

The central contribution of this research is a controller architecture which is applicable to the pointing and vibration control of flexible spacecraft. This architecture is a synthesis of three technologies.

(1) Singular, memoryless transformations of multiple-path signals (Appendix A).

(2) Asymptotic corrections (Appendix E).

(3) The optimal regulator/observer.

The resulting controller is of reduced order, and promises to provide the dynamic performance of a full-order design for slight increases in control cost. The architecture under discussion here was introduced and justified on technical grounds in Chapter 1. The intent of this chapter is to discuss the controller issues from an alternate departure point. A representative flexible spacecraft design, the M2V2 optical system, is used as a test-bed for various controller configurations. The particular focus is on exploring the benefits and penalties associated with introducing output transforms, input transforms, and asymptotic corrections to the observer. The configurations that are exhibited are, in fact, point designs. Nevertheless, the controller characteristics which are illustrated are interesting and should be more widely relevant.

This chapter begins with a brief review of the problem statement. Then, the discussion turns to the controller alternatives. The baseline option is a full-state optimal regulator; all discussions of performance and costs refer to this case.

3.1 Problem Statement

The plant of interest is the M2V2 satellite. A description is given in Chapter 2, and equations of motion are developed in Appendix F. It is a lightly damped ($\zeta = 0.05$) flexible structure which supports an optical measurement system. Optical performance criteria dictate the controller requirements.

For purposes of this chapter, the dynamics of the M2V2 are modeled with a 50-mode (100-state) state space model. Eleven of the 50 modes are to be specifically controlled. This number includes three rigid-body rotation modes, seven vibratory modes which impact optical performance, and an additional mode, mode 10, which cannot be spatially distinguished from mode 4 and thus needs to be controll in the frequency domain. The states that describe the dynamics of these controlled modes are designated $\underline{x}_1$. The states that are not specifically controlled fall into four categories. Three of these categories, $\underline{x}_2$, $\underline{x}_3$, and $\underline{x}_4$, are accounted for in the controller design, but not included in the performance requirements. The final category $\underline{x}_5$ contains residual states that are neglected by the controller design model. The dimensions of the state subspaces are: dim $[\underline{x}_1] = 22$, dim $[\underline{x}_2] = 16$, dim $[\underline{x}_3] = 34$, dim $[\underline{x}_4] = 16$, and dim $[\underline{x}_5] = 12$. The frequency spectrum of the model, Figure 15, summarizes this data.

Sixteen control inputs are available. Three are orthogonal torques from control moment gyros located in the base section. The other 13 controls are member actuators; 1 in the base section, and 12 in the upper three sections of the metering truss. Specific locations are given in Appendix F, Figure F-28.

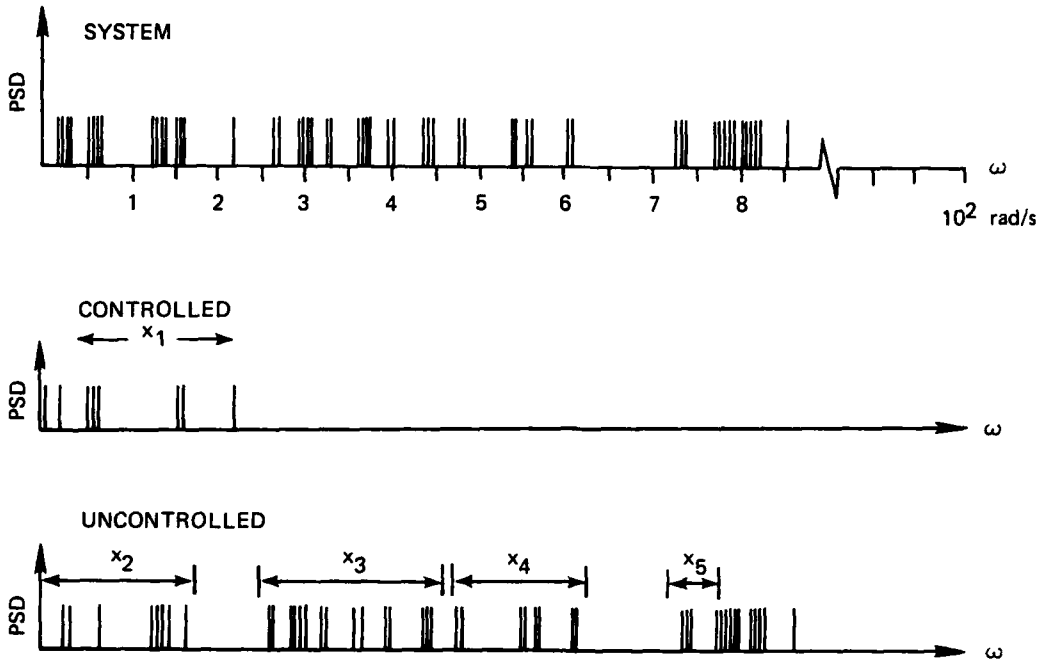

Figure 15. Frequency spectrum, evaluation model.

Thirty-eight sensors provide dynamic information. Sixteen of these are colocated with the actuators. The remaining 22 provide 12 horizontal and 10 vertical displacement measurements along the solar arrays (see Section F.9.4).

Control requirements dictate that the rigid-body time constant be 1 radian/second or smaller, that the $\underline{x}_1$ modes be damped to 10 percent, and that the set of modes {23, 26, 28, 29, 30} be isolated from the effects of the controller.

3.2 The Optimal Regulator

An optimal regulator was designed to serve as the baseline controller design. It was assumed that the M2V2 dynamic performance could

be adequately modeled by a finite element based state space model which acknowledged $\underline{x}_1$, $\underline{x}_2$, $\underline{x}_3$, and $\underline{x}_4$. The order of this model is 88. This section reviews regulator design methodology, presents a specific baseline controller, and then discusses issues and concerns. Included in this last area is the whole topic of discretization.

3.2.1 Regulator Theory

An optimal regulator for the 88-state plant consists of a control law and an estimator.

$$\underline{u} = K\hat{\underline{x}} \tag{9}$$

and

$$\dot{\hat{\underline{x}}} = A\hat{\underline{x}} + B\underline{u} + G(\underline{y} - C\hat{\underline{x}})$$

where

$$\underline{x} = \begin{bmatrix} \underline{x}_1 \\ \underline{x}_2 \\ \underline{x}_3 \\ \underline{x}_4 \end{bmatrix} \quad \text{and} \quad \hat{\underline{x}} = \begin{bmatrix} \hat{\underline{x}}_1 \\ \hat{\underline{x}}_2 \\ \hat{\underline{x}}_3 \\ \hat{\underline{x}}_4 \end{bmatrix}$$

The gain matrix K is given by

$$K = -R_2^{-1}B^TP \tag{10}$$

where the matrix P satisfies the algebraic Riccati equation

$$0 = A^TP + PA + R_1 - PBR_2^{-1}B^TP \tag{11}$$

The matrices R_1 and R_2 are weighting matrices associated with state deviations and control effort in the quadratic cost index

$$J = \int_{t_0}^{\infty} \underline{x}^T R_1 \underline{x} + \underline{u}^T R_2 \underline{u} \, dt \tag{12}$$

If K is chosen to satisfy Eq. (10), then the cost index J will be minimized. The cost associated with driving any state deviation $\underline{x}^0$ to zero is given by

$$J = \underline{x}^{0T} P \underline{x}^0 \tag{13}$$

For the problem at hand, characterized by a block diagonal A matrix, and a performance index which accounts for only a subset of $\underline{x}$ (namely $\underline{x}_1$), the R_2, R_1, P_1, and K matrices have special forms.

(1) The R_2 matrix is a diagonal 16×16 matrix which weights control effort. Equal penalties are assessed for using the member actuators, and these weights are numerically 10 times greater than the weights on the three outputs of the CMG. The intent is to acknowledge the greater control authority of the CMG. The exact choice of weights is not a central concern in this research.

(2) The R_1 matrix is a diagonal 88×88 matrix, where 88 is the dimension of x. However, only 22 of the states are weighted, and R_1 has the form

$$R_1 = \begin{bmatrix} \bar{R}_1 & & & \\ & 0 & & \\ & & 0 & \\ & & & 0 \end{bmatrix} \begin{matrix} \} x_1 \\ \} x_2 \\ \} x_3 \\ \} x_4 \end{matrix} \tag{14}$$

$\bar{R}_1$ is 22×22, and is a diagonal matrix. The diagonal elements of $\bar{R}_1$ are not all equal. They have been chosen iteratively to yield acceptable closed-loop pole placements.

(3) The P matrix is also 88×88, and again has nonzero elements only in the partition which is associated with $\underline{x}_1$. It is intuitive that states which are dynamically uncoupled (block-diagonal A matrix), and not weighted, should have no cost associated with them. To construct a rigorous proof of this see Theorem 3.8 in Linear Optimal Control Systems.[6] P has the form

$$P = \begin{bmatrix} \bar{P}_1 & & & \\ & 0 & & \\ & & 0 & \\ & & & 0 \end{bmatrix} \begin{matrix} \} x_1 \\ \} x_2 \\ \} x_3 \\ \} x_4 \end{matrix} \qquad (15)$$

$\bar{P}_1$ is 22×22, and fully populated.

(4) The gain matrix K can also be partitioned.

$$K = \lfloor K_1 \quad K_2 \quad K_3 \quad K_4 \rfloor \qquad (16)$$

Using Eq. (10) and (15), one obtains

$$K = \lfloor -R_2^{-1} B_1^T \bar{P}_1 \quad 0 \quad 0 \quad 0 \rfloor \qquad (17)$$

The elements of K_2, K_3, and K_4 are all zero.

The specific values of R_1, R_2, P, and K for the design at hand are given in Appendix H, where the method of solving Eq. (11) is also discussed.

Incorporating Eq. (17) into Eq. (9), the optimal control law becomes

$$u = K_1 \hat{x}_1 \tag{18}$$

where $\hat{x}_1$ is a partition of $\hat{x}$ and

$$\dot{\hat{x}} = A\hat{x} + Bu + G[y - C\hat{x}] \tag{19}$$

Equation (19) is an asymptotic observer. The gain matrix G is 88×38. The elements of G are chosen to give adequate closed-loop performance. In a stochastic environment, where estimates of plant noise and measurement noise are available, the matrix G should be the Kalman gain matrix. Alternately, in a deterministic design, the elements of G can be chosen to place the poles of the observer error states. This second methodology is used here.

The desired observer error pole locations represent a compromise between two constraints.

(1) Cost. If the observer poles are faster than the closed-loop system poles, then the incremental cost due to observer error will be small.[6]

(2) Robustness. If full-state feedback is available, the regulator supplies gain margins of 0.5 to ∞, and phase margins of -60° to +60° for all feedback paths.[7] With an observer or a Kalman filter in the feedback loop, these margins are degraded. However, the full-state margins are asymptotically achieved as the observer poles approach the regulator bandwidth.[8]

The actual mechanism which was used for placing the poles is the alpha-shift technique (see Sesak[11] and Strunce[5]). This technique exploits duality and chooses

$$G = -QC^T V_2^{-1} \tag{20}$$

where Q satisfies

$$0 = \bar{A}Q + Q\bar{A}^T + V_1 - QC^T V_2^{-1} CQ \tag{21}$$

V_1 and V_2 are weights on observer error states and on the use of measurement information. The matrix $\bar{A}$ is given by

$$\bar{A} = A + \alpha I \tag{22}$$

Use of Eq. (20), (21), and (22) guarantees that all poles of [A - GC] will be to the left of the line $s = -\alpha$ in the complex frequency plane. For designs in this chapter $\alpha = 6.0$, and V_1 and V_2 are diagonal. The elements of V_2 were set equal to 1.0×10^{-7}, and elements of V_1 were iterated to achieve satisfactory pole locations.

If the control law given by Eq. (18) and (19) is implemented, the closed-loop system can be described by Eq. (23).

$$\begin{bmatrix} \dot{\underline{x}}_1 \\ \dot{\underline{x}}_2 \\ \dot{\underline{x}}_3 \\ \dot{\underline{x}}_4 \\ \dot{\underline{e}}_1 \\ \dot{\underline{e}}_2 \\ \dot{\underline{e}}_3 \\ \dot{\underline{e}}_4 \end{bmatrix} = \left[\begin{array}{cccc:c} A_1 + B_1K_1 & & & & B_1K_1 \\ & A_2 & & & B_2K_1 \\ & & A_3 & & B_3K_1 \\ & & & A_4 & B_4K_1 \\ \hdashline & & 0 & & A - GC \end{array}\right] \begin{bmatrix} \underline{x}_1 \\ \underline{x}_2 \\ \underline{x}_3 \\ \underline{x}_4 \\ \underline{e}_1 \\ \underline{e}_2 \\ \underline{e}_3 \\ \underline{e}_4 \end{bmatrix} + \left[\begin{array}{c} B_1 \\ B_2 \\ B_3 \\ B_4 \\ \hdashline 0 \end{array}\right] \underline{r} \tag{23}$$

where

$$\underline{e} = \hat{\underline{x}} - \underline{x}$$

$$y = \begin{bmatrix} C_1 & C_2 & C_3 & C_4 & 0 & 0 & 0 & 0 \end{bmatrix} \begin{bmatrix} \underline{x}_1 \\ \underline{x}_2 \\ \underline{x}_3 \\ \underline{x}_4 \\ \underline{e}_1 \\ \underline{e}_2 \\ \underline{e}_3 \\ \underline{e}_4 \end{bmatrix} \quad (23) \text{ (Cont.)}$$

The closed-loop system poles are the poles of the following matrices.

$$\begin{bmatrix} A_1 + B_1 K_1 \end{bmatrix}$$

$$A_2,\ A_3,\ \text{and}\ A_4$$

$$\begin{bmatrix} A - GC \end{bmatrix}$$

If K and G are chosen by the methods described above, then these poles will all have negative real parts, and the overall system will be stable.

3.2.2 Baseline Design

The optimal regulator is used as a standard against which other controller architectures can be evaluated. The quantities of specific interest are as follows.

(1) The Regulator Weights R_1 and R_2. Numerical values for R_1 and R_2 are given in Appendix H. For purposes here, the specific values are less important than the fact that each subsequent controller option will use the same weightings.

(2) The Cost Matrix P. Numerical values for the elements of P are given in Table 3. Recall that the cost to null any state deviation $\underline{x}^0$ is given by $J = \underline{x}^{0T} P \underline{x}^0$. In Table 3 the costs are ordered to correspond to 11 displacements (modes 4, 5, 6, 7, 10, 11, 12, 13, 20, 21, 22), then 11 modal velocities.

(3) The Closed-Loop Poles. Figure 16 shows the open-loop locations of the A_1 poles. Under control action, these poles move to locations shown in Figure 17. The poles of A_2, A_3, and A_4 are not modified by the controller. The error poles of the observer are given by det [sI - A + GC] = 0. The matrix G was not calculated for the 88-state case for the following reasons.

(a) Computer limitations precluded assessing a 166-state closed-loop system.

(b) The cost matrix was assumed to be independent of the observer.

(c) The closed-loop system poles are available in closed form.

However, it is known that all the observer poles would be to the left of s = -6.

Time histories of the closed-loop full-state feedback response to a unit initial condition on each of the $\underline{x}_1$ states is shown in Figure 18. Plots of the corresponding open-loop response are given in Figure 19. (An oversight is that the solar mode 10 was not initialized as intended.)

3.2.3 Issues and Concerns

If an accurate plant model is available, optimal control theory is a very attractive design technique. The resulting controller is a

Table 3. Cost matrix P.

SOLUTION MATRIX "P" OF ALGEBRAIC RICCATI EQUATION

	1	2	3	4	5	6	7	8
1	1.716216500D+00	-1.291147112D-04	-1.411506776D-04	8.427545610D-03	0.0	-2.797714672D-03	-3.827266027D-03	1.406387163D-03
2	-1.291147112D-04	1.844829228D+00	-2.798151034D-04	1.123394670D-03	0.0	2.439929737D-05	7.897225140D-01	2.396263476D-03
3	-1.411506776D-04	-2.798151034D-04	1.651560674D+00	-1.292006659D+00	0.0	2.837423148D-04	-9.574061365D-03	-7.134399212D-01
4	8.427545610D-03	1.123394670D-03	-1.292006859D+00	2.872495935D+02	0.0	-3.709691705D-03	6.901121519D-02	-3.500643155D+01
5	0.0	0.0	0.0	0.0	0.0	3.244128927D-14	-2.037557825D-14	-7.423713480D-14
6	-2.797714672D-03	2.439929737D-05	2.837423148D-04	-3.709691705D-03	3.244128927D-14	7.314575073D+01	7.223355046D-04	-1.702703922D-03
7	-3.827266027D-03	7.697225140D-01	-9.574061365D-03	6.901121519D-02	-2.037557825D-14	7.223355046D-04	3.654520350D+01	6.827133591D-02
8	1.406387163D-03	2.396263476D-03	-7.134399212D-01	-3.500643155D+01	-7.423713480D-14	-1.702703922D-03	6.827133591D-02	5.400077117D+01
9	1.[illegible]D-02	1.134039400D-01	4.639490927D-02	-3.046252776D-02	1.542655176D-13	-8.043931380D-04	3.052137793D+00	-1.961171063D-01
10	3.573571409D-02	-2.340091400D-02	1.794481803D-01	-1.169934193D+01	1.124247161D-12	-2.035171594D-03	-4.334540935D-02	2.097283065D+00
11	2.121207945D-02	7.389726144D-04	4.476450940D-03	-3.098515290D-02	-2.204253259D-12	-3.613376207D-01	1.805213400D-03	-1.837657460D-02
12	5.023641834D-02	-1.363001359D-04	-1.523560230D-04	9.492929340D-03	4.524412026D-15	-2.987776415D-03	-4.129250760D-03	1.643643561D-03
13	-1.407184523D-04	1.877817640D-01	-3.101367630D-04	1.237037760D-03	-1.446570165D-15	2.690058136D-05	8.903415680D-01	2.669344687D-03
14	-1.537339054D-04	-3.095419916D-04	1.954772638D-01	-1.489923759D+00	4.435676399D-15	3.157970977D-04	-1.079092478D-02	-8.168246179D-01
15	-2.912892765D-04	6.291827171D-05	-1.199875950D-02	-2.997111649D-01	2.656950904D-14	1.762134101D-05	2.312853269D-03	2.106074164D+00
16	0.0	0.0	0.0	0.0	0.0	0.0	0.0	0.0
17	7.703702262D-05	-1.893232474D-07	-1.936475781D-06	-1.011594550D-05	3.520027279D-16	3.[illegible]56052900D-04	1.397655902D-06	6.641616257D-06
18	6.392630910D-05	-5.251559372D-03	2.192530453D-05	-1.187474653D-04	8.646867103D-16	-1.912471546D-05	-1.323790907D-02	-5.8[illegible]D-05
19	-4.421792263D-05	-3.319139459D-05	8.598725564D-03	-4.820564916D-01	-2.945169955D-15	1.159754150D-05	-5.160565175D-04	-6.495505400D-02
20	-2.551436626D-05	6.205503083D-04	-5.962663920D-05	-2.573157405D-04	2.415471349D-14	3.033330[illegible]D-07	2.552645420D-02	1.715170401D-03
21	-6.206424197D-05	2.963132795D-05	7.230704061D-04	-1.193557276D-02	2.639033195D-14	1.334602650D-06	8.241347244D-04	-3.695733650D-02
22	-1.458633463D-05	-1.605617431D-07	-9.263002497D-07	8.653004346D-07	9.362935787D-15	-7.112640563D-03	-1.549001054D-07	3.448093404D-07

9	10	11	12	13	14	15	16
1.299991390D-02	3.573571409D-02	2.121207945D-02	5.023641839D-02	-1.407184523D-04	-1.537339054D-04	-2.912892765D-04	0.0
1.134039400D-01	-2.340091910D-02	7.389726144D-04	-1.363001359D-04	1.877817640D-01	-3.095419916D-04	6.291827171D-05	0.0
4.639495927D-02	1.794481303D-01	4.476450940D-03	-1.523560230D-04	-3.101367630D-04	1.954772638D-01	-1.199875900D-02	0.0
-3.046252770D-02	-1.169934153D+01	-3.098515290D-02	9.492929340D-03	1.237037760D-03	-1.489923750D+00	-2.997111649D-01	0.0
1.542655176D-13	1.124247161D-12	[illegible]	4.52[illegible]D-15	-1.446570150D-15	4.43[illegible]D-15	2.[illegible]	0.0
-8.043931380D-04	-2.035171594D-03	-3.613376287D-01	-2.987776415D-03	2.690058136D-05	3.157970970D-04	1.762134101D-05	0.0
3.052137093D+00	-4.334540935D-02	1.805213406D-03	-4.129250760D-03	8.903415680D-01	-1.079092478D-02	2.312853269D-03	0.0
-1.961171065D-01	2.097283065D+00	-1.837657460D-02	1.643643561D-03	2.669944687D-03	-8.168246179D-01	2.106074164D+00	0.0
5.360357040D+02	-2.790675331D-02	8.160773760D-03	1.347249912D-02	1.160552023D-01	5.419354392D-02	-1.195027659D-02	0.0
-2.790675331D-02	5.391504611D+02	2.173191570D-02	3.699950912D-02	-2.602706375D-02	1.639381507D-01	1.210726145D+00	0.0
8.160773760D-03	2.173191576D-02	8.315590323D+03	2.186316664D-02	8.104252436D-04	4.910450051D-03	-5.129075010D-04	0.0
1.347249912D-02	3.699950912D-02	2.186316664D-02	5.173129580D-02	-1.492530633D-04	-1.657367260D-04	-2.760943770D-04	0.0
1.160552003D-01	-2.602706375D-02	8.104252036D-04	-1.492530633D-04	2.057609164D-01	-3.450079468D-04	6.742326674D-05	0.0
5.419354351D-02	1.639381507D-01	4.910450051D-03	-1.657367260D-04	-3.450079468D-04	2.145651120D-01	-1.635125516D-02	0.0
-1.195027659D-02	1.210726145D+00	-5.129075010D-04	-2.760943770D-04	6.742326674D-05	-1.635125516D-02	6.560037160D-01	0.0
0.0	0.0	0.0	0.0	0.0	0.0	0.0	0.0
2.256076564D-05	6.141904965D-05	2.608569334D-01	7.717142767D-05	-1.977916514D-07	-1.943400071D-0[illegible]	-6.751592970D-0[illegible]	-1.[illegible]D-17
-3.450211285D-01	-9.776791860D-03	6.677967474D-06	6.386110754D-05	-5.320552651D-03	1.901034[illegible]D-05	-3.022064951D-05	1.[illegible]D-16
-1.201669169D-02	3.030211090D-01	1.998201000D-04	-4.630305019D-05	-3.597629429D-05	9.274130459D-03	-4.347730767D-02	-5.[illegible]D-17
-5.313319740D-03	1.049297550D-04	-1.519154355D-05	-2.575693550D-05	6.950310640D-04	-6.470922103D-05	9.852083667D-05	-[illegible]D-16
3.311697234D-04	-9.615372351D-03	-2.170083410D-05	-6.245413370D-05	3.195423371D-05	8.199203030D-04	-2.967561630D-03	-3.[illegible]D-16
2.706209007D-06	6.679137316D-06	-1.193712150D-04	-1.467406095D-05	-1.697975360D-07	-9.361059302D-07	1.105935514D-0[illegible]	[illegible]

17	18	19	20	21	22
7.703702262D-05	6.395692912D-05	-4.421792263D-05	-2.551436626D-05	-6.20[illegible]D-05	-1.45[illegible]D-05
-1.893232474D-07	-5.251559372D-03	-3.319139459D-05	6.205503083D-04	2.963[illegible]D-05	-1.[illegible]D-07
-1.936475781D-06	2.19[illegible]D-05	8.597265564D-03	-5.962663920D-05	7.[illegible]D-04	-9.[illegible]
-1.011594550D-05	-1.187474653D-04	-4.820564916D-01	-2.573157405D-04	-1.[illegible]	8.6[illegible]
3.520027279D-16	8.64[illegible]D-16	-2.945169955D-15	2.415471349D-14	2.[illegible]D-14	9.[illegible]
3.[illegible]D-04	-1.[illegible]	1.1[illegible]D-05	3.0[illegible]D-07	1.33[illegible]	-7.[illegible]
-3.397655902D-06	-1.323790907D-02	-5.160565190D-04	2.552645420D-02	8.2[illegible]D-04	-1.5[illegible]
6.641616257D-06	-5.820[illegible]D-05	-6.495505400D-02	1.715170401D-03	-3.69[illegible]D-02	3.[illegible]
2.25[illegible]D-05	-3.450211[illegible]D-01	-1.201669169D-02	-5.313319740D-03	3.311[illegible]D-04	2.[illegible]
6.14[illegible]D-05	-9.77[illegible]D-03	3.030211090D-01	1.049297550D-04	-9.615[illegible]D-03	6.6[illegible]
2.60[illegible]D-01	6.677[illegible]D-06	1.998201000D-04	-1.519154354D-05	-2.170[illegible]D-05	-1.1[illegible]
7.717142767D-05	6.386110[illegible]D-05	-4.630305019D-05	-2.57[illegible]D-05	-6.245413[illegible]D-05	-1.4[illegible]
-1.977916514D-07	-5.320552651D-03	-3.597629429D-05	6.9[illegible]D-04	3.195[illegible]D-05	-1.69[illegible]
-1.94[illegible]D-06	1.9[illegible]D-05	9.274130459D-03	-6.470922103D-05	8.19[illegible]D-04	-9.[illegible]
-6.751592970D-07	-3.0[illegible]D-05	-4.347730737D-02	9.852083667D-05	-2.[illegible]D-03	1.1[illegible]
-1.[illegible]D-17	1.[illegible]D-16	-5.9[illegible]D-17	-2.333041199D-16	-3.[illegible]D-16	2.[illegible]
5.[illegible]D-02	2.[illegible]D-07	-2.[illegible]D-07	-1.1072165[illegible]D-06	-2.[illegible]	-2.[illegible]
[illegible]	[illegible]	1.163010630D-05	8.370635010D-04		
-2.[illegible]D-07	1.[illegible]D-05	2.507332267D-02	3.076635114D-05		
-1.[illegible]	[illegible]D-04	3.076635114D-05	2.433011401D-02		
[illegible]	2.[illegible]D-05	-7.164[illegible]D-04	1.001645127D-06		
-8.516[illegible]D-05	-5.[illegible]D-09	-6.171065701D-09	2.225751451D-08		

	REAL	IMAG
2	0.0	0.19687310795200-06
4	0.0	0.29535090725300-06
6	-0.1176609970790D+01	0.2350276575898D+02
8	-0.2007126491170D+01	0.4009232026051D+02
10	-0.7380120283550D+01	0.1474179470050D+03
12	-0.1090596025320D+02	0.2178463854387D+03
14	0.0	0.28e2622115420D-06
16	-0.1100791723045D+01	0.2193829744642D+02
18	-0.1831068375055D+01	0.3597631261500D+02
20	-0.2052281769380D+01	0.4099429523632D+02
22	-0.7380835478650D+01	0.1474332717192D+03

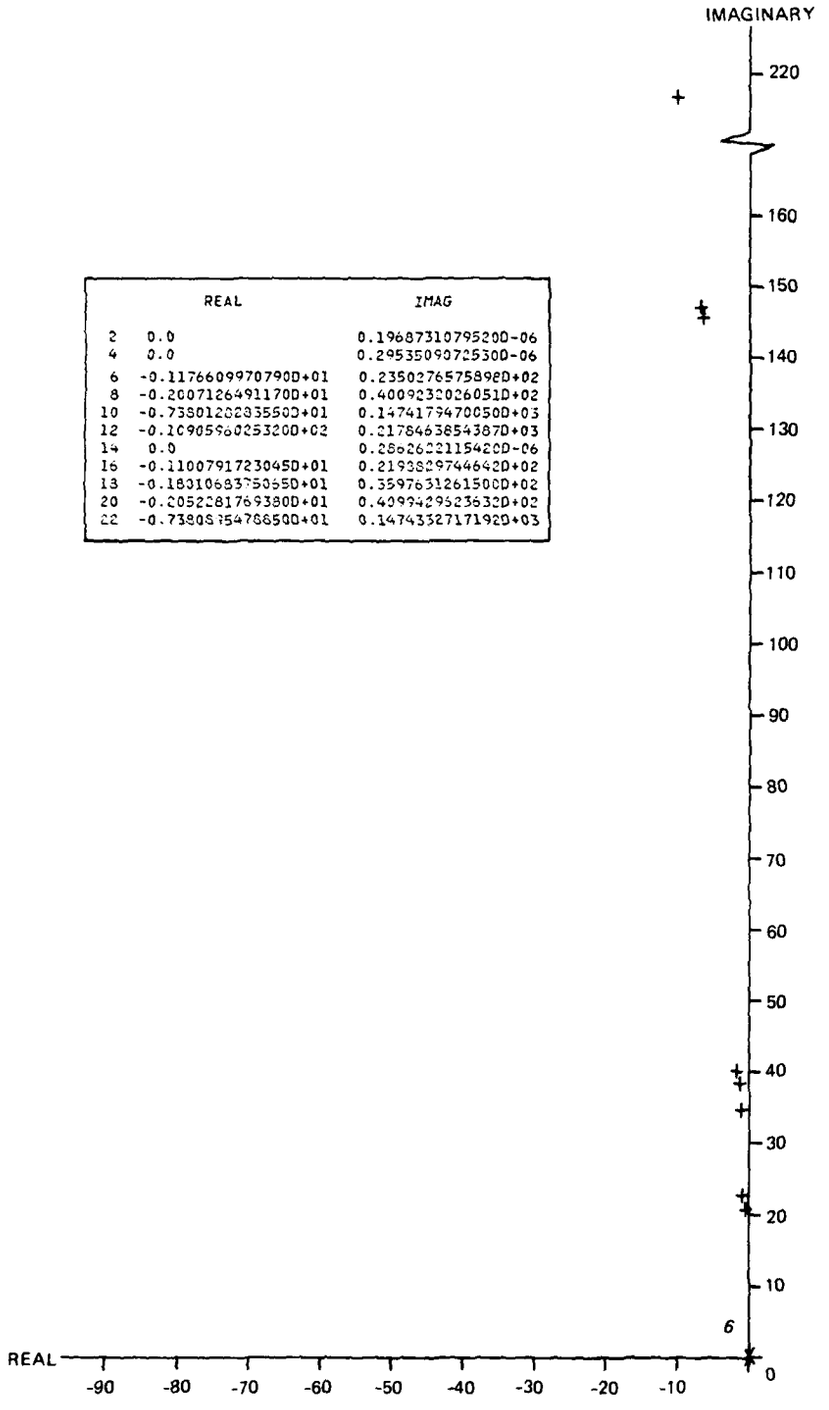

Figure 16. Poles of A_1.

	REAL	IMAG
2	-0.177048611286 5D+02	0.2173992784136D+03
4	-0.268887756371 6D+02	0.1450289392211D+03
6	-0.269005208761 5D+02	0.1450331562681D+03
7	-0.331339367568 4D+02	
9	-0.230083353877 1D+02	0.3228710821362D+02
11	-0.707603978398 9D+01	0.3532055367905D+02
13	-0.199228575139 7D+02	0.2955850046588D+02
15	-0.117660997079 0D+01	0.2350276575896D+02
17	-0.987962792408 9D+01	0.2253841623713D+02
18	-0.103625407287 2D+02	
19	-0.107437949514 5D+02	
20	-0.100045579153 3D+01	
21	-0.100494418180 7D+01	
22	-0.100491390944 1D+01	

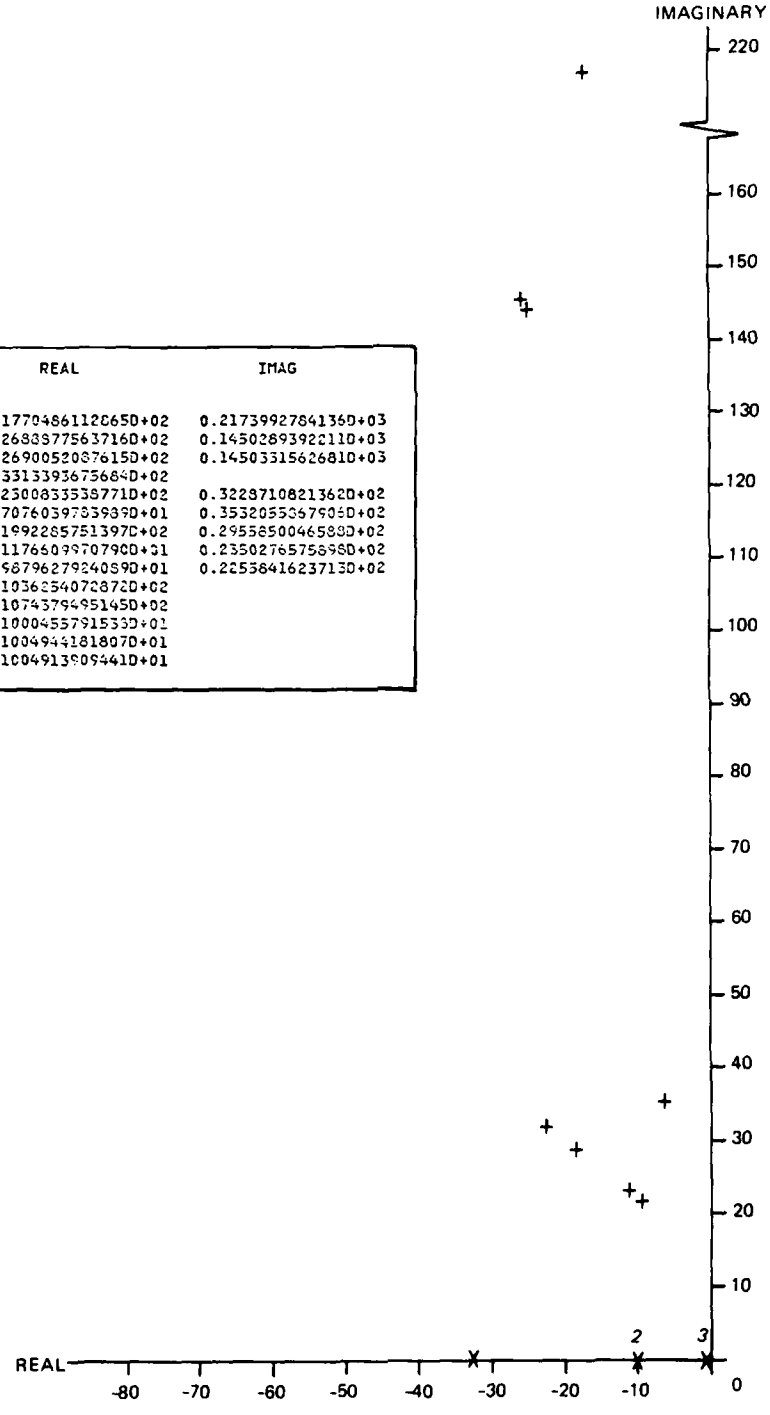

Figure 17. Optimal regulator: poles of $(A_1 + B_1K_1)$.

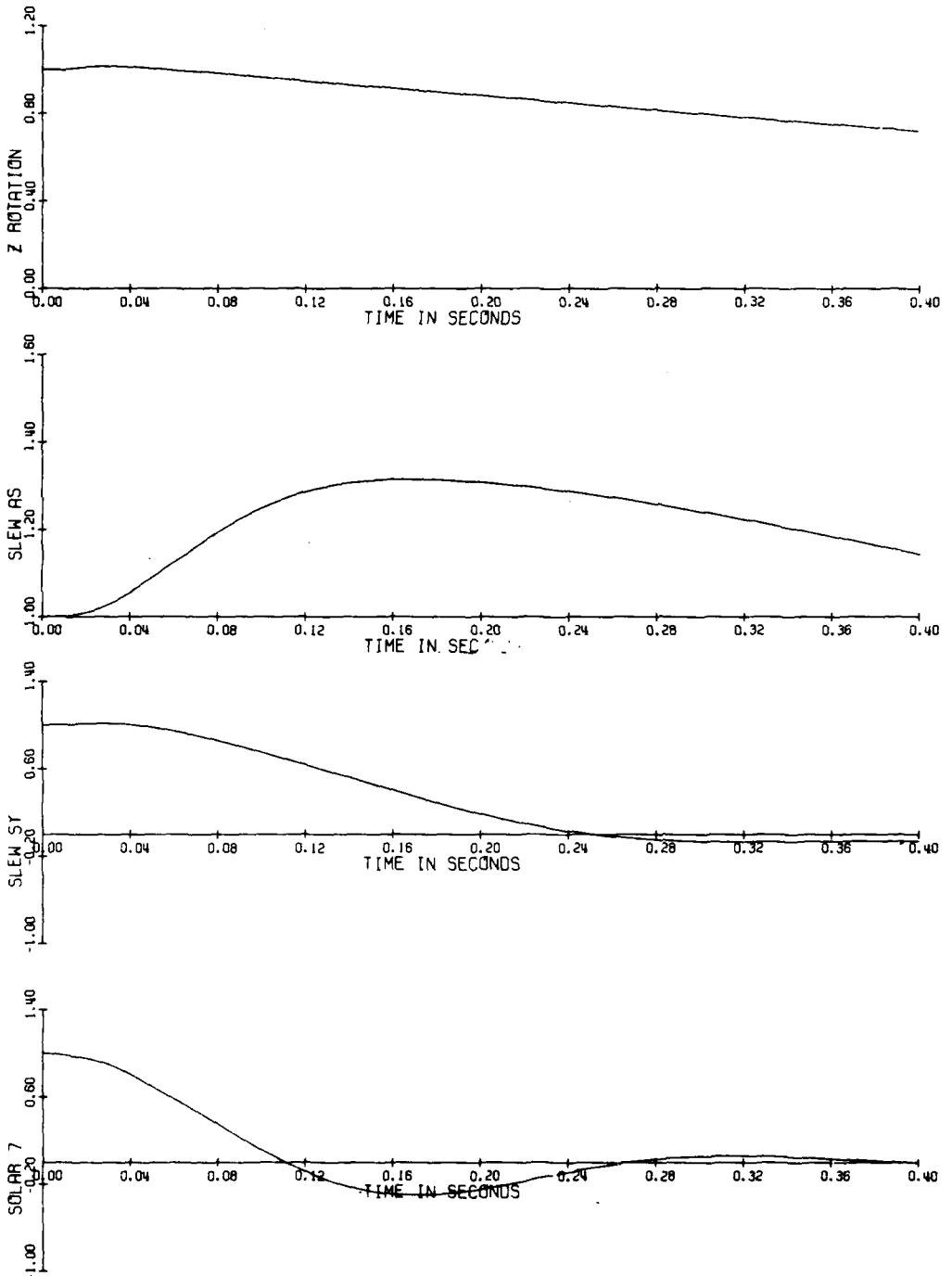

Figure 18. Full-state feedback response (sheet 1 of 6).

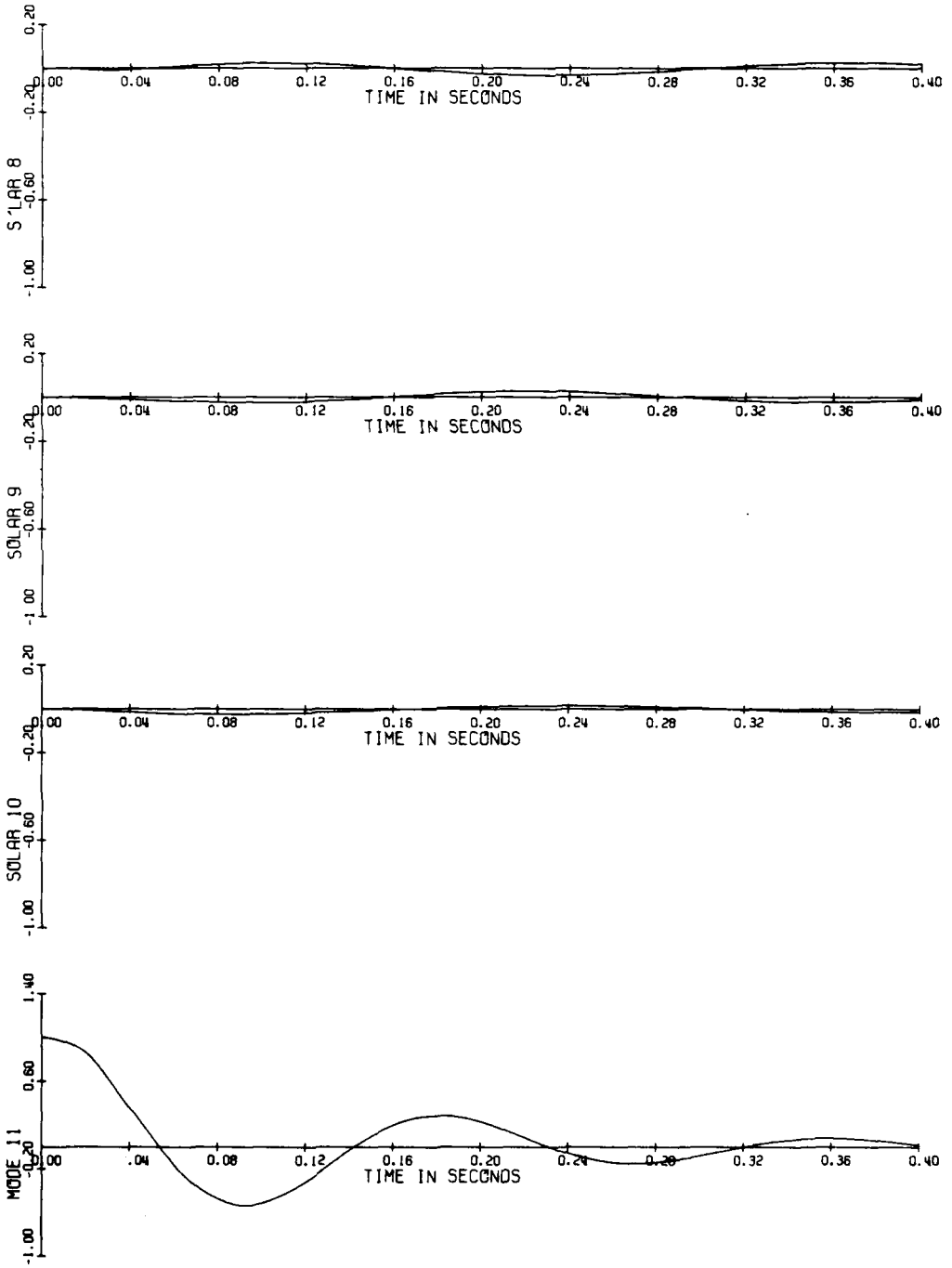

Figure 18. Full-state feedback response (sheet 2 of 6).

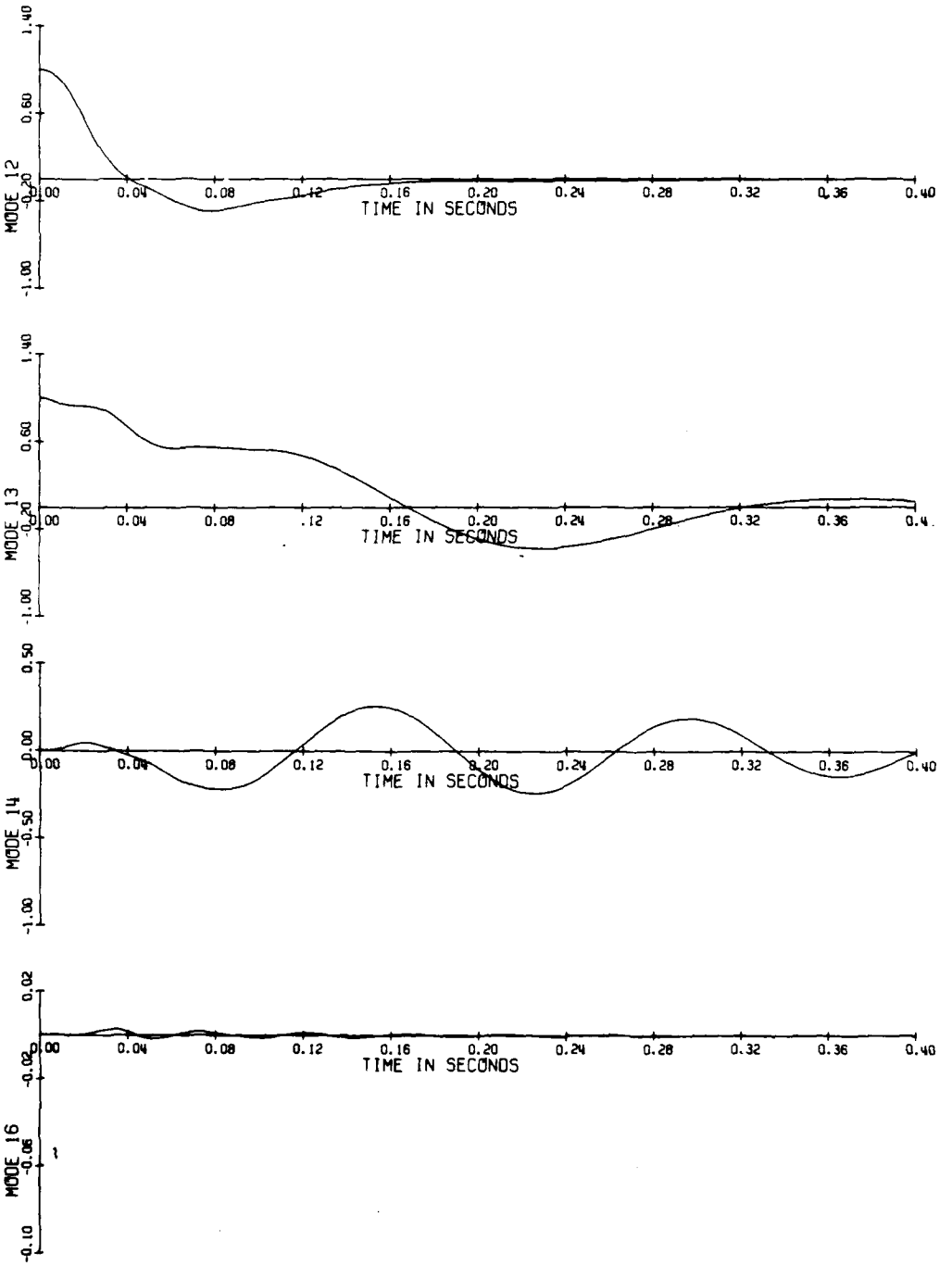

Figure 18. Full-state feedback response (sheet 3 of 6).

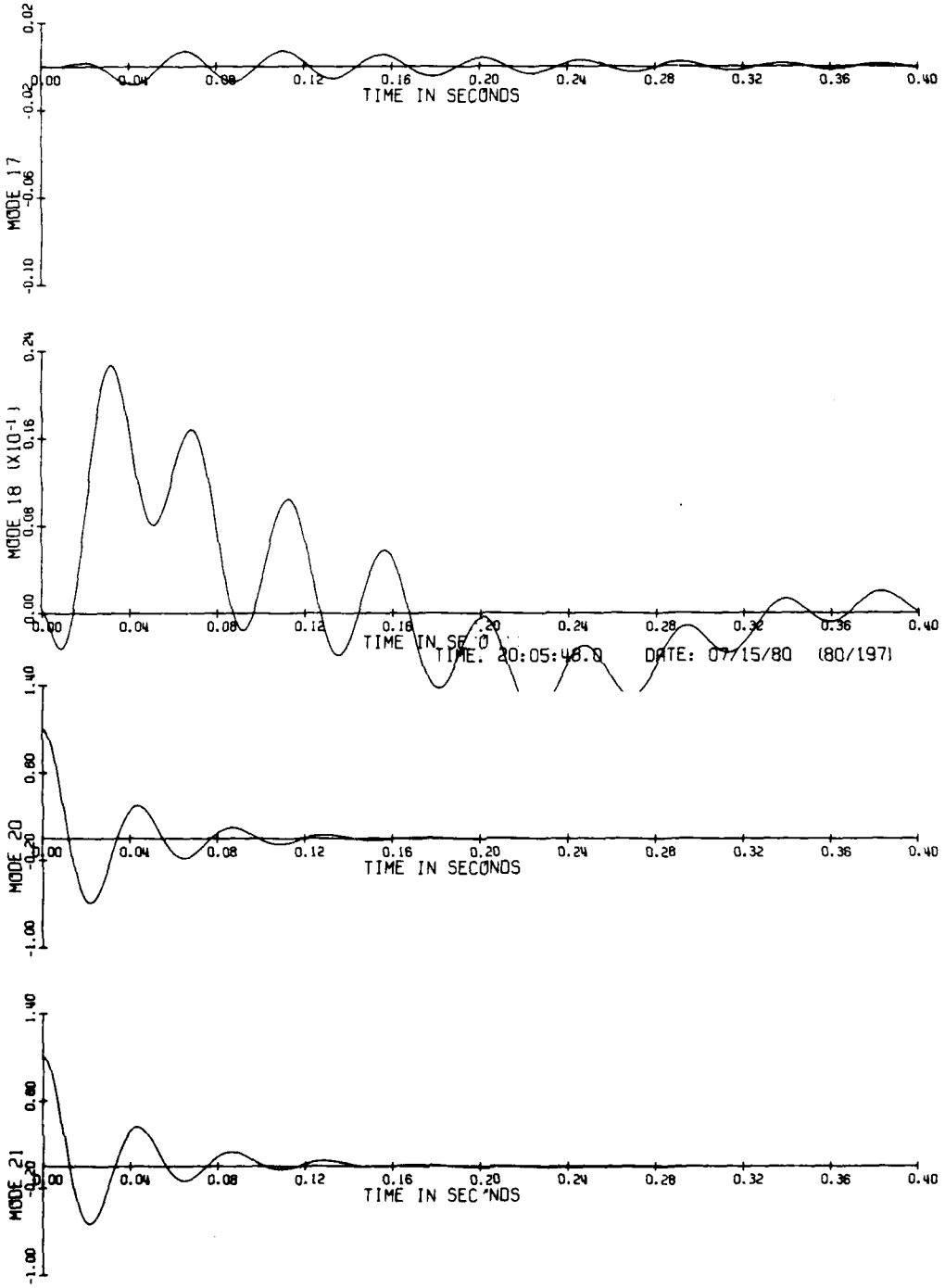

Figure 18. Full-state feedback response (sheet 4 of 6).

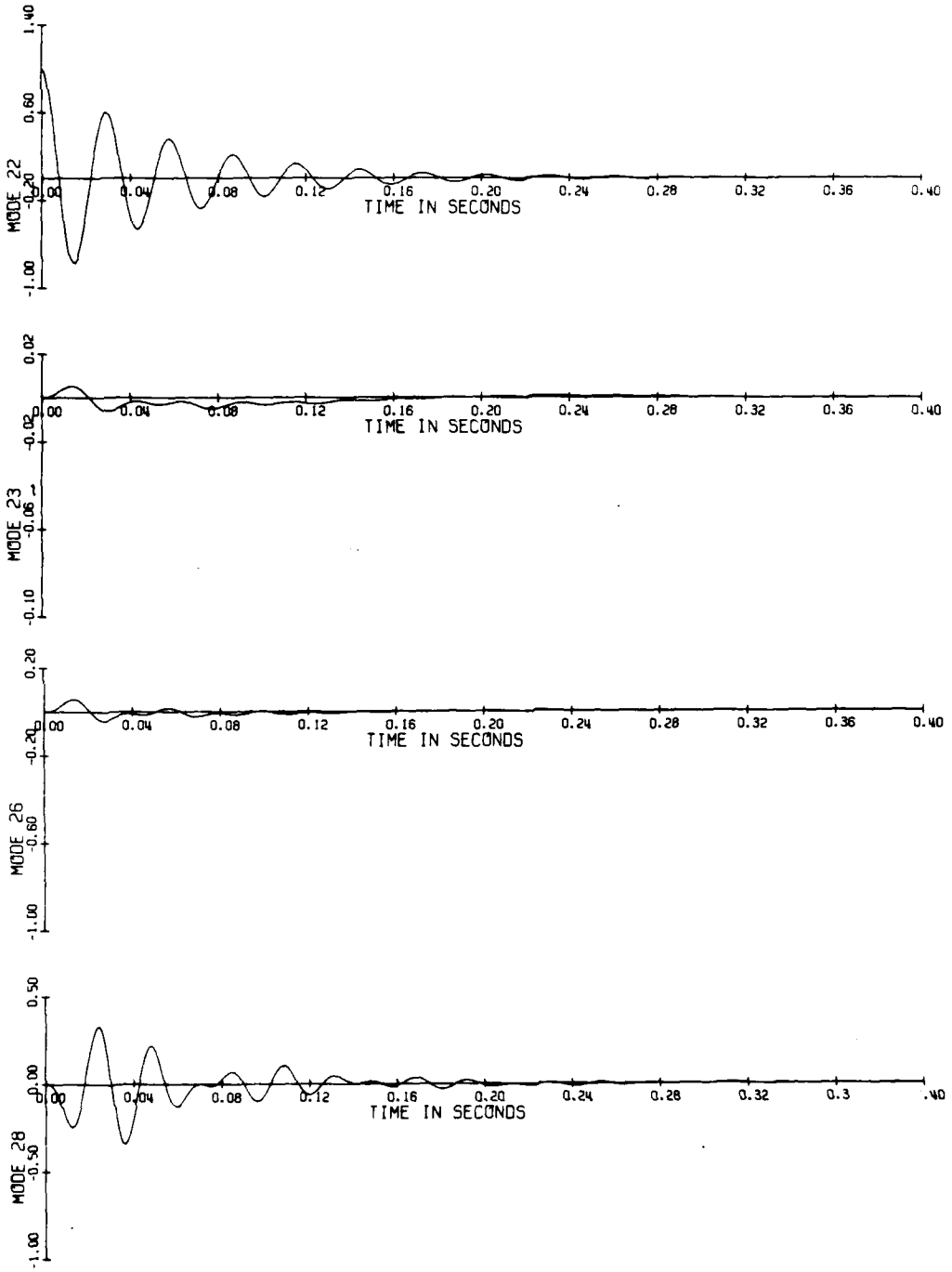

Figure 18. Full-state feedback response (sheet 5 of 6).

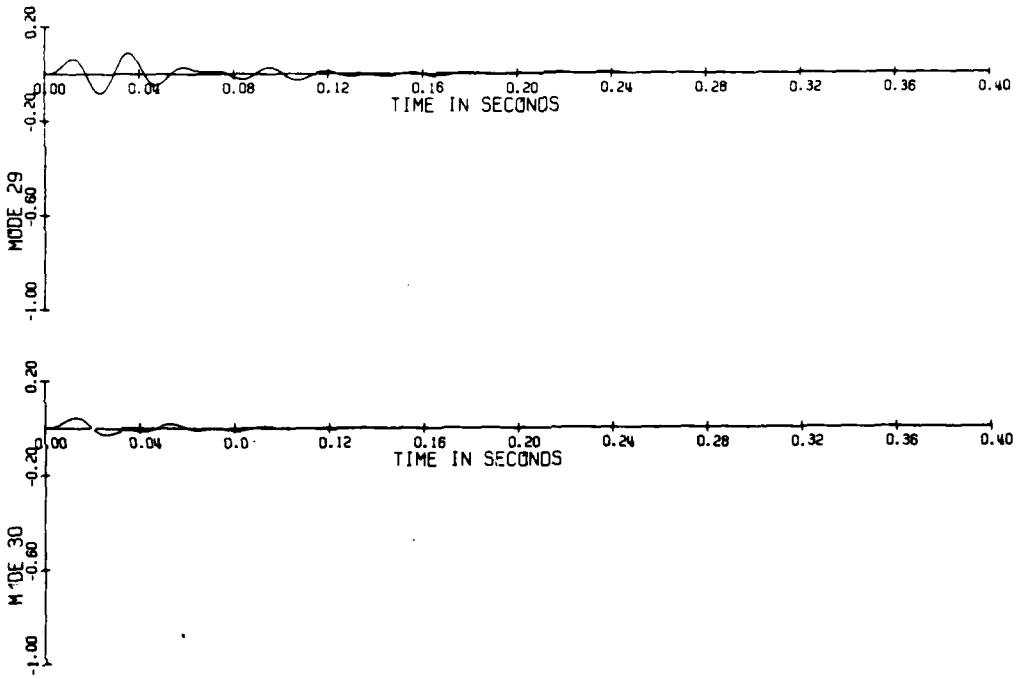

Figure 18. Full-state feedback response (sheet 6 of 6).

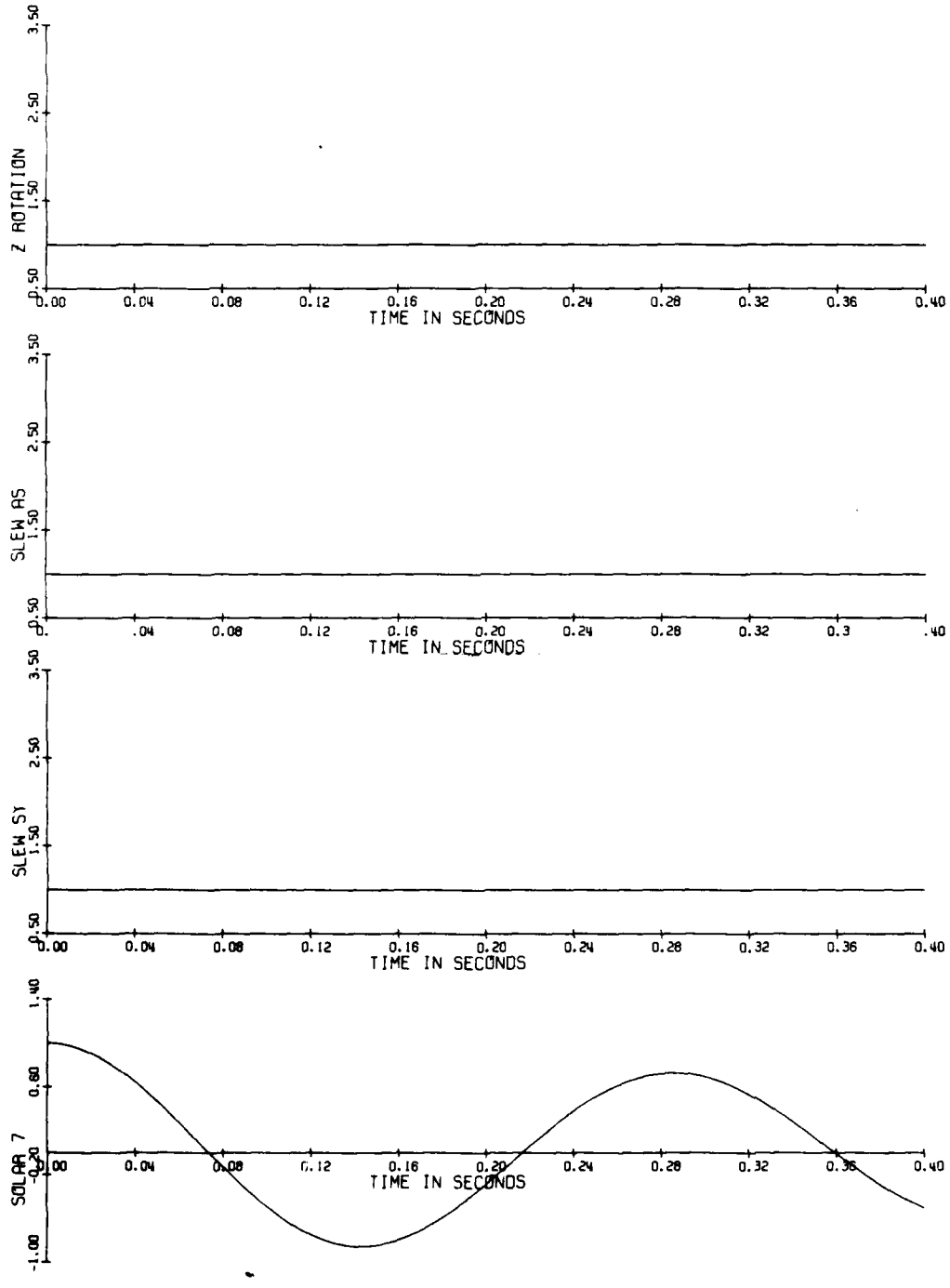

Figure 19. Open-loop feedback response (sheet 1 of 3).

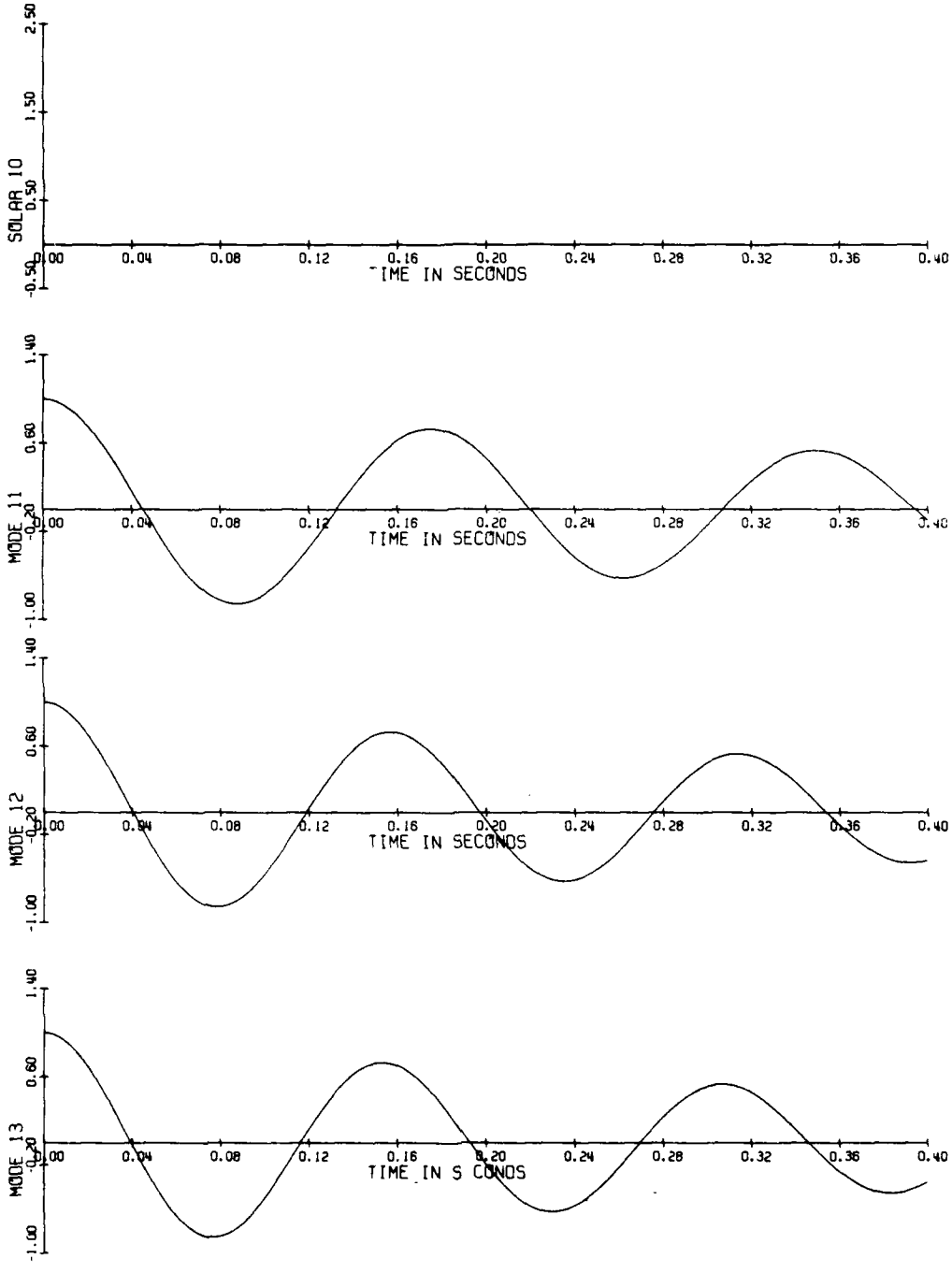

Figure 19. Open-loop feedback response (sheet 2 of 3).

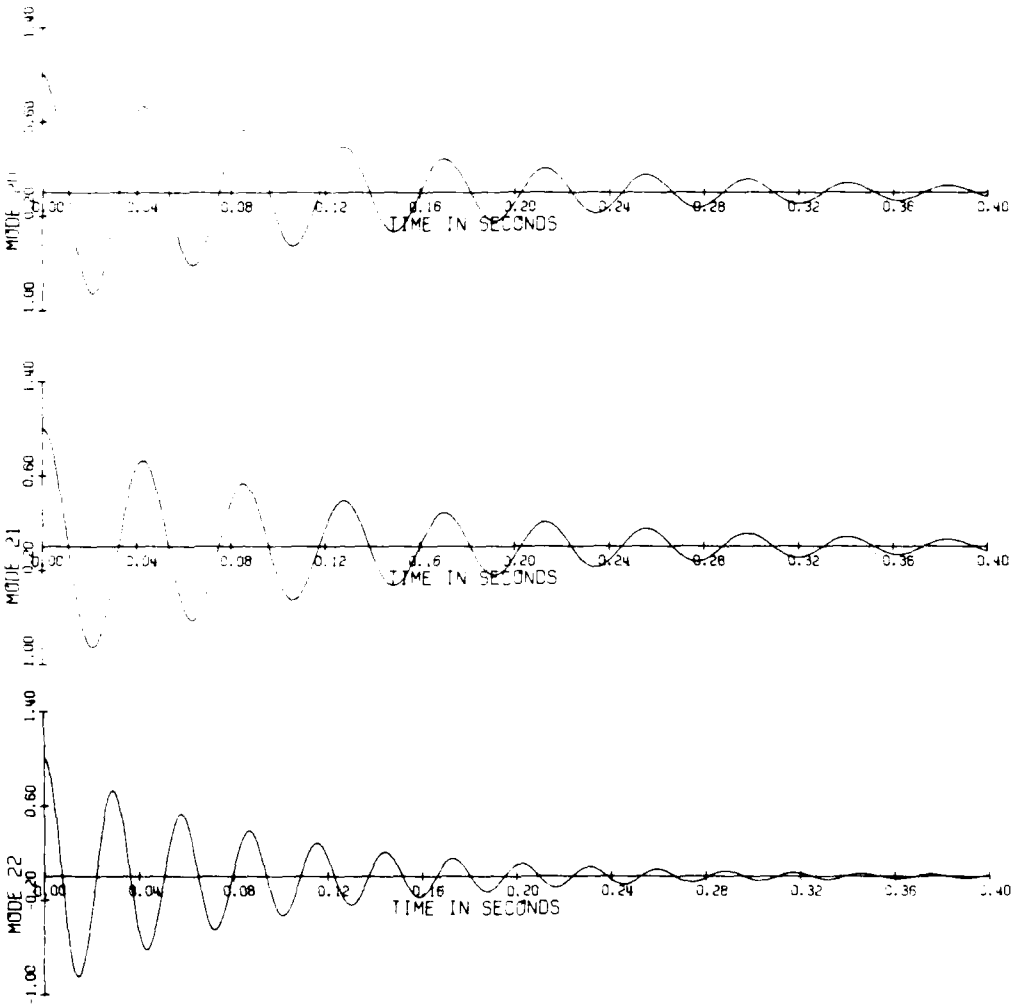

Figure 19. Open-loop feedback response (sheet 3 of 3).

cascade of steady-state regulator gains and a time-invariant asymptotic observer. If the initial observer error is zero, the controller minimizes the quadratic performance index

$$J = \int_{t_0}^{\infty} \underline{x}^T R_1 \underline{x} + \underline{u}^T R_2 \underline{u} \, dt \tag{24}$$

and has good stability margins. The design process itself is well defined, rigorous, noniterative in principle, and structured to treat the multiple-actuators/multiple-sensor plant. Despite its attractiveness, there are issues associated with implementing a regulator. This section identifies these issues and discusses them in the context of the M2V2 design.

3.2.3.1 Design Model

Regulator theory requires a finite dimension state space model as a departure point. There are two issues associated with constructing this model; the issues of discretization, and of model dimension. The validity of using a discrete model to represent a distributed parameter system is a concern. There are only two cases where a finite model can be rigorously justified.

(1) The zero spillover case where either B_5—the residual mode input distribution matrix, or C_5—the residual mode output matrix is equal to zero.

(2) The case of high-frequency residual modes.

In the first case, a truncated structural model is valid, and the controller will have the form

$$\begin{aligned} \underline{u} &= K\hat{\underline{x}} \\ \dot{\hat{\underline{x}}} &= A\hat{\underline{x}} + B\underline{u} + G[\underline{y} - C\hat{\underline{x}}] \end{aligned} \tag{25}$$

In the case of high-frequency residual modes, the dynamics of $\underline{x}_5$ may be neglected, and the $\underline{x}_5$ modes treated as dc. The coupling between controlled and residual modes is retained, but the dimension of the controller is reduced. This approach is motivated by singular perturbation theory (see Appendix E), and leads to a control law of the form

$$\begin{aligned} \underline{u} &= K\hat{\underline{x}} \\ \dot{\hat{\underline{x}}} &= A\hat{\underline{x}} + B\underline{u} + G(\underline{y} - \hat{\underline{y}}) \\ \hat{\underline{y}} &= C\hat{\underline{x}} + C_5 A_5^{-1} B_5 \underline{u} \end{aligned} \tag{26}$$

This controller design is similar to the case just shown, except the dc effect of $\underline{x}_5$ is subtracted from the system output before it drives the observer.

Neither Eq. (25) nor (26) will be valid in the general flexible-spacecraft case. Residual states are typically close in frequency to the controller bandwidth, and are both excited and observed. As mentioned in the introduction, the presence of residual modes greatly hinders the application of regulator theory to flexible-spacecraft control.

Having acknowledged the difficulties associated with residual modes and discretization, one also faces the problem of dimension. The 88-state model used in the Section 3.2.2 design is small from the structural point of view. It includes as an example only the first two axial modes and the first two bending modes. On the other hand, from the context of a spaceborne computer, it is very large. Theory demands that the observer have the same dimension as the plant model. However, the computational requirements associated with 88 coupled difference equations are significant in a limited-computer-resources environment. This practical consideration is a strong motive for reducing the order of the controller. An additional motive is the asymmetry between the dimension of the gain matrix, 16×22, and the dimension of the observer, 88. An observer of dimension 22 would be attractive.

3.2.3.2 Closed-Loop Performance

There are three performance requirements associated with the M2V2 controller design. Two of these requirements are directly reflected in the performance index.

(1) The increase in damping ratio to 10 percent for modes 7, 11, 12, 13, 20, 21, 22.

(2) The time constant of 1 radian/second for the rigid-body rotation modes 4, 5, 6.

As illustrated in Figure 17, these requirements are met. The third requirement

(3) Isolation of modes 23, 26, 28, 29, and 30 from controller action.

is not reflected in the performance index, and cannot be fulfilled by the optimal regulator (see Figure 18). The problem is caused by the term B_3K_1 in Eq. (23), a control spillover term. From a fundamental point of view, there is no mechanism in traditional regulator theory for decoupling modes from control influence.

3.2.3.3 Use of Spatial Information

The discussion here brings up a philosophic issue, in contrast to the implementation questions just presented. A structure can be modeled by a separable partial differential equation in space and time; both spatial and temperal characteristics are important. The regulator is based in the time domain, and when applied to a flexible structure, it controls modes by shaping the frequency content of the control signals. The philosophic question concerns the merit in shaping control in the spatial domain as well. It is hypothesized that a controller which blends spatial and temporal information may be attractive for this problem.

3.3 Alternate Control Architectures

Regulator theory provides a powerful methodology for the treatment of multiple-sensor/multiple-actuator, large-scale problems. However, the regulator designs are not completely satisfactory if the plant is a distributed parameter system like a spacecraft. As discussed in Section 3.2, deficiencies fall into two categories.

(1) Deficiencies associated with plant/model mismatch.

(2) Deficiencies occurring even if an accurate plant model is assumed.

This section begins by assuming that an accurate plant model exists. Within this context, options are explored which reduce the dimension of the controller and which allow some of the uncontrolled states to be isolated from controller excitation. The plant/model mismatch is then acknowledged, and the effects of residual modes are discussed.

3.3.1 Reduced-Order Observers

The baseline optimal control law has the form

$$u = K\hat{\underline{x}}_1 \tag{27}$$

where $\hat{\underline{x}}_1$ is a partition of $\hat{\underline{x}}$

$$\hat{\underline{x}} = \begin{bmatrix} \hat{\underline{x}}_1 \\ \hat{\underline{x}}_2 \\ \hat{\underline{x}}_3 \\ \hat{\underline{x}}_4 \end{bmatrix} \qquad \hat{\underline{x}}_1, \in R^{22}, \ \hat{\underline{x}}, \in R^{88} \tag{28}$$

and

$$\dot{\hat{\underline{x}}} = A\hat{\underline{x}} + B\underline{u} + G[\underline{y} - C\hat{\underline{x}}] \tag{29}$$

Equations (27) and (29) form the optimal controller. The intent of this section is to replace the 88-state dynamic observer (Eq. (29)) with an observer of lower order. There are two motivations for this. The first is practical in nature: to reduce the real-time computational burden. Propagating a 88-element state vector is expensive even on a mainframe computer. Performing a similar calculation within the computational and memory constraints of flight-qualified hardware may not be feasible. The second motivation is the asymmetry that exists between the observer, which uses 88 states to estimate $\underline{x}_1$, $\underline{x}_2$, $\underline{x}_3$, and $\underline{x}_4$, and the control law which only requires $\hat{\underline{x}}_1$ (dimension 22). It would be heuristically attractive to implement an observer of the same dimension as $\underline{x}_1$.

3.3.1.1 Alternate Designs

Three reduced-order observer designs are considered. The first design has the form

$$\dot{\hat{\underline{x}}}_1 = A_1\hat{\underline{x}}_1 + B_1\underline{u} + G[\underline{y} - C_1\hat{\underline{x}}_1] \tag{30}$$

G is picked using the method discussed in Section 3.2.1. The poles of $[A_1 - GC_1]$ are given in Figure 20. This observer is of dimension 22.

One intuitive concern regarding the first observer design is that the $\underline{x}_1$ and $\underline{x}_2$ states are interleaved in frequency (see Figure 15). It is heuristically difficult to neglect the $\underline{x}_2$ states. The second design, therefore, includes the $\underline{x}_2$ state dynamics in addition to the $\underline{x}_1$, and has the form

$$\begin{bmatrix} \dot{\hat{\underline{x}}}_1 \\ \dot{\hat{\underline{x}}}_2 \end{bmatrix} = \begin{bmatrix} A_1 & 0 \\ 0 & A_2 \end{bmatrix}\begin{bmatrix} \hat{\underline{x}}_1 \\ \hat{\underline{x}}_2 \end{bmatrix} + \begin{bmatrix} B_1 \\ B_2 \end{bmatrix}\underline{u} + G\left[\underline{y} - \begin{bmatrix} C_1 C_2 \end{bmatrix}\begin{bmatrix} \hat{\underline{x}}_1 \\ \hat{\underline{x}}_2 \end{bmatrix}\right] \tag{31}$$

	REAL	IMAG
2	-0.21787947110100+02	0.21733645832320+03
4	-0.14387263690250+02	0.14720206351560+03
6	-0.12505387062950+02	0.14728154923330+03
8	-0.10736340922340+02	0.40020814424940+02
10	-0.14310201568270+02	0.39991673154760+02
12	-0.11803578623060+02	0.35760071522930+02
14	-0.19179966548936D+02	0.24144957319710+02
16	-0.18442641125640+02	0.19260061072640+02
18	-0.12053988125330+02	0.77574067033470-01
20	-0.12036701917790+02	0.96622806004650-01
22	-0.12017719485370+02	0.16119793816160+00

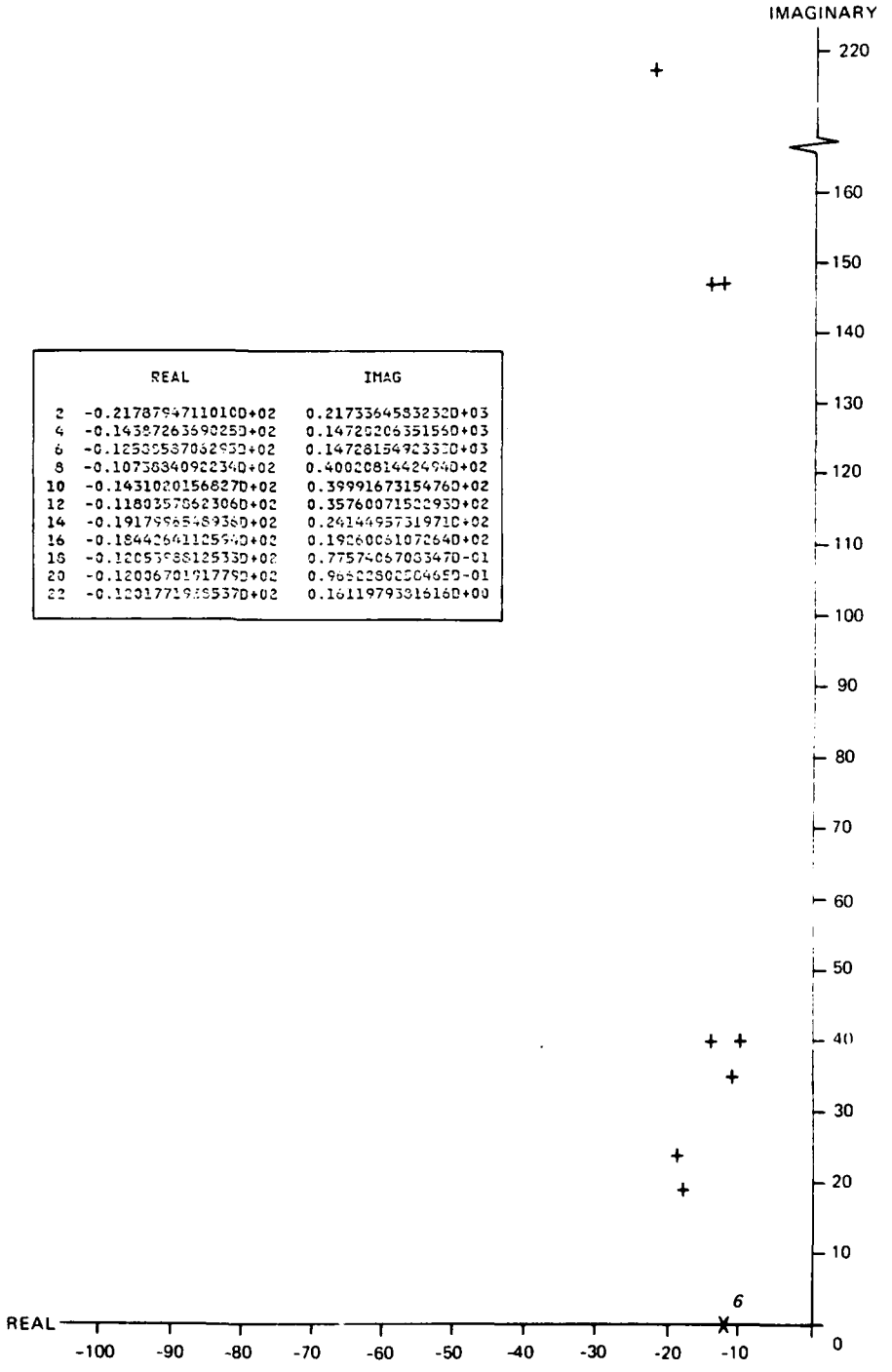

Figure 20. Observer 1: poles of $(A_1 - GC_1)$.

This design is of dimension 38. It is inefficient because it outputs unnecessary information [$\underline{x}_2$], but it is easier to justify than the previous design. The poles of

$$\left[\begin{bmatrix} A_1 & \\ & A_2 \end{bmatrix} - G[C_1 C_2] \right]$$

are given in Figure 21.

The third observer option relies on only $\underline{x}_1$ dynamic information, and has dimension 22. It is similar in structure to the first observer, but instead of using the system output to drive the estimator, it uses a singular transformation of the output. Specifically, an output transform, T_3, is introduced, where T_3 satisfies the following conditions

$$\begin{aligned} T_3 C_1 &\neq 0 \\ T_3 C_2 &= 0 \\ T_3 C_3 &= 0 \end{aligned} \tag{32}$$

The details of calculating T_3 are discussed in Appendix H. Then, an observer of the form

$$\dot{\hat{\underline{x}}}_1 = A_1 \hat{\underline{x}}_1 + B_1 \underline{u} + G T_3 [\underline{y} - C_1 \hat{\underline{x}}_1] \tag{33}$$

can be constructed. The gain matrix G is based on [A_1, $T_3 C_1$]. The poles of [$A_1 - G T_3 C_1$] are given in Figure 22. The transform T_3 affects the dimension and orientation of the unobservable subspace. If Eq. (32) is satisfied, then both $\underline{x}_2$ and $\underline{x}_3$ are unobservable. T_3 depends explicitly on spatial information. Recall that the columns of C are the mode shapes evaluated at the sensor locations.

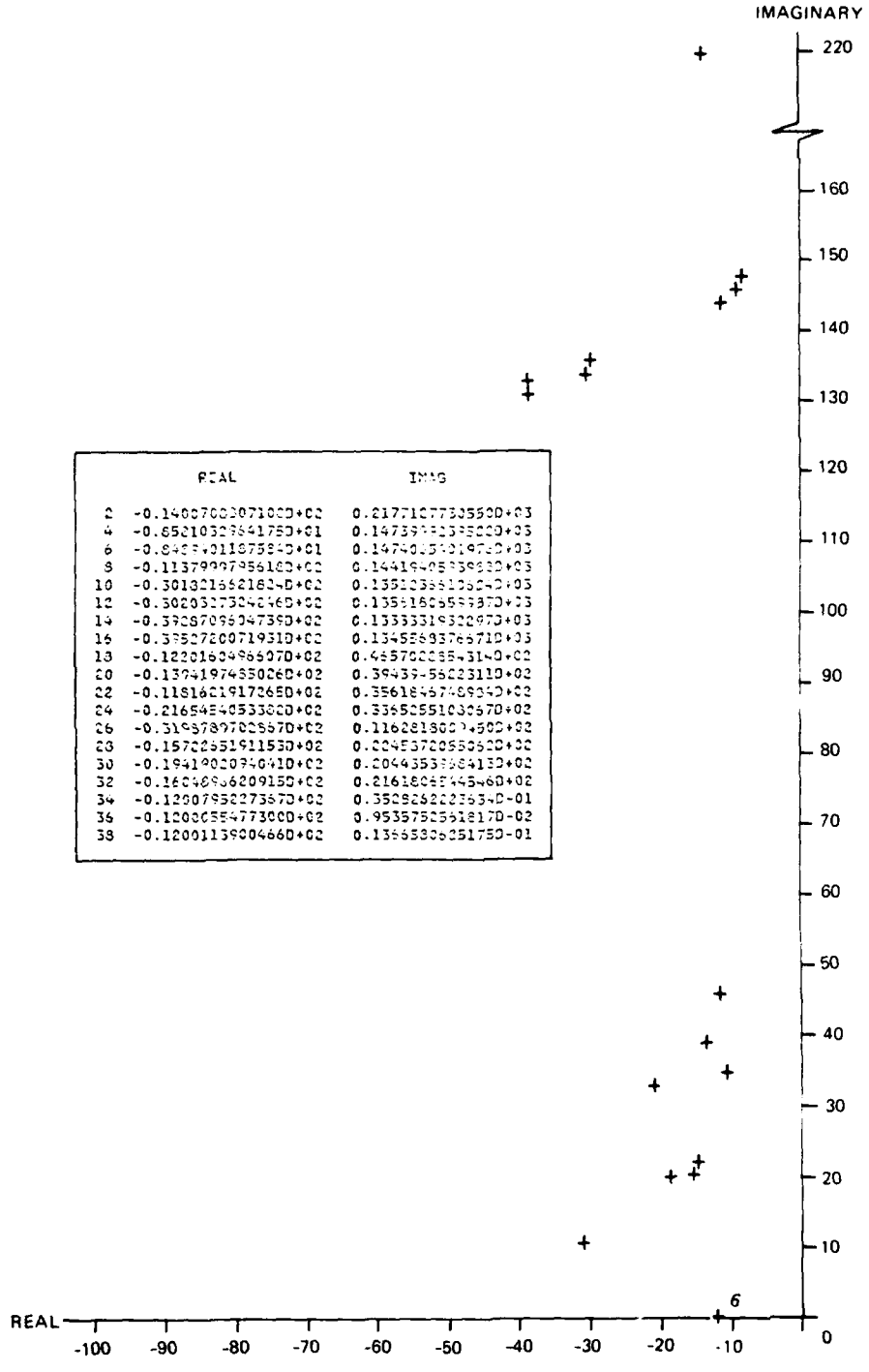

	REAL	IMAG
2	-0.1400700307100D+02	0.2177107733550D+03
4	-0.6521032864175D+01	0.1473994[illegible]
6	-0.8[illegible]	0.1474[illegible]
8	-0.1137999795618D+02	0.1441940[illegible]
10	-0.3013216621624D+02	0.1352236[illegible]
12	-0.3020327324246D+02	0.1356160[illegible]
14	-0.3928709604739D+02	0.1333331[illegible]
16	-0.3952720071931D+02	0.1345569[illegible]
18	-0.1220162496607D+02	0.4457022[illegible]
20	-0.1374197485026D+02	0.3943[illegible]
22	-0.1181621917265D+02	0.3561[illegible]
24	-0.2165424053382D+02	0.3365[illegible]
26	-0.3198787026567D+02	0.1162[illegible]
28	-0.1572265191153D+02	0.2245[illegible]
30	-0.1941902094041D+02	0.2044[illegible]
32	-0.1604896209150+02	0.2161[illegible]
34	-0.1290795227367D+02	0.3529[illegible]
36	-0.1200655477300D+02	0.9535[illegible]
38	-0.1200113900466D+02	0.1366[illegible]

Figure 21. Poles of 38-state observer.

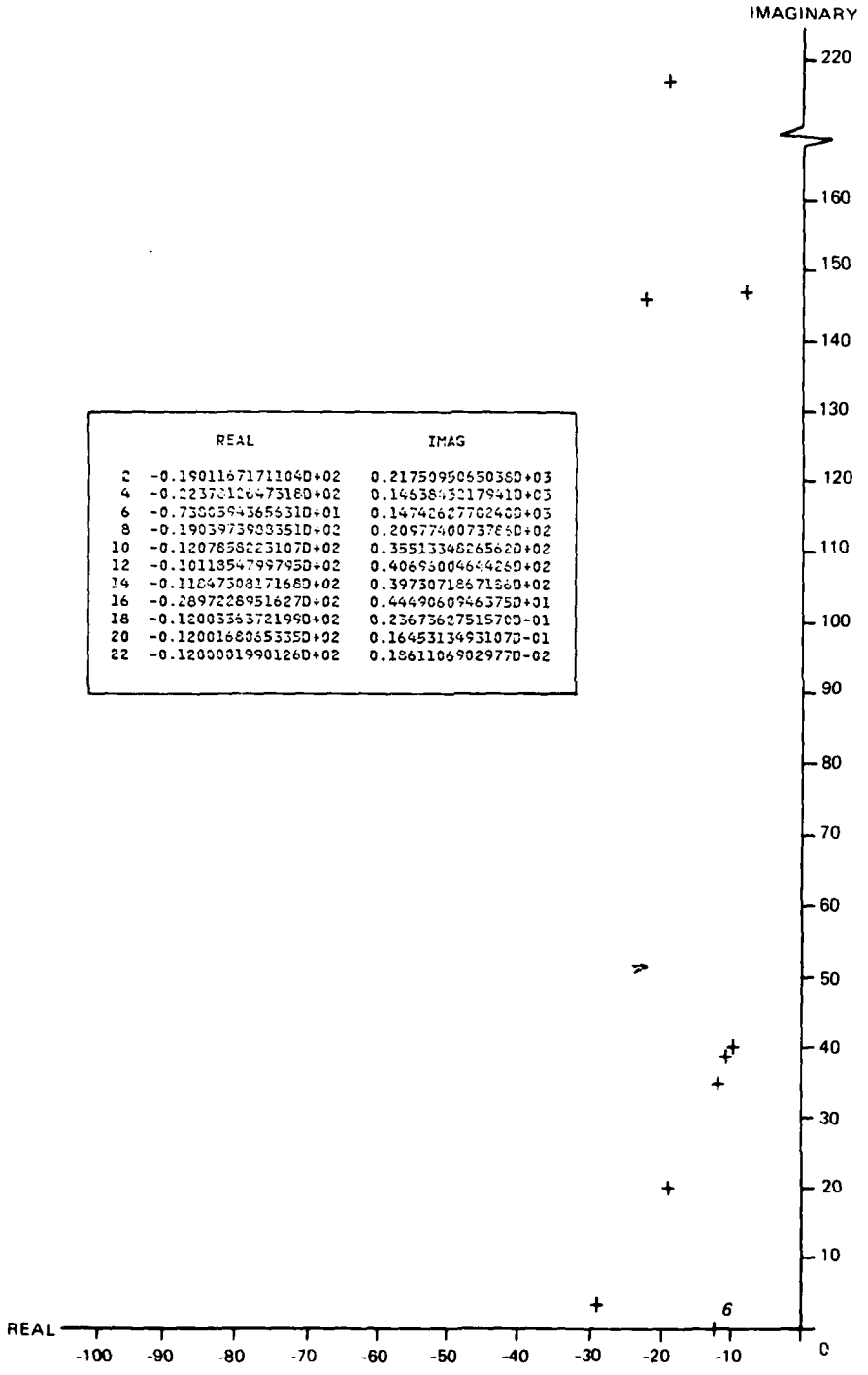

	REAL	IMAG
2	-0.1901167171104D+02	0.2175095065036D+03
4	-0.2237812647318D+02	0.1463843217941D+03
6	-0.7306394365631D+01	0.1474262770240D+03
8	-0.1903973933351D+02	0.2097740073766D+02
10	-0.1207858223107D+02	0.3551334826562D+02
12	-0.1011854799795D+02	0.4069600464426D+02
14	-0.1184730817168D+02	0.3973071867186D+02
16	-0.2897228951627D+02	0.4449060946375D+01
18	-0.1200336372199D+02	0.2367362751570D-01
20	-0.1200168065335D+02	0.1645313493107D-01
22	-0.1200001990126D+02	0.1861106902977D-02

Figure 22. Observer 3: poles of $[A_1 - GT_3C_1]$.

3.3.1.2 Closed-Loop Assessment

The three candidate reduced-order observers have similar error dynamics if evaluated against their design models. When evaluated against a higher dimension plant model the similarity disappears. This subsection presents the closed-loop performance. The evaluation plant model consists of the $\underline{x}_1$ and $\underline{x}_2$ states, and 22 of the $\underline{x}_3$ states. This model is dictated by a dimension constraint on available eigenvalue routines. The plant model is kept constant for all three evaluations. In addition, the same gain matrix (the optimal gains K_1) are used. Tables 4, 5, and 6 summarize the closed-loop transfer functions between a slew command and a slew response for three observer candidates.

3.3.1.3 Discussion

The observer based on only $\underline{x}_1$ information is not satisfactory. The observer poles and the unmodeled plant poles interact

$$\begin{bmatrix} \dot{\underline{x}}_1 \\ \dot{\underline{x}}_2 \\ \dot{\underline{x}}_3 \\ \dot{\underline{e}} \end{bmatrix} = \begin{bmatrix} A_1 + B_1K_1 & 0 & 0 & B_1K_1 \\ B_2K_1 & A_2 & 0 & B_2K_1 \\ B_3K_1 & 0 & A_3 & B_3K_1 \\ 0 & GC_2 & GC_3 & A_1 - GC_1 \end{bmatrix} \begin{bmatrix} \underline{x}_1 \\ \underline{x}_2 \\ \underline{x}_3 \\ \underline{e} \end{bmatrix} \tag{34}$$

and the closed-loop system is unstable. This is a demonstration of the adverse effects of spillover.

If the dimension of the observer design model is increased, and the $\underline{x}_2$ dynamics are included, then the observer will estimate $\underline{x}_2$ and use this estimate to reduce observation spillover. Nevertheless, there is still interaction between the observer poles and the unmodeled plant poles

Table 4. Closed-loop transfer characteristics, slew command to slew response for observer 1 (sheet 1 of 2). (In this case the evaluation model consists of the $\underline{x}_1$, $\underline{x}_2$ and $\underline{x}_3$ states.)

----------UNIQUE POLES----------

S-PLANE

NUMBER	REAL	IMAG	DAMPING	FREQUENCY
1	-1.015530			
2	-1.007584			
3	-6.814196			
5	-7.453760	3.047229	9.256356E-01	8.052586E+00
6	-11.047015			
7	-13.390049			
9	-11.449656	7.825401	8.255953E-01	1.386836E+01
10	-21.405136			
12	-18.791641	18.710480	7.086354E-01	2.651807E+01
14	-9.357993	22.301987	3.869218E-01	2.418575E+01
16	0.679920	24.189636	-2.809681E-02	2.419919E+01
18	0.476190	23.614639	-2.016094E-02	2.361943E+01
20	-19.227478	24.109787	6.235011E-01	3.083792E+01
22	-13.936120	36.655167	3.553773E-01	3.921500E+01
24	-10.019306	40.462021	2.403629E-01	4.168407E+01
26	-21.695465	36.450302	5.114639E-01	4.241837E+01
28	-25.753845	33.289597	6.118947E-01	4.209868E+01
30	-2.532052	46.953949	5.384804E-02	4.702217E+01
32	-7.124103	137.467911	5.175430E-02	1.376524E+02
34	-6.972634	137.211060	5.075137E-02	1.373881E+02
36	-7.953462	138.302078	5.741305E-02	1.385306E+02
38	-14.703921	147.527267	9.917778E-02	1.482592E+02
40	-12.433351	148.072800	8.367336E-02	1.485939E+02
42	-25.039124	142.899231	1.725927E-01	1.450763E+02
44	-26.576904	141.798431	1.842195E-01	1.442675E+02
46	-13.021539	259.915771	5.003633E-02	2.602417E+02
48	-15.169055	298.099609	5.082010E-02	2.984854E+02
50	-15.083717	296.345459	5.083331E-02	2.967290E+02
52	-16.141846	322.261230	5.002663E-02	3.226650E+02
54	-18.708339	373.757368	4.999231E-02	3.742535E+02
56	-18.916077	376.039551	5.023991E-02	3.765149E+02
58	-22.890915	457.258545	4.999860E-02	4.578311E+02

THE FOLLOWING POLES MATCHED ZEROS AND WERE ELIMINATED IN ABOVE LISTS

NUMBER	REAL	IMAGINARY
1	-1.0003605	
3	-1.1766090	23.5027618
4	-32.5592194	
6	-14.5011158	32.9516602
8	-5.9662685	37.1050110
10	-19.4964905	140.990448
12	4.6008644	139.271133
14	-19.9740753	215.519897
16	-18.2264557	218.800003
18	-13.5907898	268.270752
20	-14.9602709	298.845459
22	-15.7036667	305.726074
24	-15.4683867	310.114990
26	-18.7397308	375.975830
28	-18.6756439	372.778809
30	-19.7651672	394.580322
32	-20.4223973	408.166504
34	-22.2779388	444.873291
36	-22.4438934	448.315186

Table 4. Closed-loop transfer characteristics, slew command to slew response for observer 1 (sheet 2 of 2).

----------UNIQUE ZEROS----------

1	-1.012992			
3	-6.951283	3.413284	8.976250E-01	7.744083E+00
4	-11.046655			
6	-0.516858	8.206378	6.285793E-02	8.222638E+00
7	-13.390564			
9	-7.476950	11.432682	5.473383E-01	1.366056E+01
10	-22.202805			
12	-3.598394	22.017761	1.612917E-01	2.230986E+01
14	-0.486787	23.537735	2.067671E-02	2.354277E+01
16	0.679912	24.189636	-2.809649E-02	2.419919E+01
18	-19.227661	24.109207	6.235138E-01	3.083759E+01
20	-31.977722	19.621918	8.523321E-01	3.751791E+01
22	-11.242344	39.843384	2.715601E-01	4.139909E+01
24	-23.912643	33.227295	5.841275E-01	4.093736E+01
26	-2.532063	46.953964	5.384625E-02	4.702219E+01
28	-33.452271	40.679688	6.351567E-01	5.266774E+01
30	-7.003776	137.681641	5.080367E-02	1.378596E+02
32	-6.970445	137.211792	5.073520E-02	1.373887E+02
34	-4.729492	134.574463	3.512037E-02	1.346575E+02
36	-9.327847	147.548218	6.309301E-02	1.478428E+02
38	-12.510166	148.133362	8.415246E-02	1.486607E+02
40	-26.663437	141.809052	1.847855E-01	1.442939E+02
42	-33.193481	142.878082	2.262937E-01	1.466830E+02
44	-12.814193	257.944580	4.961689E-02	2.582627E+02
46	-15.117949	297.697266	5.071762E-02	2.980808E+02
48	-15.019808	296.079834	5.066378E-02	2.954604E+02
50	-14.401913	310.535400	4.632789E-02	3.108691E+02
52	-15.951144	335.117920	4.754477E-02	3.354973E+02
54	-18.703232	373.776611	4.997602E-02	3.742441E+02
56	-20.666031	423.620361	4.872638E-02	4.241240E+02

THE FOLLOWING ZEROS MATCHED POLES AND WERE ELIMINATED IN THE ABOVE LISTS

1	-1.0003605	
3	-1.1766090	23.5027618
5	-14.5011034	32.9516602
6	-32.5591888	
8	-5.9662676	37.1050110
10	4.6008844	139.271133
12	-19.4964905	140.990448
14	-19.9740753	215.519897
16	-18.2264557	218.800003
18	-13.5907898	268.270752
20	-14.9602709	298.845459
22	-15.7036667	305.726074
24	-15.4683867	310.114990
26	-18.6756439	372.778809
28	-18.7397308	375.975830
30	-19.7651672	394.580322
32	-20.4228973	408.166504
34	-22.2779388	444.873291
36	-22.4438934	448.315186

Table 5. Closed-loop transfer characteristics, slew command to slew response for observer 2 (sheet 1 of 2).

----------UNIQUE POLES----------

NUMBER	S-PLANE REAL	IMAG	DAMPING	FREQUENCY
1	-0.987259			
2	-1.069546			
3	-1.000226			
4	-11.659215			
6	-11.079893	0.694201	9.980430E-01	1.110162E+01
7	-12.376805			
9	-13.033106	1.044375	9.968048E-01	1.307488E+01
10	-6.282499			
11	-22.712341			
13	-19.417023	20.433807	6.888410E-01	2.818796E+01
15	-16.052307	21.669006	5.952561E-01	2.696706E+01
17	-15.698311	22.468597	5.727350E-01	2.740938E+01
19	-18.631088	23.348709	6.237172E-01	2.987105E+01
21	-1.137619	22.723938	5.000000E-02	2.275238E+01
23	-1.083267	23.482864	4.608113E-02	2.350783E+01
25	0.089596	22.793396	-3.930740E-03	2.279356E+01
27	-31.485703	11.935660	9.350682E-01	3.367209E+01
29	-16.756836	31.924820	4.647536E-01	3.605531E+01
31	-24.839035	30.254044	6.345487E-01	3.914441E+01
33	-11.940179	35.966766	3.150699E-01	3.789691E+01
35	-14.202227	39.408997	3.390362E-01	4.189000E+01
37	-1.926232	35.892975	5.358888E-02	3.594463E+01
38	-41.888321			
40	-31.986328	33.282425	6.929286E-01	4.616107E+01
42	-8.727573	46.181061	1.856989E-01	4.699852E+01
44	-8.506873	147.394333	5.761918E-02	1.476396E+02
46	-8.484466	147.412018	5.746103E-02	1.476560E+02
48	-7.380895	147.433258	5.000000E-02	1.476179E+02
50	-7.380128	147.417938	5.000000E-02	1.476026E+02
52	-6.895615	137.739792	5.000000E-02	1.379123E+02
54	-6.952700	138.680066	5.000000E-02	1.390540E+02
56	-30.203094	135.619827	2.173787E-01	1.389423E+02
58	-30.183334	135.125336	2.180005E-01	1.384554E+02
60	-39.497787	134.564545	2.816411E-01	1.402415E+02
62	-39.287430	133.329102	2.826496E-01	1.389969E+02
63	-105.252670			
64	67.066559			
66	-13.012999	259.891602	5.000825E-02	2.602170E+02
68	-14.786859	295.269775	5.001649E-02	2.956396E+02
70	-14.952042	297.097412	5.026346E-02	2.974734E+02
72	-13.806489	304.784668	4.525276E-02	3.050972E+02
74	-16.129684	322.229492	4.999394E-02	3.226326E+02
76	-18.707413	373.761719	4.998915E-02	3.742295E+02
78	-18.694656	372.771729	5.008746E-02	3.732402E+02
80	-19.345840	375.963623	5.138870E-02	3.764609E+02

THE FOLLOWING POLES MATCHED ZEROS AND WERE ELIMINATED IN ABOVE LISTS

NUMBER	REAL	IMAGINARY
2	-7.3352070	146.520645
4	-11.3795204	144.194107
6	-6.8707819	137.243759
8	-6.7724915	135.280411
10	-14.0057030	217.711624
12	-10.9059601	217.846375
14	-13.4055433	267.830322
16	-14.9545565	298.820801
18	-15.1777697	310.302002

Table 5. Closed-loop transfer characteristics, slew command to slew response for observer 2 (sheet 2 of 2).

	UNIQUE ZEROS			
1	-1.014238			
2	-1.001904			
3	-5.527421			
5	-11.603097	0.140680	9.999265E-01	1.160395E+01
6	-12.453119			
8	-12.712068	0.993790	9.969581E-01	1.275085E+01
10	-1.820453	8.797625	2.026327E-01	8.983999E+00
11	-21.852631			
13	-15.977408	21.597702	5.947253E-01	2.686519E+01
15	-15.678535	22.439590	5.727469E-01	2.737428E+01
17	-19.426849	20.445221	6.688220E-01	2.820300E+01
19	-6.972517	24.392853	2.748352E-01	2.536981E+01
21	-1.134023	22.743225	4.980015E-02	2.277147E+01
23	-0.791293	23.566193	3.355857E-02	2.357947E+01
25	0.100199	22.784088	-4.397720E-03	2.278430E+01
27	-15.495689	30.807693	4.493430E-01	3.448521E+01
29	-12.255844	36.133194	3.212110E-01	3.815512E+01
31	-1.790771	36.227997	4.937031E-02	3.627223E+01
32	-39.742004			
34	-15.999253	40.792191	3.651333E-01	4.381757E+01
36	-43.283508	10.648792	9.710442E-01	4.457419E+01
38	-8.789634	46.187195	1.869494E-01	4.701611E+01
40	-64.693405	38.276611	8.606430E-01	7.516869E+01
41	65.252930			
43	-8.481948	147.411163	5.744437E-02	1.476550E+02
45	-8.506897	147.327850	5.764526E-02	1.475732E+02
47	-7.534446	147.033630	5.117587E-02	1.472265E+02
49	-7.387407	147.422943	5.004750E-02	1.476079E+02
51	-6.899275	137.761185	5.001873E-02	1.379338E+02
53	-6.618836	134.322495	4.921600E-02	1.344855E+02
55	-30.550735	135.341415	2.201907E-01	1.387467E+02
57	-30.182831	135.124985	2.179976E-01	1.384549E+02
59	-34.438171	139.312332	2.399775E-01	1.435058E+02
61	-39.287537	133.329437	2.826496E-01	1.389973E+02
62	-105.271210			
64	-12.635200	258.243652	4.964066E-02	2.585623E+02
66	-14.735691	295.081055	4.987563E-02	2.954487E+02
68	-14.882603	296.835937	5.007458E-02	2.972037E+02
70	-13.306531	304.784912	4.525086E-02	3.050974E+02
72	-15.352722	315.840332	4.855182E-02	3.162131E+02
74	-16.479034	344.377197	4.779701E-02	3.447712E+02
76	-18.680878	373.775879	4.991651E-02	3.742424E+02
78	-18.694489	372.771240	5.008711E-02	3.732395E+02

THE FOLLOWING ZEROS MATCHED POLES AND WERE ELIMINATED IN THE ABOVE LISTS

2	-7.3352070	146.520645
4	-11.3795233	144.194138
6	-6.8707819	137.243759
8	-6.7724915	135.280411
10	-14.0057011	217.711624
12	-10.9059601	217.846375
14	-13.4055443	267.830322
16	-14.9545565	298.820801
18	-15.1777773	310.302002

Table 6. Closed-loop transfer characteristics, slew command to slew response for observer 3 (sheet 1 of 2).*

----------UNIQUE POLES----------

S-PLANE

NUMBER	REAL	IMAG	DAMPING	FREQUENCY
1	-1.004944			
2	-10.550700			
3	-10.323856			
4	-11.429878			
5	-12.440581			
7	-12.065302	0.594815	9.987870E-01	1.207995E+01
9	-11.931503	1.418213	9.930098E-01	1.201549E+01
11	-1.137760	22.723785	5.000651E-02	2.275224E+01
13	-1.287174	22.591370	5.698412E-02	2.262801E+01
15	-9.879208	22.558701	4.011520E-01	2.462709E+01
17	-19.142365	21.276001	6.688483E-01	2.861939E+01
19	-28.973267	4.480728	9.882520E-01	2.931769E+01
20	-33.133865			
22	-19.923080	29.565842	5.588202E-01	3.565204E+01
24	-23.008408	32.287338	5.803362E-01	3.964668E+01
26	-11.965508	35.538879	3.190376E-01	3.749913E+01
28	-7.103016	35.222835	1.976796E-01	3.593195E+01
30	-11.849165	39.731093	2.857937E-01	4.146056E+01
32	-10.117865	40.696777	2.412711E-01	4.193565E+01
34	-2.345220	46.851044	4.999434E-02	4.690970E+01
36	-6.895641	137.739807	5.000019E-02	1.379123E+02
38	-6.952720	138.880585	4.999996E-02	1.390545E+02
40	-6.897458	135.543747	5.082157E-02	1.357191E+02
42	-7.380588	147.426270	5.000029E-02	1.476109E+02
44	-7.235736	146.225311	4.942300E-02	1.464042E+02
46	-26.887207	145.029877	1.822847E-01	1.475011E+02
48	-26.902924	145.057587	1.823540E-01	1.475312E+02
50	-22.379166	146.365112	1.511430E-01	1.480661E+02
52	-17.697586	217.276077	8.113320E-02	2.179956E+02
54	-19.006470	217.655746	8.699244E-02	2.184340E+02
56	-13.010519	259.884033	5.000017E-02	2.602095E+02
58	-14.783208	295.295883	4.999983E-02	2.956655E+02
60	-14.876577	297.122803	5.000616E-02	2.974949E+02
62	-16.131653	322.224121	5.000083E-02	3.226277E+02
64	-18.711212	373.756104	5.000002E-02	3.742241E+02
66	-18.828690	376.067139	5.000474E-02	3.765381E+02

THE FOLLOWING POLES MATCHED ZEROS AND WERE ELIMINATED IN ABOVE LISTS

NUMBER	REAL	IMAGINARY
1	-1.0049181	
2	-1.0004549	
4	-1.1766090	23.5027618
6	-6.8707666	137.243652
8	-13.4099436	267.836914
10	-14.9596920	298.819336
12	-15.2198362	304.042236
14	-15.5362902	310.304443
16	-18.6623077	372.779541

*Input transform also included.

Table 6. Closed-loop transfer characteristics, slew command to slew response for observer 3 (sheet 2 of 2).*

	UNIQUE ZEROS			
1	-10.538695			
3	-12.005877	0.379031	9.99499[illegible]E-01	1.001198E+01
5	-11.947660	1.415541	9.930536E-01	1.203125E+01
7	-9.736929	5.696114	8.635[illegible]E-01	1.127[illegible]E+01
9	0.152455	7.464769	-2.041906E-02	7.466326E+00
11	-1.137530	22.723939	4.999593E-02	2.275246E+01
13	-1.287189	22.591400	5.688472E-02	2.262804E+01
15	-19.147766	21.292847	6.686599E-01	2.863603E+01
16	-33.134216			
18	-7.103048	35.222870	1.976807E-01	3.593193E+01
20	-11.965901	35.539001	3.190960E-01	3.749937E+01
22	-11.278847	39.950729	2.716988E-01	4.151231E+01
24	-23.069473	32.254059	5.817533E-01	3.965508E+01
26	-2.345032	46.851105	4.999027E-02	4.690976E+01
28	-43.446594	21.345001	8.975313E-01	4.840677E+01
30	-11.056975	55.068802	1.968559E-01	5.616786E+01
31	-88.561650			
32	52.545685			
34	-6.895600	137.739777	4.999991E-02	1.379122E+02
36	-6.953054	138.883392	5.000136E-02	1.390573E+02
38	-6.897305	135.543594	5.082050E-02	1.357189E+02
40	-7.380616	147.427200	5.000017E-02	1.476118E+02
42	-7.235595	146.225050	4.940074E-02	1.464041E+02
44	-26.895905	145.033401	1.823375E-01	1.475062E+02
46	-28.020569	144.397751	1.904978E-01	1.470913E+02
48	-21.191711	147.524414	1.421893E-01	1.490387E+02
50	-17.697617	217.276108	8.118331E-02	2.179957E+02
52	-19.006409	217.655685	8.699220E-02	2.184839E+02
54	-13.008091	259.848389	4.999774E-02	2.601736E+02
56	-14.782550	295.284180	4.999952E-02	2.956533E+02
58	-14.865562	297.068604	4.997832E-02	2.974402E+02
60	-16.104568	321.858887	4.997361E-02	3.222615E+02
62	-18.711197	373.755127	5.000011E-02	3.742231E+02
64	-18.517227	371.971436	4.971977E-02	3.724319E+02

THE FOLLOWING ZEROS MATCHED POLES AND WERE ELIMINATED IN THE ABOVE LISTS

1	-1.0049171	
2	-1.0004549	
4	-1.1766090	23.5027618
6	-6.8707666	137.243652
8	-13.4099426	267.836914
10	-14.9596920	298.819336
12	-15.2198453	304.042236
14	-15.5362911	310.304443
16	-18.6623077	372.779541

*Input transform also included.

$$\begin{bmatrix} \dot{x}_1 \\ \dot{x}_2 \\ \dot{x}_3 \\ \dot{e} \end{bmatrix} = \begin{bmatrix} A_1 + B_1K_1 & 0 & 0 & B_1K_1 \\ 0 & A_2 & 0 & B_2K_1 \\ B_3K_1 & 0 & A_3 & B_3K_1 \\ 0 & 0 & GC_3 & A_1 - GC_1 \end{bmatrix} \begin{bmatrix} \underline{x}_1 \\ \underline{x}_2 \\ \underline{x}_3 \\ \underline{e} \end{bmatrix} \tag{35}$$

and the closed-loop system is again unstable.

The final design is of dimension 22, and uses an output transform to spatially filter the system output. The closed-loop equation has the form

$$\begin{bmatrix} \dot{x}_1 \\ \dot{x}_2 \\ \dot{x}_3 \\ \dot{e} \end{bmatrix} = \begin{bmatrix} A_1 + B_1K_1 & 0 & 0 & B_1K_1 \\ B_2K_1 & A_2 & 0 & B_2K_1 \\ B_3K_1 & 0 & A_3 & B_3K_1 \\ 0 & GT_3C_2 & GT_3C_3 & A_1 - GT_3C_1 \end{bmatrix} \begin{bmatrix} \underline{x}_1 \\ \underline{x}_2 \\ \underline{x}_3 \\ \underline{e} \end{bmatrix} \tag{36}$$

If Eq. (32) is satisfied, then Eq. (36) becomes

$$\begin{bmatrix} \dot{x}_1 \\ \dot{x}_2 \\ \dot{x}_3 \\ \dot{e} \end{bmatrix} = \begin{bmatrix} A_1 + B_1K_1 & 0 & 0 & B_1K_1 \\ B_2K_1 & A_2 & 0 & B_2K_1 \\ B_3K_1 & 0 & A_3 & B_3K_1 \\ 0 & 0 & 0 & A_1 - GT_3C_1 \end{bmatrix} \begin{bmatrix} \underline{x}_1 \\ \underline{x}_2 \\ \underline{x}_3 \\ \underline{e} \end{bmatrix} \tag{37}$$

Observation spillover has been eliminated and the closed-loop system is stable. In fact, the poles of Eq. (37) include the poles of $[A_1 + B_1K_1]$, A_2, A_3, and $[A_1 - GT_3C_1]$. Returning to Table 6, one can verify that the numerical results can also be categorized this way.

The results presented here illustrate the effect of spillover, and demonstrate that a singular output transform can be used to eliminate the observation spillover from a finite number of modes. If observation spillover is eliminated, the unmodeled plant modes will still be excited by the controller ($B_2K_1\hat{x}$, $B_3K_1\hat{x}$), but the overall system will be stable.

In the case considered above, enough outputs are available to eliminate spillover from the $\underline{x}_2$ and $\underline{x}_3$ modes. Using an evaluation model which includes $\underline{x}_1$, $\underline{x}_2$ and all of $\underline{x}_3$, one can calculate the closed-loop eigenvalues (see Table 7). Again the regulator, observer, A_2, and A_3 poles are uncoupled. If $\underline{x}_4$ or $\underline{x}_5$ modes are included in the evaluation model, then the effects of spillover will be seen. However, by filtering the $\underline{x}_2$ and $\underline{x}_3$ states, the transform creates a frequency separation between the $\underline{x}_1$ information and the residual mode spillover.

3.3.2 Input Transforms

The optical performance requirements of the M2V2 satellite dictate that the set of modes {23, 26, 28, 29, 30} be isolated from the disturbing effect of control action. These modes are higher in frequency than all the $\underline{x}_1$ modes, and are not explicitly included in the quadratic cost expression. As illustrated earlier, the baseline optimal control law does in fact excite this set of modes. If the level of excitation is unsatisfactory from a system's viewpoint, two options are available. One alternative is to include these additional modes in the performance index. This course of action is undesirable because it increases the dimension of the optimal control law. The other alternative is to use an input transform to constrain the spatial content of the control. To illustrate the effects of the input transform, two configurations are compared. These configurations are shown in Figure 23. Both have the same plant model, and the same observer to process the plant output signal $\underline{y}$ and to estimate $\underline{x}_1$. The configurations differ only in the control law. Configuration 1 uses a control law of the form

$$\underline{u} = K_1\hat{\underline{x}}_1 \qquad (38)$$

Table 7. Closed-loop transfer characteristics, slew command to slew response for $\underline{x}_1\underline{x}_2\underline{x}_3$ plant model (sheet 1 of 2).*

----------UNIQUE POLES----------

S-PLANE

NUMBER	REAL	IMAG	DAMPING	FREQUENCY
1	-1.012941			
2	-1.005194			
3	-1.000736			
4	-6.380075			
6	-11.496717	0.171995	9.998882E-01	1.149800E+01
8	-12.032524	0.571587	9.988737E-01	1.204609E+01
9	-12.439398			
10	-12.896002			
11	-10.245658			
13	-1.137719	22.723770	5.000474E-02	2.275223E+01
15	-1.237823	22.667725	5.462604E-02	2.270149E+01
17	-8.324382	22.063034	3.530093E-01	2.358119E+01
18	-25.994095			
20	-28.965134	4.446473	9.884217E-01	2.930443E+01
22	-19.100829	20.924986	6.742216E-01	2.833316E+01
24	-21.172394	30.945003	5.646746E-01	3.749488E+01
26	-17.795761	35.359451	4.495571E-01	3.958510E+01
28	-11.983670	35.546082	3.195841E-01	3.751335E+01
30	-6.480253	35.364639	1.802400E-01	3.595346E+01
32	-11.847562	39.729355	2.857709E-01	4.145825E+01
34	-10.118303	40.696686	2.412815E-01	4.193567E+01
36	-2.345032	46.851089	4.999029E-02	4.690974E+01
38	-6.953517	138.882187	5.000510E-02	1.390561E+02
40	-6.742580	135.218918	4.980231E-02	1.353869E+02
42	-7.380596	147.426270	5.000034E-02	1.476109E+02
44	-18.366882	146.334518	1.245359E-01	1.474826E+02
46	-22.378647	146.381439	1.511232E-01	1.480822E+02
48	-23.743332	145.568058	1.609592E-01	1.475114E+02
50	-20.279205	215.581940	9.365330E-02	2.165336E+02
52	-17.621277	218.691010	8.031523E-02	2.193998E+02
54	-13.010483	259.824033	5.000003E-02	2.602093E+02
56	-13.408319	267.822590	5.000025E-02	2.681600E+02
58	-14.782457	295.295654	4.999727E-02	2.956653E+02
60	-14.874912	297.126465	4.999995E-02	2.974985E+02
62	-16.131378	322.224121	4.999998E-02	3.226277E+02
64	-18.711212	373.756104	5.000002E-02	3.742241E+02
66	-18.828568	376.067383	5.000438E-02	3.765383E+02
68	-18.848114	376.432617	5.000772E-02	3.769041E+02
70	-19.749481	394.502441	4.999915E-02	3.949963E+02
72	-22.429688	448.398682	4.999929E-02	4.489590E+02
74	-22.891510	457.258057	4.999986E-02	4.578306E+02

THE FOLLOWING ZEROS MATCHED POLES AND WERE ELIMINATED IN THE ABOVE LISTS

2	-1.1766090	23.5027618
4	-6.8957291	137.739944
6	-6.8707829	137.243713
8	-7.3597240	146.596191
10	-14.9596624	298.818848
12	-15.2212658	304.044189
14	-15.5341339	310.316162
16	-18.6623230	372.779541
18	-20.4317169	408.086914
20	-22.1532440	445.004150

* Input transform also included.

Table 7. Closed-loop transfer characteristics, slew command to slew response for $\underline{x}_1\underline{x}_2\underline{x}_3$ plant model (sheet 2 of 2).*

	UNIQUE ZEROS			
1	-1.005241			
2	-1.000740			
3	-10.416402			
5	-11.623823	0.141190	9.999263E-01	1.162468E+01
6	-12.852970			
7	-12.252294			
9	-5.330327	6.329781	6.441347E-01	8.275174E+00
11	0.908830	6.610679	-1.361980E-01	6.672857E+00
13	-1.137522	22.724045	4.999546E-02	2.275250E+01
15	-1.237846	22.667740	5.452706E-02	2.270151E+01
16	-25.981155			
18	-19.109406	20.930420	6.742507E-01	2.834169E+01
20	-19.411041	34.196747	4.936455E-01	3.932182E+01
22	-11.988814	35.546143	3.195870E-01	3.751346E+01
24	-6.480372	35.364548	1.802437E-01	3.595338E+01
26	-11.175797	40.430679	2.664276E-01	4.194684E+01
28	-2.344984	46.851273	4.998909E-02	4.690991E+01
30	-48.028336	25.204910	8.854735E-01	5.424023E+01
32	17.952972	57.511398	-2.979825E-01	6.024940E+01
34	-6.953891	138.882339	5.000773E-02	1.390563E+02
36	-6.742594	135.218903	4.980241E-02	1.353269E+02
38	-17.140594	116.660004	1.453671E-01	1.179125E+02
40	-7.372447	147.483505	4.992595E-02	1.476573E+02
42	-13.776550	146.527725	9.362072E-02	1.471741E+02
44	-24.610855	145.780365	1.664659E-01	1.478432E+02
46	-63.776683	139.703751	4.152864E-01	1.535728E+02
48	-20.277786	215.581070	9.364766E-02	2.165326E+02
50	-17.622528	218.692062	8.032107E-02	2.194009E+02
52	-13.009516	259.879883	4.999716E-02	2.602051E+02
54	-13.408500	267.829590	5.000092E-02	2.681650E+02
56	-14.761109	295.238525	4.993488E-02	2.956072E+02
58	-14.871683	297.111328	4.999168E-02	2.974832E+02
60	-16.123535	322.178223	4.998286E-02	3.225813E+02
62	-18.711029	373.754395	4.999975E-02	3.742224E+02
64	-18.984095	376.568359	5.034947E-02	3.770464E+02
66	-18.843312	376.432129	5.000831E-02	3.769036E+02
68	-19.749710	394.502441	4.999973E-02	3.949953E+02
70	-22.429733	448.393682	4.995940E-02	4.489590E+02
72	-22.846939	456.939209	4.993757E-02	4.575100E+02

THE FOLLOWING POLES MATCHED ZEROS AND WERE ELIMINATED IN ABOVE LISTS

NUMBER	REAL	IMAGINARY
2	-1.1766090	23.5027618
4	-6.8957253	137.739807
6	-6.8707829	137.243713
8	-7.3597238	146.596191
10	-14.9596577	298.818848
12	-15.2212582	304.044189
14	-15.5341311	310.316162
16	-18.6623230	372.779541
18	-20.4317169	408.086914
20	-22.1532440	445.004150

*Input transform also included.

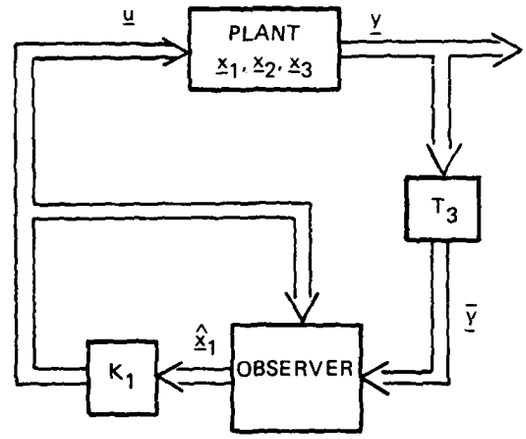

CONFIGURATION 1
OPTIMAL GAINS

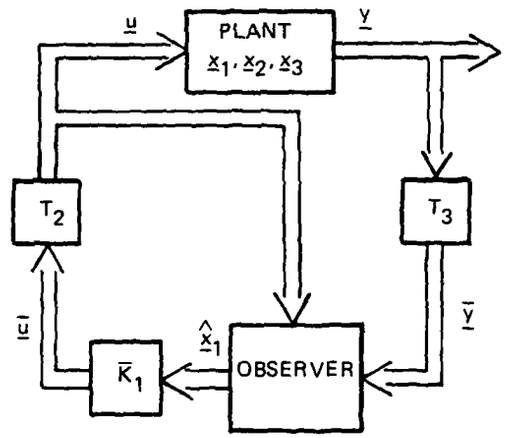

CONFIGURATION 2
INPUT TRANSFORM

Figure 23. Alternate controller configuration: mode isolation.

where K_1 is the baseline optimal gain matrix. Configuration 2 uses a control law of the form

$$\underline{u} = T_2 \bar{K}_1 \hat{\underline{x}}_1$$

where the columns of T_2 are orthogonal to the rows of the input distribution matrix B, which correspond to modes 23, 26, 28, 29, and 30. $\bar{K}_1$ is the optimal constrained gain matrix. The matrix $T_2\bar{K}_1$ has the same dimensions as the matrix K_1.

The optimal control law, Eq. (38), minimizes the quadratic performance index

$$J = \int_{t_0}^{\infty} \underline{x}_1^T \bar{R}_1 \underline{x}_1 + \underline{u}^T R_2 \underline{u} \, dt \tag{39}$$

subject to the constraint

$$\dot{\underline{x}}_1 = A_1 \underline{x}_1 + B_1 \underline{u} \tag{40}$$

Any other choice of control will imply an equal or greater cost.

The gains $\bar{K}_1$ were selected by minimizing the same performance index

$$J = \int_{t_0}^{\infty} \underline{x}_1^T \bar{R}_1 \underline{x}_1 + \underline{u}^T R_2 \underline{u} \, dt \tag{41}$$

subject to two constraints

$$\dot{\underline{x}}_1 = A_1 \underline{x}_1 + B_1 \underline{u} \tag{42}$$

$$\underline{u} = T_2 \bar{\underline{u}} \tag{43}$$

This second constraint restricts the spatial content of $\underline{u}$.

Equations (41), (42), and (43) can be rewritten

$$\bar{J} = \int_{t_0}^{\infty} \underline{x}_1^T R_1 \underline{x}_1 + \bar{\underline{u}}^T \bar{R}_2 \bar{\underline{u}} \, dt \tag{44}$$

$$\dot{\underline{x}}_1 = A_1 \underline{x} + B_1 T_2 \bar{\underline{u}} \tag{45}$$

where $\bar{R}_2$ is given by

$$\bar{R}_2 = T_2^T R_2 T_2 \tag{46}$$

The control which minimizes $\bar{J}$ is

$$\bar{\underline{u}} = \bar{K}_1 \underline{x}_1$$

where

$$\bar{K}_1 = \bar{R}_2^{-1} B_1 T_2 \bar{P}$$

and $\bar{P}$ is the solution to the appropriate algebraic Riccati equation.

$$0 = \bar{P}^T A + A\bar{P} + \bar{R}_1 - \bar{P} B_1 T_2 [\bar{R}_2]^{-1} T_2^T B^T \bar{P} \tag{47}$$

The trace elements of the cost matrices P and $\bar{P}$ are compared in Table 8. These elements reflect the cost of nulling a unit initial condition on any $\underline{x}_1$ state. As expected, the optimal control law costs are lower in every case than the corresponding costs of the spatially constrained control. Similarly, the poles of $[A_1 + B_1 K_1]$ are (see Table 9) incrementally faster than the poles of $[A_1 + B_1 T_2 \bar{K}_1]$. The decrease

Table 8. Cost comparison.

Mode	Optimal Cost	Cost with Input Transform
Displacements		
4	1.716	1.730
5	1.844	1.949
6	1.852	1.862
7	289.249	342.145
10	0	0
11	73.145	78.539
12	36.545	39.789
13	54.002	56.656
20	536.035	624.594
21	539.150	696.428
22	8315.590	13287.459
Velocities		
4	0.052	0.066
5	0.205	0.353
6	0.214	0.228
7	0.686	0.745
10	0	0
11	0.056	0.060
12	0.020	0.024
13	0.025	0.026
20	0.024	0.027
21	0.024	0.031
22	0.174	0.279

Table 9. Closed-loop eigenvalues.

OPTIMAL CONTROL LAW

CLOSED LOOP EIGENVALUES OF MATRIX (A+KB)

ERROR INDICATOR FOR EIGENVALUE ROUTINE: 0

	REAL	IMAG
2	-0.1770486112665D+02	0.2173992784136D+03
4	-0.2688877563716D+02	0.1450289392211D+03
6	-0.2690052087615D+02	0.1450331562681D+03
7	-0.3313393675684D+02	
9	-0.2300833538771D+02	0.3228710821362D+02
11	-0.7076039783989D+01	0.3532055867906D+02
13	-0.1992285751397D+02	0.2955850046588D+02
15	-0.1176609970790D+01	0.2350276575698D+02
17	-0.9879627924089D+01	0.2255841623713D+02
18	-0.1036254072872D+02	
19	-0.1074379495145D+02	
20	-0.1000455791533D+01	
21	-0.1004944181807D+01	
22	-0.1004913909441D+01	

SPATIALLY CONSTRAINED INPUT

CLOSED LOOP EIGENVALUES OF MATRIX (A+KB)

ERROR INDICATOR FOR EIGENVALUE ROUTINE: 0

	REAL	IMAG
2	-0.1893351829740D+02	0.2172958312334D+03
4	-0.2374416278885D+02	0.1455851168015D+03
6	-0.1836650478384D+02	0.1463348615205D+03
7	-0.2598670037900D+02	
9	-0.6466770857673D+01	0.3543677722509D+02
11	-0.1779526660991D+02	0.3535391100540D+02
13	-0.2116589170226D+02	0.3094400899411D+02
15	-0.1176609970790D+01	0.2350276575898D+02
17	-0.8823694945264D+01	0.2206026005629D+02
18	-0.1045717324745D+02	
19	-0.6379717219080D+01	
20	-0.1000741321590D+01	
21	-0.1012941900526D+01	
22	-0.1005180548397D+01	

in $\underline{x}_1$ dynamic performance is the penalty associated with the spatial constraint. The benefit of the constraint is best illustrated in the time domain. Figures 24 and 25 compare the time responses of the two systems to a unit initial condition on each $\underline{x}_1$ displacement state. Several observations can be made.

(1) Modes 4, 5, 6, 7, 10, 11, 12, 13, 20, 21, and 22 are $\underline{x}_1$ modes and are controlled. The time response of the $\underline{x}_1$ modes for the optimal law is slightly faster than the response provided by the constrained law. This is consistent with the closed-loop pole analysis.

(2) Modes 8, 9, 14, 15, 16, 17, and 18 are $\underline{x}_2$ modes. The dynamics of these modes are not fed back because of T_3. There is evidence of control spillover, however, for both control designs. (Mode 19 not shown.)

(3) T_2 is designed to suppress control spillover for modes 23, 26, 28, 29, and 30. The time-history traces indicate that the optimal control law excites these modes. The constrained design, on the other hand, shows sharply reduced excitation levels except for mode 29. In theory, the excitation can be suppressed completely. In practice, there is a tradeoff between suppressing modes and retaining control authority over $\underline{x}_1$ modes. This topic is discussed in Appendix H, including the reason for allowing spillover into Mode 29.

In summary, an input transform can be used to suppress control spillover into a set of uncontrolled modes. The penalty for implementing the transform is an increase in cost. The tradeoff between the spillover suppression and the cost penalty can be done at the systems level.

An additional comment, which is appropriate here, is that cost reflects the dynamics of only $\underline{x}_1$. Any plant/controller interactions which occur outside $\underline{x}_1$ space are not seen in the performance index. This point has been made previously. It is repeated here to emphasize that transforms have a much greater impact on the system than the performance index alone would indicate.

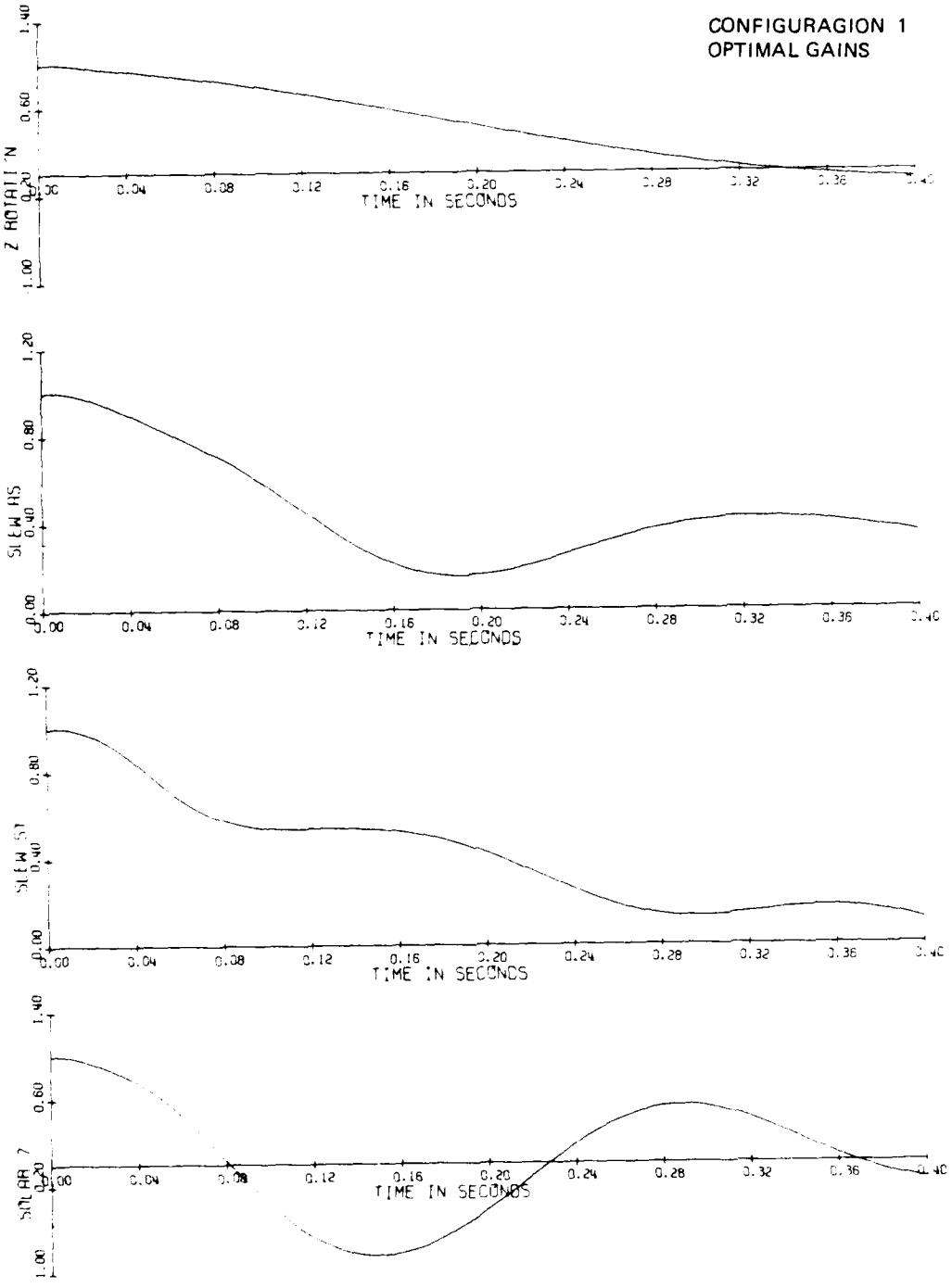

Figure 24. Output transform (sheet 1 of 6).

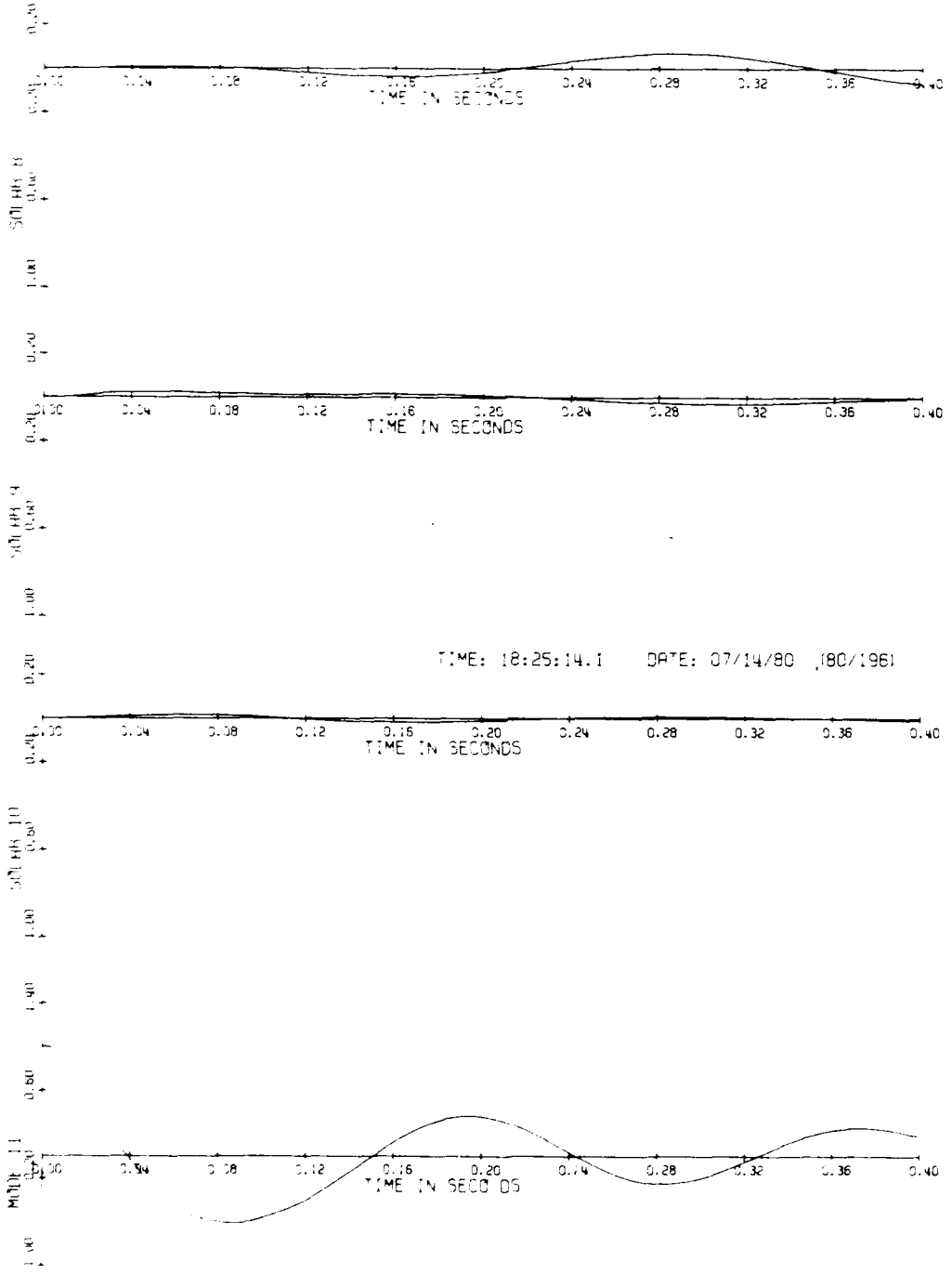

Figure 24. Output Transform (sheet 2 of 6).

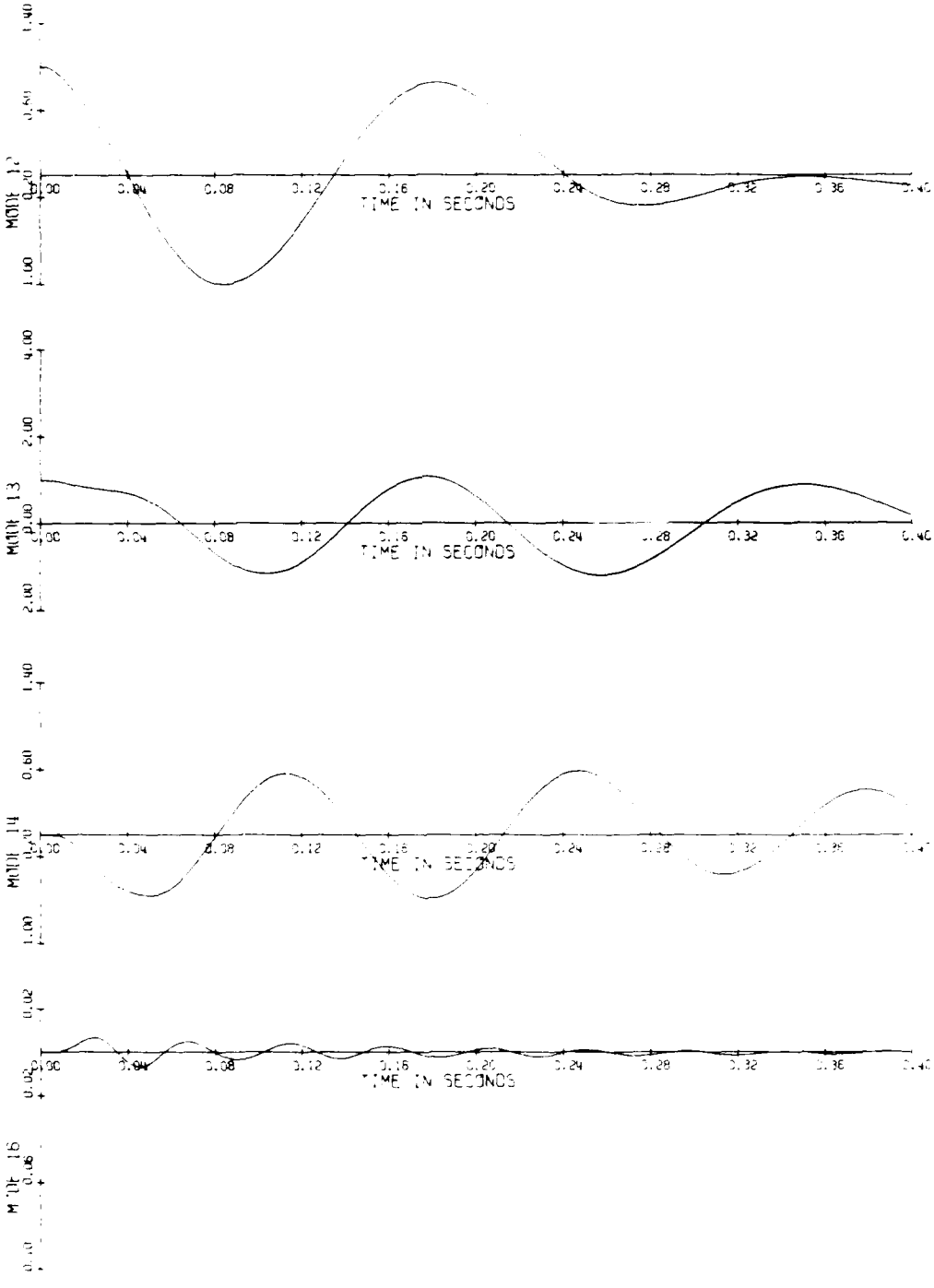

Figure 24. Output transform (sheet 3 of 6).

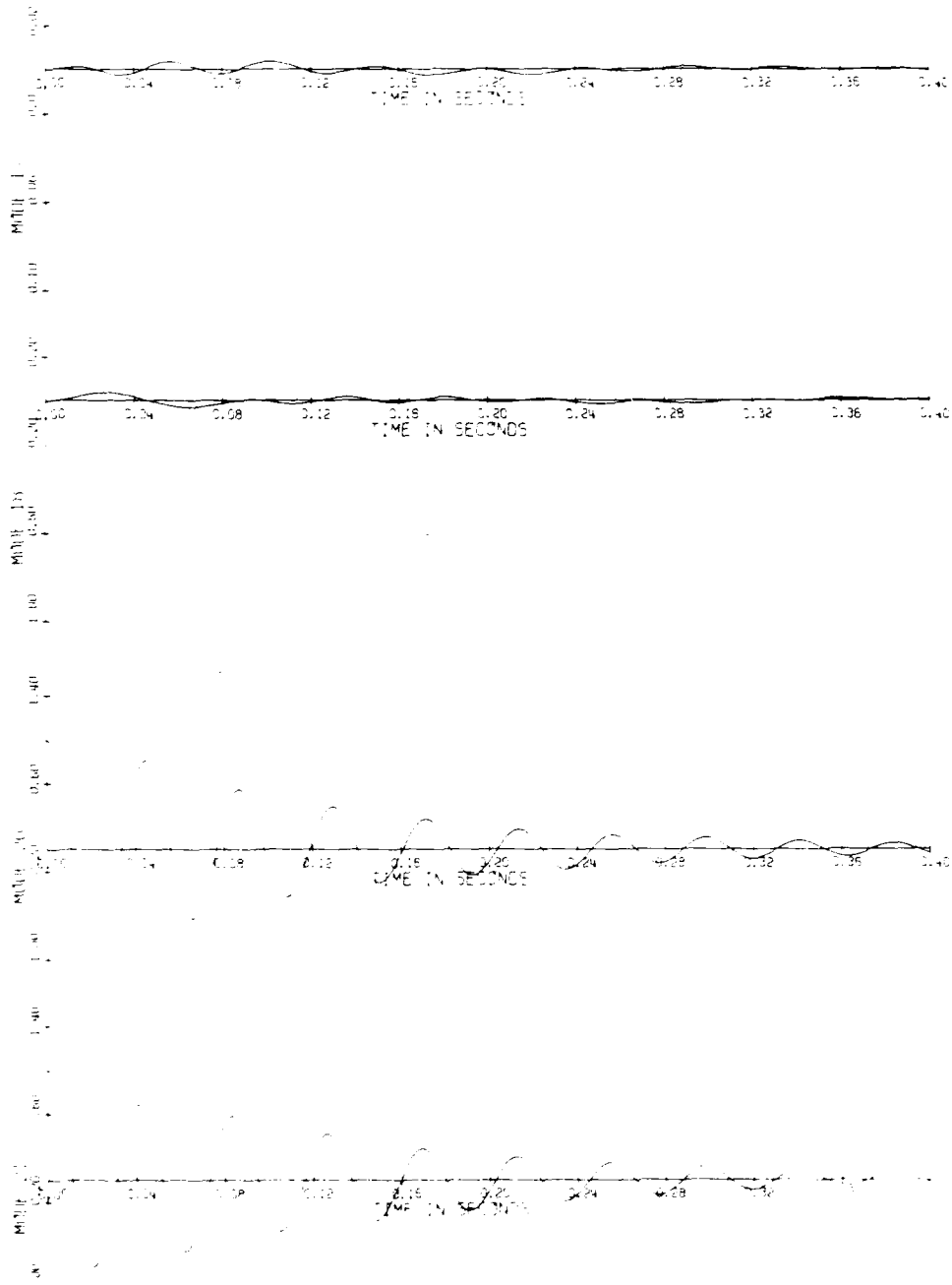

Figure 24. Output transform (sheet 4

AD-A092 547 AIR FORCE INST OF TECH WRIGHT-PATTERSON AFB OH F/G 22/2
OPTIMAL REGULATION WITHIN SPATIAL CONSTRAINTS. AN APPLICATION T--ETC(U)
AUG 80 E G TAYLOR
UNCLASSIFIED AFIT-CI-80-46D NL

2 OF 4
AD A092547

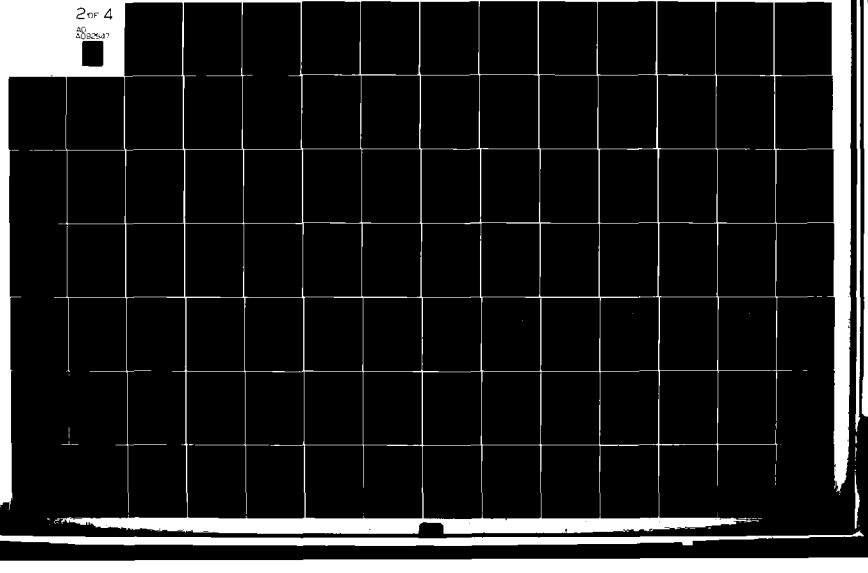

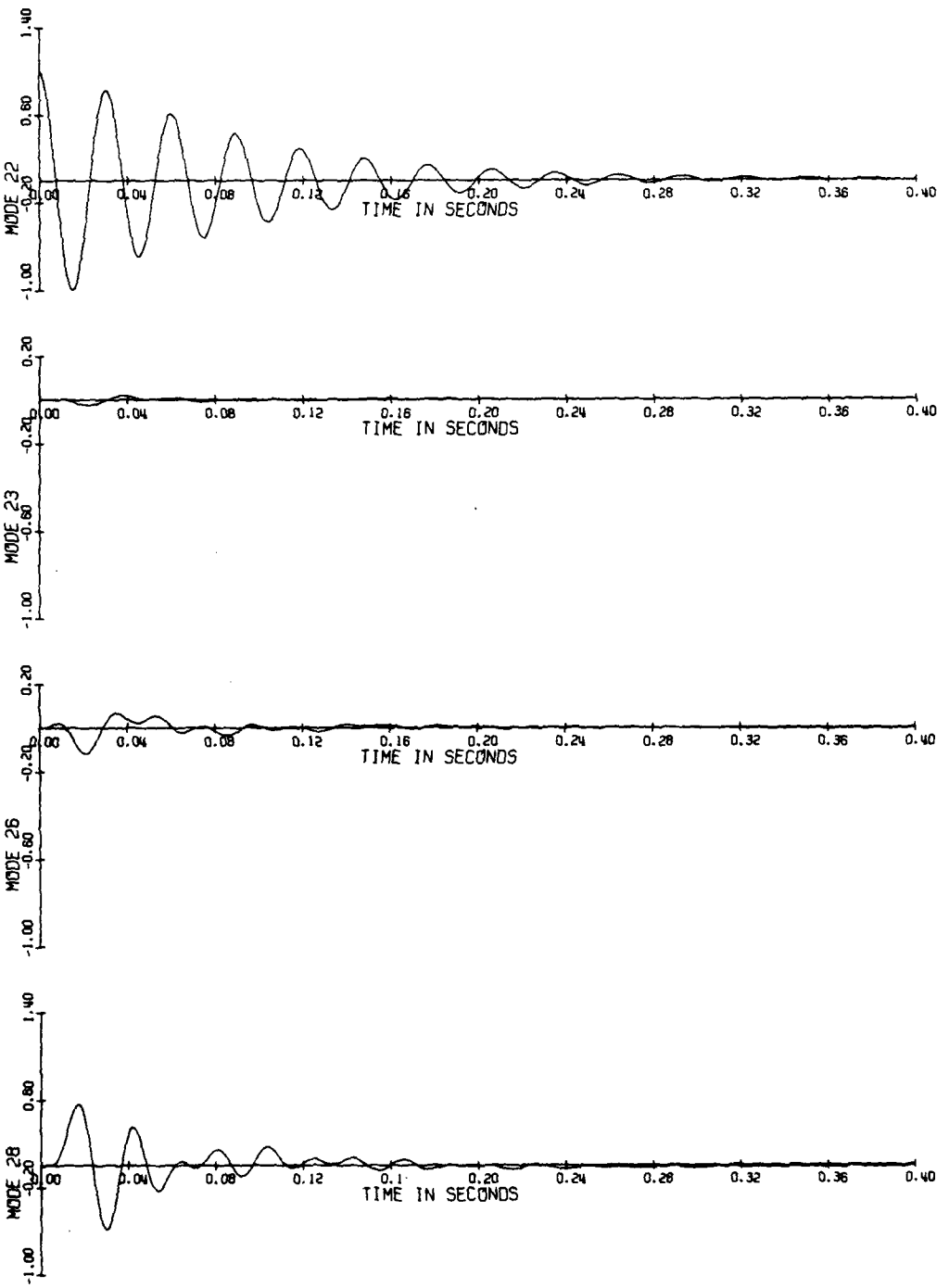

Figure 24. Output transform (sheet 5 of 6).

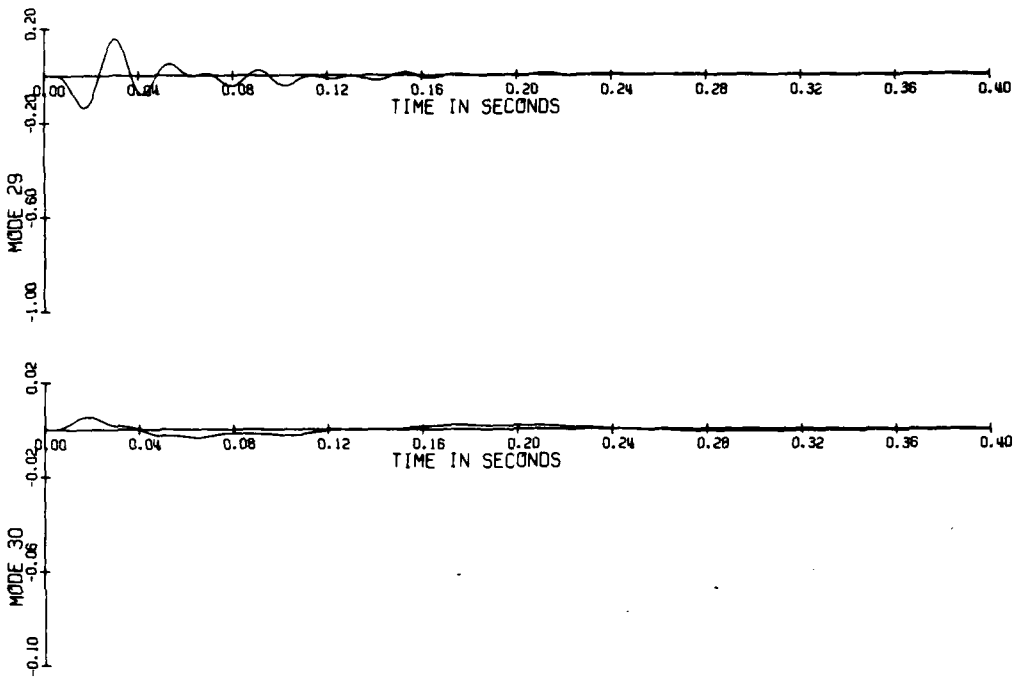

Figure 24. Output transform (sheet 6 of 6).

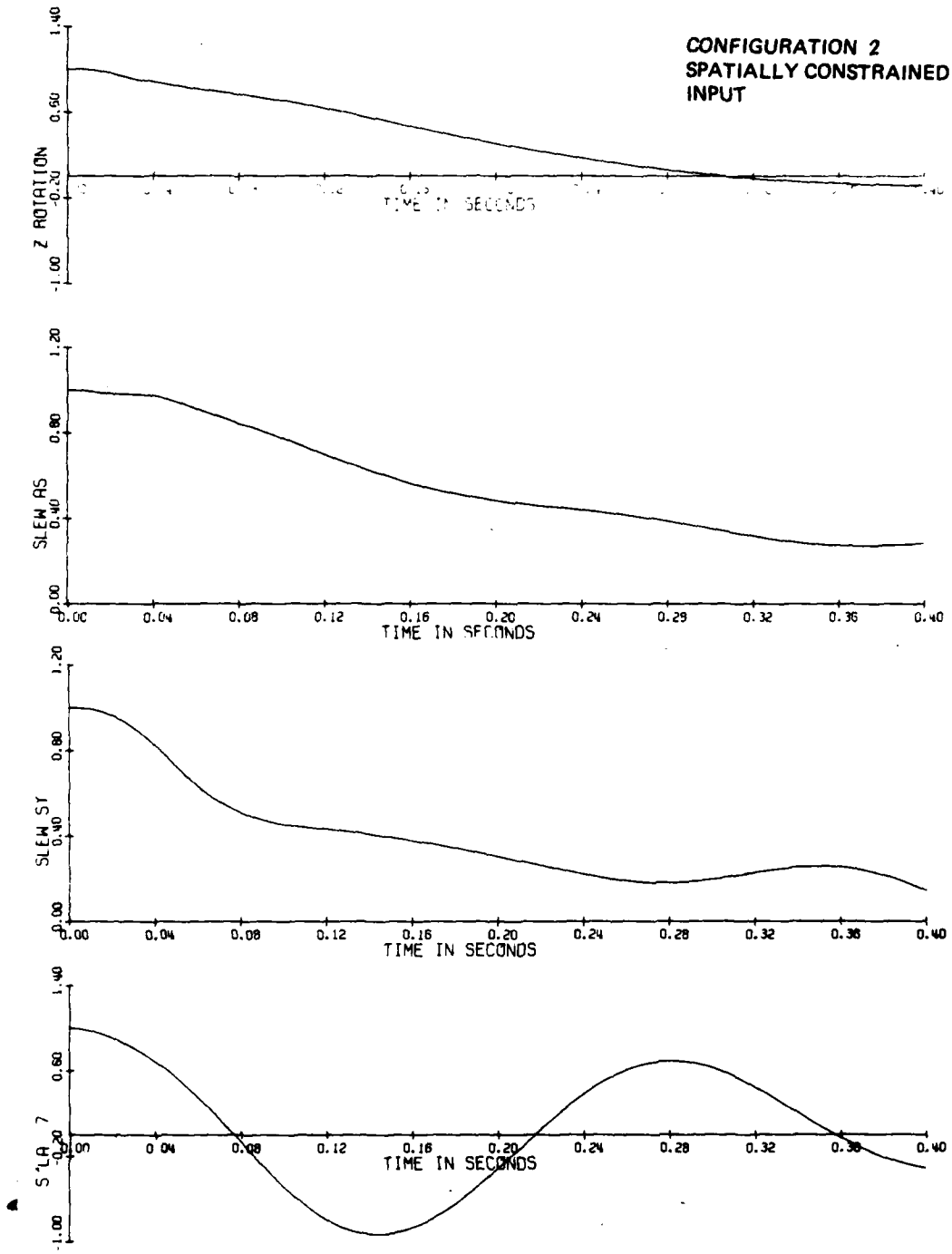

Figure 25. Input and output transforms (sheet 1 of 6).

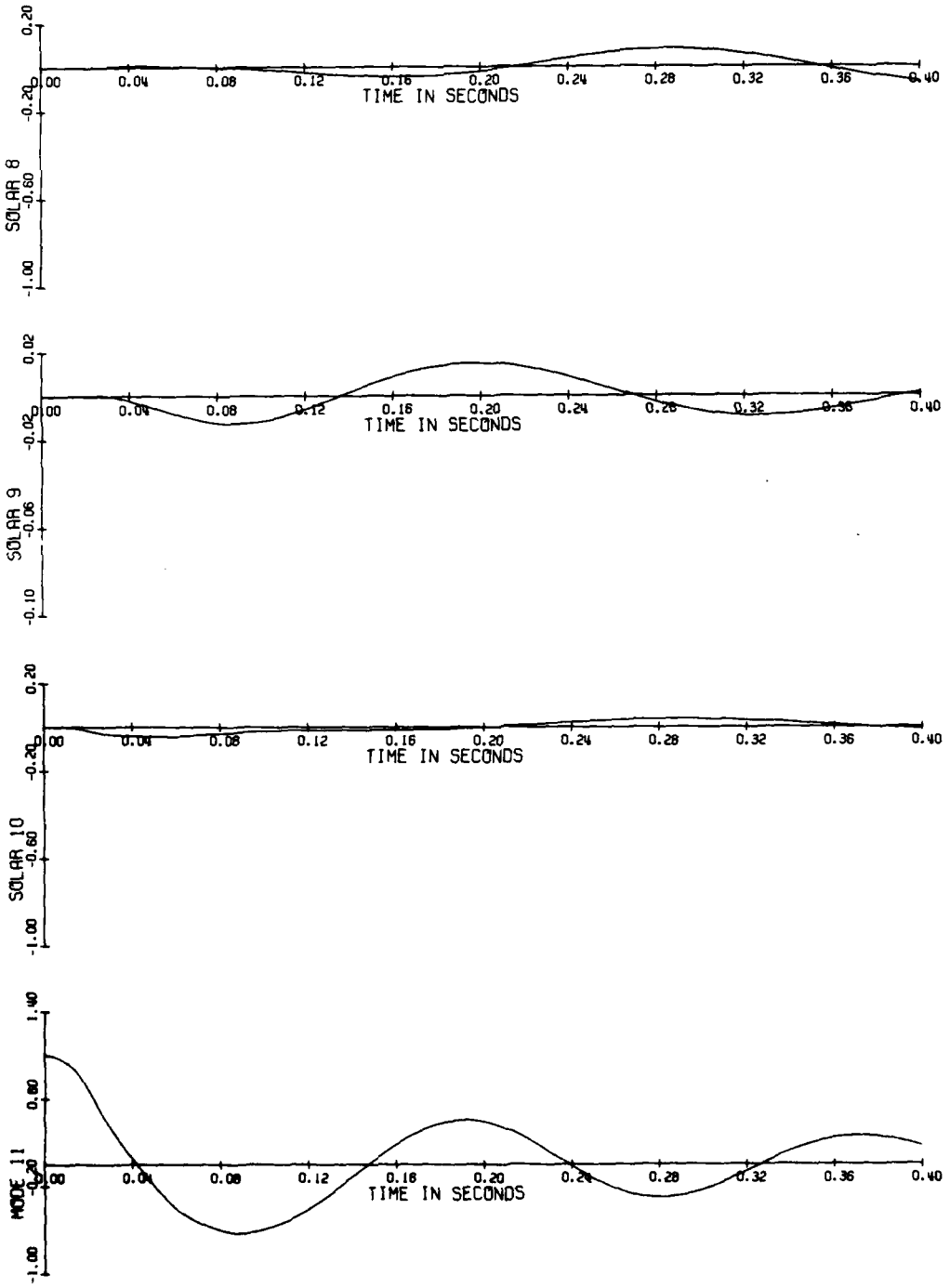

Figure 25. Input and output transforms (sheet 2 of 6).

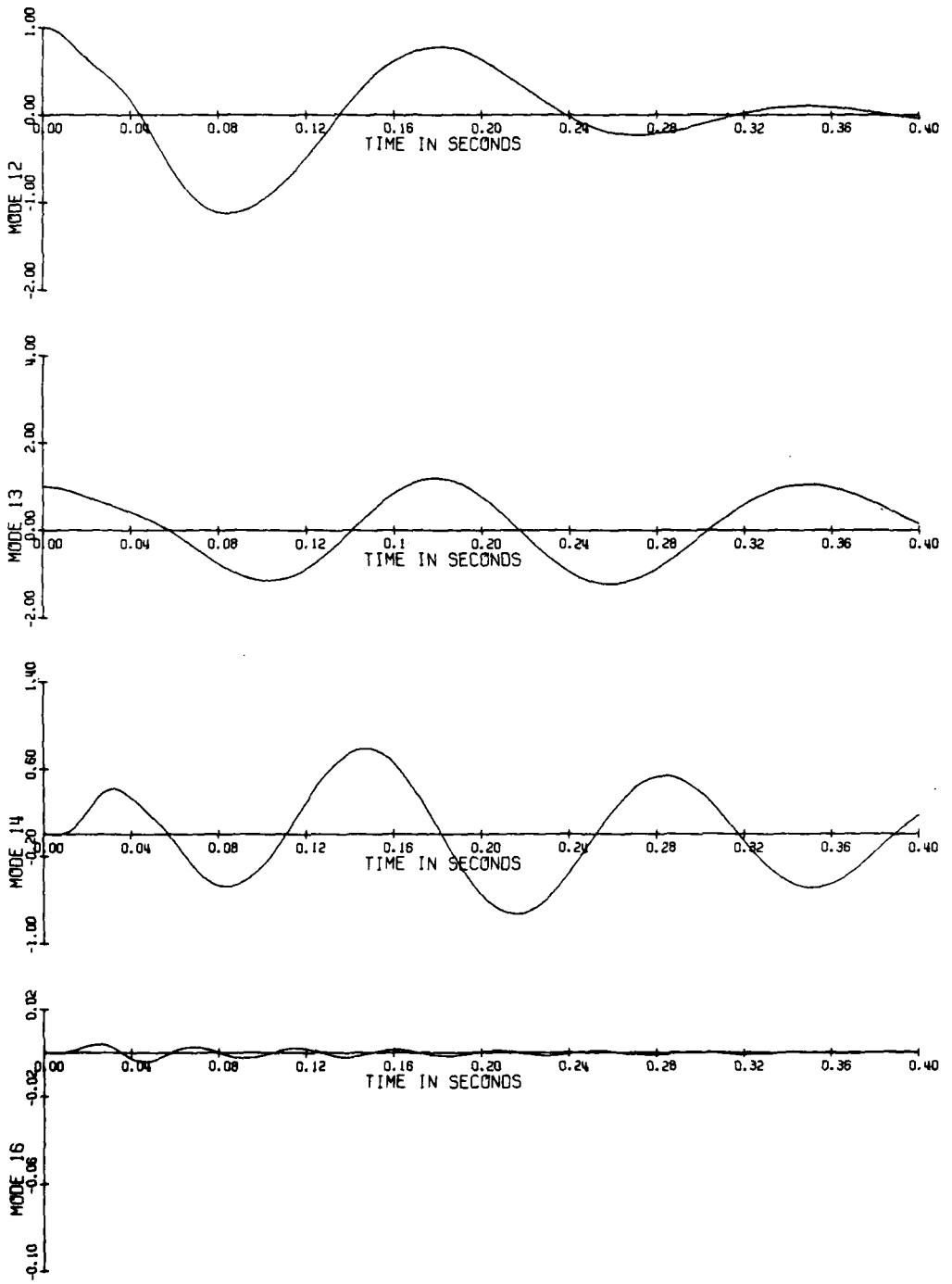

Figure 25. Input and output transforms (sheet 3 of 6).

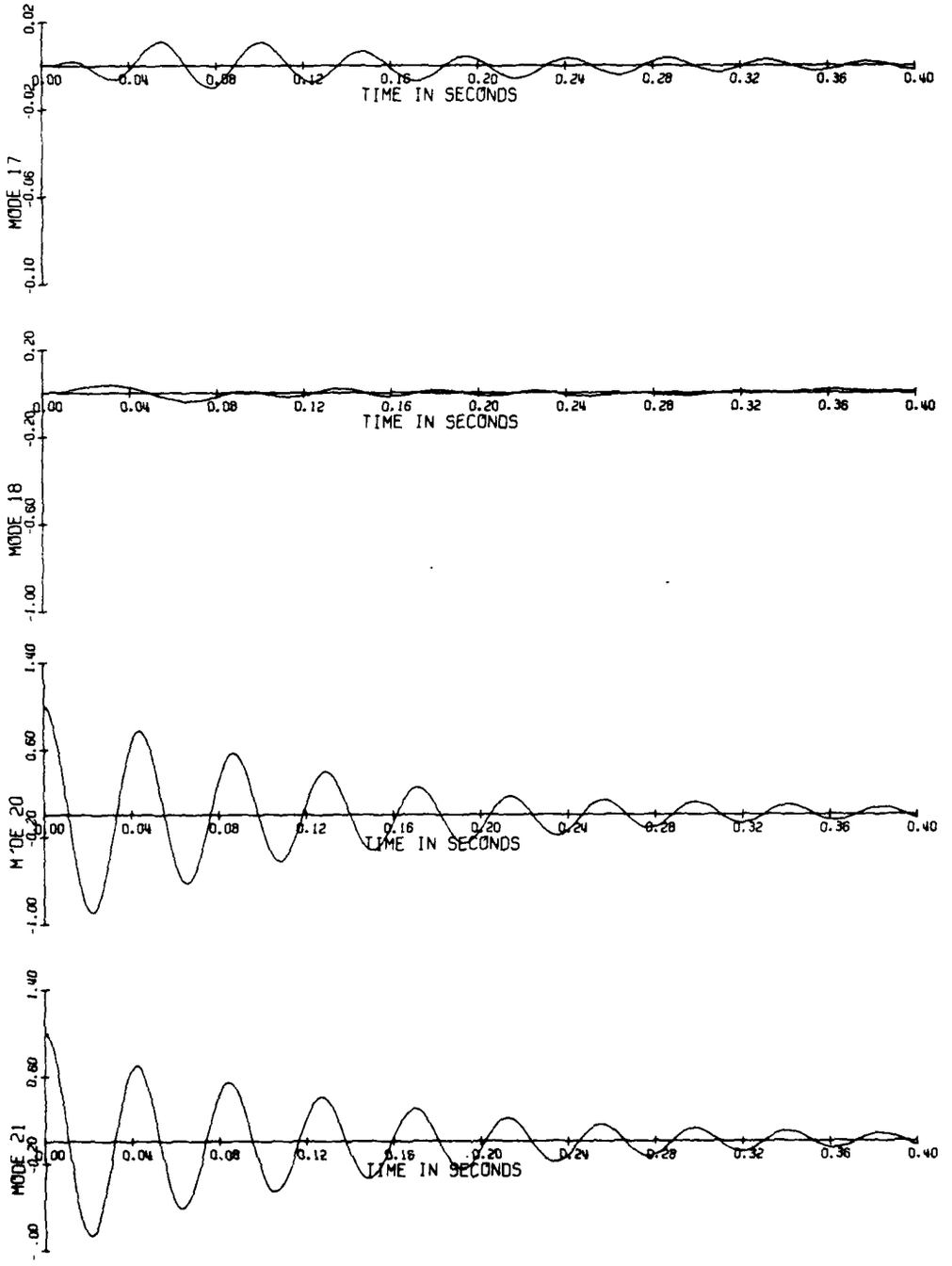

Figure 25. Input and output transforms (sheet 4 of 6).

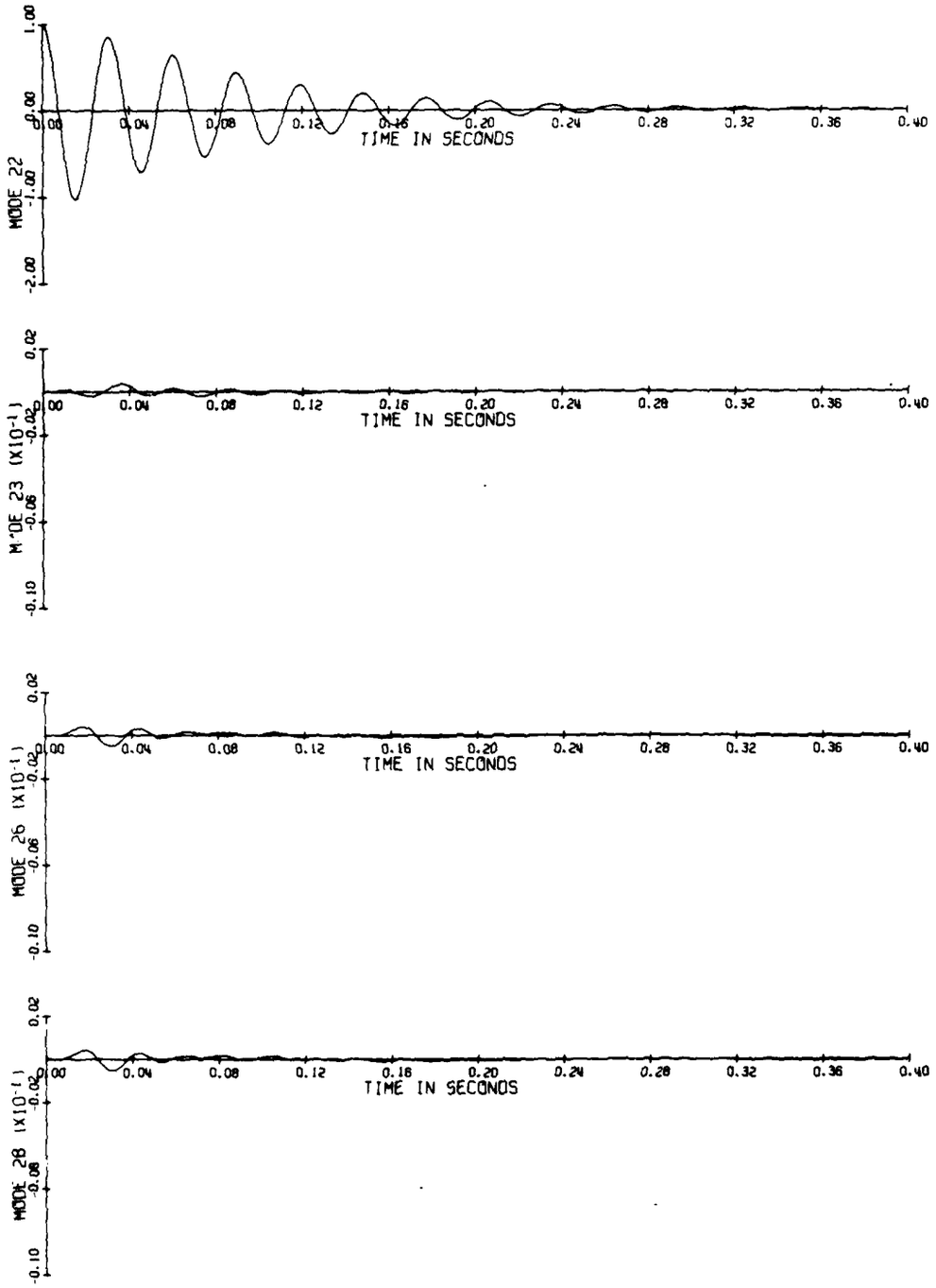

Figure 25. Input and output transforms (sheet 5 of 6).

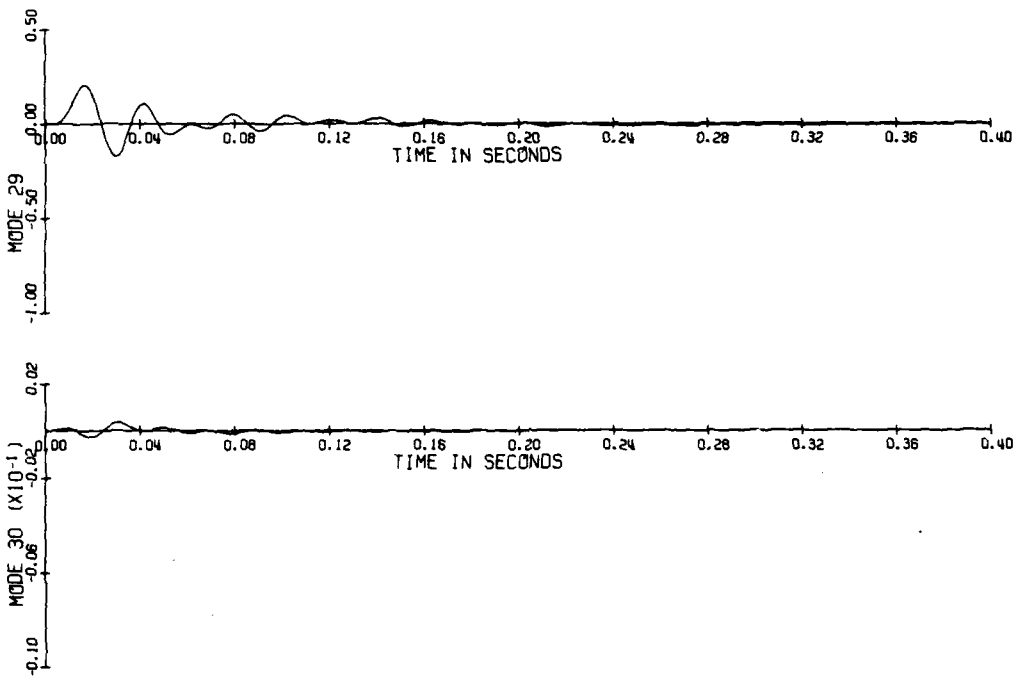

Figure 25. Input and output transforms (sheet 6 of 6).

3.3.3 Residual Mode Effects

The preceding sections illustrate the properties of input and output transforms in a closed-loop system context. Of particular interest are the control and observation spillover-suppression properties. However, the number of modes which can be suppressed is finite and, if the number of residual modes is greater than the number of suppressed modes, some spillover will occur (see Appendix A). The introduction advances the hypothesis that if input and output transforms suppress the interleaved residual modes, and enough additional modes can be suppressed so that there is a frequency separation between controlled and residual modes, then frequency-domain techniques can be used to account for the remaining residual modes. Consider the M2V2 plant as an example. If the transforms T_2 (input) and T_3 (output) are introduced, the control to observed output signal paths (see Figure 26) will contain $\underline{x}_1$, $\underline{x}_4$, and $\underline{x}_5$ information. Then, if a controller of the form

$$\underline{u} = T_2\bar{K}_1\hat{\underline{x}}_1$$

$$\dot{\hat{\underline{x}}}_1 = A_1\hat{\underline{x}}_1 + B_1\underline{u} + \bar{G}T_3[y - C_1\hat{\underline{x}}_1] \qquad (48)$$

is implemented, ($\bar{K}_1$ from Section 3.3.2, $\bar{G}$ from Section 3.3.1) spillover from $\underline{x}_4$ and higher frequency residual modes will occur. This spillover can be expected to adversely affect closed-loop performance. Specifically, a plant of $\underline{x}_1$ and $\underline{x}_4$ dynamics was cascaded with the controller above (see Figure 27). Table 10 gives the closed-loop poles for this configuration. Based on discussions in Section 3.2.3, one would expect spillover to affect both the closed-loop poles and the unmodeled plant poles. The numerical results bear this out. The observer poles (at -12 + 0j) have migrated, as have the high-frequency $\underline{x}_4$ poles. There is a distinct frequency separation between $\underline{x}_1$ and $\underline{x}_4$, however, and the singular perturbation techniques of Section 3.2 and Appendix E should be applicable.

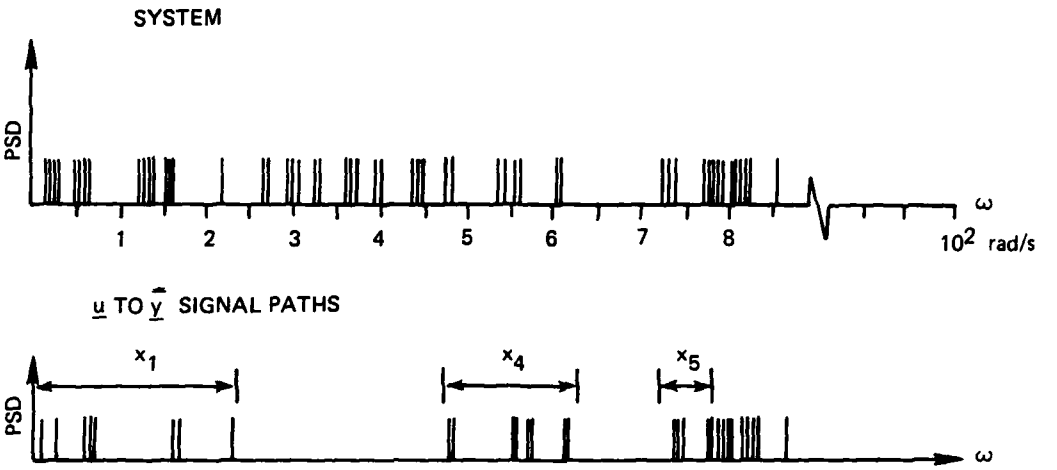

Figure 26. Spectral content.

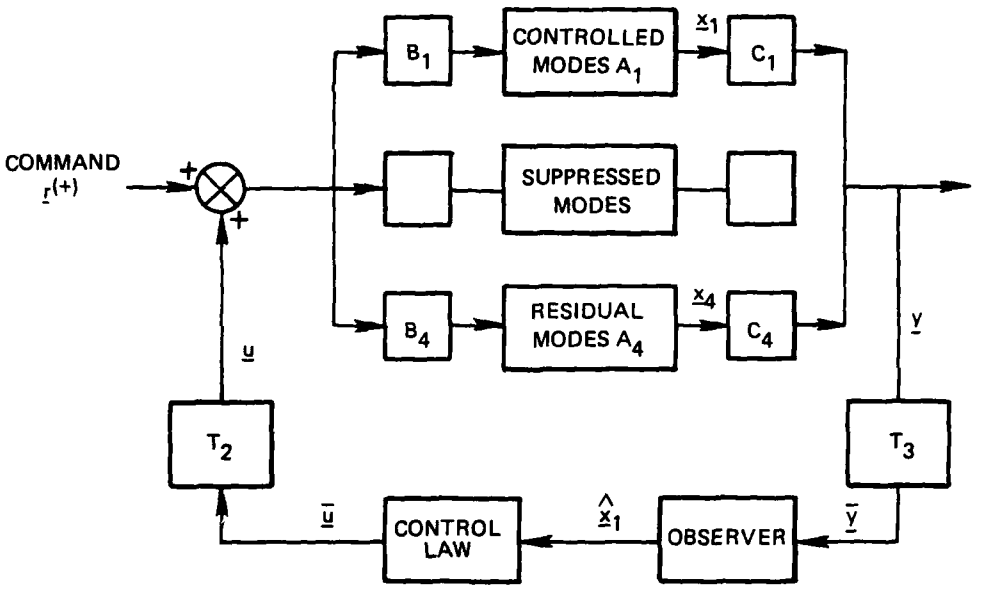

- CONTROL LAW $\bar{u} = \bar{K}_1 x_1$
- OBSERVER $\dot{\hat{x}} = A_1 \hat{x}_1 + B_1 T_2 \bar{u} + G T_3 [\underline{y} - C_1 \hat{x}_1]$

Figure 27. Closed-loop configuration—residual effects included.

Table 10. Closed-loop poles and zeros, slew command to slew response for $\underline{x}_1$, $\underline{x}_4$ plant (sheet 1 of 2).

----------UNIQUE POLES----------

S-PLANE

NUMBER	REAL	IMAG	DAMPING	FREQUENCY
1	-1.013303			
2	-1.005209			
3	-1.000392			
4	-5.090219			
6	-9.572584	0.791795	9.965966E-01	9.605274E+00
8	-12.248342	1.567404	9.919112E-01	1.234822E+01
10	-7.896777	6.165940	7.881898E-01	1.001888E+01
11	-17.293930			
12	-25.011749			
14	-7.681919	21.380539	3.381319E-01	2.271870E+01
16	-16.932022	20.992416	6.278123E-01	2.696988E+01
18	-14.261611	33.662659	3.900974E-01	3.655910E+01
20	-6.251226	35.371292	1.740347E-01	3.591943E+01
22	-16.159561	35.818222	4.112392E-01	3.929474E+01
24	-22.058914	32.533920	5.611935E-01	3.930714E+01
26	-9.925739	40.293793	2.391842E-01	4.149831E+01
28	-13.225443	40.912445	3.075900E-01	4.299689E+01
30	-33.674622	22.408234	8.325238E-01	4.044884E+01
32	-7.380591	147.426270	5.000031E-02	1.476109E+02
34	-18.239471	146.982559	1.231482E-01	1.481099E+02
36	-19.691284	143.373672	1.360651E-01	1.447196E+02
38	-26.942505	149.447433	1.774206E-01	1.518566E+02
40	-23.399048	188.200195	1.233807E-01	1.895492E+02
42	-11.963984	219.641251	5.438994E-02	2.199668E+02
44	-23.507065	469.643799	4.999039E-02	4.702317E+02
46	-24.157578	477.839844	5.049133E-02	4.784500E+02
48	-31.554672	539.892334	5.834666E-02	5.408137E+02
50	-26.593765	571.815430	4.645740E-02	5.724333E+02
52	-27.649902	607.891846	4.543793E-02	6.085203E+02

THE FOLLOWING POLES MATCHED ZEROS AND WERE ELIMINATED IN ABOVE LISTS

NUMBER	REAL	IMAGINARY
2	-1.1766090	23.5027618
4	-27.1470642	542.287109
6	-29.1265259	552.700684
8	-30.3554840	606.320557

Table 10. Closed-loop poles and zeros, slew command to slew response for $\underline{x}_1$, $\underline{x}_4$ plant (sheet 2 of 2).

	UNIQUE ZEROS			
1	-1.005443			
2	-1.000397			
3	-6.136703			
4	-9.495000			
6	-4.506025	6.337749	5.794539E-01	7.776331E+00
8	0.881102	6.590878	-1.325062E-01	6.649511E+00
9	-16.858185			
11	-15.017513	7.981828	8.830240E-01	1.700691E+01
12	-24.974045			
14	-16.935242	20.978592	6.281349E-01	2.696115E+01
16	-19.075562	33.889740	4.905069E-01	3.838948E+01
18	-16.168900	35.824432	4.113781E-01	3.930423E+01
20	-6.251682	35.371613	1.740454E-01	3.591983E+01
22	-11.387846	40.522385	2.705458E-01	4.209212E+01
24	-47.406754	25.131973	8.835236E-01	5.365646E+01
26	18.161652	57.403748	-3.016471E-01	6.020827E+01
28	-17.331757	116.419693	1.472502E-01	1.177027E+02
30	-13.793817	146.473846	9.375769E-02	1.471219E+02
32	-7.372199	147.483704	4.992420E-02	1.476578E+02
34	-24.665848	145.225693	1.674469E-01	1.473055E+02
36	-62.854874	142.773788	4.029234E-01	1.559971E+02
38	-23.409515	183.197205	1.234369E-01	1.896476E+02
40	-11.964111	219.641068	5.439056E-02	2.199267E+02
42	-23.507019	469.644043	4.999026E-02	4.702319E+02
44	-24.157547	477.839344	5.049127E-02	4.784500E+02
46	-31.527542	539.855957	5.830060E-02	5.407756E+02
48	-26.593735	571.815430	4.645735E-02	5.724333E+02
50	-27.662201	607.906250	4.545701E-02	6.085354E+02

THE FOLLOWING ZEROS MATCHED POLES AND WERE ELIMINATED IN THE ABOVE LISTS

2	-1.1766090	23.5027618
4	-27.1470642	542.287109
6	-29.1265259	552.700684
8	-30.3554840	606.320557

For the specific case under consideration here, singular perturbation theory suggests that the observer be modified.

$$\dot{\hat{\underline{x}}} = A_1\hat{\underline{x}} + B_1\underline{u} + \bar{G}(\bar{y} - \hat{y})$$

$$\hat{y} = T_3C_1\hat{x}_1 + T_3C_4A_4^{-1}B_4T_2\bar{u} \qquad (49)$$

The dc correction term $T_3C_4A_4^{-1}B_4T_2$ is a 4×10 matrix (dim $[\bar{y}]$ × dim $[\bar{u}]$). $C_4A_4^{-1}B_4$ represents the static deformation of residual modes due to unit loads at the actuators as observed at the sensors. This matrix will converge for a large enough number of residual modes because the static displacement of a structure is smooth and bounded. Table 11 shows the convergence of $T_3C_4A_4^{-1}B_4T_2$ as one, two, three, etc., of the $\underline{x}_4$ modes are included.

The modified observer was implemented for the $\underline{x}_1$, $\underline{x}_4$ plant, and the closed-loop characteristics are given in Table 12. The correction term returns the observer poles to "prespillover" values, but has a less pronounced effect on the residual modes.* This is intuitively correct: the dc term is fundamentally a low-frequency correction.

The $\underline{x}_1\underline{x}_4$ plant serves to illustrate the effect of residual modes, but it assumes that T_2 and T_3 completely suppress the $\underline{x}_2$ and $\underline{x}_3$ modes. If the modified controller is applied to an $\underline{x}_1\underline{x}_2\underline{x}_3\underline{x}_4$ plant, an interesting comparison is available.

(1) Table 13 gives the poles of an unmodified controller on an $\underline{x}_1\underline{x}_2\underline{x}_3$ plant.

(2) Table 14 gives the poles of a modified controller on an $\underline{x}_1\underline{x}_2\underline{x}_3\underline{x}_4$ plant.

(3) Table 12 gives the poles of a modified controller of an $\underline{x}_1\underline{x}_4$ plant.

* Compare Tables 6, 10, and 12.

Table 11. The dc correction term as a function of number of x_4 modes.

TRANSFER MATRIX		KK = 1						
.37758D-18	.21831D-13	-.23894D-13	-.21116D-13	-.70232D-17	.37900D-14	-.89189D-14	-.58186D-13	-.46396D-24	-.46598D-13
.78133D-18	.45175D-13	-.49443D-13	-.43696D-13	-.14533D-16	.78426D-14	-.18456D-13	-.12041D-12	-.96007D-24	-.96426D-13
-.12047D-27	-.69655D-23	.76237D-23	.67374D-23	.22409D-26	-.12093D-23	.28457D-23	.18565D-22	.14803D-33	.14868D-22
.27857D-15	.16106D-10	-.17628D-10	-.15579D-10	-.51815D-14	.27961D-11	-.65801D-11	-.42929D-10	-.34230D-21	-.34379D-10
TRANSFER MATRIX		KK = 2						
-.26888D-09	-.35069D-11	.21977D-09	-.21116D-13	-.12852D-09	.31053D-12	-.89189D-14	-.55079D-13	.48057D-11	-.75821D-13
-.11132D-16	.45175D-13	-.49434D-13	-.43696D-13	-.20227D-16	.78426D-14	-.18456D-13	-.12041D-12	.21292D-18	-.96426D-13
.23944D-09	.31423D-11	-.19572D-09	-.50824D-21	.11444D-09	-.27315D-12	-.31834D-21	-.27673D-14	-.42795D-11	.26023D-13
-.16057D-12	.16104D-10	-.17497D-10	-.15579D-10	-.82062D-13	.27963D-11	-.65801D-11	-.42929D-10	.28749D-14	-.34379D-10
TRANSFER MATRIX		KK = 3						
-.26888D-09	-.36120D-11	.21984D-09	.44169D-13	-.12852D-09	.25684D-12	.30203D-13	.27050D-12	.48057D-11	.33418D-12
-.50217D-17	-.11930D-11	.74619D-12	.72536D-12	.90191D-15	-.62458D-12	.44240D-12	.37149D-11	.21292D-18	.47334D-11
.23944D-09	.31423D-11	-.19572D-09	-.73413D-20	.11444D-09	-.27315D-12	-.44131D-20	-.27673D-14	-.42795D-11	.26023D-13
-.19162D-12	.63073D-08	-.40599D-08	-.39230D-08	-.47673D-11	.32160D-08	-.23481D-08	-.19530D-07	.28749D-14	-.24574D-07
TRANSFER MATRIX		KK = 4						
-.26888D-09	-.35609D-11	.21988D-09	-.59482D-13	-.12852D-09	.10696D-12	-.28245D-13	.30412D-12	.48057D-11	.44280D-12
.16994D-16	-.17506D-11	.31018D-12	.18556D-11	.43262D-15	.10099D-11	.10798D-11	.33483D-11	.21293D-18	.35489D-11
.23944D-09	.31423D-11	-.19572D-09	-.41940D-19	.11444D-09	-.27315D-12	-.23923D-19	-.27673D-14	-.42795D-11	.26023D-13
-.35379D-12	.10415D-07	-.84814D-09	-.12249D-07	-.13103D-11	-.88238D-08	-.70431D-08	-.16829D-07	.28749D-14	-.15849D-07
TRANSFER MATRIX		KK = 5						
-.57907D-09	-.83089D-11	.47545D-09	-.59482D-13	-.10931D-08	-.34977D-11	-.28245D-13	.26766D-12	-.10624D-10	.42142D-12
.16572D-16	-.17506D-11	.31018D-12	.18556D-11	.43131D-15	.10099D-11	.10798D-11	.33483D-11	.19196D-18	.35489D-11
.51622D-09	.73790D-11	-.42378D-09	-.25548D-19	.97517D-09	.29433D-11	-.14730D-19	.29767D-13	.94887D-11	.45103D-13
.14344D-11	.10415D-07	-.84961D-09	-.12249D-07	.42506D-11	-.88237D-08	-.70431D-08	-.16829D-07	.91827D-13	-.15849D-07
TRANSFER MATRIX		KK = 6						
-.57931D-09	-.82592D-11	.47965D-09	-.59482D-13	-.10918D-08	-.34602D-11	-.28245D-13	.26728D-12	-.93410D-11	.42183D-12
.17030D-16	-.17506D-11	.31017D-12	.18556D-11	.42889D-15	.10099D-11	.10798D-11	.33483D-11	-.22200D-17	.35489D-11
.56138D-09	-.18403D-11	-.12029D-08	.93304D-20	.73660D-09	-.40074D-11	.49475D-20	.10000D-12	-.22853D-09	-.31818D-13
.13407D-11	.10415D-07	-.84800D-09	-.12249D-07	.47457D-11	-.88237D-08	-.70431D-08	-.16829D-07	.58576D-12	-.15849D-07
TRANSFER MATRIX		KK = 7						
-.57931D-09	-.82576D-11	.47966D-09	-.14559D-13	-.10918D-08	-.35040D-11	-.41767D-14	.33270D-12	-.93410D-11	.43915D-12
.15326D-16	-.17465D-11	.33103D-12	.19742D-11	.43806D-15	.89411D-12	.11433D-11	.35210D-11	-.22200D-17	.35946D-11
.56138D-09	-.18403D-11	-.12029D-08	-.65783D-20	.73660D-09	-.40074D-11	-.35759D-20	.10000D-12	-.22853D-09	-.31818D-13
.12408D-11	.10656D-07	.37596D-09	-.52937D-08	.52836D-11	-.15615D-07	-.33167D-08	-.67015D-08	.58576D-12	-.13168D-07
TRANSFER MATRIX		KK = 8						
-.57931D-09	-.82171D-11	.47968D-09	.35567D-13	-.10918D-08	-.34250D-11	.20925D-13	.35439D-12	-.93410D-11	.52602D-12
.11135D-15	-.27192D-11	-.30751D-12	.77013D-12	-.42952D-15	-.10045D-11	.54032D-12	.29999D-11	-.22200D-17	.15078D-11
.56138D-09	-.18403D-11	-.12029D-08	-.51610D-20	.73660D-09	-.40074D-11	-.28661D-20	.10000D-12	-.22853D-09	-.31818D-13
.15586D-11	.74371D-08	-.17370D-08	-.92780D-08	.24126D-11	-.21897D-07	-.53119D-08	-.84258D-08	.58576D-12	-.20074D-07

Table 12. Closed-loop poles and zeros, slew command to slew response for $\underline{x}_1$, $\underline{x}_4$ plant, dc correction included (sheet 1 of 2).

----------UNIQUE POLES----------

S-PLANE

NUMBER	REAL	IMAG	DAMPING	FREQUENCY
1	-1.012940			
2	-1.005177			
3	-1.000744			
5	-11.691469	0.472293	9.991851E-01	1.170100E+01
7	-12.271549	0.426408	9.993969E-01	1.227895E+01
9	-11.907424	0.984103	9.966022E-01	1.194802E+01
10	-10.437132			
11	-6.378399			
12	-25.977539			
14	-29.046371	4.679237	9.872715E-01	2.942085E+01
16	-8.324968	22.054962	3.531443E-01	2.357384E+01
18	-18.976929	21.119812	6.683630E-01	2.839314E+01
20	-21.148926	30.951050	5.641731E-01	3.748659E+01
22	-17.792923	35.337494	4.497226E-01	3.956421E+01
24	-12.101912	35.529961	3.224223E-01	3.753435E+01
26	-6.467656	35.431305	1.795734E-01	3.601677E+01
28	-11.851106	39.740463	2.857761E-01	4.146989E+01
30	-10.121757	40.692001	2.413852E-01	4.193196E+01
32	-7.380593	147.426270	5.000032E-02	1.476109E+02
34	-18.347107	146.270096	1.244578E-01	1.474162E+02
36	-22.092773	145.536942	1.500824E-01	1.472042E+02
38	-24.123764	146.663467	1.623029E-01	1.486342E+02
40	-22.358002	211.578491	1.050872E-01	2.127565E+02
42	-15.382879	219.692368	6.984901E-02	2.202303E+02
44	-23.507050	469.644043	4.999033E-02	4.702319E+02
46	-24.166153	477.837158	5.050949E-02	4.784478E+02
48	-31.528839	539.871094	5.830133E-02	5.407910E+02
50	-26.542984	572.176514	4.633968E-02	5.727917E+02
52	-27.664230	607.903076	4.546058E-02	6.085322E+02

THE FOLLOWING POLES MATCHED ZEROS AND WERE ELIMINATED IN ABOVE LISTS

NUMBER	REAL	IMAGINARY
2	-1.1766090	23.5027618
4	-27.1470642	542.287109
6	-29.1354675	552.672607
8	-30.3554840	606.320557

Table 12. Closed-loop poles and zeros, slew command to slew response for $\underline{x}_1$, $\underline{x}_4$ plant, dc correction included (sheet 2 of 2).

	UNIQUE ZEROS			
1	-1.005224			
2	-1.000748			
3	-10.105846			
5	-11.938153	0.917469	9.970599E-01	1.197336E+01
7	-12.161644	1.020272	9.964994E-01	1.220437E+01
9	-5.328587	6.326995	6.441776E-01	8.271921E+00
11	0.908837	6.610736	-1.361979E-01	6.672915E+00
12	-25.982590			
14	-18.977676	21.116013	6.684443E-01	2.839081E+01
16	-19.410522	34.196396	4.936393E-01	3.932126E+01
18	-12.101197	35.529922	3.224047E-01	3.753418E+01
20	-6.467691	35.431274	1.795745E-01	3.601674E+01
22	-11.176970	40.432083	2.664449E-01	4.194852E+01
24	-48.030716	25.204117	8.854890E-01	5.424202E+01
26	17.952332	57.502731	-2.980137E-01	6.023994E+01
28	-17.155441	116.653046	1.454988E-01	1.179078E+02
30	-24.617371	145.735733	1.665584E-01	1.478002E+02
32	-13.782695	146.511215	9.365910E-02	1.471581E+02
34	-7.372384	147.483429	4.992554E-02	1.476676E+02
36	-63.925949	140.004272	4.153513E-01	1.539082E+02
38	-22.359856	211.578995	1.050910E-01	2.127571E+02
40	-15.383151	219.692276	6.965033E-02	2.202302E+02
42	-23.507019	469.644043	4.999026E-02	4.702319E+02
44	-24.166122	477.837158	5.050943E-02	4.784478E+02
46	-31.501404	539.835449	5.825463E-02	5.407537E+02
48	-26.542953	572.176758	4.633960E-02	5.727920E+02
50	-27.676620	607.917236	4.547985E-02	6.085469E+02

THE FOLLOWING ZEROS MATCHED POLES AND WERE ELIMINATED IN THE ABOVE LISTS

2	-1.1766090	23.5027618
4	-27.1470642	542.287109
6	-29.1354675	552.672607
8	-30.3554840	606.320557

Table 13. Closed-loop transfer characteristics, slew command to slew response for $\underline{x}_1$, $\underline{x}_2$, $\underline{x}_3$ plant model, unmodified controller only 20 $\underline{x}_3$ states included (sheet 1 of 2).

----------UNIQUE POLES----------

S-PLANE

NUMBER	REAL	IMAG	DAMPING	FREQUENCY
1	-1.012941			
2	-1.005194			
3	-1.000739			
4	-6.379978			
6	-12.005651	0.081773	9.999768E-01	1.200593E+01
8	-11.606636	0.748193	9.979287E-01	1.163073E+01
10	-12.472207	0.679230	9.985204E-01	1.249069E+01
11	-10.235530			
13	-1.137719	22.723770	5.000474E-02	2.275223E+01
15	-1.238274	22.667587	5.454620E-02	2.270137E+01
17	-8.324394	22.063034	3.530094E-01	2.358119E+01
18	-25.991760			
20	-28.966324	4.450431	9.884021E-01	2.930621E+01
22	-19.033051	21.091461	6.699308E-01	2.840962E+01
24	-21.172241	30.944992	5.646721E-01	3.749475E+01
26	-17.795383	35.359543	4.495526E-01	3.958524E+01
28	-12.000372	35.537125	3.199365E-01	3.750861E+01
30	-6.481998	35.369781	1.802616E-01	3.595883E+01
32	-11.847546	39.729340	2.857707E-01	4.145822E+01
34	-10.118307	40.696686	2.412816E-01	4.193567E+01
36	-2.345032	46.851089	4.999029E-02	4.690974E+01
38	-6.953511	138.882172	5.000507E-02	1.390561E+02
40	-6.742848	135.219208	4.980417E-02	1.353972E+02
42	-7.380596	147.426270	5.000034E-02	1.476109E+02
44	-18.366852	146.334412	1.245357E-01	1.474825E+02
46	-22.378693	146.381577	1.511233E-01	1.480823E+02
48	-23.743332	145.588058	1.609592E-01	1.475114E+02
50	-19.276627	217.058807	8.846015E-02	2.179131E+02
52	-18.671051	217.720505	8.544332E-02	2.185196E+02
54	-13.010483	259.864033	5.000003E-02	2.600095E+02
56	-13.408322	267.809590	5.000026E-02	2.681650E+02
58	-14.782457	295.295654	4.999727E-02	2.956653E+02
60	-14.874912	297.126465	4.999995E-02	2.974935E+02
62	-16.131378	322.224121	4.999998E-02	3.226277E+02
64	-18.711212	373.756104	5.000002E-02	3.742941E+02
66	-18.828568	376.067383	5.000438E-02	3.765383E+02

THE FOLLOWING POLES MATCHED ZEROS AND WERE ELIMINATED IN ABOVE LISTS

NUMBER	REAL	IMAGINARY
2	-1.1766090	23.5027618
4	-6.8957253	137.739807
6	-6.8707829	137.243713
8	-7.3594818	146.595718
10	-14.9596577	298.818848
12	-15.2212582	304.044189
14	-15.5341215	310.316162
16	-18.6623230	372.779541

Table 13. Closed-loop transfer characteristics, slew command to slew response for $\underline{x}_1$, $\underline{x}_2$, $\underline{x}_3$ plant model, only 20 $\underline{x}_3$ states included (sheet 2 of 2).

	UNIQUE ZEROS			
1	-1.005041			
2	-1.000743			
3	-10.402925			
5	-11.584787	0.713611	9.981082E-01	1.160674E+01
7	-12.481441	0.648710	9.986520E-01	1.249829E+01
9	-5.330287	6.329798	6.441309E-01	8.275161E+00
11	0.908833	6.610667	-1.361986E-01	6.672847E+00
13	-1.137522	22.724045	4.999546E-02	2.275250E+01
15	-1.238297	22.667603	5.454719E-02	2.270140E+01
16	-25.980469			
18	-19.039398	21.097260	6.699724E-01	2.841818E+01
20	-6.482110	35.369690	1.802651E-01	3.595876E+01
22	-12.000528	35.537201	3.199396E-01	3.750873E+01
24	-19.411072	34.196762	4.936458E-01	3.932185E+01
26	-11.175798	40.430679	2.664275E-01	4.194685E+01
28	-2.344983	46.851273	4.998907E-02	4.690991E+01
30	-48.028412	25.204819	8.854744E-01	5.424031E+01
32	17.952896	57.511246	-2.979821E-01	6.024823E+01
34	-6.953391	138.882324	5.000774E-02	1.390563E+02
36	-6.742861	135.219193	4.980427E-02	1.353872E+02
38	-7.372448	147.483505	4.992595E-02	1.476676E+02
40	-13.777969	146.527878	9.361672E-02	1.471742E+02
42	-17.142822	116.658615	1.453872E-01	1.179114E+02
44	-24.610794	145.780350	1.664655E-01	1.478432E+02
46	-63.770187	139.704300	4.152500E-01	1.535706E+02
48	-19.269455	217.055725	8.842874E-02	2.179094E+02
50	-18.678070	217.723923	8.547390E-02	2.185236E+02
52	-13.009518	259.879853	4.999717E-02	2.602051E+02
54	-13.408503	267.829590	5.000093E-02	2.681650E+02
56	-14.761139	295.238525	4.993498E-02	2.956072E+02
58	-14.871689	297.111328	4.999170E-02	2.974[illegible]E+02
60	-16.123550	322.178223	4.998290E-02	3.225813E+02
62	-18.711029	373.754395	4.999975E-02	3.742224E+02
64	-18.983688	376.566406	5.034864E-02	3.770447E+02

THE FOLLOWING ZEROS MATCHED POLES AND WERE ELIMINATED IN THE ABOVE LISTS

2	-1.1766090	23.5027618
4	-6.8707829	137.243713
6	-6.8957291	137.739944
8	-7.3594780	146.595718
10	-14.9596624	298.818548
12	-15.2212658	304.044189
14	-15.5341244	310.316162
16	-18.6623230	372.779541

The $\underline{x}_2\underline{x}_3$ spillover effects are small, and if residual modes are included and accounted for with a dc correction, the low-frequency effect is also small.

3.4 Discussion

For purposes of controller design, the dynamics of the M2V2 spacecraft were modeled by a 44-mode state space model. As a starting point, this model can be assumed to be an accurate representation. Then, one control option is the optimal regulator discussed in Section 3.2. The regulator meets $\underline{x}_1$ performance requirements with minimum control cost. Its deficiencies are dimension, and control spillover into modes 23, 26, 28, 29, and 30. The discussion in Section 3.3 motivates an alternate controller design (Eq. (49)) which is a synthesis of transform, singular perturbation, and optimal linear feedback ideas. The performance cost associated with this alternate is higher, but it is of dimension 22 instead of 88, and the excitation of modes 23, 26, 28, and 30 is dramatically lower. The closed-loop poles of this controller and an $\underline{x}_1$, $\underline{x}_2$, $\underline{x}_3$,$\underline{x}_4$ plant are given in Table 14.

The 44-mode model is, in fact, not a complete representation of the M2V2 vehicle. If distributed mass and stiffness are acknowledged, then high-frequency residual modes must be accounted for. In theory, both the regulator and the reduced-order design can be made asymptotically correct by subtracting a dc residual correction from the system measurement. In fact, this procedure is more valid for the reduced-order design because a frequency separation can be identified.

Table 14. Closed-loop transfer characteristics, slew command to slew response for $\underline{x}_1$, $\underline{x}_2$, $\underline{x}_3$, $\underline{x}_4$ plant model, modified controller, (only 20 $\underline{x}_3$ states included) (sheet 1 of 2).

----------UNIQUE POLES----------

S-PLANE

NUMBER	REAL	IMAG	DAMPING	FREQUENCY
1	-1.012940			
2	-1.005191			
3	-1.000743			
4	-11.768886			
5	-6.378666			
6	-12.244505			
7	-10.205903			
9	-11.521297	1.143831	9.951079E-01	1.157794E+01
11	-12.427792	1.004272	9.967509E-01	1.246830E+01
13	-1.137719	22.723770	5.000474E-02	2.275223E+01
15	-1.238747	22.667480	5.456723E-02	2.270129E+01
17	-8.325666	22.057739	3.531312E-01	2.357669E+01
18	-25.983063			
20	-29.033757	4.677201	9.872760E-01	2.941301E+01
22	-18.970261	21.234848	6.662224E-01	2.847437E+01
24	-21.155258	30.951843	5.642784E-01	3.749081E+01
26	-17.793549	35.343033	4.496790E-01	3.956944E+01
28	-12.023295	35.550656	3.203576E-01	3.753025E+01
30	-6.483103	35.364166	1.803190E-01	3.595351E+01
32	-11.851348	39.739105	2.857903E-01	4.146867E+01
34	-10.121520	40.692688	2.413762E-01	4.193256E+01
36	-2.345033	46.851089	4.999031E-02	4.690974E+01
38	-6.953498	138.882217	5.000496E-02	1.390562E+02
40	-6.743121	135.218048	4.980661E-02	1.353561E+02
42	-7.380596	147.426270	5.000034E-02	1.476109E+02
44	-18.347488	146.269669	1.244607E-01	1.474159E+02
46	-22.091125	145.535660	1.500728E-01	1.472027E+02
48	-24.125168	146.664932	1.623105E-01	1.486359E+02
50	-22.371307	211.548839	1.051635E-01	2.127285E+02
52	-15.372473	219.695892	6.980091E-02	2.202330E+02
54	-13.010403	259.684033	5.000003E-02	2.600095E+02
56	-13.408273	267.829590	5.000008E-02	2.681652E+02
58	-14.782454	295.295554	4.999726E-02	2.956653E+02
60	-14.874912	297.126465	4.999995E-02	2.974915E+02
62	-16.131378	322.224121	4.999998E-02	3.226277E+02
64	-18.711212	[illegible]	[illegible]	[illegible]
66	-18.828568	376.067383	5.000438E-02	3.765383E+02
68	-23.507050	469.644043	4.999033E-02	4.702319E+02
70	-24.166168	477.837158	5.050952E-02	4.784478E+02
72	-31.528854	539.671094	5.830136E-02	5.407910E+02
74	-26.542969	572.176514	4.633965E-02	5.727917E+02
76	-27.664230	607.903076	4.546058E-02	6.085322E+02

THE FOLLOWING POLES MATCHED ZEROS AND WERE ELIMINATED IN ABOVE LISTS

NUMBER	REAL	IMAGINARY
2	-1.1766090	23.5027618
4	-6.8957253	137.739807
6	-6.8707829	137.243713
8	-7.3588905	146.597519
10	-14.9596577	298.818848
12	-15.2212582	304.044189
14	-15.5341005	310.315674
16	-18.6623230	372.779541
18	-27.1470642	542.287109
20	-29.1354828	552.672607
22	-30.3554840	606.320557

Table 14. Closed-loop transfer characteristics, slew command to slew response for $\underline{x}_1$, $\underline{x}_2$, $\underline{x}_3$, $\underline{x}_4$ plant model, modified controller, (only 20 $\underline{x}_3$ states included) (sheet 1 of 2).

	UNIQUE ZEROS			
1	-1.005238			
2	-1.000746			
3	-10.095799			
5	-11.704855	1.117005	9.954774E-01	1.175805E+01
7	-12.409084	1.115681	9.959826E-01	1.245914E+01
9	-5.327983	6.327348	6.441139E-01	8.271802E+00
11	0.908804	6.610687	-1.361941E-01	6.672852E+00
13	-1.137522	22.724045	4.999546E-02	2.275250E+01
15	-1.239771	22.667511	5.456824E-02	2.270132E+01
16	-25.981216			
18	-18.975922	21.240570	6.662331E-01	2.848241E+01
20	-6.483232	35.364090	1.803229E-01	3.595346E+01
22	-12.023262	35.552948	3.203561E-01	3.753093E+01
24	-19.409821	34.196930	4.936200E-01	3.932138E+01
26	-11.176941	40.432022	2.664447E-01	4.194644E+01
28	-2.344982	46.651273	4.998995E-02	4.690991E+01
30	-48.032059	25.202240	8.855086E-01	5.424234E+01
32	17.952667	57.507050	-2.979984E-01	6.024416E+01
34	-6.953958	138.832355	5.000749E-02	1.390563E+02
36	-6.743133	135.218033	4.980670E-02	1.353960E+02
38	-7.372416	147.433536	4.992573E-02	1.476677E+02
40	-13.777948	146.524420	9.362507E-02	1.471603E+02
42	-17.165115	116.640549	1.455944E-01	1.173968E+02
44	-24.619522	145.734302	1.665735E-01	1.477997E+02
46	-63.645566	140.049118	4.148039E-01	1.539156E+02
48	-22.371918	211.548874	1.051665E-01	2.127285E+02
50	-15.372672	219.695653	6.980181E-02	2.202331E+02
52	-13.009515	259.879883	4.999716E-02	2.602051E+02
54	-13.409455	267.829346	5.000085E-02	2.681646E+02
56	-14.761032	295.238525	4.993462E-02	2.956072E+02
58	-14.871675	297.111323	4.999165E-02	2.974832E+02
60	-16.123535	322.178223	4.998066E-02	3.225813E+02
62	-18.711029	373.754395	4.999975E-02	3.742224E+02
64	-18.984787	376.567139	5.035149E-02	3.770452E+02
66	-23.507019	469.644043	4.999026E-02	4.702319E+02
68	-24.166122	477.837158	5.050943E-02	4.784478E+02
70	-31.500599	539.834473	5.825321E-02	5.407527E+02
72	-26.5-2938	570.176758	4.633138E-02	5.727920E+02
74	-27.676941	607.917725	4.548034E-02	6.095474E+02

THE FOLLOWING ZEROS MATCHED POLES AND WERE ELIMINATED IN THE ABOVE LISTS

2	-1.1766090	23.5027618
4	-6.8957300	137.739944
6	-6.8707829	137.243713
8	-7.3588877	146.597519
10	-14.9596615	298.818848
12	-15.2212658	304.044189
14	-15.5341024	310.315674
16	-18.6623230	372.779541
18	-27.1470642	542.287109
20	-29.1354675	552.672607
22	-30.3554840	606.320557

CHAPTER 4

SUMMARY AND SUGGESTIONS FOR FUTURE WORK

The contribution of this research is a candidate reduced-order control architecture for application to lightly damped, flexible spacecraft. The resulting controller is attractive in terms of dimension, performance, and stability, but there are areas where further investigation is necessary. The intent of this chapter is to highlight key points in the theoretical development of the candidate architecture, and to indicate assumptions, limitations, and areas of concern.

The plant of interest is specifically a distributed stiffness, distributed mass, flexible, lightly damped spaceborne structure with six rigid-body degrees of freedom. The deformations of the structure are assumed to be small and elastic. Within these constraints linear theory applies, and the system response can be described by a separable partial differential equation (PDE) in space and time. If modal coordinates are used, and a third assumption, "modal damping", is made, then the solution to the PDE is

$$q[\underline{y},t] = \sum_{i=1}^{\infty} \phi_i \xi_i \tag{50a}$$

where

$$\ddot{\xi}_i + 2\zeta_i\omega_i\dot{\xi}_i + \omega_i^2\xi_i = \frac{1}{m_i}\int_S \phi_i \cdot F[\underline{y},t]\, d\underline{y} \tag{50b}$$

$$m_i = \int_S \phi_i^2 \rho \, d\underline{y} \tag{50c}$$

$F[\underline{y},t]$ is the force input to the system and can be selected to control $q[\underline{y},t]$.

For purposes of this research, the control design objective is to regulate pointing and to add damping to those structural modes which impact system performance. However, before discussing the controller, several comments are appropriate.

(1) The simple form of Eq. (50) is due to two assumptions: linear structural theory, and a viscous approximation for structural damping. These assumptions are basic to the work of this text, and if they are not valid the results presented here may not apply.

(2) Equation (50b) is a semiinfinite set of second-order differential equations which describe the dynamics of the modal amplitudes. In reality, this set will be truncated; a limitation due to the state-of-the-art in structural modeling. The truncated description is accurate at low frequencies, but becomes increasingly inaccurate at higher frequencies.[23]

(3) The eigenfrequencies λ_i are densely spaced for a structure, with the potential for multiplicities of four or greater. In general, there will be no evident frequency separation between high- and low-frequency eigenvalues. The mode shapes ϕ_i are functions of spatial variables only.

(4) The time response of any particular modal coordinate ξ_i depends on the spatial and temporal characteristics of $F[\underline{y},t]$. The spatial characteristics govern the amplitude of response through the factor $\int_S \phi_i \cdot F[\underline{y},t] \, d\underline{y}$.

The temporal characteristics of F determine the actual response dynamics. If F is periodic in time, then the λ_i response can be described with a Bode plot. In this thesis, point actuators were used— either axial member actuators, or CMG torques. For this special case, the spatial characteristics of F are determined by the actuator locations, and by the way the m controls are coupled together.

$$\int_S \phi_i \cdot F[\underline{y},t]\, d\underline{y} = \sum_{k=1}^{m} \phi_i[\underline{y}_K]\, u_K[t]$$

where

m = the number of actuators.

If the control law $\underline{u}[t]$ is chosen to be a feedback signal (for all the advantages that feedback gives), then two bodies of control theory are available: classical and optimal.

Classical theory is based in the frequency domain and presents the designer with a set of powerful scalar tools to shape the frequency characteristics of input/output paths. Given a modal description of a system, the designer may phase-stabilize, gain-stabilize, notch-filter, cross feed inputs and outputs, or put dynamic compensation in the forward or feedback paths. The flexibility allowed by classical theory is both a strength and a source of criticism. Classical designs are nonunique and depend heavily on the experience and capability of the designer.

In contrast to classical techniques, optimal theory provides a feedback design which is fixed in configuration—a cascade of regulator gains and an optimal estimator. The gains of the regulator and the

dynamics of the estimator can be uniquely selected to minimize a weighted cost function of mean-square input and mean-square state deviations. Knowledge of the system eigenspectrum is not needed in the design.

Both approaches (classical and optimal) have their strengths, but in the spacecraft context neither is adequate. Classical theory is not tractable for systems with large numbers of inputs and outputs. Optimal theory can handle the multiple-input/multiple-output problem, but requires that the dimension of the controller match the dimension of the plant. This is clearly not feasible.

The control design approach which is developed in this thesis borrows classical ideas: Chapter 1 discusses categorizing modes with the intent of treating them differently in the design process and Appendix A develops input/output transform theory, which is a linear-algebraic extension of crossfeed. These ideas are blended with a reduced-order optimal regulator estimator to make up the candidate architecture discussed in detail in Chapter 1. The philosophy is to use the regulator within the bandwidth, to use the input and output transforms to decouple $\underline{x}_2$ and $\underline{x}_3$ states, and to use a singular perturbation correction to account for the high-frequency $\underline{x}_4$ states.

From a fundamental point of view, categorizing modes and using different techniques to account for them allows the designer to use information he might otherwise discard. Transforms, for instance, exploit spatial information. The advantages of this control design approach are illustrated in Chapter 3. Reduced-order designs are exhibited, which have near optimal performance and which are stable when tested against an evaluation model.

There are areas of concern, however. One serious issue that must be faced is that of the design sensitivity to parameter variations

(robustness). Ideally, a reduced-order controller should be insensitive to both the order reduction scheme and to the parameter changes within the retained model. This area has not been completely explored in this research. Two points can be made, however.

(1) At high frequencies, eigenvectors are less sensitive to parameter variations than their corresponding eigenvalues (see Appendix G).

(2) Small changes in a transform correspond to small changes in zero locations. Recall that a transform will place zeros on top of poles of suppressed modes. If the transform is perturbed, these zeros move smoothly in the frequency plane (see Appendix A, F-8 example).

The insensitivity of spatial information and the smoothness of zero movement are indications that using transforms may be a robust-order reduction scheme.

A second concern is the effect of measurement noise. Designs in this thesis are deterministic and output transforms look attractive. If measurements were noisy, an alternate set of conclusions may be reached. The concern is not that $\underline{\bar{y}}$ will have dramatically different noise characteristics than $\underline{y}$, but that the covariance of an $[A_1, T_3C_1]$ observer will be larger than the covariance of a [A, C] design.

Future work is certainly needed in the two areas just discussed. In addition, there are two other areas that may prove interesting. Appendix A indicates that transform capabilities are enhanced if transforms are given memory. This extension parallels the classical idea of a crossfeed filter. Then, Appendix C discusses making an adaptive transform. An algorithm is presented, and it is illustrated that when system outputs are run through a fast-Fourier transform (FFT), and the results are arrayed spatially, that mode-shape information can be constructed. This is a potentially powerful idea. An issue which remains is the impact of noise on the Fourier coefficient values.

CHAPTER 5

CONCLUSIONS

A new controller design methodology for application to flexible structures has been developed. This investigation shows that the spatial shaping of system inputs can effectively reduce the excitation of a defined subset of modes. When the subset is chosen to create a frequency separation between controlled and residual modes, a reduced order regulator can be used to control the performance-related modes. A dc correction term in the regulator measurement equation will adequately prevent the residual modes from causing instability.

The reduced order design methodology has been applied to two plants: the F-8 aircraft and the Draper Laboratory M2V2 space optical satellite design. For the F-8, spatial shaping of the control reproduces the rudder coordination crossfeed gains of a classical design. For the M2V2 satellite, a 22-state reduced order regulator is shown to have essentially the same quadratic cost as an 88-state, full-state feedback regulator.

APPENDIX A

TRANSFORM METHODOLOGY

Input and output transformations are integral to the control architecture which is developed in this thesis. They are used to shape the input and feedback control signals so that control authority is delivered only to the system modes of interest. The need to focus the control effort in this way is indicated earlier in the text; the interest here is in a detailed description of the transform methodology in terms of linear algebra, frequency domain, and crossfeed control ideas.

A.1 Concept Motivation

For discussions in this appendix, the finite dimensional system Σ_0, described by

$$\Sigma_0: \quad \begin{bmatrix} \dot{\underline{x}}_1 \\ \dot{\underline{x}}_2 \end{bmatrix} = \begin{bmatrix} A_{11} & 0 \\ 0 & A_{22} \end{bmatrix} \begin{bmatrix} \underline{x}_1 \\ \underline{x}_2 \end{bmatrix} + \begin{bmatrix} B_1 \\ B_2 \end{bmatrix} \underline{u} \qquad \text{(A-1)}$$

$$\underline{y} = \begin{bmatrix} C_1 & C_2 \end{bmatrix} \begin{bmatrix} \underline{x}_1 \\ \underline{x}_2 \end{bmatrix}$$

will be used. The block diagram description is given in Figure A-1. The following definitions hold.

$\underline{x}_1$ = the vector of state variables that describes the modes which have unacceptable dynamics or which are excited by external disturbances. These modes are to be controlled.

$\underline{x}_2$ = the vector of state variables that describes the modes which have acceptable open-loop dynamic characteristics.

Equation (A-1) is in the block diagonal canonical form described in Appendix E. In this form, there is no dynamic coupling between modes; the coupling is solely in the input distribution and output matrices.

The intent is to provide a reduced-order feedback controller for Σ_0; specifically, a controller based on the dynamic description of the $\underline{x}_1$ states. The control law to be applied has the form

$$\underline{u} = K\hat{\underline{x}} \tag{A-2}$$

$$\dot{\hat{\underline{x}}} = A_{11}\hat{\underline{x}} + B_1\underline{u} + G[\underline{y} - C_1\underline{x}_1] \tag{A-3}$$

where K and G are gain matrices. Using this control law, the closed-loop dynamics are given by

$$\begin{bmatrix} \dot{\underline{x}}_1 \\ \dot{\underline{x}}_2 \\ \dot{\hat{\underline{x}}} \end{bmatrix} = \begin{bmatrix} A_{11} & 0 & +B_1K \\ 0 & A_{22} & +B_2K \\ GC_1 & GC_2 & A_{11} + B_1K - GC_1 \end{bmatrix} \begin{bmatrix} \underline{x}_1 \\ \underline{x}_2 \\ \hat{\underline{x}} \end{bmatrix} \tag{A-4}$$

Introducing the variable

$$\underline{e} = \hat{\underline{x}} - \underline{x}_1 \tag{A-5}$$

There are special cases, investigated by Balas,[14] when a control law based on only $[A_{11}, B_1, C_1]$ will be adequate. He defines the quantity $B_2K\,\hat{\underline{x}}$ as "control spillover"; the quantity $GC_2\underline{x}_2$ as "observation spillover", and proves the following results.

(1) If $GC_2 = 0$ and $B_2K = 0$, the case of no observation or control spillover, then $\underline{x}_2$ and $\underline{e}$ will be uncoupled from $\underline{x}_1$ and a controller based on $[A_{11}, B_1, C_1]$ will be adequate. Because G and K will in general be nonzero, the zero spillover condition typically occurs only when $C_2 = 0$ and $B_2 = 0$.

(2) If $GC_2 = 0$ and $B_2K \neq 0$, the case of only control spillover, the $\underline{x}_2$ states will be excited by the controller, but the system will be stable if $[A_{11} - B_1K]$, A_{22}, and $[A_{11} - GC_1]$ are all stable.

(3) If $GC_2 \neq 0$ and $B_2K = 0$, the case of only observation spillover, the time response of the $\underline{x}_1$ states may be slower than ideal (case a), but the system will again be stable if $[A_{11} - B_1K]$, and $[A_{11} - GC_1]$ are all stable.

The control methodology presented in this thesis was motivated originally by Balas' discussion.[14] The transforms T_2 and T_3 (see Figure A-2) were introduced to minimize the control and observation spillover. The objective is to choose T_2 such that

$$B_1T_2 \neq 0,\ B_2T_2 = 0 \qquad \text{(A-7)}$$

and T_3 such that

$$T_3C_1 \neq 0,\ T_3C_2 = 0. \qquad \text{(A-8)}$$

If these conditions are met, then $[A_{11}, B_1T_2, T_3C]$ will be controllable and observable, and there will be no control or observation spillover from the controller.

In addition to the transforms in the feedback loop, the methodology allows a transform on the commanded input. The purpose of this transform is to shape the command to avoid exciting the $\underline{x}_2$ states.

This appendix discusses the solution of Eq. (A-7) and (A-8), and comments on the existence of solutions. In addition, the state space and frequency-domain interpretations of the transform concept are developed and related to classical crossfeed design concepts. Finally, the use of dynamic transforms is discussed and applied to a design example.

A.2 State Space Formulation

A controller configuration which provides authority to specified states, and at the same time eliminates spillover, is clearly of interest. Equations (A-7) and (A-8) offer one specification for such a configuration. Alternatively, referring to Figure A-2, one can look at three signal paths: $\underline{r}$ to $\underline{x}$, $\underline{\bar{u}}$ to $\underline{x}$, and $\underline{u}$ to $\underline{\bar{y}}$. In each of these paths, the transform, T_1, T_2, or T_3 can be chosen to exclude information about specified modes. The condition of zero observation spillover corresponds to a $\bar{y}$ which contains information only about the $\underline{x}_1$ states. Similarly, for zero control spillover from either the system input r, or the feedback control u, the output of the $\underline{r}$ to $\underline{x}$, and the $\underline{\bar{u}}$ to $\underline{x}$ signal paths must contain only $\underline{x}_1$ information. This alternate specification will be used in the following discussions.

A.2.1 Transformation Selection

In this section the actual choice of the required transforms will be addressed. The same methodology applies to the selection of all three transforms; the discussions here will focus first on the choice of T_2. Then, the results will be generalized to also include T_1 and T_3. Note that T_2 and T_3 can be chosen independently, but, because T_1 operates on the closed-loop system, it may be coupled to the choice of T_2 and T_3.

The following result applies specifically to the $\bar{u}$ to x signal path.

Theorem 1:

Given a system Σ_0, with $\underline{x}\epsilon R^n$ and $\underline{u}\epsilon R^m$

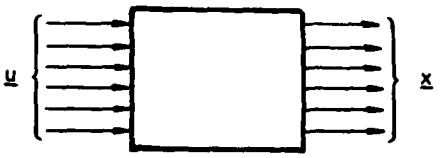

Σ_o

$$\dot{\underline{x}} = A\underline{x} + B\underline{u} \qquad \text{(A-9)}$$

$$\underline{y} = C\underline{x}$$

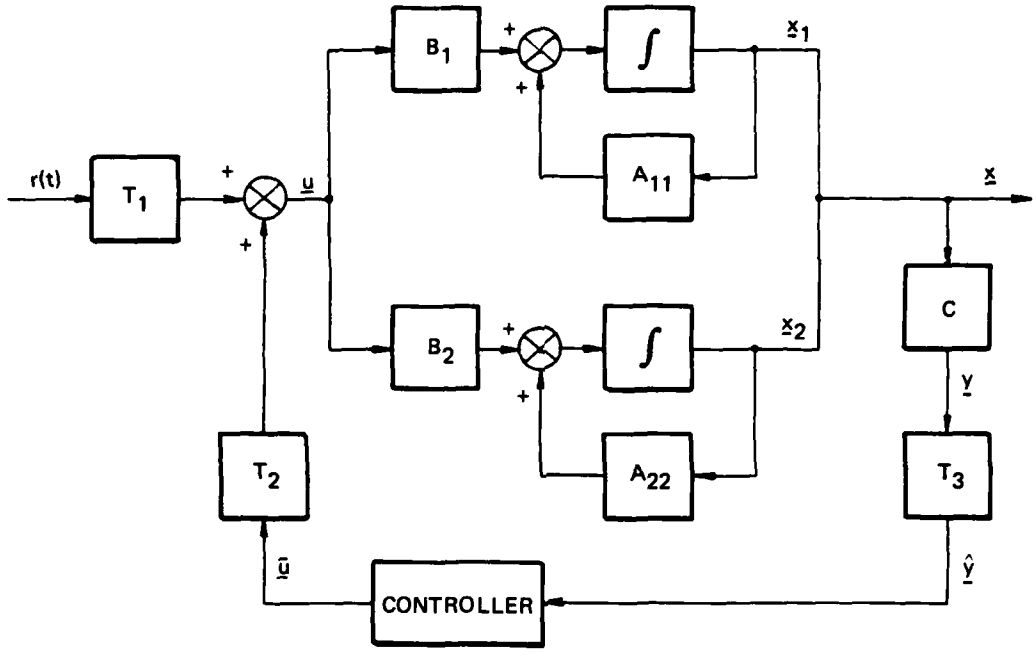

Figure A-2. Block diagram description: input/output transforms.

where Eq. (A-9) is in the block diagonal form given in Appendix E, a control can be constructed which does not excite r primary states where $r = m - 1$.

Discussion:

Assume Eq. (A-9) is in a block diagonal representation of Σ_0, and introduce as before the notation that $\underline{x}_1$ represents the states to be controlled, and $\underline{x}_2$ represents the states to be suppressed. The system Σ_0 can then be represented as

$$\begin{bmatrix} \dot{\underline{x}}_1 \\ \dot{\underline{x}}_2 \end{bmatrix} = \begin{bmatrix} A_1 & 0 \\ 0 & A_2 \end{bmatrix} \begin{bmatrix} \underline{x}_1 \\ \underline{x}_2 \end{bmatrix} + \begin{bmatrix} B_1 \\ B_2 \end{bmatrix} \underline{u} \qquad \text{(A-10)}$$

where $\underline{u} = T_2 \bar{\underline{u}}$ (see Figure A-3).

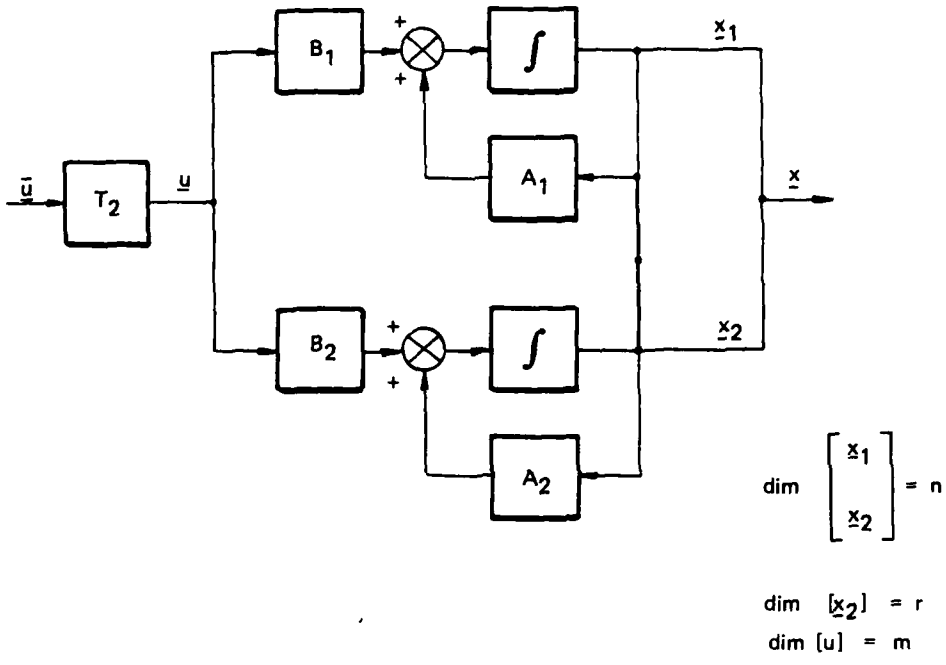

Figure A-3. $\bar{u}$ to $\underline{x}$ signal path.

To suppress $\underline{x}_2$, a singular transformation T_2 must be chosen such that

$$B_1 T_2 \neq 0$$

$$B_2 T_2 = 0 \qquad \text{(A-11)}$$

Depending on the dimensions r and m, a solution to Eq. (A-11) may not exist. (See Bryson and Ho[24] Appendix A.)

(1) If $r < m$, at least one T_2 exists although its form may not be unique.

(2) If $r \geq m$, the condition $B_2 T_2 = 0$ can only be met by $T_2 = 0$, in which case $B_1 T_2 = 0$ also.

From a geometric viewpoint, the rows of B_2 and the columns of T_2 are contained in the space R^r. If $r \leq m$, R^r will in general be completely specified by B_2, and no nonzero vectors, V, will exist in R^r for which $B_2 \cdot \underline{V} = 0$. On the other hand, if $r > m$, the rows of B_2 will only span a subspace of R^r, and the columns of T_2 can be chosen in the null space of B_2. The dimension of the null space must be at least one for Eq. (A-11) to be satisfied.

The focus of the theorem is on maximizing the suppressed subspace, given a system dimension and a control dimension. This approach results in a T_2 which is an [r × 1] matrix, and in a scalar control $\bar{u}$. Alternatively, if r and n are specified, then T_2 can be chosen to be a matrix of dimension mx[m - r], and $\underline{\bar{u}}$ will have dimension [m - r] × 1. In this case, the columns of T_2 are again chosen to span the null space of B_2. Note though, that unless r = 0, T_2 will be a singular transformation.

A.2.2 Dynamic Transforms

Theorem 1 establishes that for the system of interest, described in Eq. (A-9), a control can be constructed which does not excite r primary states where r = m - 1. If there is a requirement to suppress more modes than this, two options exist: the dimension of the control vector can be increased by adding actuators, or dynamics can be introduced into the input distribution network. The following theorem applies.

Theorem 2

Given the system Σ_0, with $\underline{x} \varepsilon R^n$ and $\underline{u} \varepsilon R^m$, and described by Eq. (A-9), a control can be constructed which does not excite r primary states where

$$r = p + m - 1$$

where p is the order of the dynamics.

Discussion:

As indicated in Appendix B, if the j^{th} input to a multiple-input/multiple-output system is filtered by a first-order filter, two effects occur: the filter dynamics must be added in parallel with the plant dynamics, and the input distribution vector associated with the j^{th} input is rotated in R^{n+1}. If Σ_0 is driven only by the j^{th} input, and the input is filtered through a first-order lag with characteristics $[a_f, b_f, c_f]$, then Eq. (A-10) can be rewritten

$$\begin{bmatrix} \dot{\underline{x}}_1 \\ \dot{\underline{x}}_2 \\ \dot{x}_f \end{bmatrix} = \begin{bmatrix} A_1 & & \\ & A_2 & \\ & & a_f \end{bmatrix} \begin{bmatrix} \underline{x}_1 \\ \underline{x}_2 \\ x_f \end{bmatrix} + \begin{bmatrix} \underline{b}'_{1j} \\ \underline{b}'_{2j} \\ b_f \end{bmatrix} u_j$$

Expressions for $\underline{b}'_{1j}$ and $\underline{b}'_{2j}$ are available from the results of Appendix B. The key point here, however, is that in R^n, the vector

$$\underline{b}'_j = \begin{bmatrix} \underline{b}'_{1j} \\ \underline{b}'_{2j} \end{bmatrix}$$

is linearly independent from $\underline{b}_j$. Using system linearity, and the above result, it is possible to augment the input matrix of Σ_0 with p additional columns, where p is the number of parallel input filters that are used. For example, for the two-input system

$$\begin{bmatrix} \dot{\underline{x}}_1 \\ \dot{\underline{x}}_2 \end{bmatrix} = \begin{bmatrix} A_1 & 0 \\ 0 & A_2 \end{bmatrix} \begin{bmatrix} \underline{x}_1 \\ \underline{x}_2 \end{bmatrix} + \begin{bmatrix} & \\ \underline{b}_1 & \underline{b}_2 \end{bmatrix} \begin{bmatrix} u_1 \\ u_2 \end{bmatrix} \qquad \text{(A-12)}$$

shown in Figure A-4, introducing dynamics into the input distribution network gives the augmented system

$$\begin{bmatrix} \dot{\underline{x}}_1 \\ \dot{\underline{x}}_2 \\ \dot{\underline{x}}_f \end{bmatrix} = \begin{bmatrix} A_1 & 0 & 0 \\ 0 & A_2 & 0 \\ 0 & 0 & A_f \end{bmatrix} \begin{bmatrix} \underline{x}_1 \\ \underline{x}_2 \\ x_f \end{bmatrix} + \left[\begin{array}{cc:c} \underline{b}_1 & \underline{b}_2 & \underline{B}' \\ \hdashline 0 & 0 & B_f \end{array}\right] \begin{bmatrix} u_1 \\ u_2 \\ u' \end{bmatrix} \qquad \text{(A-13)}$$

where

$$A_f = \begin{bmatrix} A_{f1} & & \\ & A_{f2} & \\ & & \ddots \end{bmatrix}$$

$$B_f = \begin{bmatrix} b_{f1} & & \\ & b_{f2} & \\ & & \ddots \end{bmatrix}$$

and

$$\begin{bmatrix} \underline{b}_1 & \underline{b}_2 & \underline{B}' \end{bmatrix} = \begin{bmatrix} \underline{b}_{11} & \underline{b}_{12} & \underline{B}_1' \\ \hline \underline{b}_{21} & \underline{b}_{22} & \underline{B}_2' \end{bmatrix}$$

Note that the conditions

$$\begin{aligned} [\underline{b}_{11} \ \underline{b}_{12} \ \underline{B}_1']\ T_2 &\neq 0 \\ [\underline{b}_{21} \ \underline{b}_{22} \ \underline{B}_2']\ T_2 &\neq 0 \end{aligned} \qquad \text{(A-14)}$$

can be met if $r \leq p + 1$. As discussed, T_2 is chosen in the null space of $[\underline{b}_{21} \ \underline{b}_{22} \ \underline{B}_2']$.

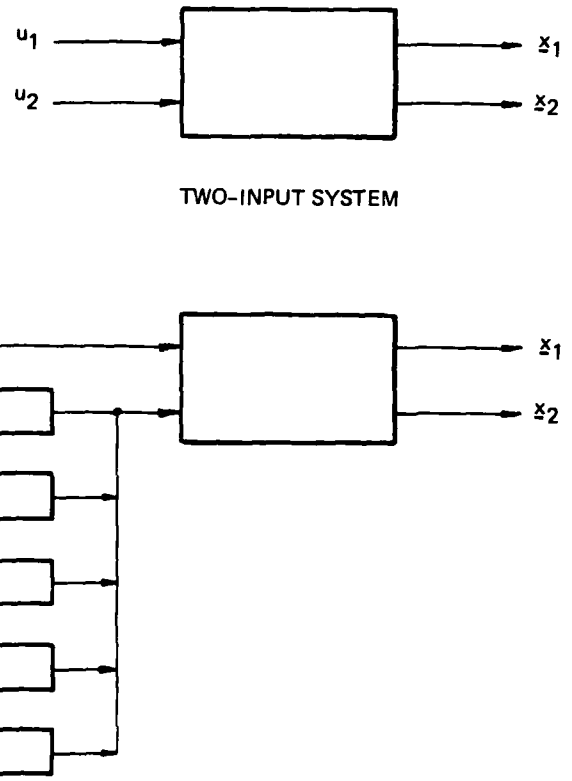

Figure A-4. Two-input system with filtered inputs.

The geometric concepts which motivate the use of transform dynamics are relatively straightforward. The actual choice of filter eigenvalues is more involved. The filters must be chosen to give input distribution vectors which are linearly independent. In addition, the filter dynamics should be significantly faster than the dynamics of the $\underline{x}_1$ states. If these conditions are met, Eq. (A-11) can be satisfied and the $\underline{x}_2$ states suppressed.

It should be stressed that for the multiple-input/multiple-output case, the methodology outlined above will not yield a unique nor an optimal design. Concerns which certainly would arise in any general implementation include how to partition the dynamics among the cross-feeds, and what values for the dynamics eigenvalues are really optimal in some sense.

A.2.3 Generalization

Sections A.2.1 and A.2.2 focus primarily on the $\underline{u}$ to $\underline{x}$ signal path, and on the selection of T_2. The extension to the $\underline{u}$ to $\underline{y}$ signal path is straightforward. The rows of T_3 are chosen to be in the column null space of C_2. If the dimension of the output is ℓ, then q primary states can be suppressed in the output where $q = \ell - 1$. If dynamics are included in the output transform, then the appropriate condition is $q = \ell + p - 1$, where p is the order of the dynamics. These results parallel the input distribution results exactly.

The choice of T_1 is similar to the choice of T_2 in methodology. The difference is that T_1 should be based on closed-loop-system input distribution characteristics. The procedure recommended is to choose T_2 and T_3 to avoid spillover, to choose G and K based on $[A_{11}, B_1T_2, T_3C_1]$, and then block diagonalize the closed-loop system. This will result in a description $[A_{CL}, B_{CL}, C_{CL}]$ that is in the block diagonal canonical form used throughout this appendix. If the columns of B_{CL} which correspond to the $\underline{x}_2$ states are identified, and designated B_{CL_2}, then the rows of T_1 can be chosen in the null space of B_{CL_2}. This procedure will shape the command input so that $\underline{x}_2$ is not excited.

A.3 Frequency Domain Interpretation

The system descriptions used thus far in this appendix, specifically Eq. (A-1), (A-4), and (A-6), are state space descriptions in the time domain. Additional insights are evident if Σ_0 is described in the frequency domain, and the implications of the choices of T_1, T_2, and T_3 are discussed in terms of the effect on pole and zero locations.

Classical control theory, as originally derived, uses scalar functions of complex frequency to describe system response characteristics. The scalar formulation is natural for single-input/single-output plants, but becomes cumbersome for multiple-input/multiple-output systems. The theory has been reformulated in terms of vector functions of frequency,

and is available in the literature. The vector formulation is appropriate for describing MIMO systems, although generalized definitions of scalar concepts are required. Appendix D reviews the vector theory in detail. Of specific interest here are the generalized descriptions of poles and zeros, and the theorems which discuss the conditions under which these quantities are invariant.

A.3.1 System Description

The system under discussion, Σ_0, is described in the time domain by Eq. (A-1), which is repeated here for convenience.

$$\Sigma_0: \begin{bmatrix} \dot{\underline{x}}_1 \\ \dot{\underline{x}}_2 \end{bmatrix} = \begin{bmatrix} A_{11} & 0 \\ 0 & A_{22} \end{bmatrix} \begin{bmatrix} \underline{x}_1 \\ \underline{x}_2 \end{bmatrix} + \begin{bmatrix} B_1 \\ B_2 \end{bmatrix} \underline{u} \qquad \text{(A-1)}$$

$$y = [C_2 \; C_2] \begin{bmatrix} \underline{x}_1 \\ \underline{x}_2 \end{bmatrix}$$

The poles of Σ_0 are given by the eigenvalues of $\begin{bmatrix} A_{11} & 0 \\ 0 & A_{22} \end{bmatrix}$; specifically the poles are the set λ_i, i = 1 to n, where

$$[\lambda_i I - A] = 0 \qquad \text{(A-15)}$$

Because Eq. (A-1) is in block diagonal form, the solutions of Eq. (A-15) are available by inspection.

The zeros of Σ_0 can be determined from the Rosenbrock Matrix P[s]

$$P[s] = \begin{bmatrix} sI - A & -B \\ C & 0 \end{bmatrix} \qquad \text{(A-16)}$$

The actual determination is computationally involved, particularly if multiplicity of zeros occurs. Kontakos[25] has developed a method which derives the complete set of zeros from the minors of P[s]. The subject is discussed further in Appendix D. Note, though, that while determining the entire set of zeros can be complicated, certain subsets of zeros are more readily accessible. Output decoupling zeros occur at those values of complex frequency s for which P[s] loses column rank. Similarly, input decoupling zeros occur at those values of s for which P[s] loses row rank.

A.3.2 Transformation Effects

If transformations are introduced into the command, feedback control, and output paths, the system Σ_0 will have the configuration shown in Figure A-2. As before, it is convenient to focus attention on the three signal paths $\underline{u}$ to $\underline{\bar{y}}$, $\underline{\bar{u}}$ to $\underline{x}$, and $\underline{r}$ to $\underline{x}$. The discussion below will evaluate their transmission-blocking characteristics.

The dynamic relationship between u and $\bar{y}$ can be described by the linear system

$$\begin{bmatrix} \dot{\underline{x}}_1 \\ \dot{\underline{x}}_2 \end{bmatrix} = \begin{bmatrix} A_{11} & 0 \\ 0 & A_{22} \end{bmatrix} \begin{bmatrix} \underline{x}_1 \\ \underline{x}_2 \end{bmatrix} + \begin{bmatrix} B_1 \\ B_2 \end{bmatrix} \underline{u} \qquad \text{(A-17)}$$

$$\bar{y} = [T_3C_1 \; T_3C_2] \begin{bmatrix} \underline{x}_1 \\ \underline{x}_2 \end{bmatrix}$$

The Rosenbrock matrix for this system is

$$P_1[s] = \begin{bmatrix} sI - A_{11} & 0 & -B_1 \\ 0 & sI - A_{22} & -B_2 \\ T_3C_1 & T_3C_2 & 0 \end{bmatrix} \qquad \text{(A-18)}$$

If T_3 is chosed to satisfy Eq. (A-9) specifically

$$T_3C_1 \neq 0 \quad T_3C_2 = 0 \qquad \text{(A-9)}$$

then, the transfer matrix between $\underline{u}$ and $\underline{\bar{y}}$ will be characterized by poles at values of s equal to the eigenvalues of A_{11} and A_{22}, and zeros at values of s equal to eigenvalues of A_{22}. Note that choosing T_3 to avoid observation spillover, will, in effect, place output decoupling zeros at the same locations in the complex plane as the poles of the modes which are to be suppressed in the output.

The relationship between $\underline{\bar{u}}$ and $\underline{x}$ can be described by the system

$$\begin{bmatrix} \dot{\underline{x}}_1 \\ \dot{\underline{x}}_2 \end{bmatrix} = \begin{bmatrix} A_{11} & 0 \\ 0 & A_{22} \end{bmatrix} \begin{bmatrix} \underline{x}_1 \\ \underline{x}_2 \end{bmatrix} + \begin{bmatrix} B_1T_2 \\ B_2T_2 \end{bmatrix} \underline{\bar{u}} \qquad \text{(A-19)}$$

The corresponding Rosenbrock matrix is

$$P_2[s] = \begin{bmatrix} sI - A_{11} & 0 & -B_1T_2 \\ 0 & sI - A_{22} & -B_2T_2 \\ I & 0 & 0 \\ 0 & I & 0 \end{bmatrix} \qquad \text{(A-20)}$$

If T_2 is chosen to null control spillover, specifically to satisfy

$$B_1T_2 \neq 0 \quad B_2T_2 = 0 \tag{A-8}$$

then, $P_2[s]$ will lose row rank at values of s equal to the eigenvalues of $[A_{22}]$. This indicates that the $\bar{u}$ to $\underline{x}$ transfer matrix will have input decoupling zeros on top of the $\underline{x}_2$ poles, and therefore will pass only $\underline{x}_1$ information.

The analysis of the effect of T_1 on the transmission-blocking properties of the $\underline{r}[t]$ to $\underline{x}$ path is more complex because T_1 depends on T_2, T_3, K, and G.

For the special case where T_2 and T_3 are chosen to satisfy Eq. (A-8) and (A-9) and the feedback loop is closed, then the dynamic response of $\underline{x}$ to $\underline{r}[t]$ is given by:

$$\begin{bmatrix} \dot{\underline{x}}_1 \\ \dot{\underline{x}}_2 \\ \dot{\underline{e}} \end{bmatrix} = \begin{bmatrix} A_{11} + B_1T_2K & 0 & -B_1T_2K \\ 0 & A_{22} & 0 \\ 0 & 0 & A_{11} - GT_3C_1 \end{bmatrix} \begin{bmatrix} \underline{x}_1 \\ \underline{x}_2 \\ \underline{e} \end{bmatrix} + \begin{bmatrix} B_1T_1 \\ B_2T_1 \\ 0 \end{bmatrix} \underline{r}(t) \tag{A-21}$$

The poles of this system are given by the eigenvalues of $[A_{11} - B_1T_2K]$, $[A_{22}]$, and $[A_{11} - GC_1]$. The Rosenbrock matrix is

$$P_3(s) = \begin{bmatrix} sI - A_{11} - B_1T_2K & 0 & -B_1T_2K & -B_1T_1 \\ 0 & sI - A_{22} & 0 & -B_2T_1 \\ 0 & 0 & sI - A_{11} + GT_3C_1 & 0 \\ I & 0 & 0 & 0 \\ 0 & I & 0 & 0 \\ 0 & 0 & I & 0 \end{bmatrix} \tag{A-22}$$

In this instance, the choice of T_1 to satisfy

$$B_1T_1 \neq 0 \quad , \quad B_2T_1 = 0 \tag{A-23}$$

will place input decoupling zeros at values of s given by the poles of $[A_{22}]$ and the path $\underline{r}[t]$ to $\underline{x}$ will not pass $\underline{x}_2$ information. However, in the more general case, where T_2 and T_3 do not satisfy Eq. (A-8) and (A-9) exactly, Eq. (A-21) becomes

$$\begin{bmatrix} \dot{\underline{x}}_1 \\ \dot{\underline{x}}_2 \\ \dot{\underline{e}} \end{bmatrix} = \begin{bmatrix} A_{11} + B_1T_2K & 0 & + B_1T_2K \\ + B_2T_2K & A_{22} & + B_2T_2K \\ 0 & GT_3C_2 & A_{11} - GT_3C_1 \end{bmatrix} \begin{bmatrix} \underline{x}_1 \\ \underline{x}_2 \\ \underline{e} \end{bmatrix} + \begin{bmatrix} B_1T_1 \\ B_2T_1 \\ 0 \end{bmatrix} \underline{r}(t) \tag{A-24}$$

and Eq. (A-22) becomes

$$P_3[s] = \begin{bmatrix} sI - A_{11} - B_1T_2K & 0 & - B_1T_2K & - B_1T_1 \\ - B_2T_2K & sI - A_{22} & - B_2T_2K & - B_2T_1 \\ 0 & - GT_3C_2 & sI - A_{11} + GT_3C_1 & 0 \\ I & 0 & 0 & 0 \\ 0 & I & 0 & 0 \\ 0 & 0 & I & 0 \end{bmatrix} \tag{A-25}$$

In general, satisfying Eq. (A-23) will not cause $P_3[s]$ to lose row rank. Instead, Eq. (A-24) must be block diagonalized. Then, as discussed in Section 2.3, some number of the closed-loop modes can be

suppressed by choosing the columns of T_1 in the null space of the rows of the closed-loop input-distribution matrix. This choice of T_1 will again place input decoupling zeros at the same locations in the complex plane as the poles of the suppressed modes.

The discussion so far has assumed a state-space description, Eq. (A-1), and focused on the characteristics of specific signal paths. The description that is chosen uses modal coordinates as state variables. This choice is convenient because it allows an easy identification of the states which correspond to any particular mode; but it is not unique. A possible concern involves the potential changes in the poles and zeros of the signal paths with changes in state variable choice. Theorems are given in Appendix D, which establish the invariance of poles and zeros under state transformations.

A.4 Correspondance to Classical Crossfeed

The design objectives, as motivated earlier in the text, are to produce a feedback controller with specified authority, which does not excite the suppressed $\underline{x}_2$ states, and, in addition, to shape the command input so that again, only the modes of interest respond. Transformations T_1, T_2, and T_3 have been introduced into the control configuration specifically to meet these objectives. Appropriate transformations exist within some constraints, as detailed earlier, but these transformations will in general be singular. In effect, the inputs of a multiple-input/multiple-output system are coupled into specific linear combinations. The structure of each combination is chosen so that the $\underline{x}_2$ states will not be excited. In general, the number of appropriate linear combinations is fewer than the number of system inputs. Similarly, the system outputs are combined linearly to form observation residuals which do not contain suppressed mode information.

The idea of coupling inputs to avoid exciting a mode, or the idea of blending outputs to produce a feedback signal which excludes certain

states, is not new. The classical concept of crossfeed in the input or output has been used extensively. Two representative exar 'os are:

(1) Rudder Crossfeed.

Figure A-5 describes the F-8 lateral dynamics control system.[26] Note the crossfeeds in the command, feedback control, and output feedback paths. Crossfeed between aileron and rudder is provided to prevent a roll command from exciting the clutch roll mode. Note, also, the presence of dynamics in the crossfeed.

(2) Missile Pitch Control

Figure A-6 describes the pitch control loop for a missile.[27] In the design shown, pitch rate output from two locations are blended to suppress the first bending mode information in the feedback signal.

The examples above are given to illustrate that the transform concept, discussed originally in terms of spillover reduction, is just a matrix extension of established design techniques.

A.5 Spatial Filtering

It is worth discussing the actual mechanism which is being exploited in the crossfeed or transform selection. Appendix E derives the system equations of motion and contends that flexible systems are best described by a partial differential equation in space and time. This equation is separable, which uncouples the spatial and temporal descriptions. When a designer controls the spectral content of a signal by using a filter, say a notch filter, he is operating on the temporal characteristics. By contrast, the use of crossfeed operates in the spatial domain; shaping the signal in space. For the systems which are of interest in this report, temporal and spatial methods represent independent uses of the available information.

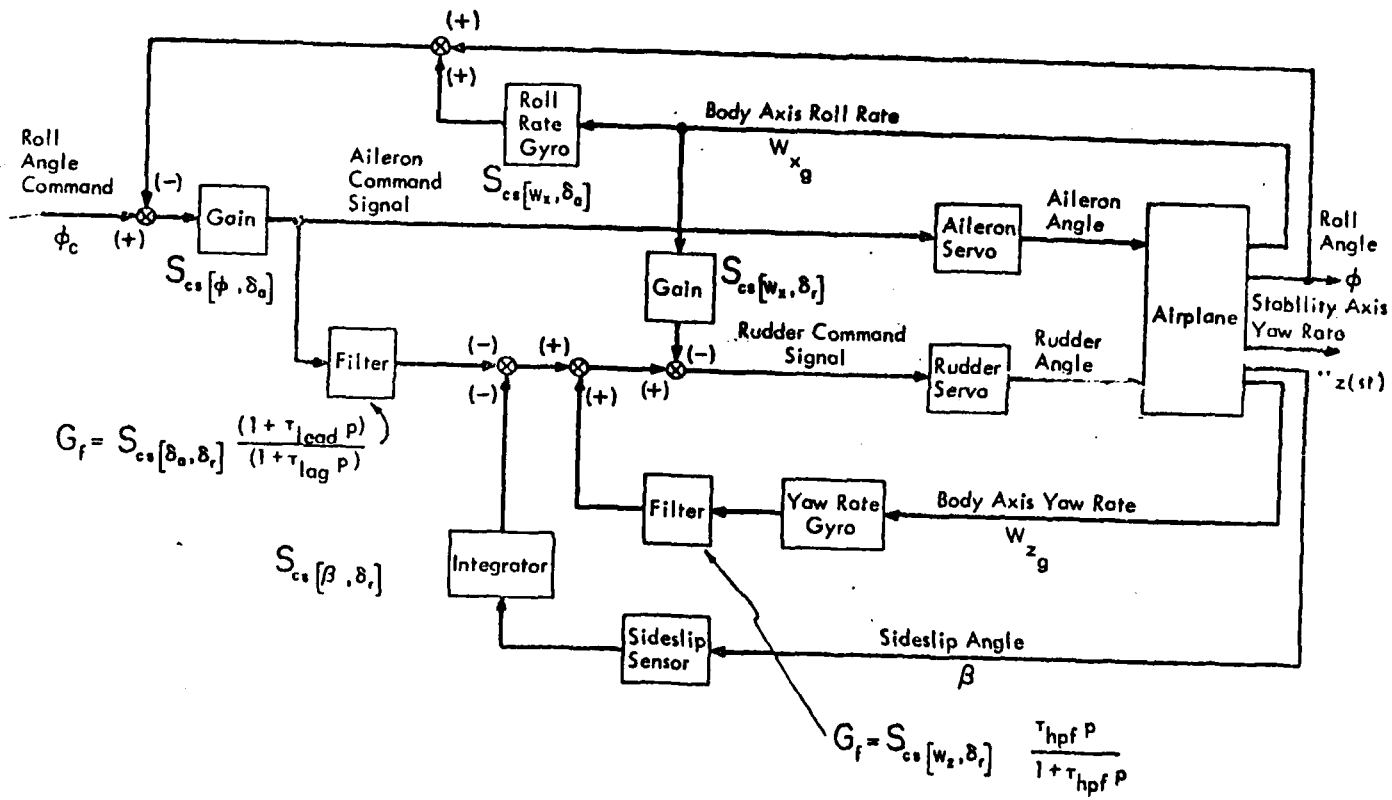

Figure A-5. Functional block diagram of the lateral-directional flight control system.

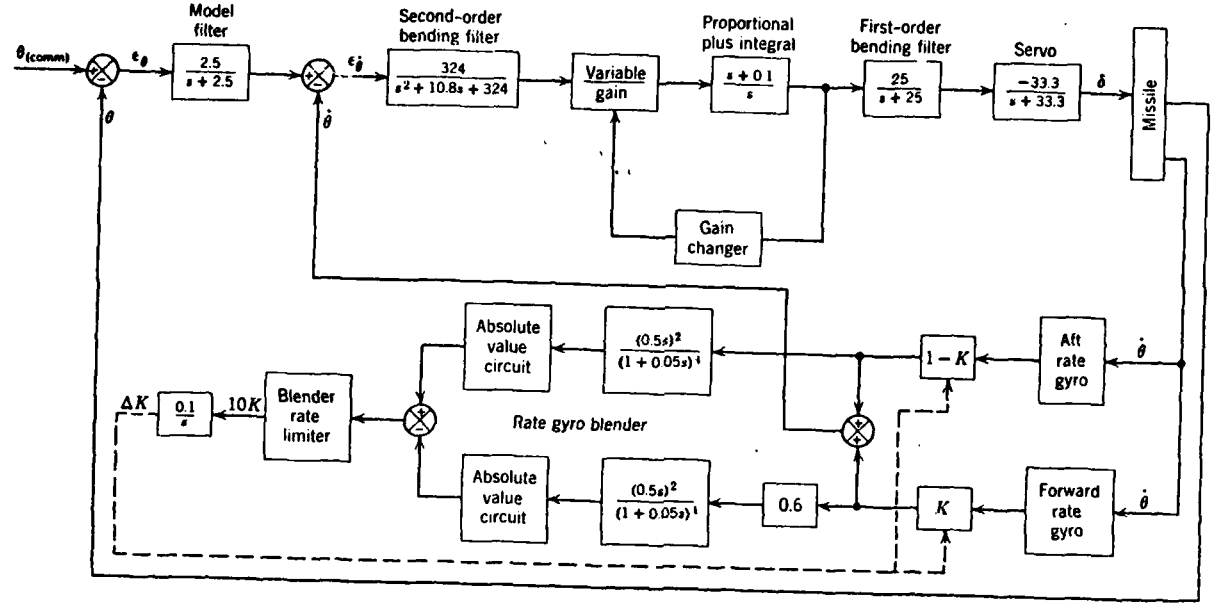

Figure A-6. Block diagram of the control system for an advanced booster system.

A.6 Summary

This appendix applies specifically to the linear dynamic system Σ_0 described by Eq. (A-1) and shown in Figure A-1. A methodology is developed which provides a reduced-order controller for Σ_0. This controller is structured to meet two specific constraints.

(1) It provides feedback control for a specified subset of the system states.

(2) It is decoupled from the remaining states.

Transformations on the system input and output are introduced, as illustrated in Figure A-2. The decoupling mentioned above is achieved by enforcing the conditions

$$\begin{aligned} B_1T_1 &\neq 0 \quad , \quad B_2T_1 = 0 \\ B_1T_2 &\neq 0 \quad , \quad B_2T_2 = 0 \\ T_3C_1 &\neq 0 \quad , \quad T_3C_2 = 0 \end{aligned} \tag{A-26}$$

If solutions to Eq. (A-26) are available (the specific existance conditions are presented in Section A.2.1), then the appropriate reduced-order controller will only depend on $[A_{11}, B_1T_2, T_3C_1]$. This is the key result. Some additional comments are offered to provide insight into the various implications of the use of input/output transforms.

(1) Structural response can be described by a separable partial differential equation in space and time. In contrast to many control system filters, the transforms used here operate in the spatial domain. In effect, decoupling is achieved by a spatial shaping of the input and output.

(2) Picking T_1, T_2, and T_3 to satisfy Eq. (A-26) is equivalent to

   (a) Choosing T_1 and T_2 in the row null space of B_2 and choosing T_3 in the column null space of C_2.

(b) Specifying that the zeros of the $\underline{r}[t]$ to $\underline{x}$, $\underline{\bar{u}}$ to $\underline{x}$, and $\underline{u}$ to $\underline{y}$, cancel the poles which correspond to $\underline{x}_2$.

(c) In Balas' terminology,[14] nulling control and observation spillover.

(3) The transform concept is a vector extension of classical crossfeed techniques.

(4) If the dimension of the system input and output are specified, there are simple limits on the number of $\underline{x}_2$ states from which the controller can be decoupled. If dynamics are used in the crossfeeds, which in effect makes the transforms specified functions of time, then the number of decoupled states can be expanded in direct proportion to the order of the dynamics.

An example—the design of an aircraft rudder coordination system—is included at this point to illustrate the transform concept and methodology.

A.7 Design Example

This design example is intended to illustrate the major points which are detailed earlier in this appendix. The aircraft was chosen as an appropriate plant for three reasons.

(1) It is of relatively low order.

(2) It is a multiple-input system.

(3) Classical design analyses are available to use as a comparison.

An actual aircraft flight controller can be quite complex; the discussion here will be limited to the design of a rudder coordination system. This system is of particular interest because the rudder coordination crossfeed has traditionally been used to prevent a roll command from exciting oscillatory modes.

A.7.1 Aircraft Description

The lateral dynamic response of an F-8 to aileron and rudder inputs is given by Eq. (A-27). This equation is written in body axes and is valid for small perturbations from straight and level flight. The body axis frame has its x axis inclined to the trimmed velocity vector by the angle $\alpha_0 = 7.75°$. The nominal flight conditions are altitude = 20,000 feet, and Mach = 0.56. The state variables are sideslip, β, roll angle ϕ, which are taken about the aircraft x axis, body axis roll rate, ω_x, and body axis yaw rate ω_z.

Aircraft

F-8

At Mach = 0.56, 6706 m altitude

$\alpha_0 = 7.75°$

Lateral Equations

$$\dot{\underline{x}}_c = A_c \underline{x}_c + B_c \underline{u} \qquad \text{(A-27)}$$

where

$$\underline{x}_c = \begin{bmatrix} \phi \\ \omega_x \\ \omega_z \\ \beta \end{bmatrix} \qquad \underline{u} = \begin{bmatrix} \delta_a \\ \delta_r \end{bmatrix}$$

$$A_c = \begin{bmatrix} 0 & 1.0 & 0.1361 & 0 \\ 0 & -2.625 & 1.91 & -29.8 \\ 0 & -0.0759 & -0.426 & 2.65 \\ 0.0555 & 0.1359 & -0.9974 & -0.2173 \end{bmatrix}$$

$$B_c = \left[\underline{b}_a \; \underline{b}_r\right] = \begin{bmatrix} 0 & 0 \\ 27.0 & 6.13 \\ 1.42 & -3.55 \\ 0.002315 & 0.0422 \end{bmatrix}$$

Eigenvalues

-1.9826

-2.856×10^{-2}

$-6.2855 \times 10^{-1} \pm 2.35\ j$

Aircraft lateral dynamics are characterized by three response modes:

(1) The role subsidence mode governs the aircraft response to a pure roll input.

(2) The spiral divergence mode is a very slow, often unstable mode. If it is unstable the resulting motion is a combination of increasing yaw angle and increasing roll angle, and finally a high-speed spiral dive.

(3) The dutch-roll mode is an oscillatory mode, in sideslip, yaw, and roll which is lightly damped.

Aileron and rudder inputs each excite all these modes. The pole zero plots of the significant input-output transfer functions are shown: aileron-to-roll angle (see Figure A-5), aileron-to-roll rate (see Figure A-6), and rudder to sideslip (see Figure A-7). Note that in the aileron transfer functions (see Figure A-8), a pair of complex zeros nearly cancels the oscillatory poles, while in the rudder transfer functions there is no cancellation, and the residues associated with the dutch-roll mode can be expected to be large.

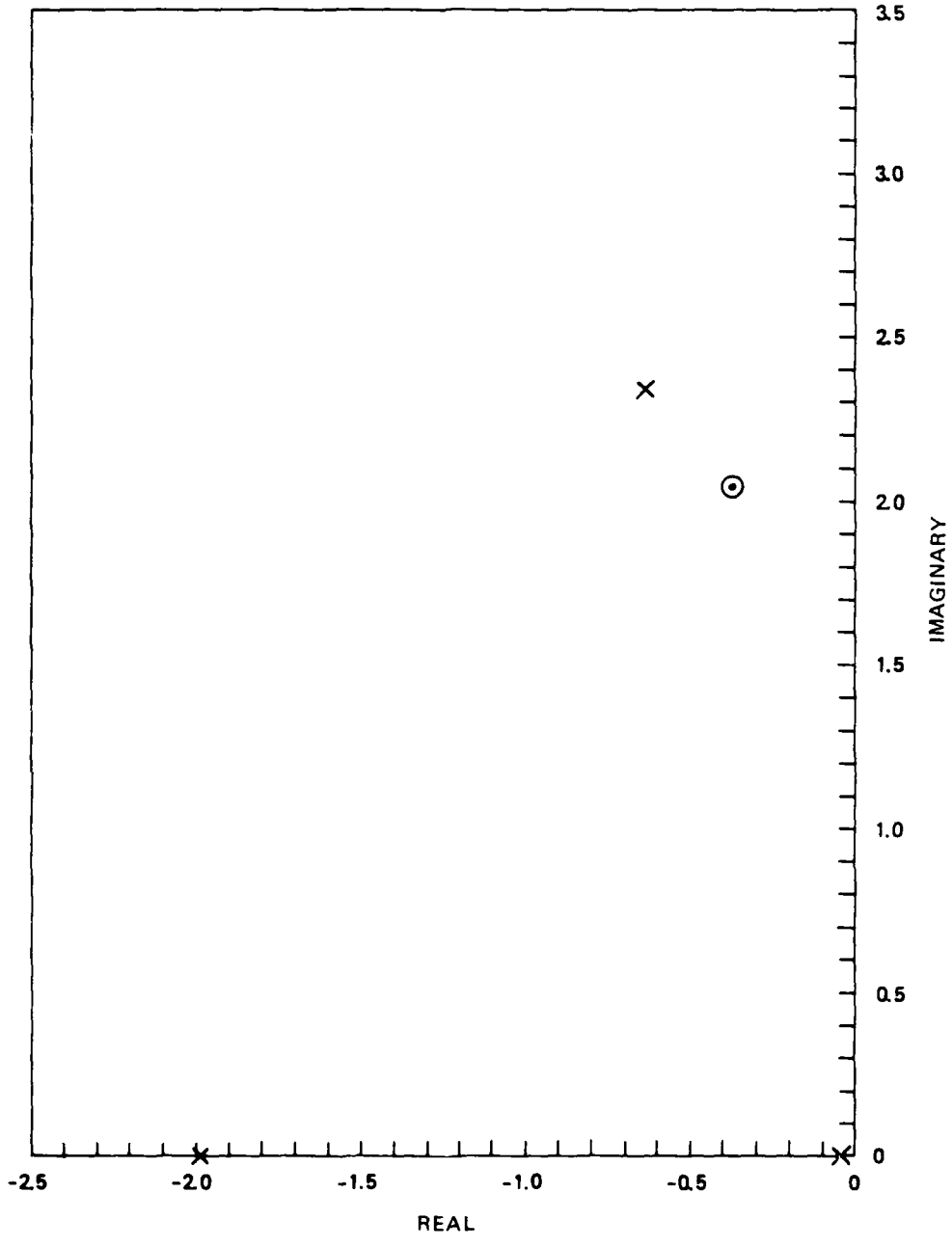

Figure A-7. Pole/zero locations—aileron to roll angle.

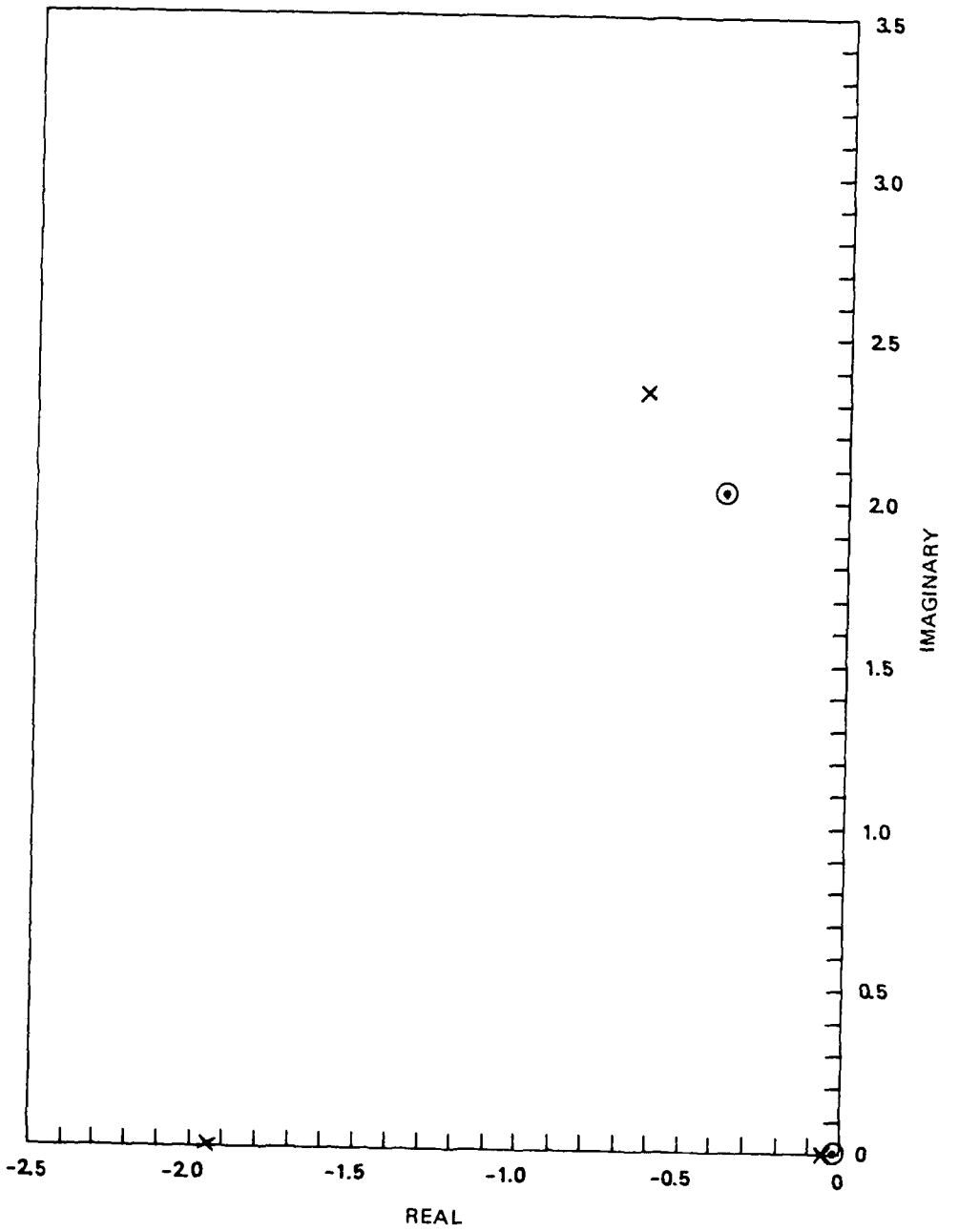

Figure A-8. Pole/zero locations—aileron to ω_x.

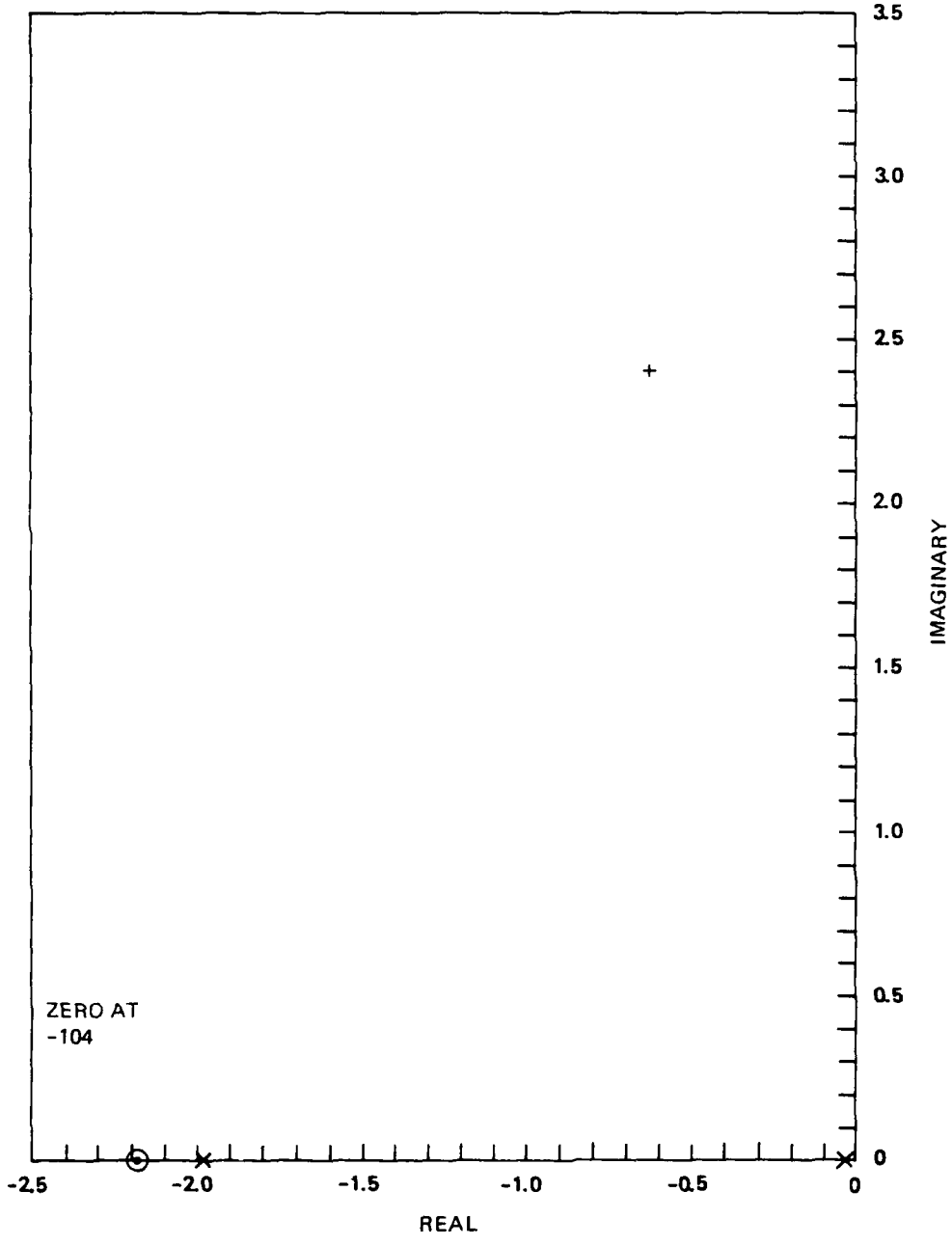

Figure A-9. Pole/zero locations—rudder to sideslip.

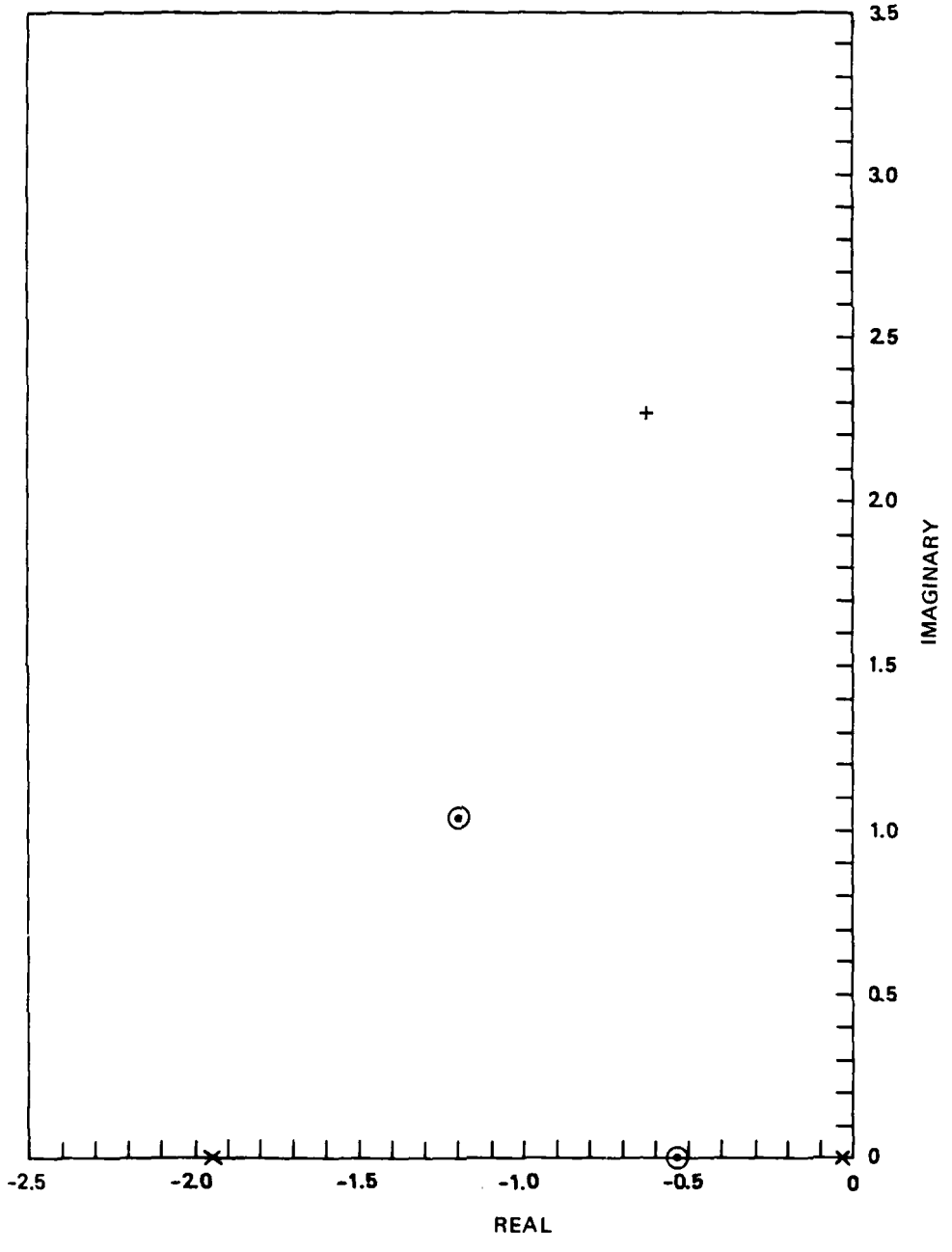

Figure A-10. Pole/zero locations—rudder to ω_z.

A.7.2 Controller Configuration

The lateral controller presented in this section achieves two objectives.

(1) It adds damping to the dutch-roll mode to improve the aircraft disturbance response.

(2) It couples the rudder to the aileron through a dynamic crossfeed to prevent the dutch roll mode from appearing in the response to a roll command.

The baseline controller was designed by Whitaker,[26] and is shown in Figure A-11. Yaw rate feedback, S_{ω_z}, is used to add the required oscillatory mode damping. The crossfeed gain S_{CF}, and the crossfeed-filter time constant, τ_{CF}, are chosen to place the complex zeros of the aileron-to-roll angle transfer function at the same location in the complex plane as the poles of the dutch-roll mode. Figure A-12, shows the design parameters, S_{ω_z}, S_{CF}, and τ_{CF}, in the structure of a state space description. A key point that is evident here is that changes in S_{ω_z} will change the system A matrix, and therefore can be expected to influence both pole and zero locations. By contrast changes in S_{CF} will change only the B matrix, and hence should only affect zero locations.

The influence of S_{ω_z}, S_{CF}, and τ_{CF} on the closed loop system characteristics will be presented two ways. First, the results from Whitaker[26] will be duplicated; then, an alternate design based on transform techniques, will be presented. The two methods produce identical results.

A.7.3 Classical Design Analysis

The analysis presented here duplicates the results obtained by Whitaker.[26] The influences of S_{ω_z}, S_{CF}, and τ_{CF} are investigated parametrically, and presented in terms of changes to the poles and zeros of the aileron-to-roll angle transfer function. Recall that the two objectives of the design are to add damping to the dutch roll, and

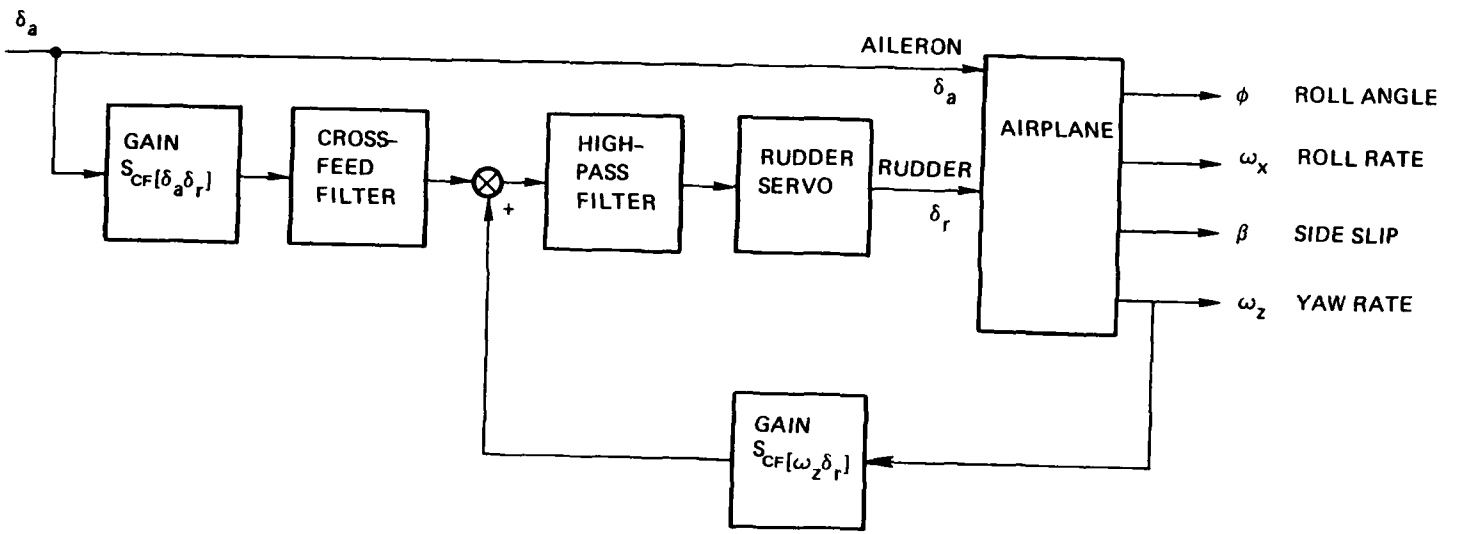

Figure A-11. Functional block diagram of the rudder coordination.

STATE SPACE EQUATIONS

- Aircraft

$$\dot{x}_c = A_c x_c + [\underline{b}_a \; \underline{b}_r] \begin{bmatrix} \delta_a \\ \delta_r \end{bmatrix}$$

- Rudder & Crossfeed — 1^{st} Order Lags

  $\tau_R \qquad \tau_{CF}$

- High-Pass Filter $\quad \frac{s}{s+1}$

  $\tau_{HP} = 1.0$

- Composite Equations

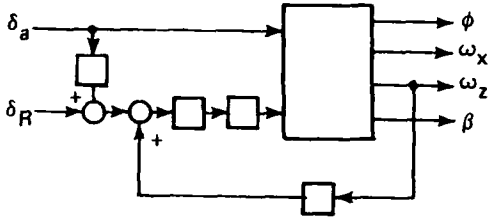

$$x_c = \begin{bmatrix} \phi \\ \omega_x \\ \omega_z \\ \beta \end{bmatrix}$$

$$\begin{bmatrix} \underline{\dot{x}}_c \\ \dot{x}_{HP} \\ \dot{x}_r \\ \dot{x}_{CF} \end{bmatrix} = \left[\begin{array}{c|c|c|c} A_c & & \underline{b}_r & \\ 4\times4 & & & \\ \hline & S_{\omega_z}/\tau_{HP} & -1/\tau_{HP} & 1/\tau_{HP} \\ & S_{\omega_z}/\tau_R & -1/\tau_R \quad -1/\tau_R & 1/\tau_R \\ \hline & & & 1/\tau_{CF} \end{array}\right] \begin{bmatrix} x_c \\ x_{HP} \\ x_r \\ x_{CF} \end{bmatrix} + \left[\begin{array}{c|c} \underline{b}_a & \\ & \\ \hline & 1/\tau_{HP} \\ & 1/\tau_R \\ \hline S_{CF}/\tau_{CF} & 0 \end{array}\right] \begin{bmatrix} \delta_a \\ \delta_R \end{bmatrix} \qquad \text{(A-28)}$$

Figure A-12. Rudder coordination system—state space equations.

then to specifically suppress the effect of this mode in the roll response to an aileron input. In the complex plane, these objectives correspond to moving the aircraft oscillatory poles to the left, and then cancelling them with complex zeros, Figures A-13 to A-20 summarize the key parametric results. Specific effects that should be noted include the following.

(1) The effect of crossfeed with no yaw feedback and no crossfeed filter (see Figures A-13 and A-14). The crossfeed gain, S_{CF}, affects only the B matrix, and therefore the system poles stay at their open-loop locations. The zeros do move, and crossfeed can be chosen to put the complex zeros close to, but not on top of, the oscillatory modes.

(2) The effect of yaw feedback to the rudder with no crossfeed (see Figures A-15 and A-16). Yaw feedback causes both the zeros and the poles to migrate. Increasing the feedback gain adds damping to the oscillatory mode, but also increases the separation between the dutch-roll poles and the complex zeros. The increase in separation increases the residue associated with this mode, and adversely affects the roll angle response.

(3) The effect of crossfeed with the yaw damper loop closed (see Figures A-17 and A-18). The yaw damper gain is chosen to give adequate damping; then rudder crossfeed is added. The trajectory of the complex zeros misses the pole location by a wide margin.

(4) The effect of crossfeed dynamics with the yaw damper loop closed (see Figures A-19 and A-20). This case is identical to the case just discussed, except that a lag filter, $\tau_{CF} = 0.25$, is added to the crossfeed. Note that a crossfeed gain can now be selected so that the complex zeros nearly cancel the damped dutch-roll poles.

STATE SPACE EQUATIONS

- CROSSFEED GAIN

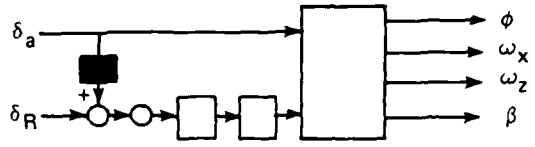

- NO CROSSFEED FILTER
- NO YAW FEEDBACK
- S_{CF} = 0.3, 0.6, 0.9

$$\dot{\underline{x}} = \begin{bmatrix} \text{AIRCRAFT: } A_c & \begin{matrix}0\\0\\0\\0\end{matrix} & \underline{b}_r & \begin{matrix}0\\0\\0\\0\end{matrix} \\ 0 & \begin{matrix}-1.0\\-25.0\end{matrix} & \begin{matrix}\\-25.0\end{matrix} & \begin{matrix}\\\\1/\tau_{CF}\end{matrix} \end{bmatrix} \underline{x} + \begin{bmatrix} \underline{b}_a & \underline{0} \\ \begin{matrix}S_{CF} \times 1\\ S_{CF} \times 25\end{matrix} & \begin{matrix}1.0\\25.0\end{matrix} \\ 0 & 0 \end{bmatrix} \underline{u} \qquad \text{(A-29)}$$

VARIATION: NO CHANGE IN A: SAME POLES, ZEROS CHANGE

Figure A-13. Effect of crossfeed with no yaw feedback and no crossfeed filter—state space equations.

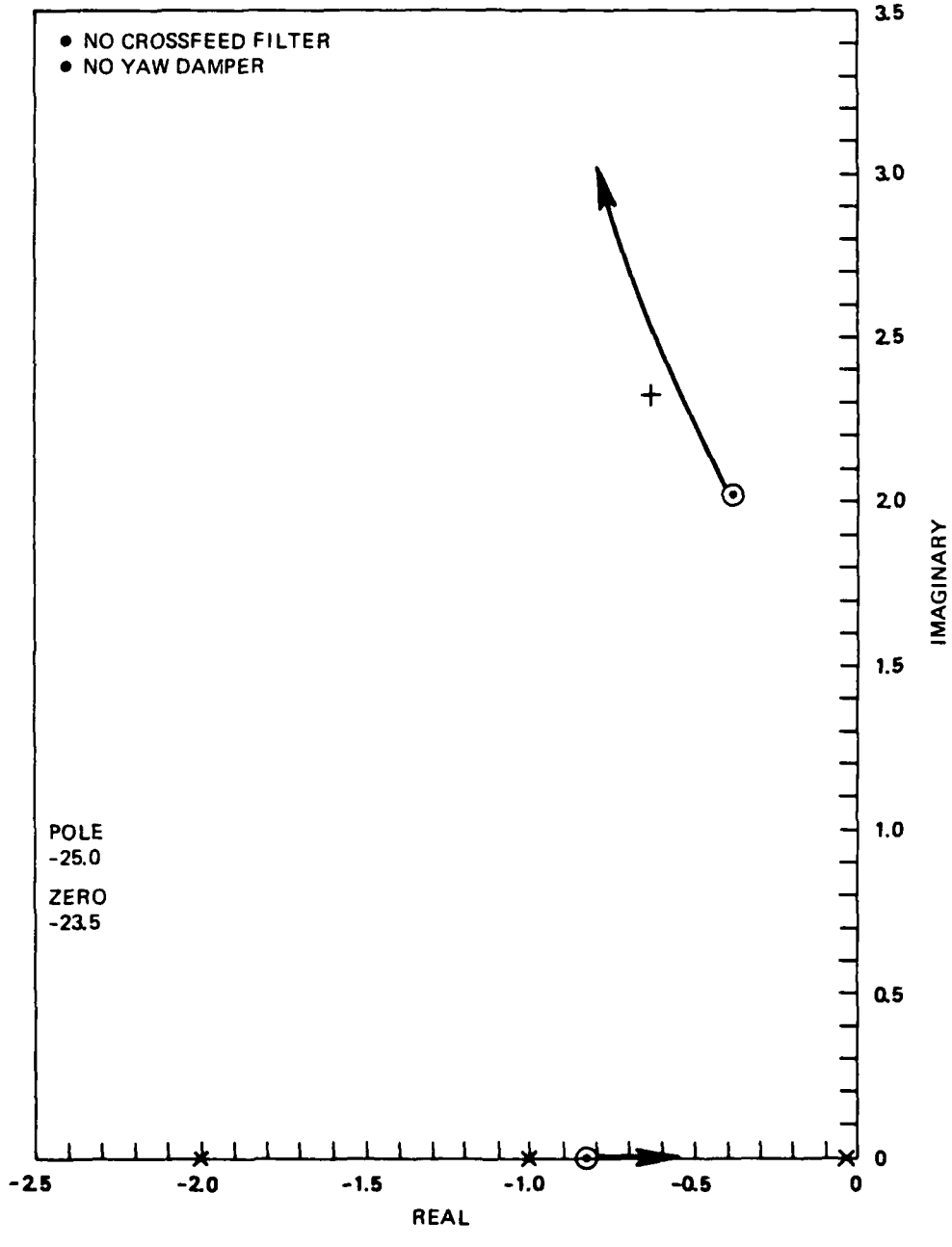

Figure A-14. Aileron to roll—zero location change with crossfeed.

• NO CROSSFEED

STATE SPACE EQUATIONS

• YAW DAMPER

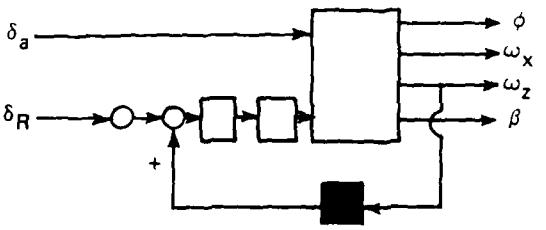

$$\dot{\underline{x}} = \begin{bmatrix} \text{AIRCRAFT: } A_a & \underline{b}_r \\ S_{\omega_z} & -1 \\ S_{\omega_z} \cdot 25 & -25.0 \quad -25.0 \end{bmatrix} \underline{x}$$

VARIATION IN A MATRIX:

CHANGE IN BOTH POLES & ZEROS

$$+ \begin{bmatrix} \underline{b}_a \\ 0 \quad 1.0 \\ 0 \quad 25.0 \end{bmatrix} \underline{u} \qquad \text{(A-30)}$$

Figure A-15. Effect of yaw feedback to the rudder with no crossfeed—state space equations.

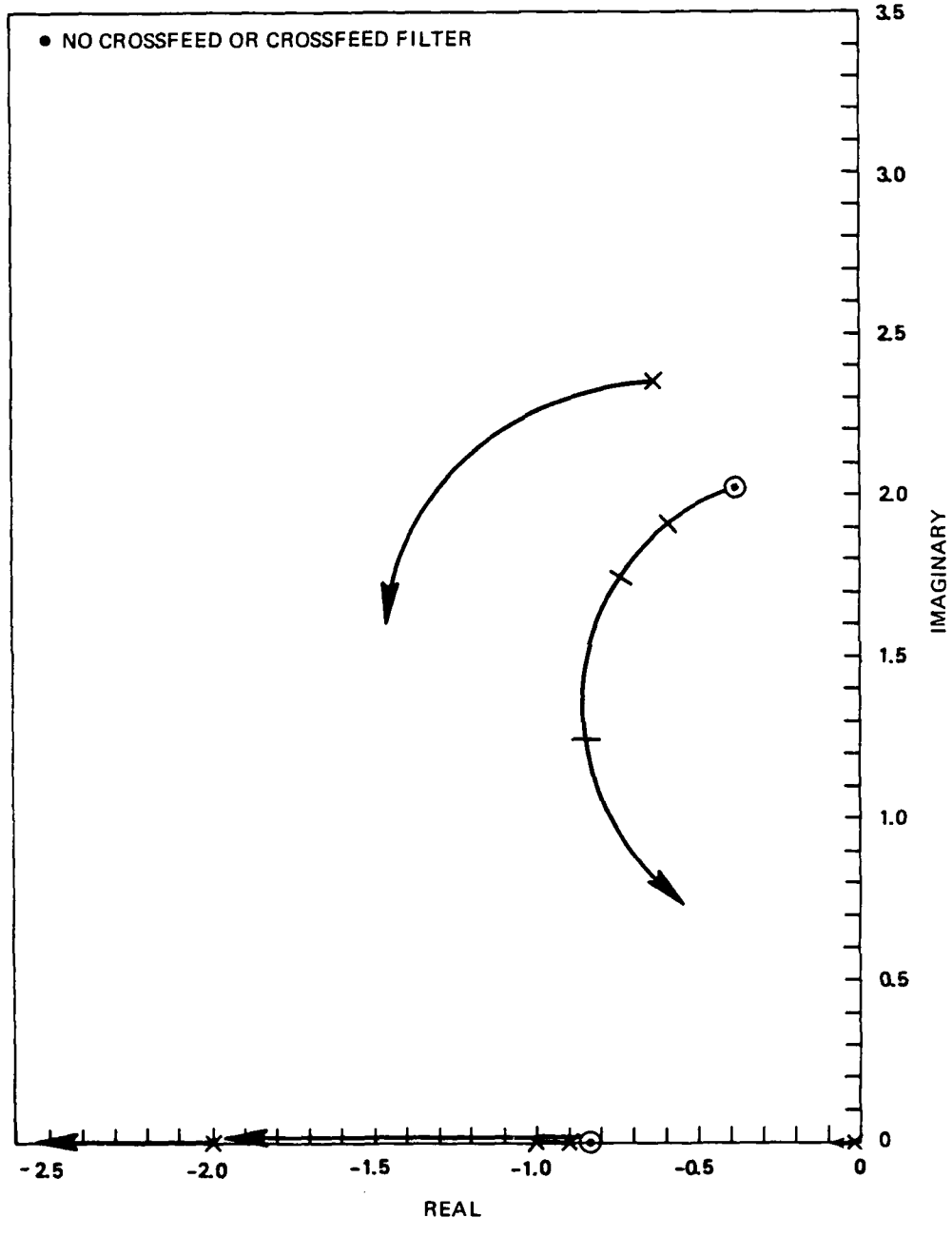

Figure A-16. Aileron to roll angle pole—zero location change with yaw damper gain.

STATE SPACE EQUATIONS

- CROSSFEED WITH YAW DAMPER

- NO CROSSFEED FILTER
- YAW DAMPER GAIN = 0.45

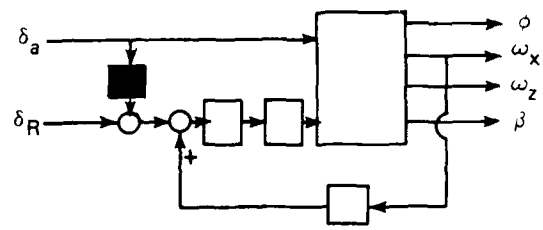

$$\dot{\underline{x}} = \begin{bmatrix} \text{AIRCRAFT } A_c & \underline{b}_r \\ 0.45 & -1.0 \\ 11.25 & -25.0 \quad -25.0 \end{bmatrix} \underline{x} + \begin{bmatrix} \underline{b} \\ S_{CF} \times 1.0 & 1.0 \\ S_{CF} \times 25 & 25.0 \end{bmatrix} \underline{u} \qquad \text{(A-31)}$$

VARIATION: NO CHANGE IN A: SAME POLES, ZEROS CHANGE

Figure A-17. Effect of crossfeed with yaw damper loop closed—state space equations.

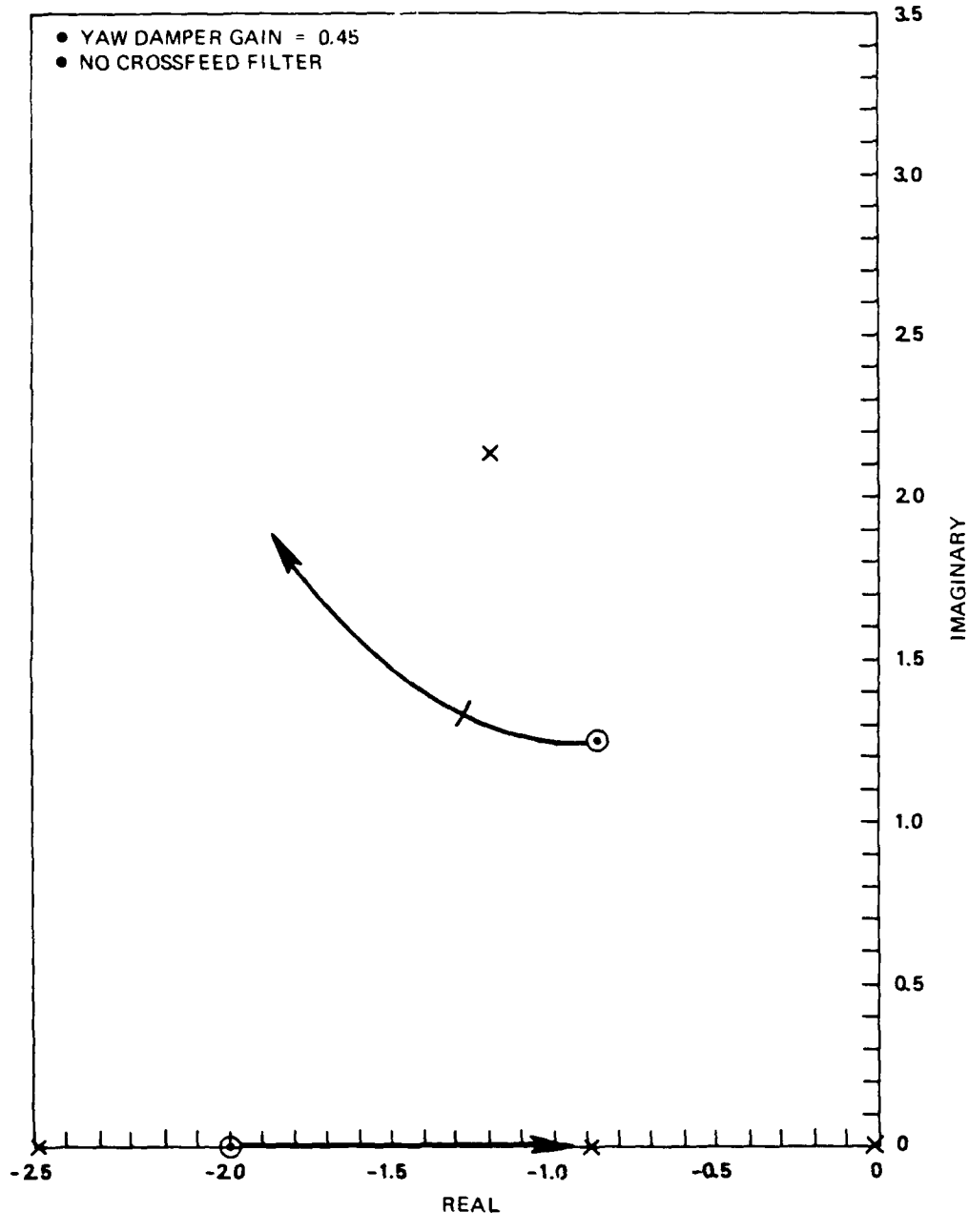

Figure A-18. Aileron to roll angle—zero location change with crossfeed gain.

- CROSSFEED FILTER τ_{CF} = 0.25
- YAW DAMPER GAIN = 0.45

STATE SPACE EQUATIONS

- CROSSFEED
  WITH YAW DAMPER
  CROSSFEED FILTER

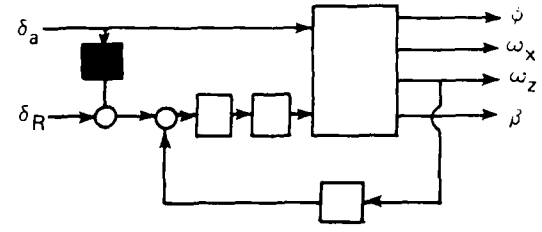

$$\dot{x} = \begin{bmatrix} \text{AIRCRAFT: } A_c & \underline{b}_r \\ \begin{matrix} 0.45 \\ 11.25 \end{matrix} & \begin{matrix} -1.0 & 1.0 \\ -25.0 & -25.0 \end{matrix} \quad \begin{matrix} 25.0 \\ -4.0 \end{matrix} \end{bmatrix} x + \begin{bmatrix} \underline{b}_a \\ \begin{matrix} 1.0 \\ 25.0 \end{matrix} \\ 4 \times S_{CF} \end{bmatrix} u \qquad \text{(A-32)}$$

VARIATION: NO CHANGE IN A: POLES REMAIN THE SAME, ZEROS CHANGE

Figure A-19. Effect of crossfeed dynamics with yaw damper loop closed—state space quations.

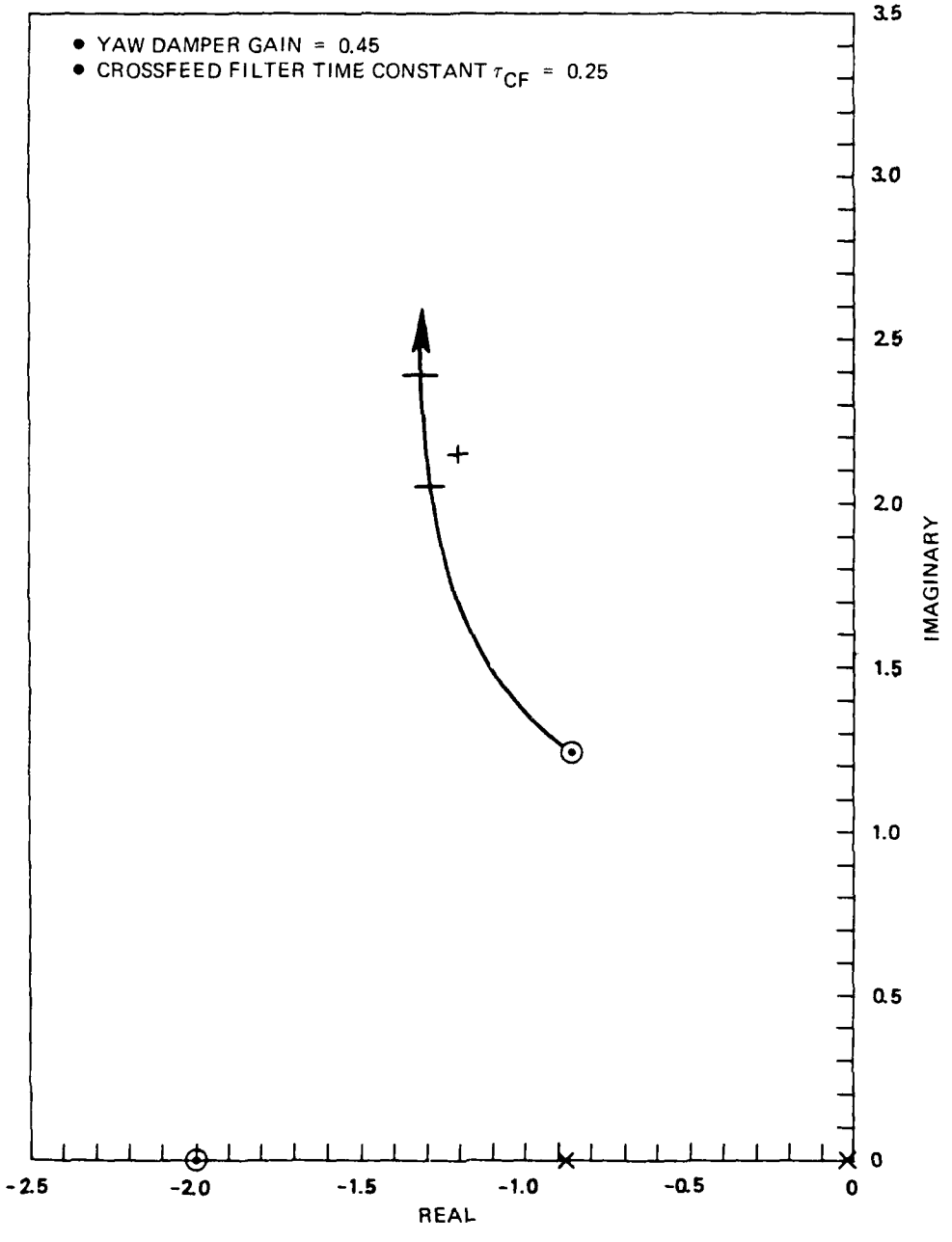

Figure A-20. Aileron to roll angle—zero location change with crossfeed gain.

Figure A-21 is a composite map, in the complex plane, of the migration of the poles and zeros of the aileron-to-roll angle transfer function with design changes. The parameter values $S_{\omega_z} = 0.45$, $S_{CF} = -0.55$, and $\tau_{CF} = 0.25$ were selected as design values based on this analysis. The corresponding poles and zeros are shown in Figure A-21.

The aforementioned trends were obtained from numerical pole zero analyses of Eq. (A-27), with, of course, the appropriate parameter values. This is, in effect, a trial-and-error method, which, though adequate for this example, would become inefficient if multiple crossfeeds, or multiple filters were required. Alternatively, once the yaw damper gain is selected, the system equations could be recast in root locus form, with the crossfeed gain as the parameter [26]. The resulting locus of zero locations would be identical to Figure A-21. This formulation is particularly nice because the crossfeed filter can then be designed, using standard root locus compensation techniques, to make the locus pass through the dutch-roll pole locations. This technique gives the crossfeed parameter values $S_{CF} = -0.55$ and $\tau_{CF} = 0.263$. Again, however, if multiple crossfeeds, or multiple pole cancellations are required, this method becomes cumbersome.

It is interesting at this point to look at the closed-loop state space equations. If the appropriate parameter and gain values are substituted into Eq. (A-28), the numerical state space description is given by Eq. (A-33) in Figure A-22. This form can be block diagonalized [see Appendix E] which results in the Eq. (A-34) in Figure A-23. The closed-loop system eigenvalues are evident along the diagonal. In addition, note that the aileron input to the oscillatory dutch-roll mode is almost nulled.

A.7.4 Transform Methodology Analysis

This analysis is presented to illustrate the transformation methodology. As noted earlier, the parameters of interest in the rudder coordination design are the yaw damper gain, and the crossfeed gain and time constant. The focus here will be on the crossfeed design. S_{ω_z}, the

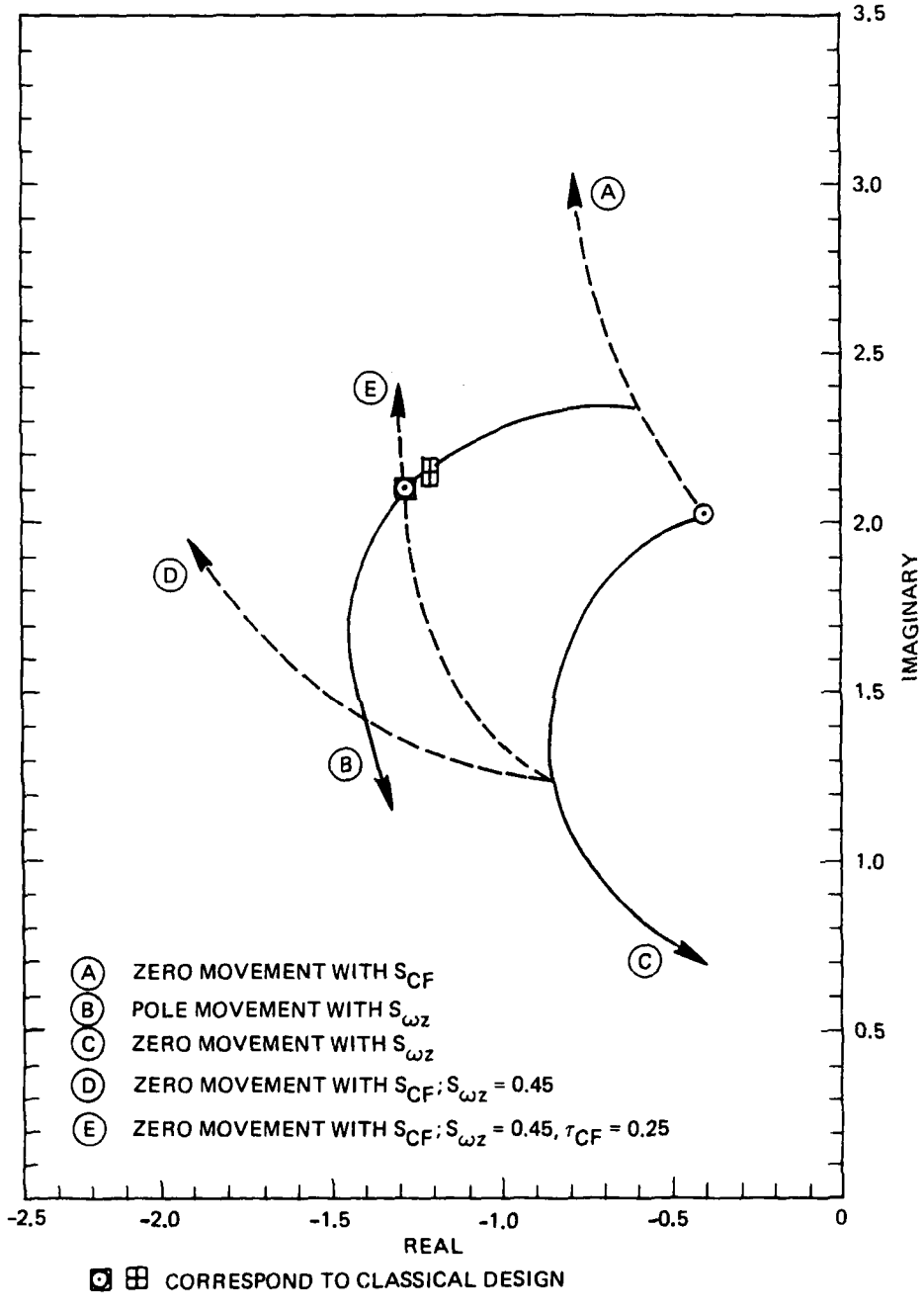

Figure A-21. Composite map of pole/zero changes—aileron to roll angle.

STATE SPACE EQUATIONS

CLASSICAL DESIGN

YAW DAMPER GAIN = 0.45

CROSSFEED GAIN = -0.55

τ_{CF} = 0.25

$$\dot{x} = \begin{bmatrix} 0 & 1.0 & 0.1361 & 0 & 0 & 0 & 0 \\ 0 & -2.625 & 1.91 & -2.90 & 0 & 6.13 & 0 \\ 0 & -0.0759 & -0.426 & 2.65 & 0 & -3.55 & 0 \\ 0.0555 & 0.135 & -0.997 & -0.217 & 0 & 0.0422 & 0 \\ 0 & 0 & 0.45 & 0 & -1.0 & 0 & 1.0 \\ 0 & 0 & 11.25 & 0 & -25.0 & -25.0 & 25.0 \\ 0 & 0 & 0 & 0 & 0 & 0 & -4.0 \end{bmatrix} \underline{x}$$

$$+ \begin{bmatrix} 0 & 0 \\ 27.0 & 0 \\ 1.42 & 0 \\ 0.002315 & 0 \\ 0 & 1.0 \\ 0 & 2.5 \\ -2.2 & 0 \end{bmatrix} \underline{u} \qquad \text{(A-33)}$$

Figure A-22. Numerical state space description—classical design.

STATE SPACE EQUATIONS

CANONICAL FORM

YAW DAMPER GAIN = 0.45

CROSSFEED GAIN = -0.55

$\tau_{CF} = 0.25$

$$\dot{\underline{x}} = \begin{bmatrix} 23.19 & & & & & & \\ & -0.877 & & & & & \\ & & -2.80 & & & & \\ & & & -0.02518 & & & \\ & & & & -4.0 & & \\ & & & & & -1.189 & 2.182 \\ & & & & & 2.182 & -1.189 \end{bmatrix} \hat{\underline{x}}$$

$$+ \begin{bmatrix} 2.94 & 34.84 \\ -0.25569 & 2.4045 \\ 6.3911 & 2.2399 \\ -0.69199 & -0.01411 \\ -2.2 & 0 \\ -0.0510 & 1.8052 \\ 0.1208 & 1.6074 \end{bmatrix} \underline{u} \qquad \text{(A-34)}$$

Figure A-23. Numerical state space description—canonical form classical design.

yaw gain, will be taken as $S_{\omega_z} = 0.45$—the same value used in the earlier analysis. The crossfeed parameters are to be chosen so that the dutch-roll mode is suppressed in the system response to an aileron input. The appropriate system functional block diagram is shown in Figure A-24.

The first step is to put the system state space description in block diagonal canonical form. This particular form is useful because the system response modes are not coupled in the A matrix. Equation (A-35) in Figure A-25 gives the appropriate canonical expression. This equation is a block diagonalization of Eq. (A-28) with $S_{\omega_z} = 0.45$, $S_{CF} = 0$, and $\tau_{CF} = 0$.

The mode of interest is the dutch-roll mode. Ideally, the choice of the crossfeed gain and filter time constant will place zeros directly on top of the dutch-roll poles in the aileron-to-roll transfer function. Equivalently, one can view the choice of crossfeed parameters as making the dutch-roll mode uncontrollable from an aileron input.

In the block-diagonal form, the system modes are dynamically decoupled and the state vector can be partitioned into

$$\hat{\underline{x}} = \begin{bmatrix} \hat{\underline{x}}_1 \\ \hat{\underline{x}}_2 \end{bmatrix} \tag{A-36}$$

where $\hat{\underline{x}}_2$ describes the aircraft oscillatory mode dynamics. Let

$$\hat{\underline{x}}_2 = \begin{bmatrix} x_1 \\ x_2 \end{bmatrix} \tag{A-37}$$

Then, the dutch-roll dynamic description can be written

$$\begin{bmatrix} \dot{x}_1 \\ \dot{x}_2 \end{bmatrix} = \begin{bmatrix} -1.189 & 2.18 \\ -2.18 & 1.189 \end{bmatrix} \begin{bmatrix} x_1 \\ x_2 \end{bmatrix} + \begin{bmatrix} 0.221 & 1.805 \\ 1.590 & 1.607 \end{bmatrix} \underline{u} \tag{A-38}$$

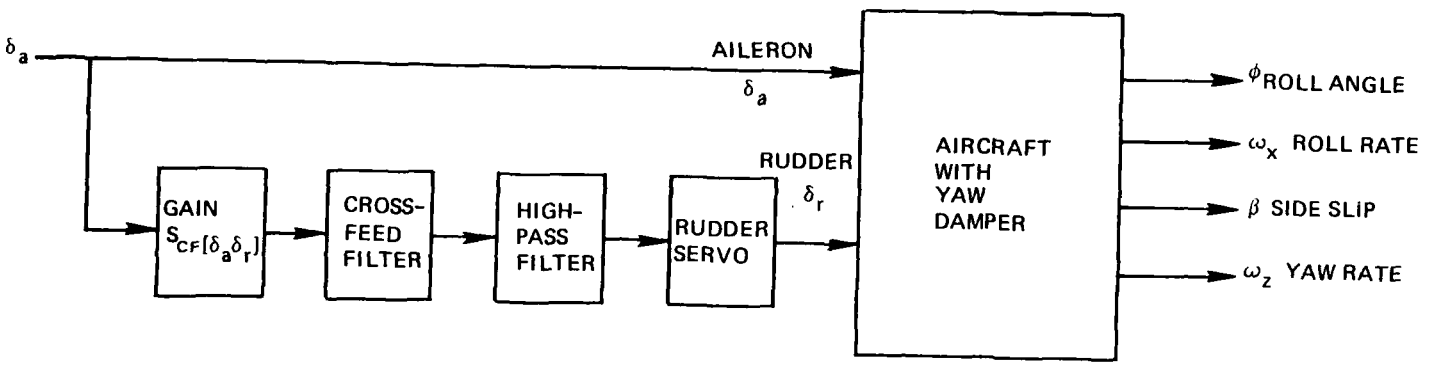

Figure A-24. Functional block diagram of the crossfeed design.

STATE SPACE EQUATIONS

CANONICAL FORM

- YAW DAMPER
- NO CROSSFEED

$$\dot{\underline{x}} = \begin{bmatrix} -23.19 & & & & & \\ & -0.877 & & & & \\ & & -2.80 & & & \\ & & & -0.02518 & & \\ & & & & -1.189 & 2.182 \\ & & & & 2.182 & -1.189 \end{bmatrix} \hat{\underline{x}}$$

$$+ \begin{bmatrix} -1.0545 & 34.84 \\ 1.438 & 2.4045 \\ 2.2829 & -2.2399 \\ -0.6998 & -0.01411 \\ 0.221216 & 1.8052 \\ 1.5904 & 1.6074 \end{bmatrix} \underline{u} \qquad \text{(A-35)}$$

Figure A-25. System state space equation - block diagonalization.

If the identifications

$$\underline{b}_1 = \begin{bmatrix} 0.221 \\ \\ 1.590 \end{bmatrix}, \quad \underline{b}_2 = \begin{bmatrix} 1.805 \\ \\ 1.607 \end{bmatrix}, \quad \text{and} \quad B_2 = \begin{bmatrix} \underline{b}_1 & \underline{b}_2 \end{bmatrix}$$

are made, where $\underline{b}_1$ is associated with the aileron input, and $\underline{b}_2$ with the rudder, then the design objectives can be reduced to finding a transform T such that

$$B_2 T = 0 \qquad \text{(A-39)}$$

There is no nonzero T that meets this condition because the rows of B_2 span R^2. This is consistent with Figure A-14, where it is evident that crossfeed alone will not produce the required locus of zero locations. If no solution to Eq. (A-39) exists, dynamics can be added to the crossfeed; specifically, since there are two controls, and two states to be suppressed, the order of the dynamics must be at least 1; a lag filter.

If a filter is added to the rudder input (see Appendix B), an additional, linearly independent system input vector is formed. Of interest here are the elements of this new vector which corresponds to the dutch-roll mode, designated $\underline{b}_2^{\cdot}$. With this new input

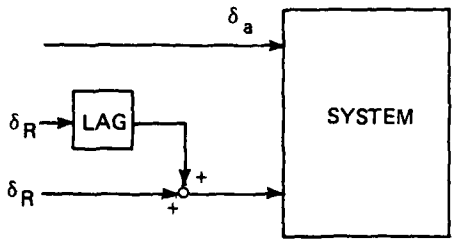

Eq. (A-38) becomes

$$\begin{bmatrix} \dot{x}_1 \\ \dot{x}_2 \end{bmatrix} = \begin{bmatrix} -1.189 & 2.18 \\ -2.18 & -1.189 \end{bmatrix} \begin{bmatrix} x_1 \\ x_2 \end{bmatrix} + \begin{bmatrix} \underline{b}_1 & \underline{b}_2' & \underline{b}_2 \end{bmatrix} \begin{bmatrix} \delta_a \\ \delta_R \\ \delta_R \end{bmatrix} \qquad \text{(A-40)}$$

The input vector $\underline{b}_2'$ is a function of τ_{CF} and $\underline{b}_2$. If $\underline{b}_2$ is regarded as a vector in R^2, then $\underline{b}_2'$ is the result of rotating $\underline{b}_2$ through the angle

$$\tan^{-1} \frac{-\beta}{\alpha + 1/\tau_{CF}}$$

and changing its magnitude by

$$\frac{1}{\tau_{CF}\sqrt{Q}}$$

where

$$Q^2 = \alpha^2 + \beta^2$$

$$\alpha = -1.189$$

$$\beta = 2.18$$

These relations are motivated and developed in Appendix B.

In this example, the vectors $\underline{b}_1$, b_2', and $\underline{b}_2$ define the way an input is distributed between the states x_1 and x_2, which describe the dutch-roll mode. Thus, x_1 and x_2 can be taken as phase-plane coordinates, and in this plane, the state vector rotates at the damped natural frequency, 2.18 radians/second. It is perhaps intuitive that if an input were filtered then its representation in the phase plane might change, and the time history of the distribution of energy between states might be effected. The change in angle and the change in magnitude mentioned previously are the description of this effect.

Given Eq. (A-40), a transform T' can be found which is orthogonal to the two row vectors of $[\underline{b}_1, \underline{b}_2', \underline{b}_2]$. This transform is a vector in R^3, and will couple together the aileron, rudder, and filtered rudder input. The details of this approach will not be pursued. Instead, because a direct comparison with Whitaker's design is desirable, a transform T will be found in R^2 which couples together the aileron and the filtered rudder input. This requires that, for the system

$$\begin{bmatrix} \dot{x}_1 \\ \dot{x}_2 \end{bmatrix} = \begin{bmatrix} -1.189 & 2.18 \\ -2.18 & -1.189 \end{bmatrix} \begin{bmatrix} x_1 \\ x_2 \end{bmatrix} + \begin{bmatrix} \underline{b}_1 & \underline{b}_2' \end{bmatrix} \begin{bmatrix} \delta_a \\ \hat{\delta}_r \end{bmatrix} \tag{A-41}$$

the condition

$$[\underline{b}_1 \quad \underline{b}_2']T = 0 \tag{A-42}$$

must be met. There are two inputs, so the only solution to Eq. (A-42) will occur when $\underline{b}_1$ and $\underline{b}_2'$ span R^1, that is, they are linearly dependent, or more simply, parallel.

Note that

$$\underline{b}_1 = \begin{bmatrix} 0.221 \\ 1.590 \end{bmatrix} \rightarrow 1.605 \angle 7.918° \tag{A-43}$$

$$\underline{b}_2 = \begin{bmatrix} 1.805 \\ 1.607 \end{bmatrix} \rightarrow 2.417 \angle 48.316° \tag{A-44}$$

For $\underline{b}_1$ and $\underline{b}_2'$ to be parallel, $\underline{b}_2$ must be rotated through -40.398°, which implies

$$\tan^{-1} \frac{-\beta}{\alpha + 1/\tau_{CF}} = -40.398° \tag{A-45}$$

Substituting for α and β, this results in

$$\tau_{CF} = 0.2666$$

and

$$\underline{b}_2' = \begin{bmatrix} 0.3713 \\ 2.6696 \end{bmatrix} \rightarrow 2.6952 \angle 7.9187° \qquad \text{(A-46)}$$

Equation (A-41) becomes

$$\begin{bmatrix} \dot{x}_1 \\ \dot{x}_2 \end{bmatrix} = \begin{bmatrix} -1.189 & 2.18 \\ -2.18 & -1.189 \end{bmatrix} \begin{bmatrix} x_1 \\ x_2 \end{bmatrix} + \begin{bmatrix} 0.2212 & 0.3713 \\ 1.5904 & 2.6696 \end{bmatrix} \begin{bmatrix} \delta_a \\ \hat{\delta}_r \end{bmatrix} \qquad \text{(A-47)}$$

T is chosen to satisfy

$$[\underline{b}_1 \quad \underline{b}_2']T = 0 \qquad \text{(A-48)}$$

or

$$T = \begin{bmatrix} 1 \\ -0.59575 \end{bmatrix} \qquad \text{(A-49)}$$

T is orthogonal to $\lfloor 0.2212 \quad 0.3713 \rfloor$ and $\lfloor 1.5904 \quad 2.6696 \rfloor$; the first element of T was chosen to be 1 to allow a direct feed through of aileron. With the crossfeed closed, Eq. (A-47) becomes

$$\begin{bmatrix} \dot{x}_1 \\ \dot{x}_2 \end{bmatrix} = \begin{bmatrix} -1.189 & 2.18 \\ -2.18 & -1.189 \end{bmatrix} \begin{bmatrix} x_1 \\ x_2 \end{bmatrix} + \begin{bmatrix} 0 \\ 0 \end{bmatrix} \delta_a \qquad \text{(A-50)}$$

The corresponding system equations are

$$\dot{\underline{x}} = \begin{bmatrix} -23.1 & & & & & & \\ & -0.8769 & & & & & \\ & & -2.80 & & & & \\ & & & -0.02518 & & & \\ & & & & -3.7507 & & \\ & & & & & -1.189 & 2.18 \\ & & & & & 2.18 & -1.189 \end{bmatrix} \underline{x}$$

$$+ \begin{bmatrix} 2.94 & 34.84 \\ -0.4324 & 2.409 \\ 7.550 & -2.239 \\ -0.6913 & 0.01411 \\ 2.2315 & 0 \\ 0 & 1.8052 \\ 0 & 1.6075 \end{bmatrix} \underline{u} \qquad \text{(A-51)}$$

Note that the dutch-roll mode is not controllable by an aileron input. The poles and zeros of Eq. (A-51) are given in Table A-1.

Table A-1. Poles and zeros of system equation (sheet 1 of 2).

PROGRAM: POLZERO TIME: 11:26:35.9 DATE: 01/03/80 (80/003)
REVN# 2, MOD# 00.

* COORDINATED AIRPLANE

INPUT QUAD = S100

NX = 9
NU = 2
NY = 4
T = .0

TRANSITION MATRIX A

	1	2	3	4	5
1	0.0	1.000000000D+00	1.361000000D-01	0.0	0.0
2	0.0	-2.625000000D+00	1.910000000D+00	-2.900000000D+01	0.0
3	0.0	-7.590000000D-02	-4.260000000D-01	2.650000000D+00	0.0
4	5.550000000D-02	1.359000000D-01	-9.974000000D-01	-2.173000000D-01	0.0
5	0.0	0.0	4.500000000D-01	0.0	-1.000000000D+00
6	0.0	0.0	1.125000000D+01	0.0	-2.500000000D+01
7	0.0	0.0	0.0	0.0	0.0
8	0.0	0.0	0.0	0.0	0.0
9	0.0	0.0	0.0	0.0	0.0

	6	7	8	9
1	0.0	0.0	0.0	0.0
2	6.130000000D+00	0.0	0.0	0.0
3	-3.550000000D+00	0.0	0.0	0.0
4	4.222000000D-02	0.0	0.0	0.0
5	0.0	1.000000000D+00	0.0	0.0
6	-2.500000000D+01	2.500000000D+01	0.0	0.0
7	0.0	-3.750300000D+00	0.0	0.0
8	0.0	0.0	0.0	0.0
9	0.0	0.0	0.0	0.0

INPUT MATRIX B

	1	2
1	0.0	0.0
2	2.700000000D+01	0.0
3	1.420000000D+00	0.0
4	2.315000000D-03	0.0
5	0.0	1.000000000D+00
6	0.0	2.500000000D+01
7	-2.234253076D+00	0.0
8	0.0	0.0
9	0.0	0.0

Table A-1. Poles and zeros of system equation (sheet 2 of 2).

OUTPUT MATRIX C

	1	2	3	4	5
1	1.000000000D+00	0.0	0.0	0.0	0.0
2	0.0	1.000000000D+00	0.0	0.0	0.0
3	0.0	0.0	1.000000000D+00	0.0	0.0
4	0.0	0.0	0.0	1.000000000D+00	0.0

	6	7	8	9
1	0.0	0.0	0.0	0.0
2	0.0	0.0	0.0	0.0
3	0.0	0.0	0.0	0.0
4	0.0	0.0	0.0	0.0

TRANSMISSION MATRIX D

	1	2
1	0.0	0.0
2	0.0	0.0
3	0.0	0.0
4	0.0	0.0

OUTPUT POLES = P200 COORD AIRPLANE

NP = 9
T = .0

NUMBER	REAL	IMAG
1	-3.750299E+00	
2	0.0	
3	0.0	
4	-2.421546E-02	
5	-8.866659E-01	
6	-2.786338E+00	
8	-1.191922E+00	2.151013E+00
9	-2.318723E+01	

OUTPUT ZEROS = Y2000101 AILERON TO ROLL

NZ = 7
GAIN = 27.1935

NUMBER	REAL	IMAG
1	0.0	
2	0.0	
3	-7.766402E-01	
5	-1.199915E+00	2.153101E+00
6	-2.369135E+01	
7	-3.628448E+00	

APPENDIX B

EFFECT OF FILTERING A CONTROL INPUT

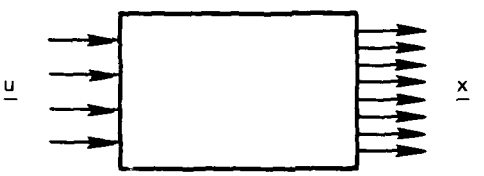

The system (I), m inputs—n states, can be represented in block-diagonal form

$$\dot{\underline{x}} = A\underline{x} + B\underline{u} \qquad \text{(B-1)}$$

where

$$A = \begin{bmatrix} A_1 & & & & \\ & A_2 & & & \\ & & \ddots & & \\ & & & A_i & \\ & & & & \ddots \\ & & & & & A_\ell \end{bmatrix}$$

$$A_i = \lambda_i \text{ or } \begin{bmatrix} \alpha_i & \beta_i \\ -\beta_i & \alpha_i \end{bmatrix}$$

$$B = [\underline{b}_1, \underline{b}_2, \ldots \underline{b}_n]; \ \underline{b}_j \text{ is a column vector}$$

If a lag filter of the form $\frac{\omega}{s + \omega}$ is added to the j^{th} input

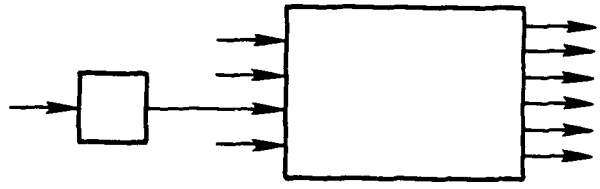

an augmented system description is required.

$$\begin{bmatrix} \dot{\underline{x}} \\ \dot{x}_f \end{bmatrix} = \begin{bmatrix} A & \underline{b}_j \\ 0 & -\omega \end{bmatrix} \begin{bmatrix} \underline{x} \\ x_f \end{bmatrix} + \begin{bmatrix} \underline{b}_1 \; \underline{b}_2 \cdots & 0 & b_{j+1} \cdots b_m \\ 0 & \omega & 0 \end{bmatrix} \underline{u} \qquad \text{(B-2)}$$

Equation (B-2) can be put in block-diagonal form using the transformation

$$T\tilde{\underline{x}} = \begin{bmatrix} \underline{x} \\ x_f \end{bmatrix} \qquad \text{(B-3)}$$

where

$$T = \begin{bmatrix} I & \underline{V}_f \\ 0 & 1 \end{bmatrix}$$

$\begin{bmatrix} \underline{V}_f \\ 1 \end{bmatrix}$ is the eigenvector associated with the filter eigenfrequency $\lambda_f = -\omega$.

The inverse of T is

$$T^{-1} = \begin{bmatrix} I & -\underline{V}_f \\ 0 & 1 \end{bmatrix}$$

and

$$\dot{\underline{\tilde{x}}} = \begin{bmatrix} A & \\ & -\omega \end{bmatrix} \underline{\tilde{x}} + \left[\begin{array}{ccc|c|ccc} \underline{b}_1 & \underline{b}_2 \cdots & \underline{b}_{j-1} & \tilde{\underline{b}}_j & \underline{b}_{j+1} & \cdots & \underline{b}_m \\ 0 & 0 \quad & 0 & & 0 & & 0 \end{array}\right] \underline{u} \qquad \text{(B-4)}$$

$$\tilde{\underline{b}}_j = -\omega \begin{bmatrix} \underline{V}_f \\ 1 \end{bmatrix}$$

B.1 Expression for $\underline{V}_f$

$\begin{bmatrix} \underline{V}_f \\ 1 \end{bmatrix}$ is an eigenvector of the matrix $\bar{A}$

$$\bar{A} = \begin{bmatrix} A & \underline{b}_j \\ 0 & -\omega \end{bmatrix}$$

which implies

$$\bar{A} \begin{bmatrix} \underline{V}_f \\ 1 \end{bmatrix} = -\omega \begin{bmatrix} V_f \\ 1 \end{bmatrix} \qquad \text{(B-5)}$$

Let

$$\underline{b}_j = \begin{bmatrix} b_{1j} \\ b_{2j} \\ b_{ij} \\ b_{nj} \end{bmatrix} \text{ and } \quad \underline{V}_f = \begin{bmatrix} V_1 \\ V_2 \\ \vdots \\ V_i \\ \vdots \\ V_n \end{bmatrix}$$

Due to the near block-diagonal form of $\bar{A}$, a set of uncoupled equations for the elements of $\underline{V}_f$ can be written. If the i^{th} eigenvalue is real, then

$$\lambda_i V_i + b_{ij} = -\omega V_i \tag{B-6}$$

or

$$V_i = \frac{-b_{ij}}{\lambda_i + \omega} \tag{B-7}$$

Combining Eq. (B-7) with Eq. (B-4) yields the relation

$$\tilde{b}_{ij} = \frac{\omega}{\lambda_i + \omega} b_{ij} \tag{B-8}$$

Recall that the filter on the j^{th} input is of the form $\frac{\omega}{s + \omega}$. Also, note that there is an apparent singularity at $\omega = -\lambda_i$. This singularity is not real. Equation (B-6) is valid only for cases where $\underline{V}_f$ is linearly independent of the other eigenvectors of $\bar{A}$; a condition that is not guaranteed if $\omega = -\lambda_i$.

If the i^{th} and $[i+1]^{th}$ eigenvalues are complex conjugates, the correct expressions are

$$\begin{aligned} \alpha_i V_i + \beta_i V_{i+1} + b_{ij} &= -\omega V_i \\ -\beta_i V_i + \alpha_i V_{i+1} + b_{i+1,j} &= -\omega V_{i+1} \end{aligned} \tag{B-9}$$

or

$$\begin{aligned} V_i &= -\frac{1}{Q}\left[(\alpha_i + \omega) b_{ij} - B_i b_{i+1,j}\right] \\ V_{i+1} &= -\frac{1}{Q}\left[B_i b_{ij} + (\alpha_i + \omega) b_{i+j,j}\right] \end{aligned} \tag{B-10}$$

where

$$Q_i = [\alpha_i + \omega]^2 + \beta^2$$

Then, using Eq. (B-4), the relationship for $\tilde{b}_{ij}$ and $\tilde{b}_{i+1,j}$ is

$$\begin{bmatrix} \tilde{b}_{ij} \\ \tilde{b}_{i+1,j} \end{bmatrix} = \frac{\omega}{\sqrt{Q}} \begin{bmatrix} \frac{[\alpha+\omega]}{\sqrt{Q}} & -\frac{\beta}{\sqrt{Q}} \\ \frac{\beta}{\sqrt{Q}} & \frac{[\alpha+\omega]}{\sqrt{Q}} \end{bmatrix} \begin{bmatrix} b_{ij} \\ b_{i+1,j} \end{bmatrix} \tag{B-11}$$

The matrix

$$\begin{bmatrix} \frac{\alpha+\omega}{\sqrt{Q}} & -\frac{\beta}{\sqrt{Q}} \\ \frac{\beta}{\sqrt{Q}} & \frac{\alpha+\omega}{\sqrt{Q}} \end{bmatrix}$$

is of the form

$$\begin{bmatrix} \cos\theta & \sin\theta \\ -\sin\theta & \cos\theta \end{bmatrix}$$

a matrix which rotates a vector through an angle θ. Making appropriate identifications, the vector $\begin{bmatrix} b_{ij} \\ b_{i+1,j} \end{bmatrix}$, by use of a filter on the j^{th} input, will have a change in magnitude of $\left[\frac{\omega}{\sqrt{Q}} - 1\right]$, and will be rotated through an angle $\tan^{-1}\frac{-\beta}{\alpha+\omega}$.

The information available in Eq. (B-5) and (B-11) can be compactly presented as

$$\hat{\underline{b}}_j = [\omega I + A]^{-1}\, \underline{b}_j \tag{B-12}$$

B.2 Summary

Filtering the j^{th} input produces the following results.

(1) The system dynamical matrix is changed only by the addition of the filter mode. It remains block-diagonal.

(2) Only the input distribution matrix column associated with the j^{th} control changes. Equations (B-8) and (B-11), or Eq. (B-12) describe these changes as a function of filter break frequency.

APPENDIX C

ADAPTIVE TRANSFORMS

C.1 Introduction

This appendix discusses the adaptive shaping of a system output to control the modal information content. The discussion focuses on the output characteristics of the linear, time-invariant, plant Σ_0,

$$\Sigma_0: \qquad \dot{\underline{x}} = A\underline{x} + P\underline{u} \qquad \underline{x}[0] = \underline{x}_0 \tag{C-1}$$

$$\underline{y} = C\underline{x} + \underline{\nu}_m$$

where

$\underline{x} \in R^n$, $\underline{u} \in R^m$, $y \in R^{\ell}$

Modal coordinates are used as state variables.

$\underline{\nu}_m$ is a vector of white, zero mean, measurement noise.

The state vector $\underline{x}$ can be partitioned

$$\underline{x} = \begin{bmatrix} \underline{x}_1 \\ \underline{x}_2 \end{bmatrix} \tag{C-2}$$

Then Eq. (C-1) becomes

$$\Sigma_0: \qquad \begin{bmatrix} \dot{\underline{x}}_1 \\ \underline{x}_2 \end{bmatrix} = \begin{bmatrix} A_{11} & 0 \\ 0 & A_{22} \end{bmatrix} \begin{bmatrix} \underline{x}_1 \\ \underline{x}_2 \end{bmatrix} + \begin{bmatrix} B_1 \\ B_2 \end{bmatrix} \underline{u} \tag{C-3}$$

$$\underline{y} = C_1\underline{x}_1 + C_2\underline{x}_2 + \underline{\nu}_m$$

where

$$\underline{x}_2 \in R^q$$

Two output quantities can be defined

$$\underline{y}_1 = C_1\underline{x}_1 \tag{C-4}$$

$$\underline{y}_2 = C_1\underline{x}_2 \tag{C-5}$$

Σ_0 is shown in block-diagram form in Figure C-1.

An output transformation T_3 can be introduced. T_3 is a singular transformation which operates on the output $\underline{y}$ to produce a signal $\bar{\underline{y}}$. The selection of T_3 is discussed in detail in Appendix A. The following results are of interest here.

(1) If $\ell > q$, then a T_3 exists which excludes all $\underline{x}_2$ information from $\bar{\underline{y}}$.

(2) T_3 satisfies the equations

$$T_3C_1 \neq 0, \; T_3C_2 = 0 \tag{C-6}$$

(3) If T_3 exists, and is implemented, it corresponds to placing the zeros of the $\underline{u}$ to $\bar{\underline{y}}$ transfer function at the same complex plane locations as the poles of $[A_{22}]$.

(4) T_3 operates on the spatial characteristics of Σ_0 to separate the $\underline{x}_1$ and $\underline{x}_2$ states.

This appendix assumes that $\ell > q$, and that a transform T_3, has been implemented. If the system model, Eq. (C-1), corresponds identically to the true system, then T_3 can be chosen to satisfy Eq. (C-6) exactly. However, model errors or system parameter changes may lead to the condition $T_3C_2 \neq 0$, a condition Balas calls observation spillover.

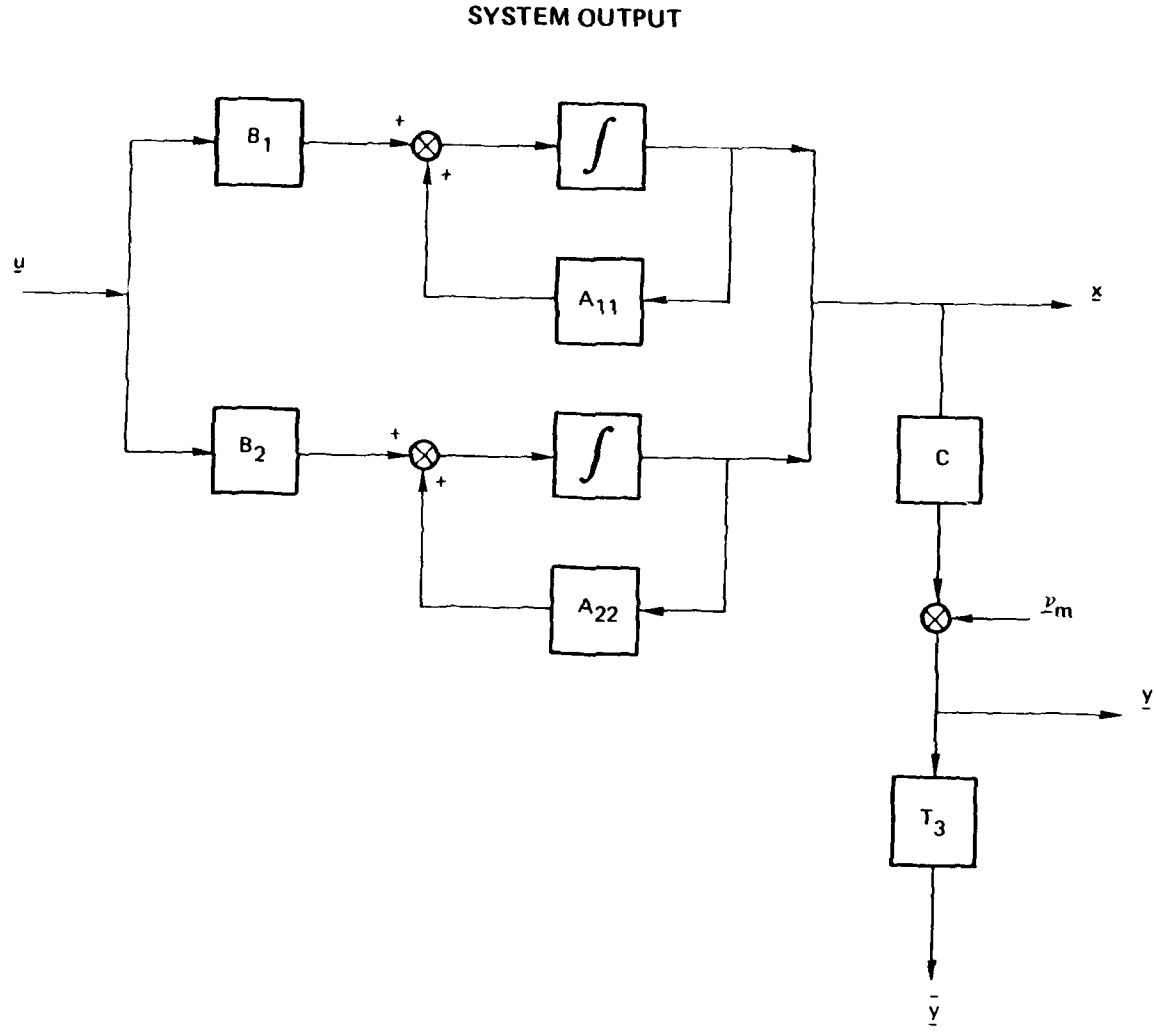

Figure C-1. Block diagram decsription of the system output.

The following distinctions are useful at this point.

(1) Subscripts: $[\ ]_T$ implies quantities which accurately describe the system of interest. $[\ ]_m$ are model values, and may be subject to errors.

(2) Transforms:

(a) T_3 is a controller quantity which was chosen to satisfy

$$T_3[C_1]_m \neq 0 \ ; \ T_3[C_2]_m = 0 \tag{C-7}$$

Spillover occurs specifically when

$$T_3[C_2]_T \neq 0 \tag{C-8}$$

The rows of T_3 can be designated $\underline{r}_j$, j=1, ℓ-q, such that

$$T_3 = \begin{bmatrix} r_1 \\ \cdot \\ \cdot \\ r_j \end{bmatrix} \tag{C-9}$$

(b) $\bar{T}_3$ is a transform which, in fact, satisfies the true conditions

$$\bar{T}_3[C_1]_T \neq 0 \qquad \bar{T}_3[C_2]_T = 0 \tag{C-10}$$

The row vectors of $\bar{T}_3$ are designated $\bar{r}_j$, j=1, ℓ-q, so that

$$\bar{T}_3 = \begin{bmatrix} \bar{r}_1 \\ \vdots \\ \bar{r}_j \end{bmatrix} \tag{C-11}$$

T_3 and $\bar{T}_3$ are related by

$$\bar{T}_3 = T_3 - \Delta T_3 \qquad \text{(C-12)}$$

where ΔT_3 reflects the error in T_3. If the row vectors of ΔT_3 are designated E_j, j=1, ℓ-q, then Eq. (C-12) can be written as a set of ℓ-q equations.

$$\bar{r}_j = r_j - E_j \qquad j = 1, \ell - q \qquad \text{(C-13)}$$

Observation spillover has a negative influence on system performance, and an adaptive scheme which minimizes spillover in real time is of obvious interest, The system implications of spillover are discussed earlier in the text; the discussion here focuses on estimating the row vectors E_j, j=1, ℓ-q. If $[E_j]$ is known, then T_3 can be updated, and the revised transform, $\bar{T}_3$, will satisfy Eq. (C-10) as desired. The actual algorithm is based on geometric arguments in vector space, so these will be discussed first. Then, the actual adaptive scheme will be presented, along with an illustrative example.

C.2 Geometric Interpretation of Transform Error

The signal of interest is the output of Σ_0:

$$\underline{y} = [C_1]_T \underline{x}_1 + [C_2]_T \underline{x}_2 + \underline{\nu}_m \qquad \text{(C-14)}$$

The design model approximates $[C_1]_T$ with $[C_1]_m$ and $[C_2]_T$ with $[C_2]_m$. $\underline{\nu}_m$ is assumed to be Gaussian white noise, and is therefore characterized on a per-element basis by a mean and a variance. The dimension of y is known exactly, ℓ, as are the dimensions of $\underline{x}_1$, n-q, and $\underline{x}_2$, q.

The work here assumes that $\ell > q$. If this is true the columns of $[C_2]_m$ span a subspace of R^{ℓ}. This subspace is designated S. Similarly, the columns of $[C_2]_T$ will span a subspace T.

Recall that a transform T_3 is introduced, which operates on $\underline{y}$ to produce a signal $\underline{\bar{y}}$. System requirements dictate that T_3 should be chosen so that $\underline{\bar{y}}$ contains only $\underline{x}_1$ information. In equation form

$$\underline{\bar{y}} = T_3[C_1]_T\underline{x}_1 + T_3[C_2]_T\underline{x}_2 + T_3\underline{\nu}_m \tag{C-15}$$

Note that the system requirements will be satisfied if

$$T_3[C_2]_T = 0 \tag{C-16}$$

However, in the design process, T_3 is picked to satisfy

$$T_3[C_2]_m = 0 \tag{C-17}$$

If there are no modeling errors, then these two relationships will be identical. If there are modeling errors, then Eq. (C-16) will not be satisfied exactly by T_3. At this point, it is useful to interpret the problem geometrically. As discussed in Appendix A, satisfying Eq. (C-17) is equivalent to picking the row vectors of T_3; i.e., r_j, $j=1, \ell-q$, in the nullspace of S. In effect, each r_j is orthogonal to all the column vectors of $[C_2]_m$. If S and τ do not coincide exactly, then the $\underline{r}_j$ will have components in τ. It is these components, in fact, which imply that

$$T_3[C_2]_T \neq 0 \tag{C-18}$$

and if these components were nulled, then the updated T_3 would be the desired transform. This discussion can be summarized in the following points.

(1) If T_3 is chosen to satisfy Eq. (C-17), and there are modeling errors, then T_3 will be inaccurate.

(2) If T_3 is inaccurate, the inaccuracy will correspond exactly to the projection of T_3 on τ.

(3) (2) implies that the error in T_3 is contained in the subspace τ. This is an important idea.

If the notation introduced in Section C.1 is used, then we can note that $\bar{T}_3$ is in the null space of τ by definition. Since the error in T_3 is in τ then the relationship

$$\bar{r}_j \cdot E_j = 0 \tag{C-19}$$

holds for all j. Using Eq. (C-13), this becomes

$$(r_j - E_j) \cdot E_j = 0 \tag{C-20}$$

Geometrically, Eq. (C-20) corresponds to requiring that the rows of the updated transform to be orthogonal to the estimates of the errors in the transform rows.

C.3 Adaptive Loop Implementation

The adaptive loop which is presented here is based on the geometric insights discussed in Section C.2. It uses the measured system output $\underline{y}$ and the initial estimate of T_3 to derive the true transform $\bar{T}_3$.

The true transform satisfies two conditions, which can be written in terms of the row vectors of $\bar{T}_3$, namely

$$\bar{r}_j [C_1]_T \neq 0 \qquad j = 1, \ell - q \tag{C-21}$$

$$\bar{r}_j [C_2]_T = 0 \qquad j = 1, \ell - q \tag{C-22}$$

Equation (C-21) implies that the dot product of $\bar{r}_j$ and any column of $[C_1]_T$ is not zero, while Eq. (C-22) specifies that the dot product of

$\underline{x}_j$ and any column of $[Q_2]_{-1}$ is equal to zero. Recall that that column vectors of $[Q_{2-1}]$ span the subspace Γ. Our interest here is in rewriting Eq. 3-22 as

$$\langle \underline{x}_j, \underline{\hat{y}}^1 \rangle = 0 \qquad j = 1, \ell - q \qquad 3\text{-}23$$

where $\underline{\hat{y}}^1$ is a vector in Γ.

If a set of vectors $\{\hat{y}^1,\ldots\hat{y}^q\}$ were available, all in Γ, then Eq. 3-22 and 3-23 would be equivalent if $\{y^1,\ldots y^q\}$ spanned Γ. Equation 3-23 can be rewritten

$$\langle \underline{x}_j - \underline{E}_j, \underline{\hat{y}}^1 \rangle = 0 \qquad j = 1, \ell - q \qquad 3\text{-}24$$

In addition, as developed earlier

$$\langle \underline{x}_j - \underline{E}_j, \underline{E}_j \rangle = 0 \qquad j = 1, \ell - q \qquad 3\text{-}25$$

These two equations form the basis of the adaptive loop. The following specific steps are involved (reference also Figure 3-2).

1. The signal $\underline{\hat{y}}^1$, valid at $t = t_\ell$, is derived from $\underline{y}$ using discrete Fourier-transform techniques. $\underline{\hat{y}}^1$ is contained in Γ.

2. The product $T_\ell \underline{\hat{y}}^1$ is formed. This product is a vector $\underline{e}^1$, $\underline{e}^1 \in F^{\ell-q}$. If T_ℓ is error free and $\hat{y}^1$ is contained in Γ, then the elements of $\underline{e}^1$ will all be zero.

3. $\underline{e}^1$ is used to drive an iterative R_ℓ estimator. The gains of this estimator are chosen so that the output converges to the true values in the row vectors of T_ℓ.

AD-A092 547 AIR FORCE INST OF TECH WRIGHT-PATTERSON AFB OH F/G 22/2
OPTIMAL REGULATION WITHIN SPATIAL CONSTRAINTS. AN APPLICATION T--ETC(U)
AUG 80 E G TAYLOR
UNCLASSIFIED AFIT-CI-80-46D NL

3 OF 4
AD A092547

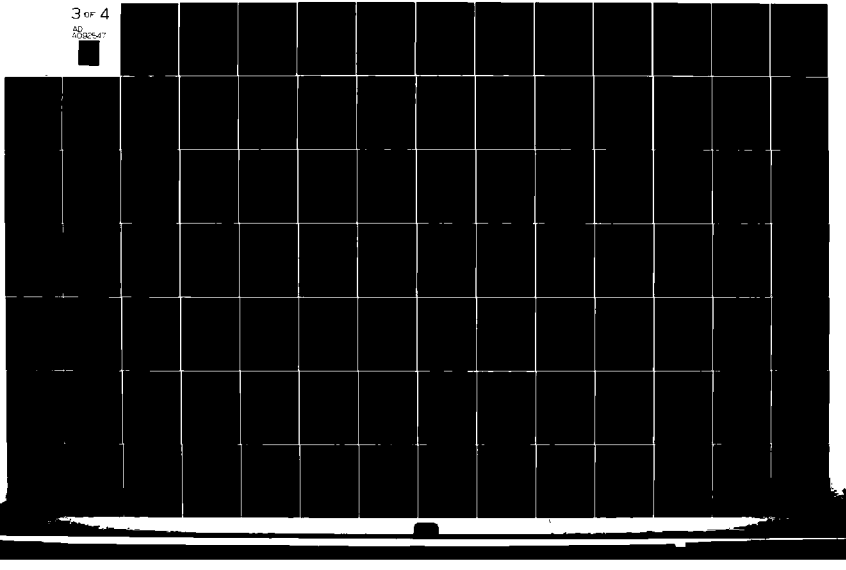

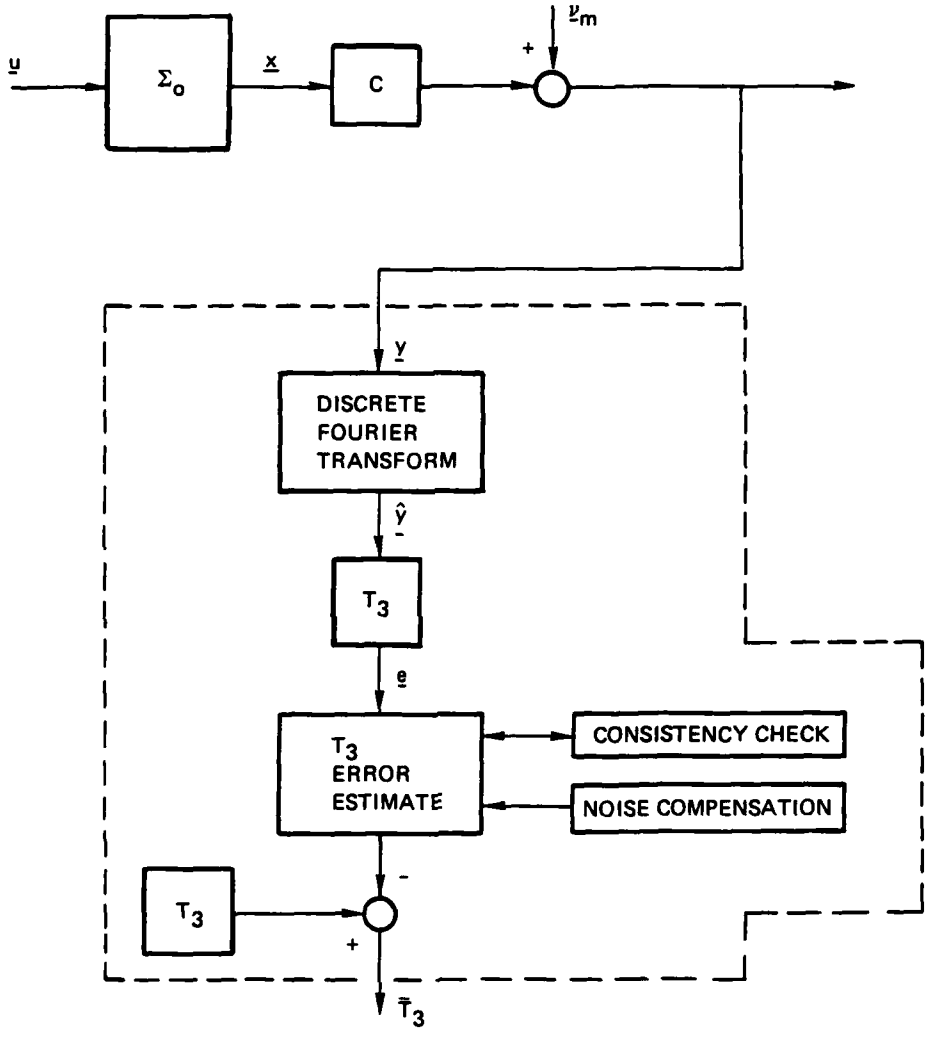

Figure C-2. Adaptive loop configuration.

(4) Once $[E_j]$ is known, then $\bar{T}_3$ is formed from

$$\bar{r}_j = r_j + E_j \qquad j = 1, \ell - q \tag{C-26}$$

These steps are now discussed in detail.

C.3.1 $\hat{y}^i$ Processing

Recall that $\underline{y}$ is the output of the linear system Σ_0:

$$\underline{y} = C_1\underline{x}_1 + C_2\underline{x}_2 + \underline{\nu}_m \tag{C-27}$$

where

$$\underline{y} \in R^{\ell}, \ \underline{x}_2 \in R^{q} \ ; \ \ell > q$$

Σ_0 describes the time variation of the state vectors $\underline{x}_1$ and $\underline{x}_2$, and $\underline{\nu}_m$ is white zero mean measurement noise. The column vectors of C_2 span τ, where τ is a subspace of R^{ℓ}. The objective of this section is to define a filter which, when driven by $\underline{y}$, will produce an ℓ dimensional vector output $\hat{\underline{y}}^i$, valid at the i^{th} time instant, where $\hat{\underline{y}}^i$ is contained in τ.

The signal $\underline{y}$ is a vector function of time. The elements of $\underline{y}$ are physically the outputs of individual sensors. Restricting attention to a specific single-sensor output $y[t]$, we note that over the interval $[0,T]$, the function $y[t]$ can be represented by the complex Fourier series

$$y[t] = \sum_{n=\infty}^{\infty} C_n e^{jn\omega_0 t} \tag{C-28}$$

where

ω_0 = $2\pi/T$

T = period (seconds)

n = harmonic number (integer)

C_n = Fourier coefficient

$$C_n = \frac{1}{T}\int_0^T y[t]e^{-jn\omega_0 t}\,dt \qquad \text{(C-29)}$$

This representation assumes that y[t] is known and well behaved everywhere in the interval [0,T]

If y[t] is sampled at a uniform rate, the sequence y[i] can be represented by

$$y(i) = \sum_{n=0}^{N-1} F[n]e^{j\frac{2\pi ni}{N}} \qquad \text{(C-30)}$$

where

ΔT = sampling time (seconds)

i = denotes the i^{th} sampled value

N = total number of sampled points in [0,T]

where

$$\left.\begin{array}{l} T = N\,\Delta T \\ \omega_0 = \dfrac{2\pi}{N\,\Delta T} \\ t = i\,\Delta T \end{array}\right\}$$

and

$$F(n) = \frac{1}{N} \sum_{i=0}^{N-1} y[i] e^{-j\frac{2\pi ni}{N}} \qquad \text{(C-31)}$$

Equation (C-31) is known as the discrete Fourier transform, and hardware is available which accepts sampled values of a signal, and which outputs F[n].[28]

If we generalize Eq. (C-30) to the vector case, where $\underline{y}^i \in R^{\ell}$, then we get

$$\underline{y}^i = \sum_{n=0}^{N-1} \underline{F}[n] e^{j\frac{2\pi ni}{N}} \qquad \text{(C-32)}$$

where the elements of $\underline{F}[n]$ represent the values of F[n] which correspond to the appropriate elements of $\underline{y}^i$.

If the $\underline{x}_2$ states are oscillatory and lightly damped, a set of associated characteristic frequencies Ω_α, $\alpha = 1, q/2$ can be identified. Then $C_2 \underline{x}_2{}^i$ can be approximated by

$$C_2 \underline{x}_2{}^i \approx \underline{y}_2{}^i = \underline{F}[n_1] e^{j\frac{2\pi n_1 i}{N}} + \ldots \underline{F}[n_k] e^{j\frac{2\pi n_k i}{N}} \qquad \text{(C-33)}$$

where the parameters n_k are all integers such that the quantities $\frac{2\pi n_k}{N\,\Delta T}$ fall within some small neighborhood, $[\Omega_\alpha - \varepsilon_\alpha, \Omega_\alpha + \varepsilon_\alpha]$, of the characteristic frequencies, for $\alpha = 1, g/2$. This approximation may, in fact, be poor, with the error coming from the following two sources.

(1) The Fourier representation of any individual mode, based only on series terms within $[\Omega - \varepsilon, \Omega + \varepsilon]$, may be inadequate.

(2) The values of $F[n_k]$ will reflect the measurement noise $\underline{\nu}_m$.

The development of a Fourier representation of $\underline{y}[t]$ is to some extent a digression. Recall that the basic intent of this section is to define a filter which, when driven by $\underline{y}[t]$, will produce a set of ℓ dimensional vectors $[\hat{y}^1 \ldots \hat{y}^k]$, where each $\hat{\underline{y}}^i$ is in τ, and where the set of vectors $\hat{\underline{y}}^i$, $i = 1, \ell = q$ spans τ.

The Fourier discussion was introduced because, in cases where y_2^i is a sufficiently accurate approximation of $C_2\underline{x}_2$, then all the vectors $\underline{F}^i[n_k]$ will be in τ and the set of $\underline{F}^i[n_k]$, where the n_k are defined for Eq. (C-33), will span τ. This is a useful idea because it allows a transform error estimate directly from the spatial distributions of the Fourier coefficients, and the inverse transform (estimate of $C_2\underline{x}_2{}^i$) does not need to be calculated. The issue of the error in this procedure remains.

In general, if the $\underline{x}_1$ and $\underline{x}_2$ states are interlaced in frequency, then the errors may be large. However, for the special case where $\underline{x}_1$ and $\underline{x}_2$ are separated in frequency, and where specifically $\underline{x}_2$ falls in the band $[\omega_1, \omega_2]$, $\hat{y}_2^i$ can be formed

$$\underline{y}_2^i = \sum_{n=n_1}^{n_2} F[n] e^{j\frac{2\pi ni}{N}} \qquad \text{(C-34)}$$

where

$$n_1 = \text{integer } [\omega_1 \frac{N\ \Delta T}{2\pi}]$$

$$n_2 = \text{integer } [\omega_2 \frac{N\ \Delta T}{2\pi}]$$

If N and ΔT can be picked so that $\omega_1 N\ \Delta T/_{\pi 2}$ and $\omega_2 N\ \Delta T/_{\pi 2}$ are in fact integers, and there is no noise, then $\hat{\underline{y}}_2^i$ will correspond to $C_2\underline{x}_2$ exactly; and $\underline{F}^i[n_k]$, $k = n, \ldots n_2$ will span τ. For applications in this thesis, the set of vectors $\underline{F}^i[n_k]$ are used to drive the transform error estimates.

The presence of measurement noise will introduce a random error to each element of $\underline{F}[n]_1 n = n_1, n_2$. The magnitudes of these errors can be described statistically based on knowledge of the noise characteristics. This thesis does not treat this area definitively. Instead, it is argued heuristically that the effect of noise is small for the case of real interest—the case of an $\underline{x}_2$ mode which is excited, and lightly or negatively damped. Here, the structural amplitudes, would tend to be significant and the resulting signal-to-noise ratio would be large. Additionally, spectral filtering, which is normally introduced to account for discrete effects in the FFT may have desirable noise suppression qualities. In the illustration of the adaptive process, which is presented later in this appendix, a Hanning window is used to process the output before the FFT is calculated. However, a detailed investigation of the effect of noise was not undertaken.

C.3.2 Estimation of E_j

The estimation algorithm which is developed here is driven by the signal $\underline{\hat{y}}$ and produces an estimate of the error in T_3, that is an estimate of $[E_j]$. Specifically, it is assumed that a set of measurements $\{y^1 \ldots y^{k_j}\}$ is available, where each y^i is in the subspace τ. These y^i may be spatial arrays of Fourier coefficients. In any event, the relation

$$\langle [r_j - E_j], \underline{y}^i \rangle = 0 \qquad \text{(C-35)}$$

must hold for all j, $j = 1, \ell - q$, and all i. In effect, the estimation problem reduces to finding the E_j, so that each quantity $[r_j - E_j]$ is orthogonal to the set of measurement vectors. The Gram-Schmidt formulation provides an iterative method of finding the E_j. Specifically, the iteration

$$E_j^{i+1} = E_j^i + K_j^i \underline{y}^i \qquad \text{(C-36)}$$

where

$$E_j^0 = \underline{0}$$

$$K_j^i = \langle r_j - E_j^i, \underline{y}^i \rangle / |\underline{y}^i|^2$$

where

$| \; |$ ⇨ geometric mean

$\langle \; \rangle$ ⇨ inner product

will converge to E_j when $\{\underline{y}^1 \ldots \underline{y}^k\}$ span the subspace τ. The term

$$\frac{\langle r_i - E_j^i, \underline{y}^i \rangle \underline{y}^i}{|\underline{y}^i|^2} \tag{C-37}$$

is the orthogonal projection of $r_j - E_j^i$ on $\underline{y}^i$. The algorithm assumes that $r_j - E_j^i$ is orthogonal to the subspace spanned by $\{y^1 \ldots y^{i-1}\}$, and then ensures that $r_j - E_j^{i+1}$ will be orthogonal to the subspace spanned by $\{\underline{y}^1 \ldots \underline{y}^i\}$ by subtracting out the projection of $r_j - E_j^i$ on $\underline{y}^i$. The Gram-Schmidt gain is optimal, but alternate gains are possible. Any gain sequence G_j^i, such that

$$G_j^i = \gamma_j K_j^i$$

$$0 < \gamma_j < 2 \tag{C-38}$$

will converge. Convergence will be fastest for γ close to 1.

C.3.3 Transform Update

If a converged estimate of the transform error $[E_j]$ is available, then the output transform can be updated using the relationship

$$\bar{T}_3 = T_3 - [E_j] \tag{C-39}$$

Prior to taking this step, the calculated $[E_j]$ can be checked for consistency. By definition, the true error associated with any r_j must lie totally in the subspace τ. It is, therefore, legitimate to require that, at any step, the condition

$$\bar{T}\, E_j^i = 0 \tag{C-40}$$

must hold. If the condition does not hold, then E_j^i will have components in the C_1 space which can be subtracted out by

$$\bar{E}_j^i = E_j^i - \sum_k \frac{\langle \bar{r}_k, E_j^i \rangle F_k}{|\bar{r}_k|^2} \tag{C-41}$$

where the $\bar{r}_k$ are the row vectors of the true transform $\bar{T}$. In reality, the transform $\bar{T}$ will be unavailable for use in an algorithm. However, the approximation

$$\frac{(r_j - E_j^i)}{|r_j - E_j^i|} \approx \frac{\bar{r}_j}{|\bar{r}_j|} \tag{C-42}$$

will become increasingly good as the τ components of E_j^i converge. It is suggested, therefore, that that equation be modified to

$$\bar{E}_j^i = E_j^i - \sum_k \frac{\langle r_k - E_k^i, E_k^i \rangle (r_k - E_k^i)}{|r_k - E_k^i|^2} \tag{C-43}$$

and that that equation be invoked prior to the actual update of the transform T_3.

C.4 Summary

The intent has been to develop an adaptive scheme that corrects the output transform T_3 to account for system variations and model inaccuracies. The particular scheme which is presented uses the measured-system output to form spatial arrays of Fourier coefficients, which are then used to drive an error estimator. The estimator itself uses geometric concepts to ensure that the updated transform meets the required conditions

$$T_3[C_1]_T \neq 0$$

$$T_3[C_2]_T = 0$$

Alternate schemes are of course possible. Some of the strengths of this approach include the following.

(1) Frequency information is used to check T_3, where T_3 is initially selected based on the system spatial response characteristics.

(2) The Fourier coefficients are outputs from common, commercially available digital processing elements.

(3) The use of nonlinear (Gram-Schmidt) gains in the estimator aids convergence rate.

This scheme will perform best when $\underline{x}_1$ and $\underline{x}_2$ are in separate frequency bands. Note also that in this special case, the scheme is insensitive to the specific frequency characteristics of $\underline{x}_2$. The only value that is needed with precision is ω_1, the lower bound of the $\underline{x}_2$ frequencies.

There are issues which remain. Perhaps the most troublesome is the treatment of measurement noise. For a discussion of noise effects on spectral estimates, see Kay.[29] He also evaluates several noise compensation schemes. Despite the issues, the idea that frequency-based descriptions can be arrayed spatially and used to update input and output transforms is significant. Two examples are included in this appendix to illustrate that this spatial arraying can result in mode shape estimates.

C.5 Examples: Mode Shape Estimates From Spatial Arraying of Fourier Coefficients

For illustrative purposes, the horizontal solar panel vibration modes (modes 4, 8, 10, 16, 17, 31, 32) were given a unit initial displacement. The output of six solar panel sensors was monitored. The placement of sensors is detailed in Figure C-3; the mode shapes of interest are shown in Figures C-4 and C-5; and the output time histories are given in Figures C-6 through C-9. In addition, mode shape values at sensor locations are given in Table C-1. The objective is to derive the mode shapes at the sensor locations using just the output time histories. To do this, each sensor output was passed through a fast-Fourier transform, and then the resulting coefficients were arrayed spatially. This data flow is presented graphically in Figure C-10. Power spectral density plots ($PSD[n] = 2 \times C[n]^2$) indicate the variation in the Fourier coefficients with sample frequency for each output. These plots are given in Figures C-11 through C-16. There is strong evidence of resonances in the data, as expected. The output of the fast-Fourier transform (FFT) processors can be arrayed spatially; here a six-element row vector is available for each n. Table C-2 is a printout of all such vectors with lengths greater than 10^{-4}. The available vectors are superpositions of modes 8 and 10 at 3.9 hertz, 16 and 17 at 21 hertz, and 31 and 32 at 60 hertz.

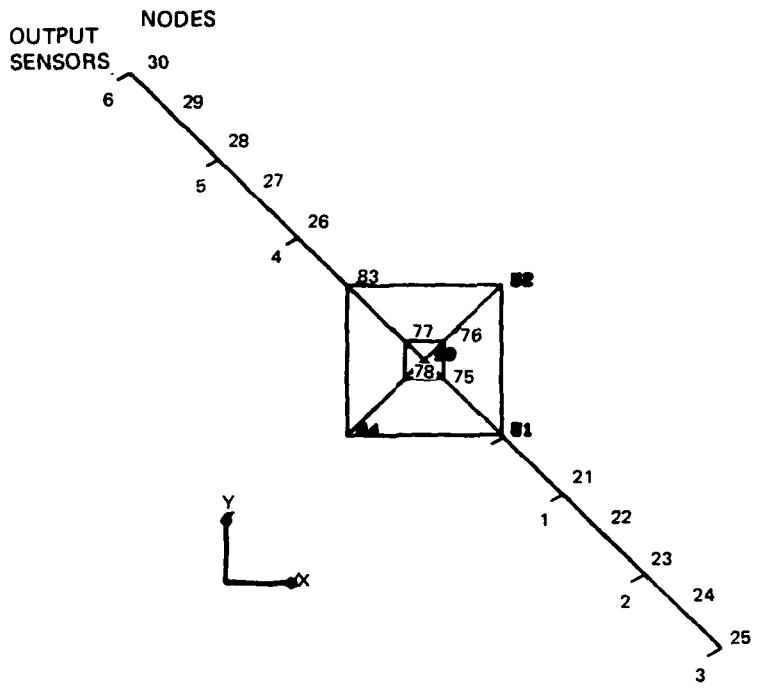

Figure C-3. Solar-panel output sensor locations.

The following points can be noted.

(1) The vectors which result from the spatial arraying of Fourier coefficients are linear combinations of the made. shapes which occur at the frequency of interest.

(2) If a transform T_3 were chosen to exclude modes (8, 10, 16, 17, 31, 32), then the vectors of Table C-2, V_i, will meet the criteria

$$T_3 V_i = 0$$

(3) Frequency methods cannot separate the effects of two different modes which have the same natural frequency.

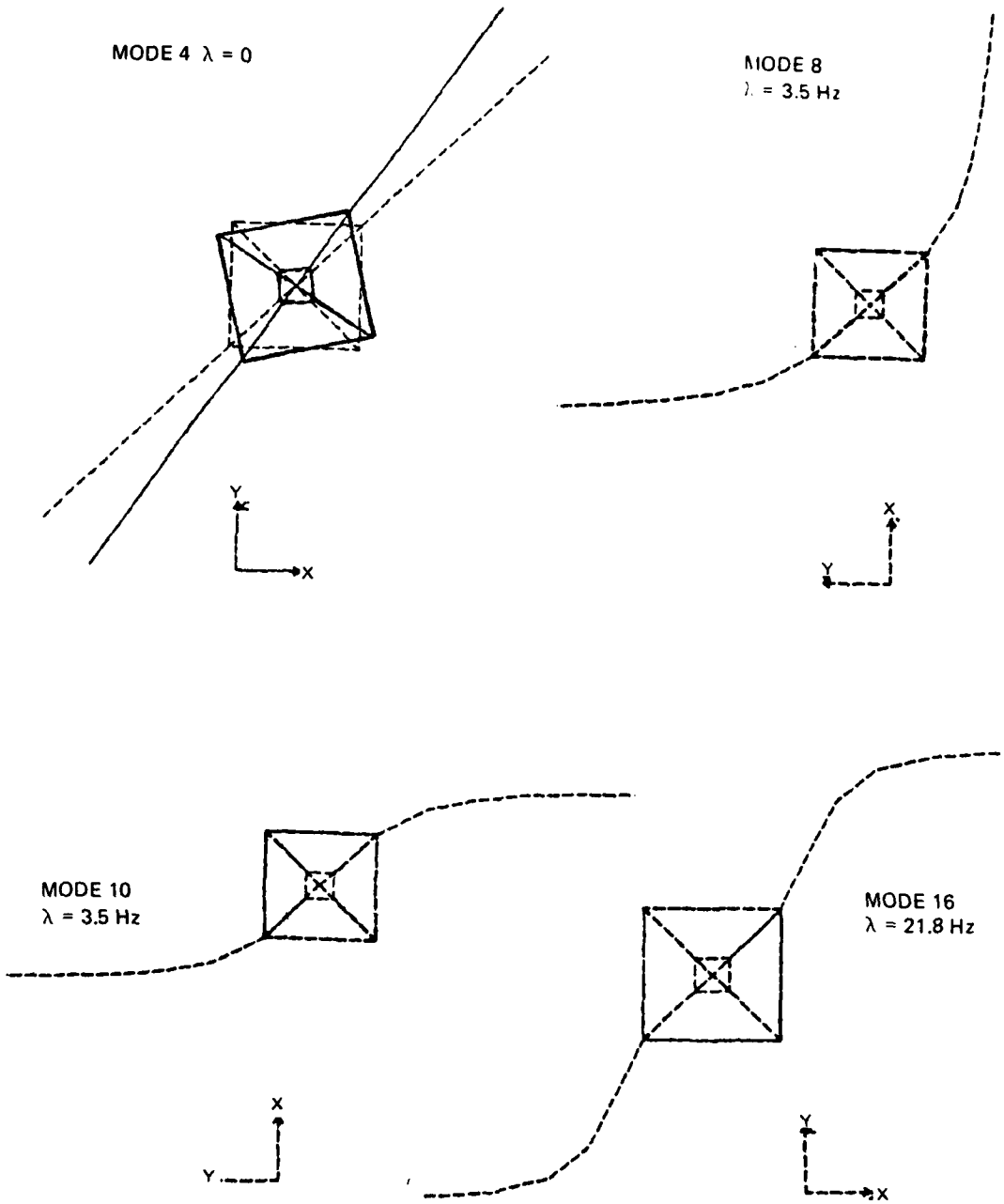

Figure C-4. Shapes for Modes 4, 8, 10, and 16.

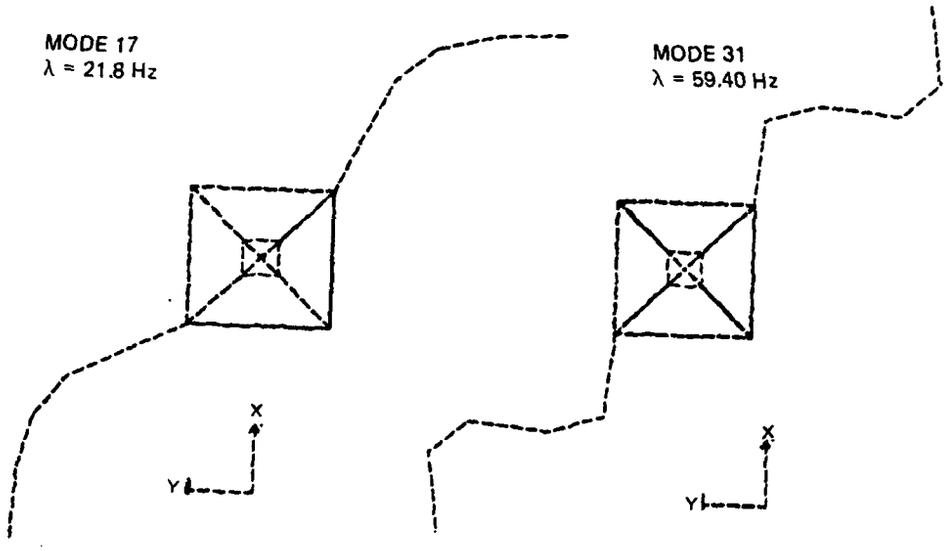

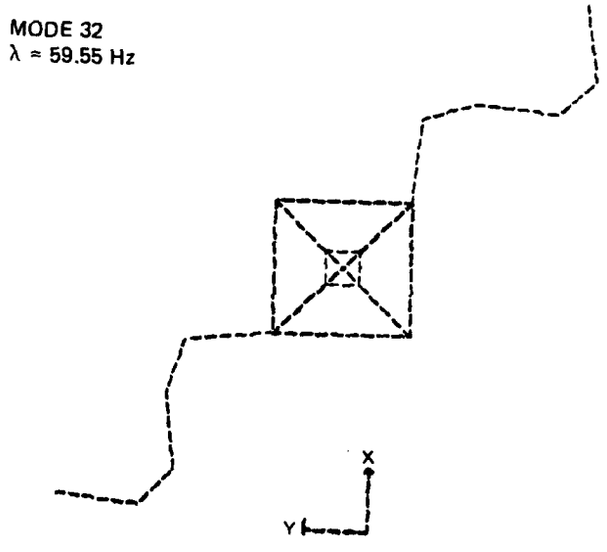

Figure C-5. Shapes for Modes 17, 31, and 32.

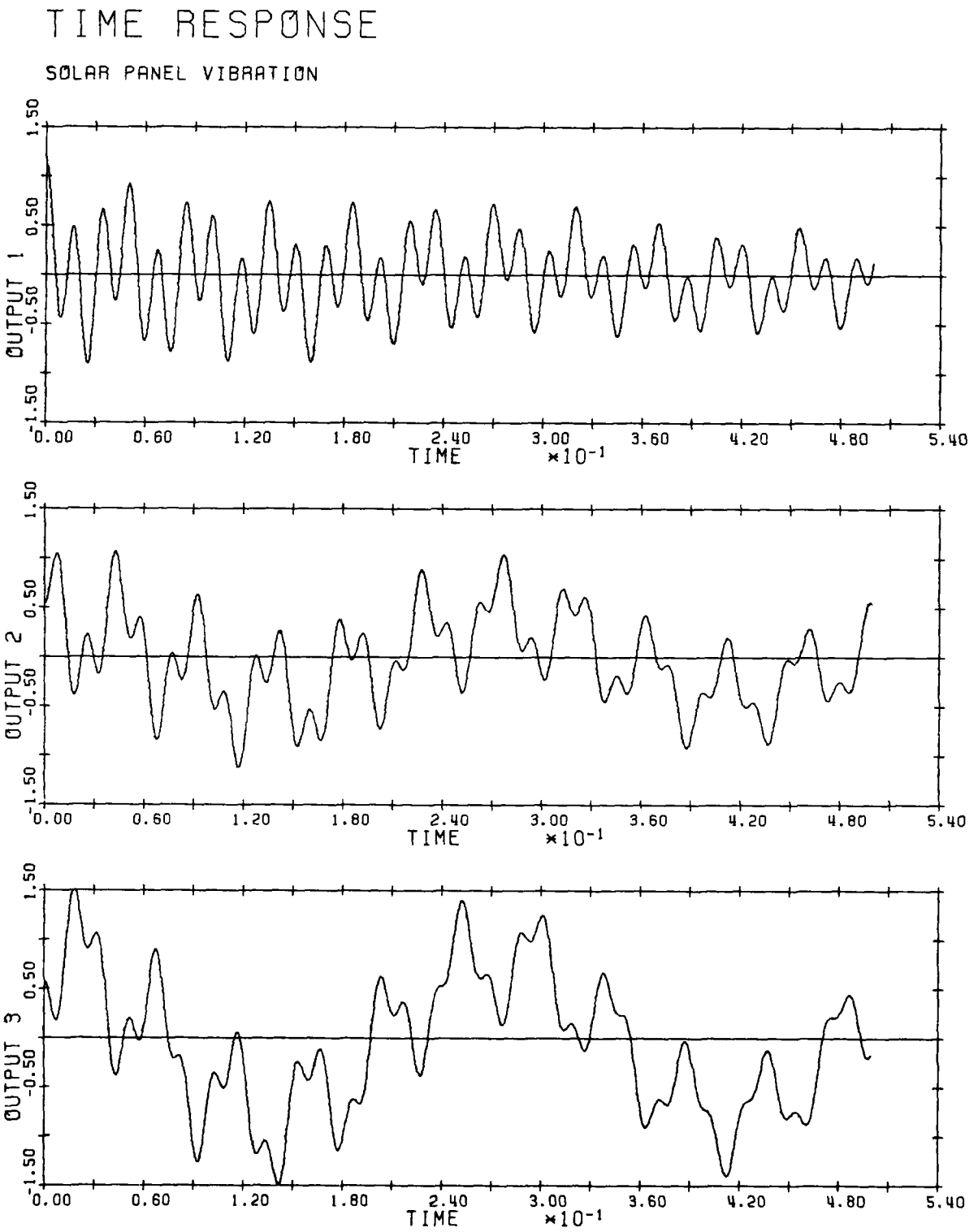

Figure C-6. Example 1: output time histories (outputs 1 through 3).

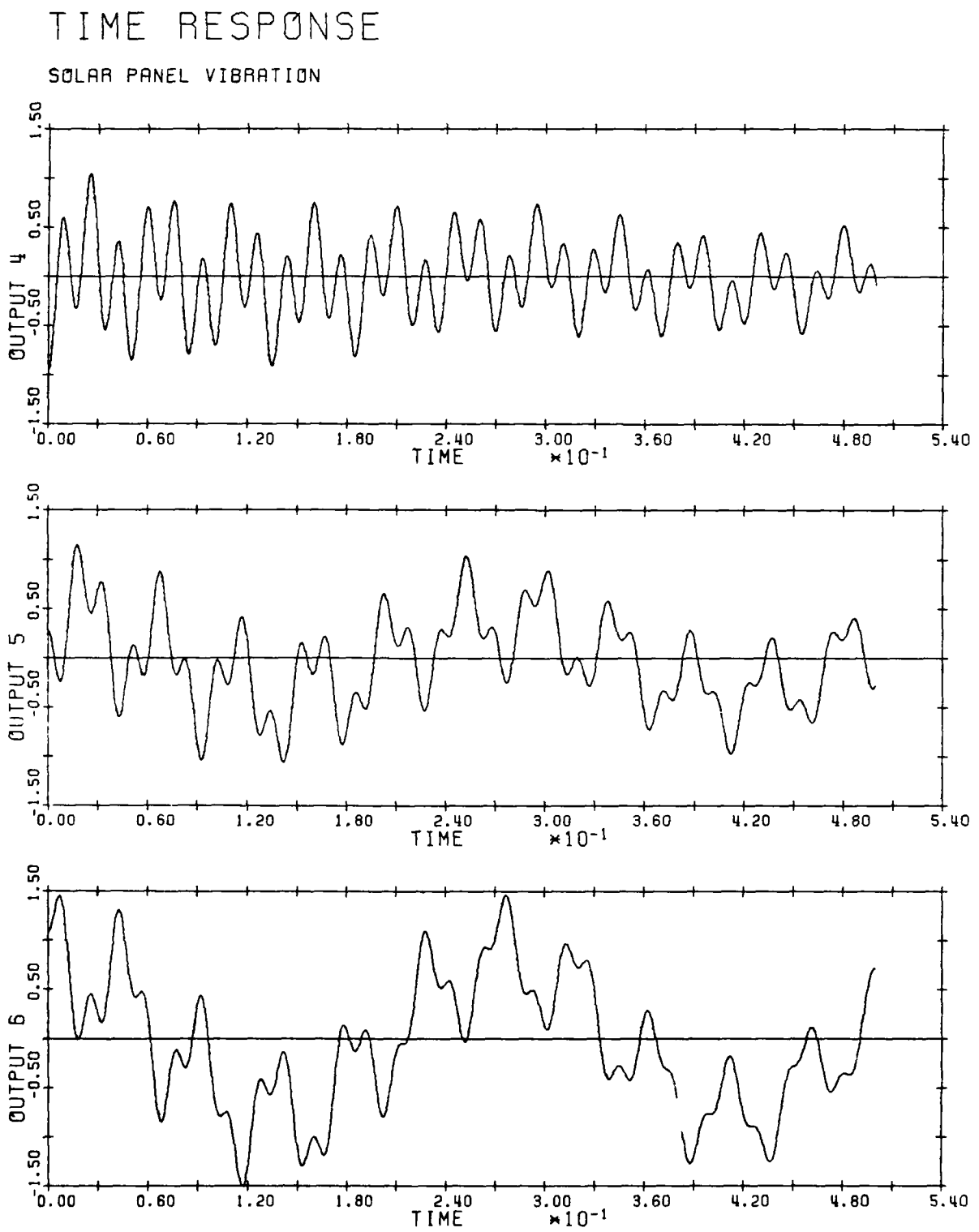

Figure C-7. Example 1: output time histories (outputs 4 through 6).

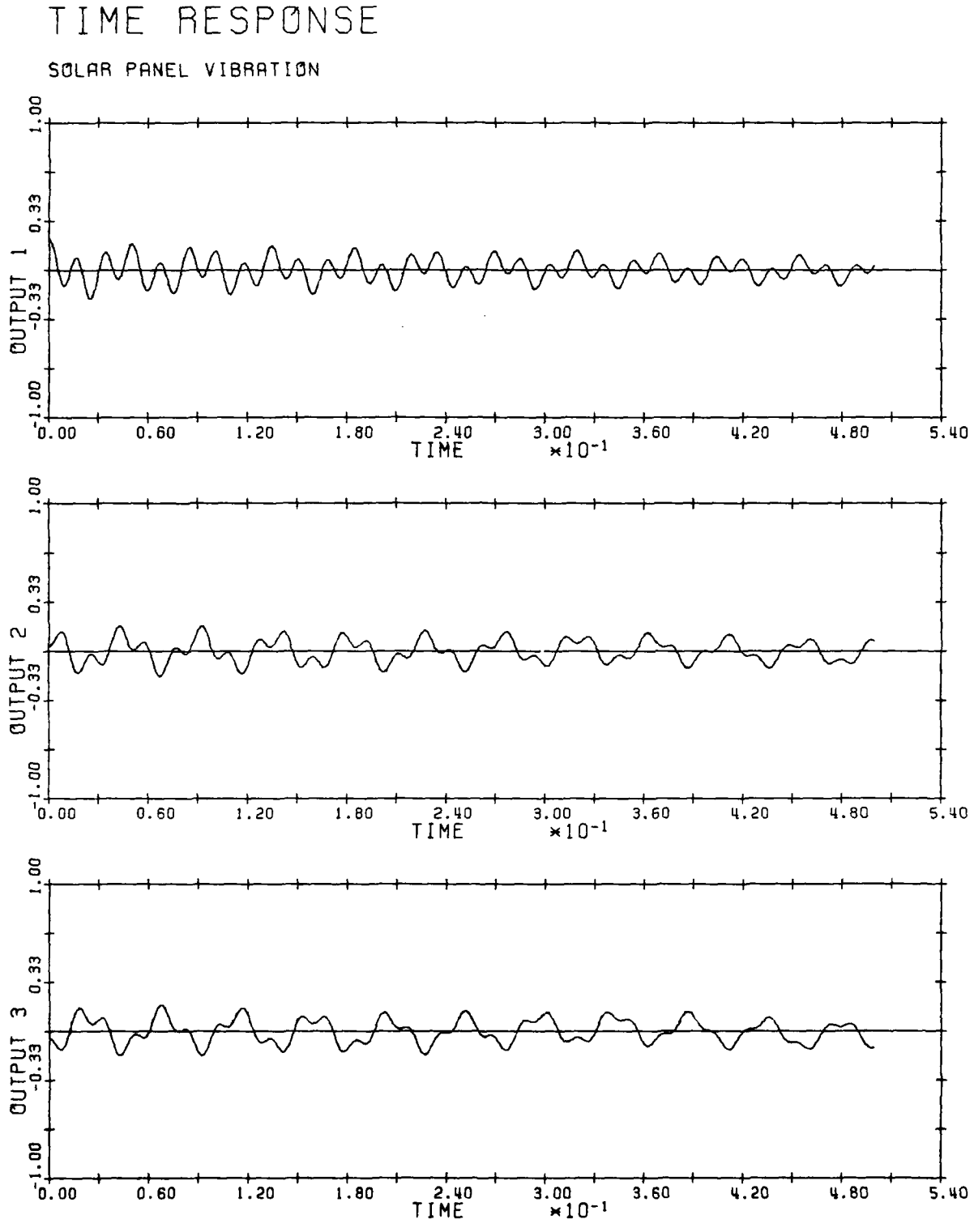

Figure C-8. Example 2: output time histories (outputs 1 through 3).

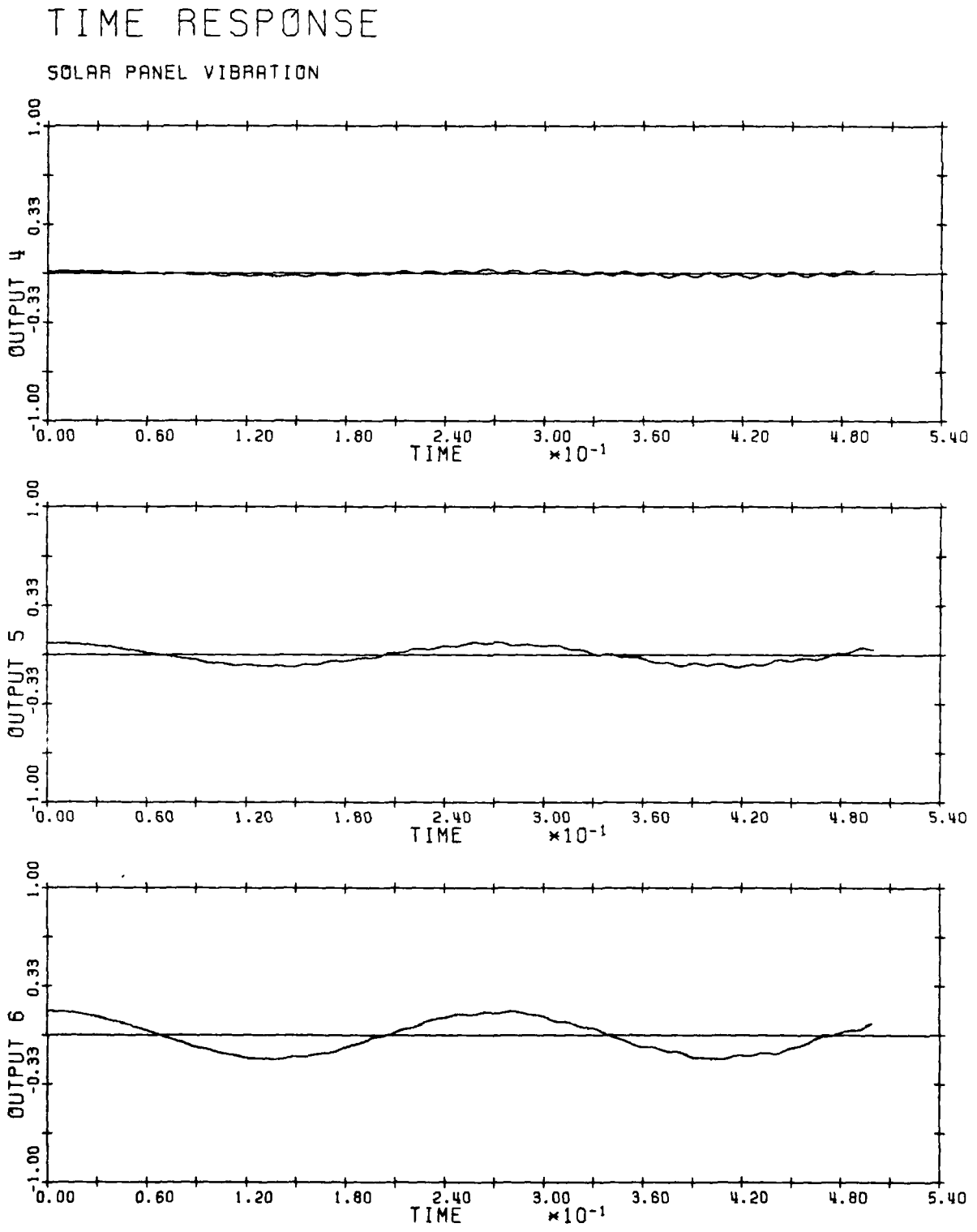

Figure C-9. Example 2: output time histories (outputs 4 through 6).

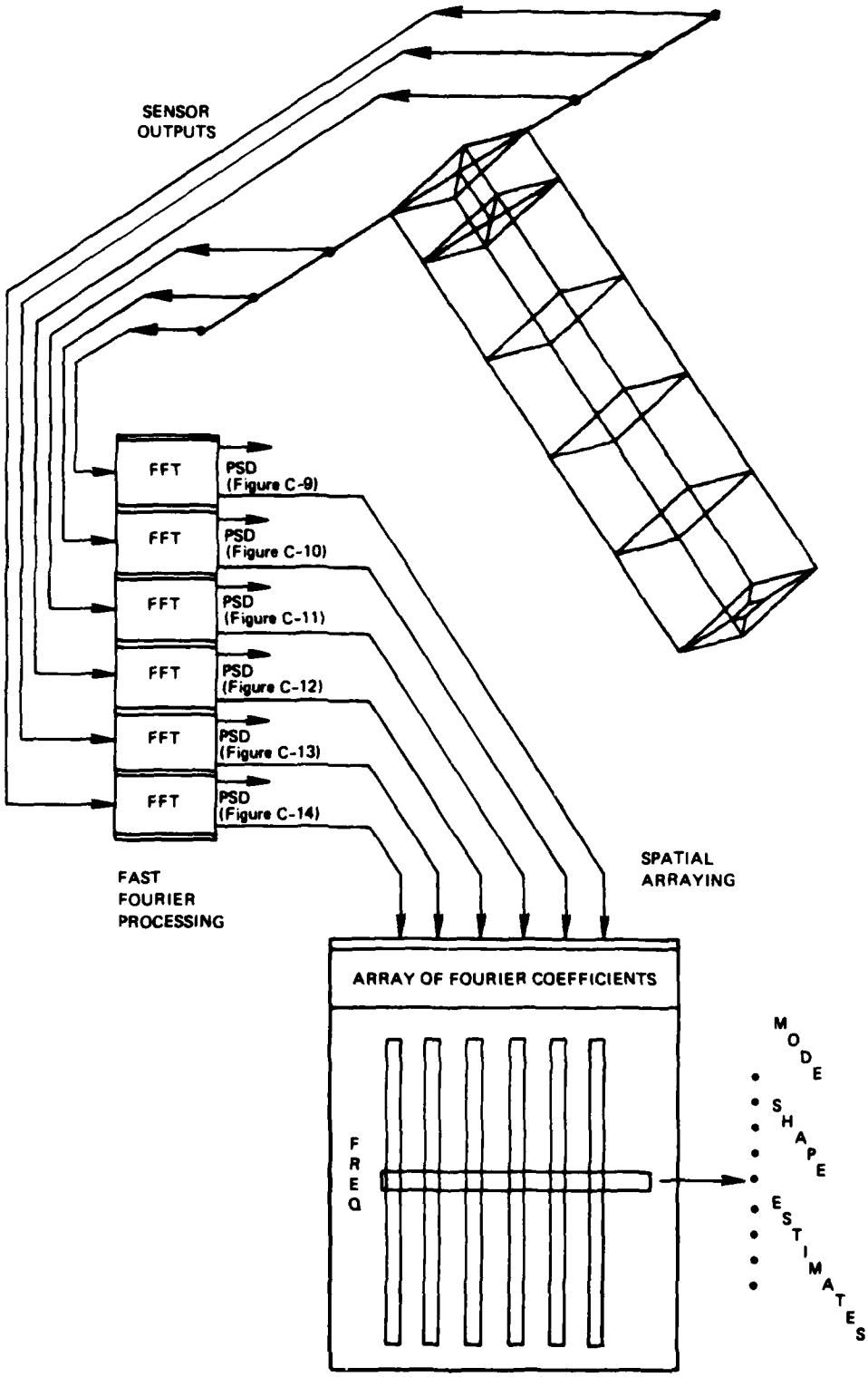

Figure C-10. Data-processing flow.

Table C-1. True values of mode shapes evaluated at sensor locations.

Mode	Frequency (Hz)	Sensors					
		3	2	1	4	5	6
4	0	0.1866	0.1399	0.0789	-0.0789	-0.1399	-0.1866
8	3.5	0.826	0.4067	0.0836	0.0836	0.4067	0.826
10	3.5	-0.8062	-0.3861	-0.0662	0.0662	0.3861	0.8062
16	21.8	-0.6034	0.5358	0.3618	-0.3618	-0.5358	0.6034
17	21.8	-0.6045	0.5884	0.3591	0.3591	0.5384	-0.6045
31	59.4	0.3422	-0.4003	0.6639	-0.6639	0.4003	-0.3422
32	59.4	0.3435	-0.4011	0.6676	0.6676	-0.4011	0.3435

The FFT/power spectral density software package, which was used in the examples, was developed by Konigsberg.[28] It includes a Hanning window to account for the discrete effects and to enhance resolution.

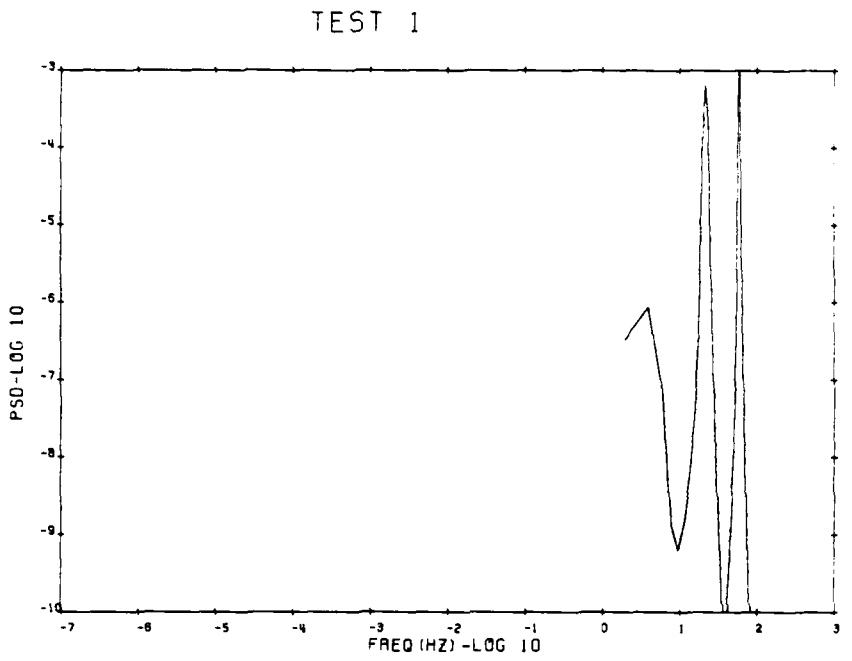

Figure C-11. Power spectral density plot of output 1, example 1.

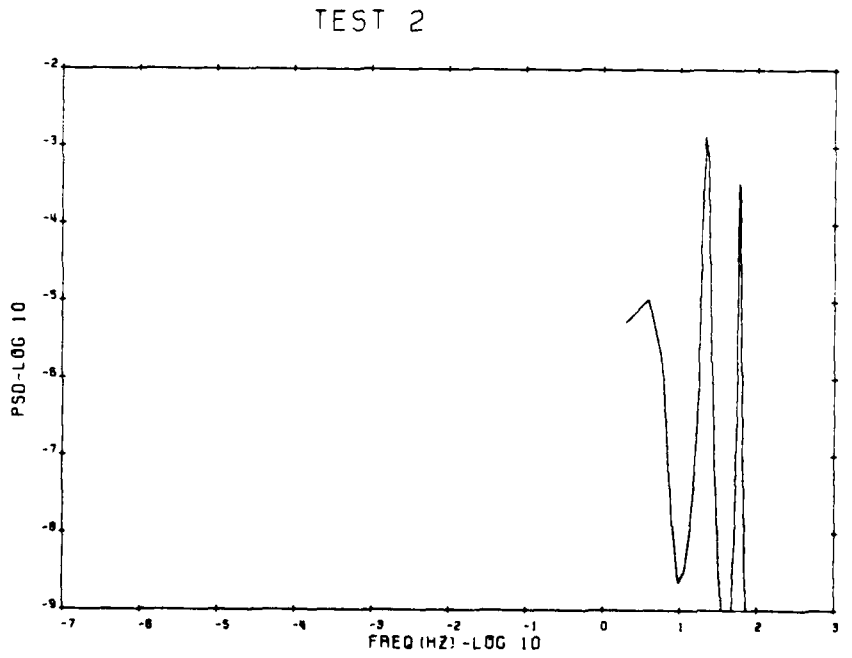

Figure C-12. Power spectral density plot of output 2, example 1.

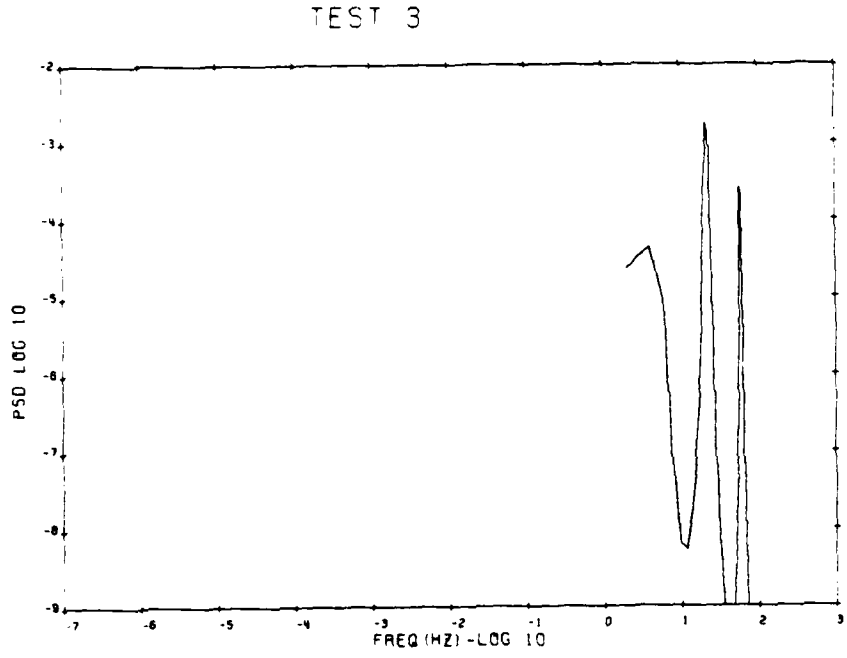

Figure C-13. Power spectral density plot of output 3, example 1.

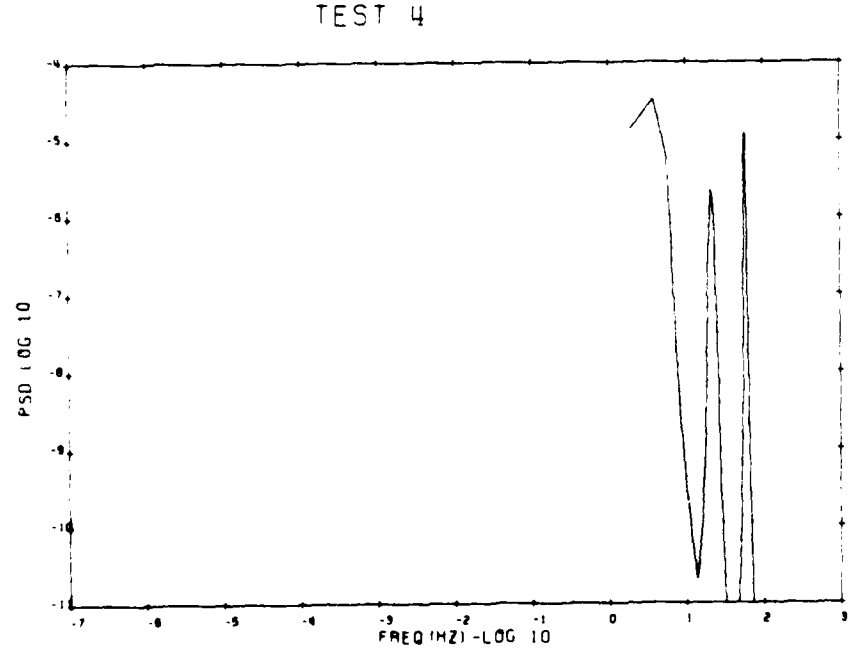

Figure C-14. Power spectral density plot of output 4, example 1.

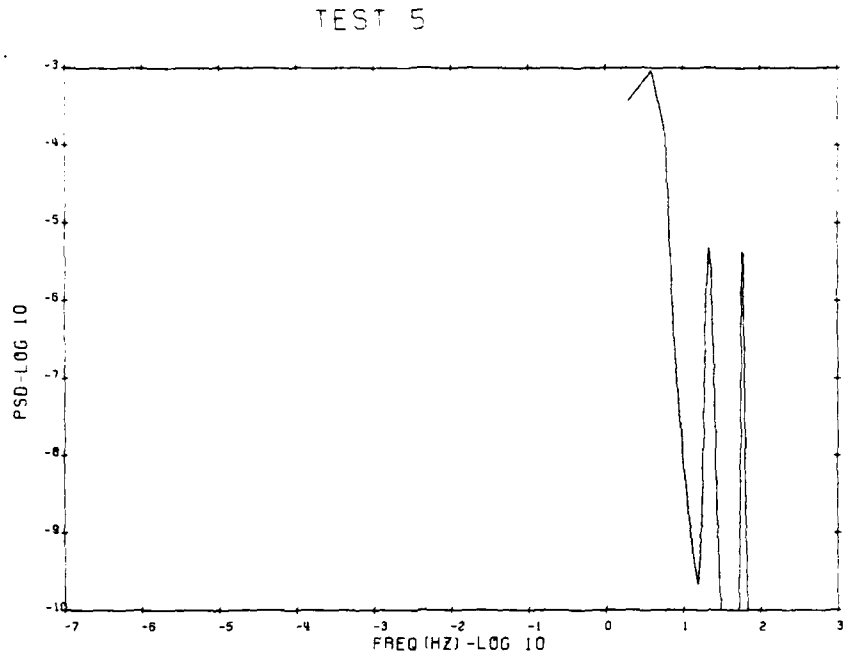

Figure C-15. Power spectral density plot of output 5, example 1.

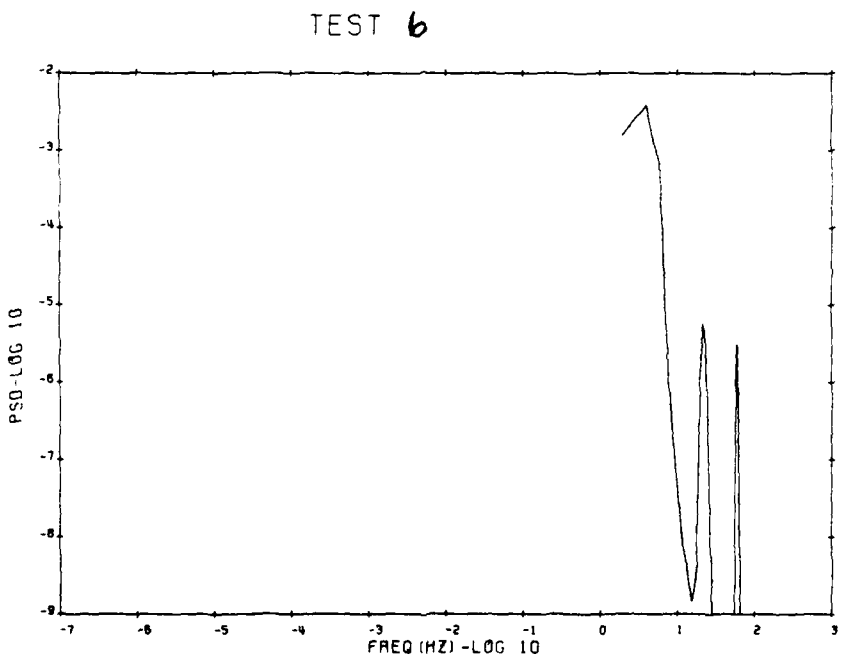

Figure C-16. Power spectral density plot of output 6, example 1.

Table C-2. Vectors with lengths greater than 10^{-4}. (Case 1)

Frequency (Hz)	Mode Shapes					
3.9062	-0.39064D-01	-0.18990D-01	-0.36310D-02	-0.56636D-03	-0.22762D-02	-0.47391D-02
5.8594	0.61234D-01	0.29802D-01	0.56364D-02	0.91575D-03	-0.32103D-02	-0.64670D-02
21.484	-0.99315D-03	0.86292D-03	0.60967D-03	-0.88606D-02	-0.12876D-01	0.14505D-02
23.437	0.23863D-02	-0.21333D-02	-0.14451D-02	0.24982D-01	0.36319D-01	-0.40910D-01
25.391	-0.17368D-02	0.15539D-02	0.10132D-02	-0.17095D-01	-0.24853D-01	0.27994D-01
58.594	0.49342D-03	-0.57952D-03	0.95444D-03	-0.72130D-02	0.42390D-02	-0.36330D-02
60.547	-0.17470D-02	0.20494D-02	-0.33958D-02	0.31017D-01	-0.18215D-01	0.15611D-01
62.500	0.16665D-02	-0.19495D-02	0.32517D-02	-0.29199D-01	0.17148D-01	-0.14697D-01

A second test case was run where only modes 8, 16, and 31 were excited. The time histories of the output are given in Figures C-17 and C-18. The output PSD calculations is given in Figures C-19 through C-24. The spatial arraying of Fourier coefficients results in the vectors given in Table C-3. In this case, there was no multiplicity among the excited eigenfrequencies, and the output closely approximates the true mode shapes.

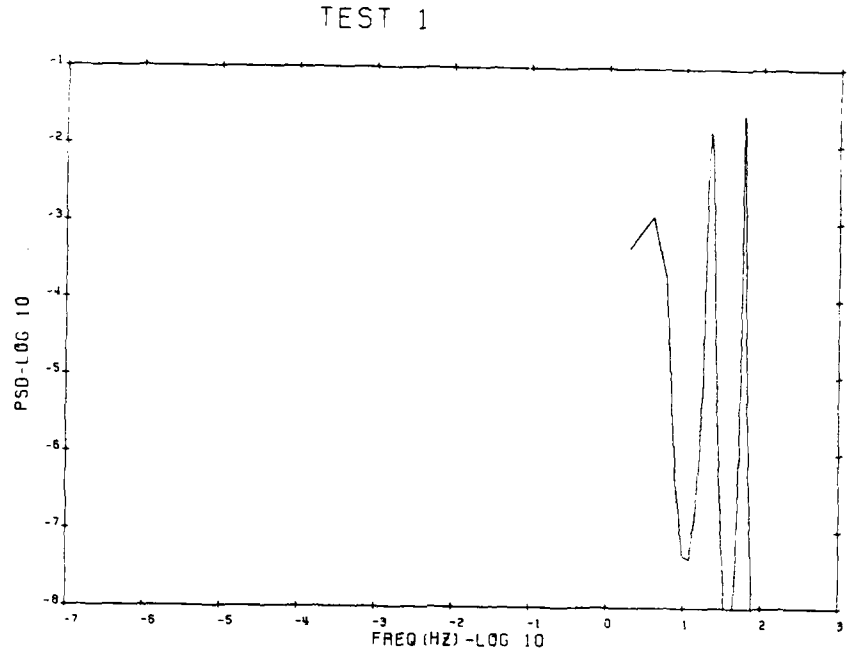

Figure C-19. Power spectral density plot of output 1, example 2.

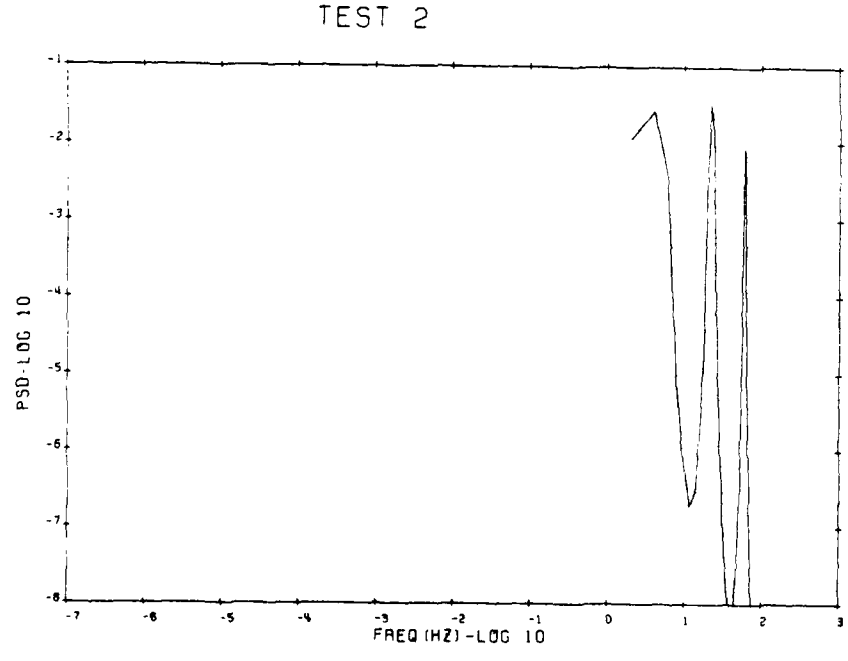

Figure C-20. Power spectral density plot of output 2, example 2.

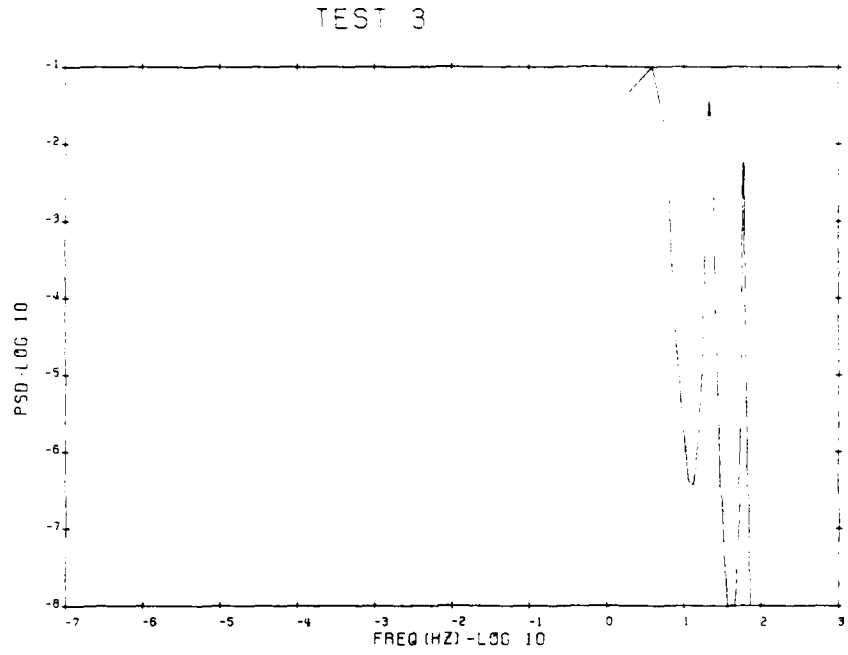

Figure C-21. Power spectral density plot of output 3, example 2.

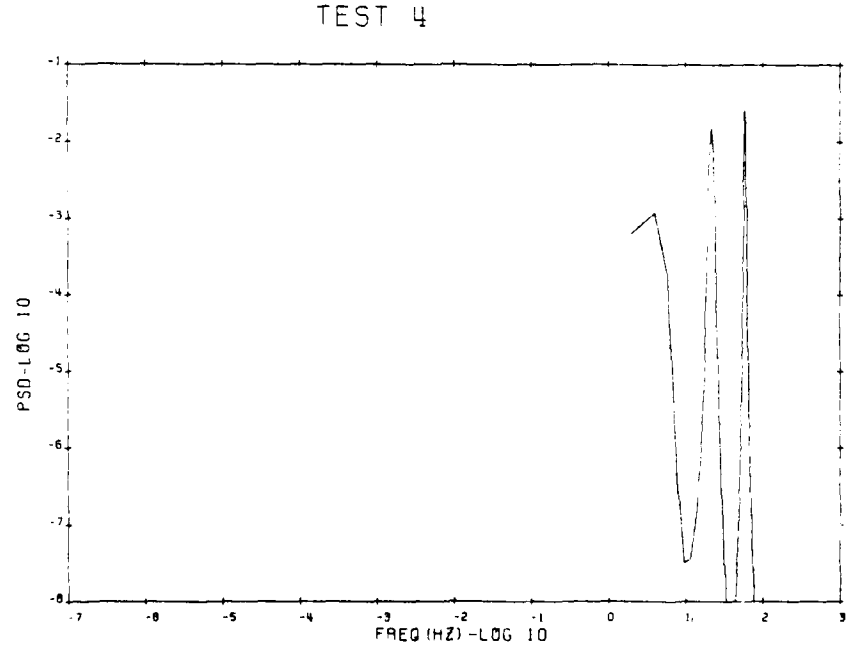

Figure C-22. Power spectral density plot of output 4, example 2.

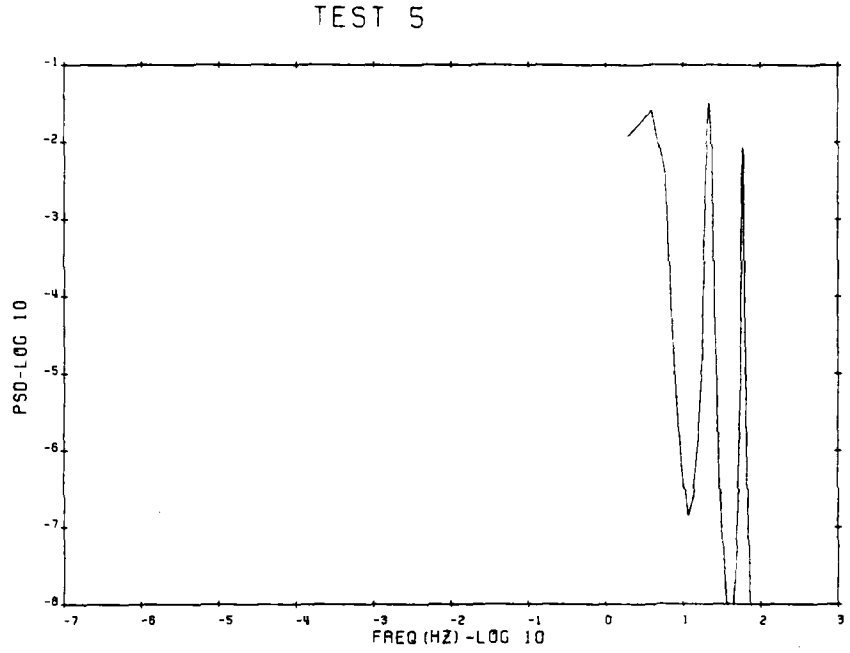

Figure C-23. Power spectral density plot of output 5, example 2.

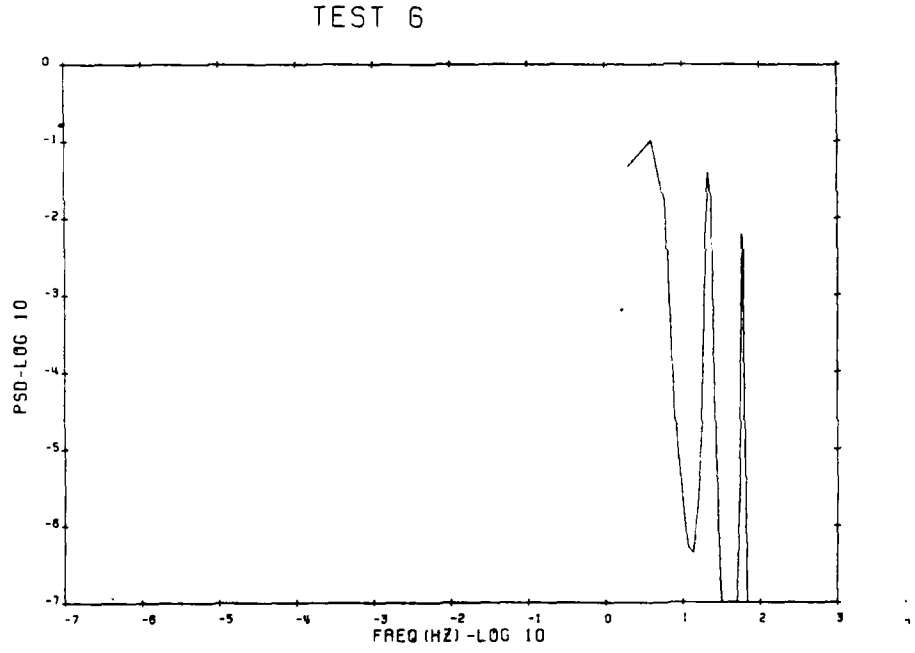

Figure C-24. Power spectral density plot of output 6, example 2.

Table C-3. Vectors with lengths greater than 10^{-4}. (Case 2)

Frequency (Hz)	Mode Shapes					
3.9062	-0.21213	-0.10755	-0.24740D-01	-0.21240D-01	-0.10592	-0.21227
5.8594	0.31781	0.15725	0.34056D-01	0.34183D-01	0.15975	0.31240
7.8125	-0.12635	-0.62454D-01	-0.13504D-01	-0.13614D-01	-0.63526D-01	-0.12411
21.484	-0.72722D-01	0.64880D-01	0.46108D-01	-0.46340D-01	-0.65945D-01	0.71443D-01
23.437	0.19824	-0.17692	-0.12570	0.12632	0.17979	-0.19483
25.391	-0.13188	0.11770	0.83640D-01	-0.84054D-01	-0.11961	0.12962
60.547	-0.77333D-01	0.90913D-01	-0.15866	0.15945	-0.92383D-01	0.76000D-01
62.500	0.69071D=01	-0.81193D-01	0.14168	-0.14238	0.82510D-01	-0.67877D-01

Table C-2. Vectors with lengths greater than 10^{-4}.

Frequency (Hz)	Mode Shapes					
3.9062	-0.39064D-01	-0.18990D-01	-0.36310D-02	-0.56636D-03	-0.22762D-02	-0.47391D-02
5.8594	0.61234D-01	0.29802D-01	0.56364D-02	0.91575D-03	-0.32103D-02	-0.64670D-02
21.484	-0.99315D-03	0.86292D-03	0.60967D-03	-0.88606D-02	-0.12876D-01	0.14505D-02
23.437	0.23863D-02	-0.21333D-02	-0.14451D-02	0.24982D-01	0.36319D-01	-0.40910D-01
25.391	-0.17368D-02	0.15539D-02	0.10132D-02	-0.17095D-01	-0.24853D-01	0.27994D-01
58.594	0.49342D-03	-0.57952D-03	0.95444D-03	-0.72130D-02	0.42390D-02	-0.36330D-02
60.547	-0.17470D-02	0.20494D-02	-0.33958D-02	0.31017D-01	-0.18215D-01	0.15611D-01
62.500	0.16665D-02	-0.19495D-02	0.32517D-02	-0.29199D-01	0.17148D-01	-0.14697D-01

APPENDIX D

ZEROS OF LINEAR MULTIPLE-INPUT/MULTIPLE-OUTPUT SYSTEMS

The fundamental concepts of classical control theory—poles, zeros, transfer functions, frequency response—were originally expressed in terms of scalar functions of a complex variable. Recent work has generalized the scalar results to matrix functions of a complex variable, and related the frequency response concepts to state-space system descriptions. This appendix reviews the definitions and theorems which are applicable to multiple-input/multiple-output systems. The primary source of this review is MacFarlane & Karcanias.[30]

D.1 System Description

The systems considered in this section are assumed to be described by

$$\begin{aligned} \dot{\underline{x}}[t] &= A\,\underline{x}[t] + B\,\underline{u}[t] \\ \underline{y}[t] &= C\,\underline{x}(t) \end{aligned} \qquad \text{(D-1)}$$

$$\underline{x}[t] \in R^{n}$$

$$\underline{u}[t] \in R^{\ell}$$

$$\underline{y}[t] \in R^{m}$$

This is a restricted case; more general results are available which allow y to be a function of the state, the control, and time derivatives of the control.

Taking the single-sided Laplace transform of Eq. (D-1) yields

$$s\,\underline{x}[s] - \underline{x}[0] = A\,\underline{x}[s] + B\,\underline{u}[s] \qquad \text{(D-2)}$$

$$\underline{y}[s] = C\,\underline{x}[s]$$

If the initial conditions are all zero, so that

$$\underline{x}[0] = 0$$

then, the input and output vectors are related by

$$\underline{y}[s] = C[sI - A]^{-1} B\,\underline{u}[s] \qquad \text{(D-3)}$$

The matrix

$$G[s] = C[sI - A]^{-1} B \qquad \text{(D-4)}$$

can be defined, and is commonly designated the transfer-function matrix. Additionally, the system matrix, P[s], can be defined.[30] Equation (D-2) can be written

$$\begin{bmatrix} sI - A & -B \\ C & 0 \end{bmatrix} \begin{bmatrix} \underline{x}[s] \\ \underline{u}[s] \end{bmatrix} = \begin{bmatrix} \underline{x}[0] \\ \underline{y}[s] \end{bmatrix} \qquad \text{(D-5)}$$

Then P[s] is taken to be

$$P[s] = \begin{bmatrix} sI - A & -B \\ C & 0 \end{bmatrix} \qquad \text{(D-6)}$$

Both G[s] and P[s] are useful in defining system poles and zeros, and establishing the links between state space and frequency response descriptions of system behavior.

D.2 Definitions of Zeros

Zeros are characteristic of the way in which the system dynamics are coupled to the environment in which the system is imbedded, and are associated with specific values of complex frequency at which transmission through the system is blocked.[30] In the literature, three interrelated classes of zeros are defined.

D.2.1 System zeros[31]

The system zeros are defined as the zeros of P[s]; those values of complex frequency $s = z_i$ for which

$$\begin{bmatrix} z_i I - A & -B \\ C & 0 \end{bmatrix} \begin{bmatrix} \underline{x}_o \\ \underline{g} \end{bmatrix} = \begin{bmatrix} 0 \\ 0 \end{bmatrix} \qquad \text{(D-7)}$$

where

$\underline{u}[t] = \underline{g} \exp [zt] \, 1 [t]$

$1[t]$ = Heaviside step function

D.2.2 Transmission zeros[30]

The transmission zeros are defined as the zeros of G(s); those values of complex frequency $s = z_i$ for which

$$C[z_i I - A]^{-1} B = 0 \qquad \text{(D-8)}$$

These zeros are physically associated with the transmission blocking properties of the system. Equations (D-7) and (D-8) can be solved directly from the minors of P[s] or G[s] using the method developed by Kontakos.[25]

D.2.3 Decoupling Zeros[31]

Output decoupling zeros are defined as the values of complex frequency $s = z_i$ for which the matrix

$$P_o[s] = \begin{bmatrix} z_i I - A \\ C \end{bmatrix}$$

loses column rank. Analogously, input-decoupling zeros are defined as the values of complex frequency $s = z_i$ for which the matrix

$$P_i[s] = \left[\begin{array}{c:c} z_i I - A & -B \end{array}\right]$$

loses row rank. Input/output decoupling zeros occur at frequencies where both P_o and P_i lose rank.

D.3 Relationships Between Various Types of Zeros

Rosenbrock[32] has established that the system zero definition is the most general, and that the following relationship holds.

{system zeros} = {transmission zeros
+ input dedoupling zeros
+ output decoupling zeros}
- {input/output decoupling zeros}

He also has proven that if Eq. (D-1) is controllable and observable, then there will be no decoupling zeros, and the set of transmission zeros will be identical to the set of system zeros.

D.4 Theoretical Results

D.4.1 Invariance of Transmission Zeros[34]

Transmission zeros are invariant under the following transformations.

(1) Nonsingular coordinate transformations in state space.

(2) Nonsingular transformations of the inputs.

(3) Nonsingular transformations of the outputs.

(4) State feedback to the inputs.

(5) Output feedback to the rates of change of the states.

In terms of the quantities shown in Figure D-1, transmission zeros are invariant under all choices of L and K, and all nonsingular choices of T, G, and F.

Proof: (See Reference 34.)

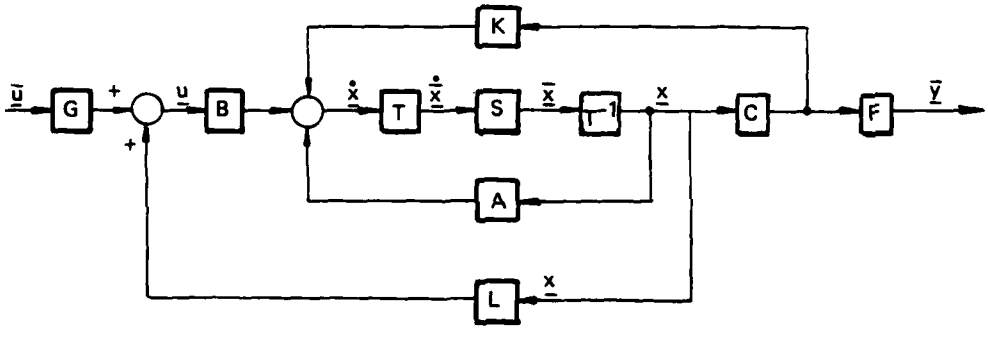

Figure D-1. Summary of transformations under which transmission zeros are invariant.

D.4.2 Relation Between Decoupling Zeros and Controllability, Observability

If a mode is uncontrollable, the real pole (or pair of complex conjugate poles) associated with the mode in question will be directly cancelled by an input decoupling zero, or complex conjugate pair of zeros.

Proof: The proof treats the case of an oscillatory mode. The arguments for a real mode are similar. The system equations are given by Eq. (D-7). A transform can be chosen (see Appendix E), which allows the system equations to be written in block diagonal form

$$\begin{aligned} \dot{\tilde{x}} &= \tilde{A}\,\tilde{x} + \tilde{B}\,u \\ y &= \tilde{C}\,\tilde{x} \end{aligned} \qquad \text{(D-9)}$$

where

$$\tilde{A} = \begin{bmatrix} A_1 & & & \\ & A_2 & & \\ & & \ddots & \\ & & & A_n \end{bmatrix} \quad \tilde{B} = \begin{bmatrix} B_1 \\ B_2 \\ \vdots \\ B_n \end{bmatrix}$$

and

$$A_i = \begin{bmatrix} -\zeta\omega_i & \omega_i\sqrt{1-\zeta^2} \\ -\omega_i\sqrt{1-\zeta^2} & -\zeta\omega_i \end{bmatrix}$$

The i^{th} mode will be uncontrollable if $B_i = 0$. Also, note that the matrix P_i

$$P_i = \left[[sI - \tilde{A}] \quad -\tilde{B} \right]$$

will lose rank for the case when $B_i = 0$, when $s = -\zeta\omega_i \pm \sqrt{1 - \zeta^2}\omega_i$, which implies directly that input decoupling zeros will exist which cancel the poles of the i^{th} mode, Q.E.D.

If a mode is unobservable, the real pole, or pair of complex conjugate poles associated with the mode in question will be directly cancelled by an output decoupling zero or conjugate pair of poles.

Proof: The proof is the dual of the controllability/input decoupling zero proof above. It involves relating the conditions for unobservability of the i^{th} mode to the frequency at which the matrix P_o

$$P_o = \begin{bmatrix} sI - A \\ C \end{bmatrix}$$

loses rank.

D.4.3 Movement of Poles with Output Feedback

Poles that correspond to modes which are uncontrollable or unobservable are not affected by output feedback.

Proof: The system described by Eq. (D-1) can be put in controllability/observability canonical form[6]

$$\begin{bmatrix} \dot{\underline{x}}_1 \\ \dot{\underline{x}}_2 \\ \dot{\underline{x}}_3 \\ \dot{\underline{x}}_4 \end{bmatrix} = \begin{bmatrix} A_{11} & A_{12} & 0 & 0 \\ 0 & A_{22} & 0 & 0 \\ A_{31} & A_{32} & A_{33} & 0 \\ 0 & 0 & 0 & A_{44} \end{bmatrix} \begin{bmatrix} \underline{x}_1 \\ \underline{x}_2 \\ \underline{x}_3 \\ \underline{x}_4 \end{bmatrix} + \begin{bmatrix} B_1 \\ 0 \\ B_3 \\ 0 \end{bmatrix} \underline{u} \qquad \text{(D-10)}$$

$$\underline{y} = \begin{bmatrix} C_1 & C_2 & 0 & 0 \end{bmatrix} \begin{bmatrix} \underline{x}_1 \\ \underline{x}_2 \\ \underline{x}_3 \\ \underline{x}_4 \end{bmatrix}$$

where

the $\underline{x}_1$ states = controllable and observable.

the $\underline{x}_2$ states = uncontrollable but observable.

the $\underline{x}_3$ states = controllable but unobservable.

the $\underline{x}_4$ states = uncontrollable and unobservable.

The poles of Eq. (D-10) are given by the characteristic equation

$$\det [A_{11}] \det [A_{22}] \det [A_{33}] \det [A_{44}] = 0$$

If an output feedback law $u = -Ky$ is used, the closed-loop poles are given by

$$\det [A_{11} - B_1 K C_1] \det [A_{22}] \det [A_{33}] \det [A_{44}] = 0$$

Note that the poles associated with unobservable or uncontrollable states are invariant for all choices of gain matrix K, Q.E.D.

If a system which is controllable and observable and which has an equal number of inputs and outputs has output feedback of the form

$$\underline{u} = -KI\underline{y}$$

then, as $K \to \infty$, a number of closed-loop poles equal in number to the finite transmittance zeros will tend asymptotically to the zero locations, while the remainder will tend to infinity.[30]

APPENDIX E

SINGULAR PERTURBATION THEORY

Singular Perturbation Theory is applicable to dynamic systems which can be modeled by

$$\begin{aligned} \dot{\underline{x}} &= f[\underline{x},\underline{z},\underline{u},t,\mu] \\ \mu\dot{\underline{z}} &= g[\underline{x},\underline{z},\underline{u},t,\mu] \\ \underline{y} &= h[\underline{x},\underline{z},\underline{u},t] \end{aligned} \qquad \text{(E-1)}$$

where

μ is a scalar $\mu > 0$

$\underline{x} \in R^n$, $\underline{z} \in R^r$, $\underline{u} \in R^m$, $\underline{y} \in R^\ell$

$\underline{x}$ and $\underline{z}$ are state variables associated with dynamic states; $\underline{y}$ is the system output.

If the system of interest is linear and time-invariant (LTI), Eq. (E-1) can be written

$$\begin{aligned} \dot{\underline{x}} &= A_{11}\underline{x} + A_{12}\underline{z} + B_1\underline{u} \qquad \underline{x}[0] = \underline{x}_0 \\ \mu\dot{\underline{z}} &= A_{21}\underline{x} + A_{22}\underline{z} + B_2\underline{u} \qquad \underline{z}[0] = \underline{z}_0 \\ \underline{y} &= C_1\underline{x} + C_2\underline{z} + D\underline{u} \end{aligned} \qquad \text{(E-2)}$$

For applications in this thesis, the $\underline{x}$ states represent low-frequency modes, the $\underline{z}$ states represent modes of higher frequency, and

μ is the square of the ratio of the frequency of the fastest x mode to the frequency of the slowest z mode.

Linear system theory provides the methodology to completely assess the forced and unforced response and the stability of any system which can be represented by Eq. (E-2). It is necessary, however, to consider the entire [n + r] order system in pursuing this assessment.

There are engineering motivations to develop appropriate reduced-order representations of Eq. (E-2) for use in control system design, particularly if the design requirements focus primarily on performance in set frequency bands. In amplifier design, for example, low-, middle-, and high-frequency models are typically used in designing to meet sinusoidal steady-state specifications. In this application, and others, reduced-order models can introduce significant efficiencies into the design process, and greatly reduce the complexity of the controller configuration. It is important to note, however, that the reduced-order model must be an adequate representation. There are numerous examples in the control literature[35,36] which indicate that undesirable and even unstable designs can result from heuristic order reduction schemes.

Singular Perturbation Theory offers a mathematically rigorous approach for constructing an asymptotically correct reduced-order approximation of Eq. (E-2). Specifically, the eigenvalues associated with the slow behavior of Eq. (E-2) can be represented as a series expansion

$$\underline{\lambda} = \underline{\lambda}_0 + \underline{\lambda}_1\mu + \underline{\lambda}_2\mu^2 \ldots \qquad \text{(E-3)}$$

Formal results are available which investigate the asymptotic behavior of this series[37] and establish that

$$\mu \to 0 \quad \Rightarrow \quad \underline{\lambda} \to \underline{\lambda}_0 \qquad \text{(E-4)}$$

where the λ_0 are the eigenvalues of the system

$$\dot{\underline{x}} = A_{11}\underline{x} + A_{12}\underline{z} + B_1\underline{u}$$

$$0 = A_{21}\underline{x} + A_{22}\underline{z} + B_2\underline{u}$$

Furthermore, for some neighborhood $\mu \in [0,\mu_0]$, it is valid[38] to approximate the unforced low-frequency behavior of Eq. (E-2) as

$$\dot{\underline{x}} = [A_{11} - A_{12}A_{22}^{-1}A_{21}]\underline{x} \qquad \text{(E-5)}$$

and the unforced high-frequency behavior as

$$\mu\dot{\underline{z}} = A_{22}\underline{z} \qquad \text{(E-6)}$$

Equations (E-5) and (E-6) are asymptotically correct reduced-order models. They account for the coupling between low- and high-frequency modes, but for the slow system, they treat the fast modes as dc values.

The work of Klimoshev and Krasovskii is key to the discussions of this report, and is presented in the following.

Lemma (Klimoshev and Krasovskii[38])

For a system governed by

$$\dot{\underline{x}} = A_{11}\underline{x} + A_{12}\underline{z} \qquad \underline{x}[0] = \underline{x}_0$$

$$\mu\dot{\underline{z}} = A_{12}\underline{x} + A_{22}\underline{z} \qquad \underline{z}[0] = \underline{z}_0 \qquad \text{(E-7)}$$

Let $\hat{A} = A_{11} - A_{12}A_{22}^{-1}A_{21}$ and A_{22} be stable matrices (all the eigenvalues of the matrices have negative real parts). Then, there exists a positive number μ such that for every $\mu \in [0,\mu_0]$, this system is asymptotically stable.

For the cases of state or output feedback control laws, and no-control feedthrough in the output

$$\underline{u} = -K_1C_1\underline{x} - K_2C_2\underline{z} \tag{E-8}$$

the closed-loop equations of an LTI singularly perturbed system can be written

$$\begin{aligned} \dot{\underline{x}} &= [A_{11} - B_1K_1C_1]\underline{x} + [A_{12} - B_1K_2C_2]\underline{z} \qquad \underline{x}[0] = \underline{x}_0 \\ \mu\dot{\underline{z}} &= [A_{21} - B_2K_1C_1]\underline{x} + [A_{22} - B_2K_2C_2]\underline{z} \qquad \underline{z}[0] = \underline{z}_0 \end{aligned} \tag{E-9}$$

Equation (E-9) is of the same form as Eq. (E-7). Exploiting this fact, the KK lemma has been applied to stabilizing feedback controllers,[9] optimal regulators,[40] and controller configurations which include dynamics in the feedback loop.[10]

It is clear that the approximate models given in Eq. (E-5) and (E-6) are strictly valid only for $\mu = 0$, and that asymptotic stability conclusions based on these reduced-order models are valid only for $\mu \in [0,\mu_1]$. A theoretical bound on μ_1, particularly as a function of the system dynamical matrix, is not available in the literature. Numerical investigations have placed μ_1 in the 0.3 range for specific problems.[36,40,41]

However, Mahapatra[42] has developed a bound for E[t], the error in $\underline{x}$ as approximated by Eq. (E-5) due to treating the high-frequency modes as dc. If the eigenvalues of A

$$A = \begin{bmatrix} A_{11} & A_{12} \\ A_{21}/\mu & A_{22}/\mu \end{bmatrix} \tag{E-10}$$

are designated λ_i, i = 1...r, $|\lambda_1| < |\lambda_2| < \ldots < |\lambda_r|$, and are assumed distinct, then $\|E[t]\|$ is bounded by

$$\|E[t]\| < K\left[[r-n]^{1/2}+1\right]\left[\sum_{i=n+1}^{r}\left[\frac{1}{\lambda_i}\right]^2\right]^{1/2} \qquad \text{(E-11)}$$

where

$$K = \left[\|B_1\| + \frac{1}{\mu}\|B_2\|\right]u_0$$

and u[t] is a step input of magnitude u_0.

The error can be made small if

$$\left[(r-n)^{1/2}+1\right]\left[\sum_{i=n+1}^{r}\left[\frac{1}{\lambda_i}\right]^2\right]^{1/2} \to 0 \qquad \text{(E-12)}$$

This condition is reached when $n \to r$, an obvious point, or when the neglected dynamics are very high frequency—in other words $\mu \to 0$.

E.1 Application of Singular Perturbation Theory to the Space Vehicle Problem

The singular perturbation formulation applied here is due to Balas.[10] He treats the specific case of controlling a system with fast and slow modes where the full state vector is unavailable and must be reconstructed from available measurements by a Kalman filter or a Luenberger observer. In this case, the appropriate low-frequency reduced-order model is

$$\begin{aligned}\dot{\underline{x}} &= \bar{A}_{11}\underline{x} + \bar{B}_1\underline{u}\\ \underline{y} &= \bar{C}_1\underline{x} + \bar{D}\underline{u}\end{aligned} \qquad \text{(E-13)}$$

where

$$\bar{A}_{11} = A_{11} - A_{12}A_{22}^{-1}A_{21}$$

$$\bar{B}_1 = B_1 - A_{12}A_{22}^{-1}B_2$$

$$\bar{C}_1 = C_1 - C_2A_{22}^{-1} - A_{21}$$

$$\bar{D} = C_1 - C_2A_{22}^{-1}B_2$$

A_{22} is assumed to have an open left-half-plane spectrum. Balas establishes that the feedback compensator has the form

$$\dot{\hat{\underline{x}}} = [\bar{A}_{11} + \bar{B}_1G - K\bar{C}_1 - K\bar{D}G]\hat{\underline{x}} + K\underline{y}$$

$$\underline{u} = G\hat{\underline{x}} \qquad \text{(E-14)}$$

which accepts the system output y and produces a stabilizing control u, and proves that if the system described by Eq. (E-9) is controllable and observable, there exists a μ_1, such that for all $\mu \in [0,\mu_1]$, the gains G and K can be chosen so that the full system (Eq. (E-2) with compensator feedback from a reduced-order observer (Eq. (E-10)) will be stabilized, and the observer estimate will converge to the actual state of the slow system.

The dynamical system of interest is summarized in Figures E-1 (configuration), and E-2 (the open- and closed-loop system equations). The $\underline{x}_1$ states are to be controlled; the $\underline{x}_a$ actuator states, $\underline{x}_s$ sensor states, and $\underline{x}_4$ structural modes are higher frequency and are not explicitly included in the controller design. The detailed development of these equations is given in Appendix F.

Using Balas' notation, the following identifications can be made.

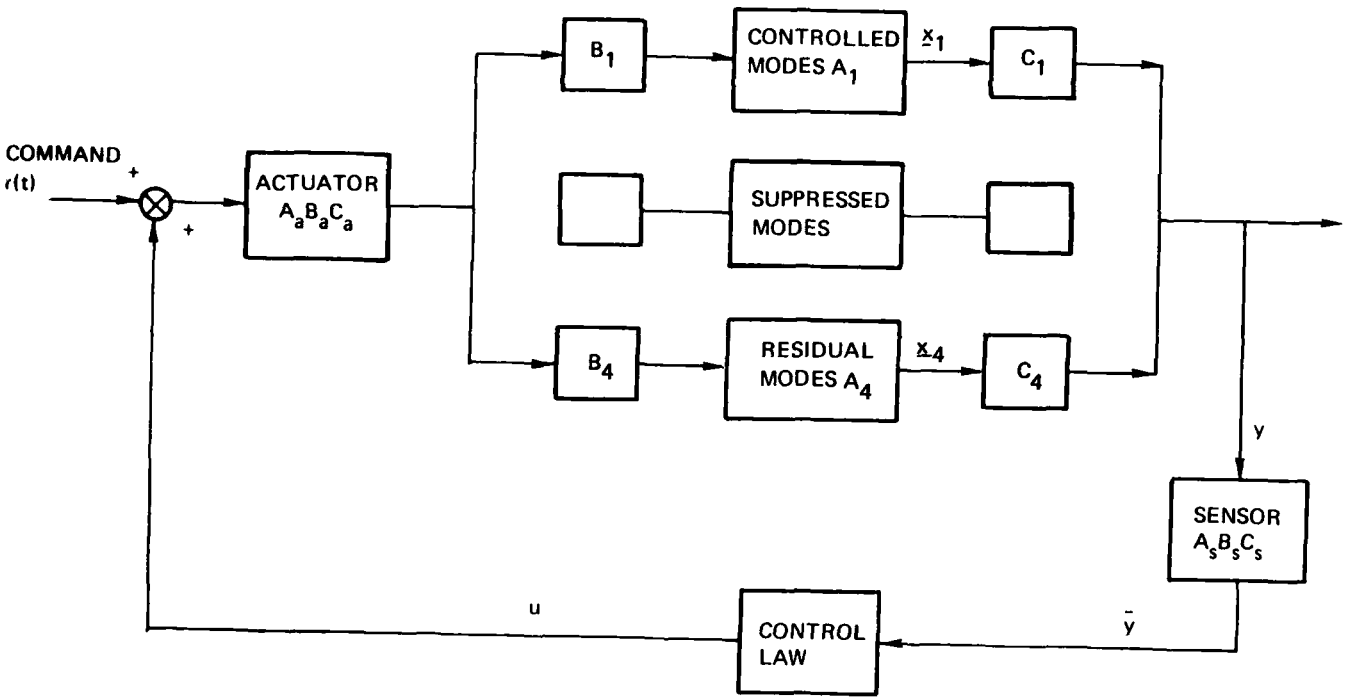

Figure E-1. Control law of the form $u = -K\hat{x}$.

OPEN LOOP

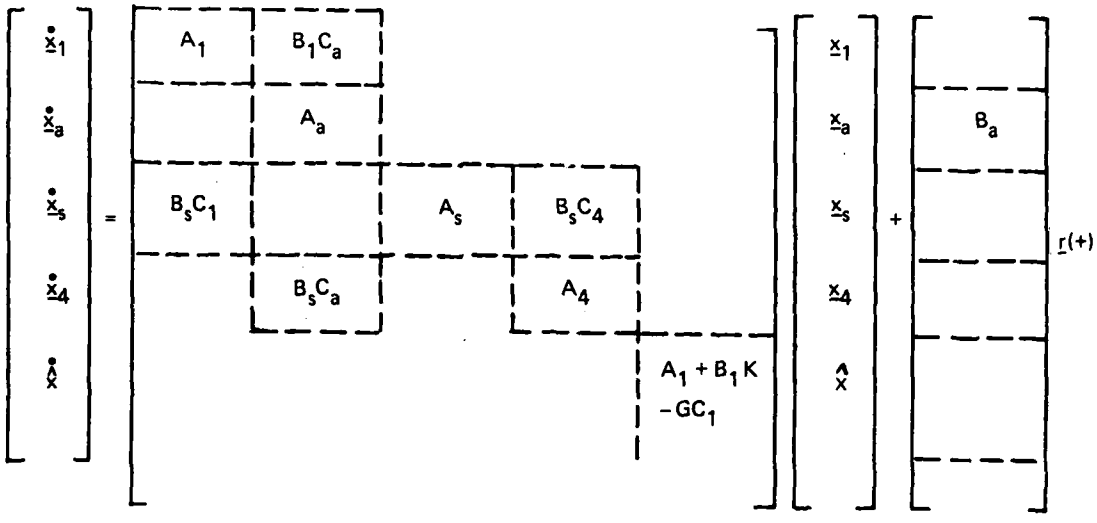

CLOSED LOOP

- CLOSING THE LOOP INTRODUCES THE TERMS

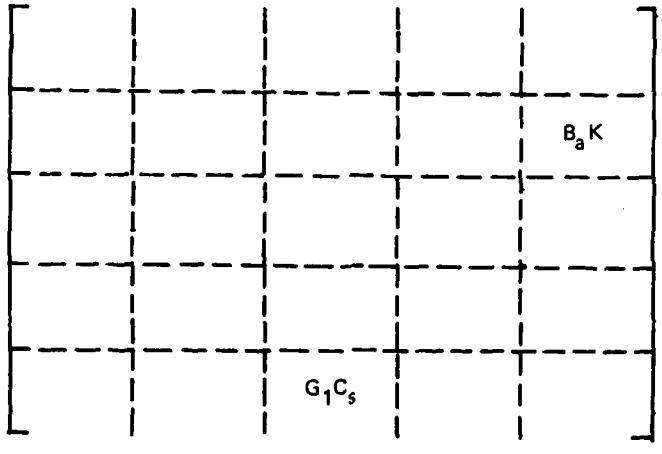

Figure E-2. Control system equations.

$$A_{11} = A_1$$

$$A_{22} = \begin{bmatrix} A_a & 0 & 0 \\ 0 & A_s & B_s C_4 \\ B_4 C_a & 0 & A_4 \end{bmatrix} \qquad A_{22}^{-1} = \begin{bmatrix} A_a^{-1} & 0 & 0 \\ -A_s^{-1} B_s C_4 A_4^{-1} B_4 C_a A_a^{-1} & A_s^{-1} & -A_s^{-1} B_s C_4 A_4^{-1} \\ A_4^{-1} B_4 C_a A_a^{-1} & 0 & A_4^{-1} \end{bmatrix}$$

$$A_{12} = \begin{bmatrix} B_1 C_a & 0 & 0 \end{bmatrix}$$

$$A_{21} = \begin{bmatrix} 0 \\ B_s C_1 \\ 0 \end{bmatrix}$$

$$B_1 = 0 \qquad B_2 = \begin{bmatrix} B_a \\ 0 \\ 0 \end{bmatrix} \qquad C_1 = 0 \qquad C_2 = \begin{bmatrix} 0 & C_s & 0 \end{bmatrix}$$

$$D = 0$$

Then the system model becomes

$$\dot{\bar{x}} = \bar{A}_{11} \bar{x} + \bar{B}_1 u$$

$$\bar{y} = \bar{C}_1 x + \bar{D} u \qquad \text{(E-15)}$$

where

$$\bar{A}_{11} = A_{11} - A_{12} A_{22}^{-1} A_{21} = A_1$$

$$\bar{B}_1 = B_1 - A_{12} A_{22}^{-1} B_2 = B_1$$

$$\bar{C}_1 = C_1 - C_2 A_{22}^{-1} A_{21} = C_1$$

$$\bar{D} = C_1 - C_2 A_{22}^{-1} B_2 = C_4 A_4^{-1} B_4$$

Implicit in these relations are the assumptions

$$C_a A_a^{-1} B_a = -I$$

$$C_s A_s^{-1} B_s = -I$$

The compensator that Balas' theory suggests is

$$\dot{\hat{x}} = [A_1 + B_1 G - KC_1 - KC_4 A_4^{-1} B_4 G]\hat{x} + Ky$$

$$u = G\hat{x} \qquad \text{(E-16)}$$

for application to the space vehicle. This controller form is increasingly valid as μ gets small.

By contrast, a compensator which neglects the fast modes completely would have the form

$$\dot{\hat{x}} = [A_1 + B_1 G - KC_1]\hat{x} + Ky$$

$$u = G\hat{x}$$

APPENDIX F

EQUATIONS OF MOTION

General formulations of the elastic equations of motion of a free vehicle in flight consider a three-dimensional body with six translational and rotational degrees of freedom and acknowledge the distributed nature of inertia, stiffness and damping forces. Vehicle motion and deformation are described in terms of coupled partial differential equations in space and time, and the appropriate boundary and initial conditions. Simplifying assumptions, which decouple, linearize, or discretize these equations, are justified for specific vehicles and sets of initial conditions.

This appendix is included to detail the simplifying assumptions which were made in this report, and to specifically exhibit the resulting vehicle equations of motion. Bisplinghoff and Ashley[43] derive the forced and unforced response equations for a three-dimensional, flexible, zero-damping vehicle. They use continuous representations for space and time, and restrict their attention to the small-deflection, zero-net angular-momentum case. These response equations are fundamental to this report, so this appendix begins with an outline of the Bisplinghoff-Ashley derivation. Then the response equations are put in state space form, and the effect of including damping is discussed. The appendix also discusses the eigenfunction normalization convention and presents the numerical state space descriptions of the satellite and the F-8 aircraft.

F.1 Coordinate Systems

The vehicle of interest is modeled as a three-dimensional elastic body which is unrestrained in space. Referring to Figure F-1, the body is allowed to assume small deformations with respect to the orthogonal x-y-z axis system, a body fixed-axis system with its origin at the vehicle center of mass.

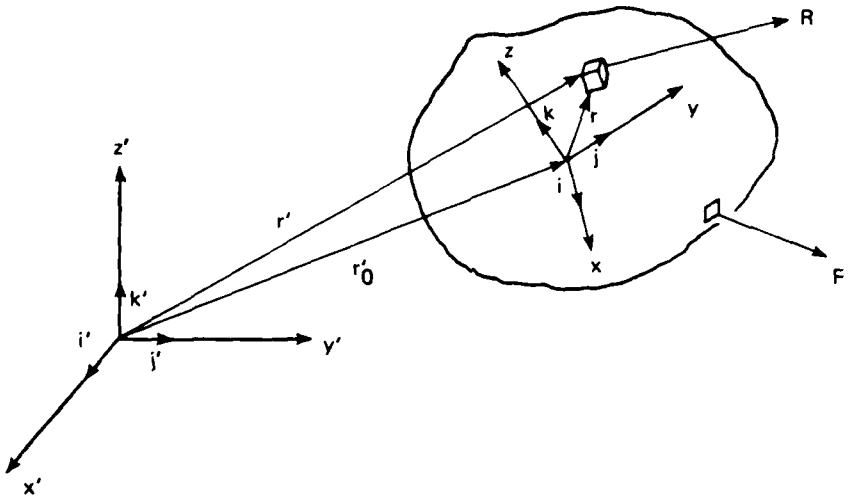

Figure F-1. Three-dimensional unrestrained elastic body.

Vehicle motions may also be described in terms of inertial coordinates. The position vector $\underline{r}'$ is referred to an orthogonal-axis system x',y',z' which is fixed in space. The body is allowed to assume large rigid-body displacements with respect to this inertial system. The vector $\underline{r}'_0$ is also referred to inertial coordinates; it represents the position vector of the vehicle center of mass.

Two vector relationships are useful in describing vehicle motion. The equation

$$\underline{r}' = \underline{r}_0' + \underline{r}$$

where $\underline{r}$ is the particle position vector in the x-y-z axis system, relates motion in inertial coordinates to motion relative to the vehicle center of mass. The second equation

$$\underline{r} = \tilde{\underline{r}} + \underline{q}$$

where $\tilde{\underline{r}}$ is the position vector from the center of mass to a particle in an unstrained vehicle, and where the vector $\underline{q}$ is an elastic deformation vector, relates deformations to the static equilibrium configuration.

The developments in this appendix will use these coordinate systems and position vectors.

F.2 Equations of Equilibrium[43]

If the body of interest, shown in Figure F-1, is acted on by surface tractions per unit area, designated by the vector $\underline{F}$, and body forces per unit volume, designated by the vector $\underline{R}$, then three vector equations of equilibrium must hold.

(1) Force Equilibrium

$$\underline{P} = \frac{d\underline{G}}{dt} \qquad \text{(F-1)}$$

where

$$P = \iiint_V R\, dV + \iint_S F dS$$

$$\underline{G} = M \frac{d\underline{r}_0'}{dt}$$

$$M\underline{r}_0' = \iiint_V \underline{r}'\,dV$$

$\underline{P}$ is the resultant of applied forces, $\underline{G}$ is the momentum vector, and M is vehicle mass.

(2) Moment Equilibrium

$$\underline{L} = \frac{d\underline{H}}{dt} \qquad \text{(F-2)}$$

where

$$\underline{L} = \iiint_V \underline{r} \times \underline{R}\,dV + \iint_S \underline{r} \times \underline{F}\,dS$$

$$\underline{H} = \iiint_V \underline{r} \times \frac{d\underline{r}}{dt}\,dV$$

$\underline{L}$ is the resultant of applied moments and $\underline{H}$ is the angular momentum vector.

(3) Elastic Equilibrium

$$\ddot{q} + \ddot{q}_0 + \frac{1}{2}\left[\dot{q} \times q_0\right] \times \bar{r} = -\iiint_V \Gamma \cdot \underline{a}\rho\,dV + \iiint_V \Gamma \cdot [F]\delta[r - \underline{r}_s]\,dV \qquad \text{(F-3)}$$

where

$$\ddot{q} = \frac{d}{dt}\left[\frac{d\underline{r}'}{dt}\right] = \frac{d}{dt}\left[\frac{d\underline{r}_0}{dt} + \frac{d\vec{r}}{dt} + \frac{d\underline{q}}{dt}\right]$$

$( )_0$ refers to quantities evaluated at the center of mass.

$\underline{r}_s$ is the position vector to the point of application of F.

Γ is the Maxwell second-order tensor of flexibility influence functions.

These equations assume small deflections, which allows the use of linear stress strain relationships.

F.3 Free Vibration

In the absence of external forces, the x-y-z system remains inert and the simplified forms of Eq. (F-1), (F-2) and (F-3), which are appropriate for the free-vibration case, are as follows.

$$\iiint_V \frac{d^2\underline{q}}{dt^2}\,\rho\,dV = 0 \qquad \text{(F-4)}$$

$$\iiint_V [\bar{r} + \underline{q}] \times \frac{d^2\underline{q}}{dt^2}\,\rho\,dV = 0 \qquad \text{(F-5)}$$

$$\underline{q} - \underline{q}_0 - \frac{1}{2}[\nabla \times \underline{q}_0] \times \bar{r} = -\iiint \Gamma \cdot \frac{d^2\underline{q}}{dt^2}\,\rho\,dV \qquad \text{(F-6)}$$

The solution to these equations is assumed to be

$$\underline{q}[x,y,z,t] = \underline{\phi}[x,y,z]T[t] \qquad \text{(F-7)}$$

where $\underline{\phi}[x,y,z] = \phi_x[x,y,z]\underline{i} + \phi_y[x,y,z]\underline{j} + \phi_z[x,y,z]\underline{k}$ is an eigenfunction in vector form which represents a natural mode shape, and T[t] is a function of time.

Equation (F-7) will be the solution to Eq. (F-4), (F-5), (F-6) provided the following dynamic conditions hold

$$\ddot{T} + \omega^2 T = 0 \tag{F-8}$$

$$\underline{\phi}[x,y,z] = \omega^2 \iiint_V G[x,y,z\,;\,\xi,\eta,\zeta]\,\underline{\phi}\,[\xi,\eta,\zeta]\rho d\xi d\eta d\zeta \tag{F-9}$$

where G is a second-order influence function dependent on system stiffness, mass, and inertia properties. The exact relation is given in Reference 43.

The unrestrained elastic vehicle has three translational modes of zero frequency which can be represented by the vector forms

$$\begin{aligned} \underline{\phi}_1 &= a_1\underline{i} \\ \underline{\phi}_2 &= b_2\underline{j} \\ \underline{\phi}_3 &= c_3\underline{k} \end{aligned} \tag{F-10}$$

and three rotational modes, also of zero frequency, which are

$$\begin{aligned} \underline{\phi}_4 &= -z\underline{j} + y\underline{k} \\ \underline{\phi}_5 &= z\underline{i} - x\underline{k} \\ \underline{\phi}_6 &= -y\underline{i} + x\underline{j} \end{aligned} \tag{F-11}$$

In addition, there are an infinite number of modes of finite frequency defined by the solutions to Eq. (F-8) and (F-9). Each pairwise combination of these solutions satisfies the orthogonality relation

$$\iiint_V \underline{\phi}_i \cdot \underline{\phi}_j \,\rho\, dV = 0 \qquad i \neq j \tag{F-12}$$

Note that the rotational modes are uncoupled. This is a result of the assumption that internal angular momentum is small.

F.4 Forced Motion

The forced motion of an unrestrained elastic vehicle can be described in terms of the natural vibration modes of the free vehicle. As defined earlier, the displacement vector of a particle in inertial coordinates is

$$\underline{r}' = \underline{r}_0' + \underline{r} \tag{F-13}$$

where $\underline{r} = \tilde{\underline{r}} + \underline{q}$

The elastic deformation vector $\underline{q}$ can be defined in terms of the free-vehicle natural modes

$$\underline{q} = \sum_{i=1}^{\infty} \underline{\phi}_i[x,y,z]\xi_i[t] \tag{F-14}$$

The normal coordinates ξ_i and the vectors $\underline{r}_0'$ and $\tilde{\underline{r}}$ are determined from the equilibrium equations.

Equations (F-1) and (F-2) provide six scalar relationships which define the translation and rotation of the x-y-z body axis system. Equation (F-3) defines the deformation displacements of the vehicle with respect to this axis system. Using Eq. (F-12) in Eq. (F-3) yields

$$\sum_{i=1}^{\infty} \left\{ \underline{\phi}_i - \underline{\phi}_i(0) - \frac{1}{2}\left[\nabla \cdot \underline{\phi}_i(0)\right] \times \underline{r} \right\} \left[\xi_i + \frac{\ddot{\xi}_i}{\omega_i^2} \right]$$

$$= -\iiint_V \Gamma \cdot [\ddot{\underline{r}}_0' + \ddot{\tilde{\underline{r}}}]\rho \, dV + \iiint_V \Gamma \cdot F \, \delta[\underline{r} - \underline{r}_s] \, dV \tag{F-15}$$

Using orthogonality Eq. (F-11) can be simplified to

$$M_j \ddot{\xi}_j + M_j \omega_j^2 \xi_j = \Xi_j \qquad [j = 1,2,\ldots,\infty] \qquad \text{(F-16)}$$

where

$$M_j = \iiint_V |\phi_j|_\rho^2 \, dv$$

$$\Xi_j = \iint_S [F \cdot \phi_j] \, dS$$

F.5 State Space Representation of Forced Motion Equations

If instead of $\underline{q}$ being a function valued three vector, $\underline{q}$ is taken to be the vector of displacements at structural node points then the forced deformation response of an unrestrained elastic vehicle to a single input, as derived from Eq. (F-3), can be presented as

$$M\ddot{\underline{q}} + K\underline{q} = \underline{b}u \qquad \text{(F-17)}$$

M and K are mass and stiffness matrices, b is an input distribution vector, and the dimension of q is three times the number of points used in the analysis. Use of orthogonality, and the displacement representation given in Eq. (F-12), allow Eq. (F-17) to be uncoupled and written as

$$[I]\ddot{\xi} + \begin{bmatrix} \ddots & & \\ & \omega_i^2 & \\ & & \ddots \end{bmatrix} \xi = \begin{bmatrix} \ddots & & \\ & \frac{1}{m_i} & \\ & & \ddots \end{bmatrix} \underline{b}u \qquad \text{(F-18)}$$

or in terms of first-order differential equations, as

$$\dot{\underline{x}} = \begin{bmatrix} A_1 & & & \\ & A_2 & & \\ & & \ddots & \\ & & & A_i \\ & & & & \ddots \end{bmatrix} \underline{x} + \begin{bmatrix} b_1 \\ b_2 \\ \vdots \\ b_i \\ \vdots \end{bmatrix} \underline{u} \qquad \text{(F-19)}$$

$$A_i = \begin{bmatrix} 0 & 1 \\ -\omega_i^2 & 0 \end{bmatrix} \qquad b_i = \begin{bmatrix} 0 \\ \frac{1}{m_i} \end{bmatrix}$$

which is block diagonal.

F.6 Viscous Damping Effects

If viscous damping effects are modeled and included in the formulation, Eq. (F-18) becomes

$$[I]\ddot{\underline{\xi}} + \left[\begin{smallmatrix} \ddots & & \\ & m_i & \\ & & \ddots \end{smallmatrix}\right]^{-1} C\dot{\underline{\xi}} + \left[\begin{smallmatrix} \ddots & & \\ & \omega_i^2 & \\ & & \ddots \end{smallmatrix}\right]\underline{\xi} = \left[\begin{smallmatrix} \ddots & & \\ & m_i & \\ & & \ddots \end{smallmatrix}\right]^{-1} \underline{u} \qquad \text{(F-20)}$$

C is a matrix of damping coefficients. If C is a linear function of either M or K, the term $\left[\begin{smallmatrix} \ddots & & \\ & m_i & \\ & & \ddots \end{smallmatrix}\right]^{-1} C$ will be diagonal, and Eq. (F-20) can be represented in state space by

$$\dot{\underline{x}} = \begin{bmatrix} A_1 & & & \\ & A_2 & & \\ & & \ddots & \\ & & & A_i \\ & & & & \ddots \end{bmatrix} \underline{x} + \begin{bmatrix} b_1 \\ b_2 \\ \vdots \\ b_i \\ \vdots \end{bmatrix} \underline{u} \qquad \text{(F-21)}$$

$$A_i = \begin{bmatrix} 0 & 1 \\ -\omega_i^2 & -2S_i\omega_i \end{bmatrix} \qquad B_i = \begin{bmatrix} 0 \\ \frac{1}{m_i} \end{bmatrix}$$

This special case is called modal damping, and has as one consequence that the system eigenvectors remain real, and the displacements remain in-phase at all frequencies.[44]

If [C] is not a linear function of [M] or [K], then $\left[\begin{smallmatrix} \ddots & & \\ & m_i & \\ & & \ddots \end{smallmatrix}\right]^{-1} C$ will not be diagonal, and the scalar differential equations in ξ_i will be

coupled. The cross-coupling terms will depend directly on the values of the damping coefficients, and if damping is low, then a representation of the form of Eq. (F-21) may be approximately correct. However, an exact damped system block-diagonalization transformation, valid for arbitrary C matrices, is given by D'Azzo and Houpis.[45] They show that any dynamical system can be put in the canonical form

$$\dot{x} = \begin{bmatrix} A_1 & & & \\ & A_2 & & \\ & & \ddots & \\ & & & A_i \\ & & & & \ddots \end{bmatrix} x + \begin{bmatrix} b_1 \\ b_2 \\ \vdots \\ b_i \\ \vdots \end{bmatrix} u \qquad \text{(F-22)}$$

where

$$A_i = \lambda_i \qquad b_i = b_i \quad \text{for real roots}$$

$$A_i = \begin{bmatrix} \lambda_i & 1 & 0 \\ 0 & \lambda_i & 1 \\ 0 & 0 & \lambda_i \end{bmatrix} \qquad b_i = \begin{bmatrix} 0 \\ \vdots \\ b_i \end{bmatrix} \quad \text{for repeated roots}$$

and

$$A_i = \begin{bmatrix} \alpha & \beta \\ -\beta & \alpha \end{bmatrix} \qquad b_i = \begin{bmatrix} b_{1i} \\ b_{2i} \end{bmatrix}$$

$$\lambda_i = \alpha + \beta_j \qquad \text{for conjugate roots}$$

$$\overline{\lambda}_i = \alpha - \beta_j$$

The advantage of these canonical forms, Eq. (F-19), (F-21) and (F-22), is that the modes are uncoupled dynamically, and the dynamic response characteristics are immediately evident. The coupling has shifted to the input distribution, and output matrices.

F.7 Conventions

Normalization

(1) The mode shapes are determined only within an arbitrary factor. A normalization can be used, provided that it is consistently applied. For this work each mode will be divided by $\max_{x,y,z} [\phi]$, which ensures that the maximum magnitude of any normalized eigenfunction will be 1.

(2) The discrete eigenvectors, which are calculated by NASTRAN (specifically the satellite mode shapes), are normalized so that each eigenvector $\underline{\phi}_i$ satisfies the relationship $\underline{\phi}_i^T m \underline{\phi}_i = 1$.

(3) Note that in the representation

$$\underline{q}(x,y,z,t) = \sum_{j=1}^{\infty} \underline{\phi}_j(x,y,z)\,\xi_j(t)$$

$$\ddot{\xi}_j + \omega_j^2 \xi_j = \iint_S \frac{F(x,y,z,t)\,\underline{\phi}_j(x,y,z)\ dS}{\iint_S \phi_j \phi_j\ \rho\ dS}$$

multiplying $\underline{\phi}_j$ by any constant will not change the relationship between $F(x,y,z,t)$ and $\underline{q}(x,y,z,t)$.

F.8 Equations of Motion of the F-8 Aircraft[26]

The F-8 aircraft is in a controller design example in Appendix A. The mass and geometric data for this aircraft are given in Table F-1.

Table F-1. Mass and geometric data for the F-8 aircraft.

Mass	9994 kg	(648.8 slug)
Chord	3.59 m	(11.8 ft)
Wing Area	34.87 m^2	(374.9 $(ft)^2$)
Tail Length	4.8 m	(15.7 ft)
Sensor Location	4.57 m	(15 ft)

For purposes of Appendix A, rigid-aircraft lateral dynamic behavior can be described by

$$\dot{\underline{x}} = A\underline{x} + B\underline{u}$$

where

$$\underline{x} = \begin{bmatrix} \phi \\ \omega_x \\ \omega_z \\ \beta \end{bmatrix} \qquad \underline{u} = \begin{bmatrix} \delta_a \\ \delta_r \end{bmatrix}$$

These state equations are written for a body axis coordinate frame whose X-axis is inclined to the trimmed velocity vector by the angle of attack α_0. The roll angle, ϕ, is the Euler angle rotation about the aircraft X axis and its rate of change, therefore it contains components of the angular velocity of the aircraft along both X and Z axes (see Figure F-2).

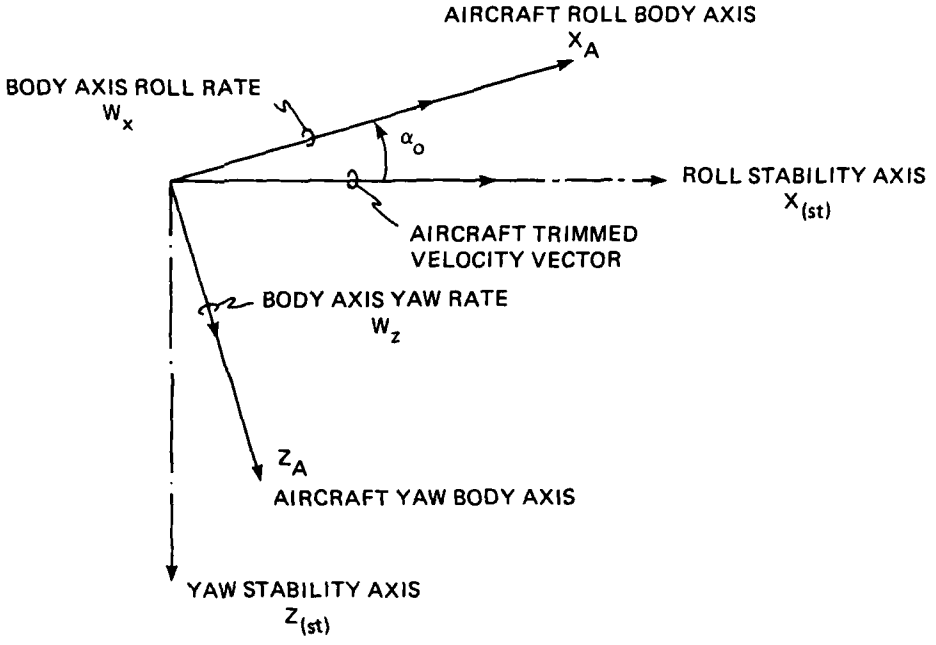

Figure F-2. Coordinate axis for aircraft equation of motion.

The flight condition of interest is Mach = 0.56, 6706 meters altitude, and α_0 = 7.75°. For this condition

$$A = \begin{bmatrix} 0 & 1.0 & 0.1361 & 0 \\ 0 & -2.625 & 1.91 & -29.80 \\ 0 & -0.0759 & -0.427 & 2.650 \\ 0.0555 & 0.1359 & -0.9974 & -0.2173 \end{bmatrix}$$

$$B = \begin{bmatrix} 0 & 0 \\ 27.0 & 6.13 \\ 1.420 & -3.55 \\ 0.002315 & 0.04222 \end{bmatrix}$$

F.9 Equations of Motion for the Spacecraft

F.9.1 Spacecraft Description

The spacecraft of interest in this thesis is a spaceborne optical imaging system similiar in design to the space telescope. The design and performance considerations, operation, and geometry of this system are discussed in Section 2. The intent here is to describe the structural and dynamic modeling that led to the satellite equations of motion.

The optical system consists of two mirrors and focal plane arrayed in a Cassegrain configuration. The structure which supports the optical system consists of a rigid base and a metering truss. The rigid base supports the primary mirror and the focal plane, and contains auxilliary equipment for cooling the focal-plane sensors and for processing data. The metering truss is configured to support the secondary mirror within the geometric constraints of the optical design. Two-flexible solar panels are rigidly attached to the base section and are sized to meet the power requirements of spaceborne cryogenic optics.

The structural configuration and node-point numerical designations are shown in Figures F-3 and F-4. Truss members are hollow graphite-epoxy tubes, joined at nodes with metallic connectors. For design purposes, the moment carrying capacity of the joints is assumed to be small. Graphite epoxy was chosen as a primary material because its strength-to-weight ratio is equivalent to aluminum or steel, and its thermal expansion coefficient is very small.

The components of the structure are shown in Figures F-5 through F-7. There is a basic box configuration (Figure F-5) which is extensively stiffened in the base area (Figure F-6) and along the truss (Figure F-7). Truss-element descriptions are given in Table F-1.

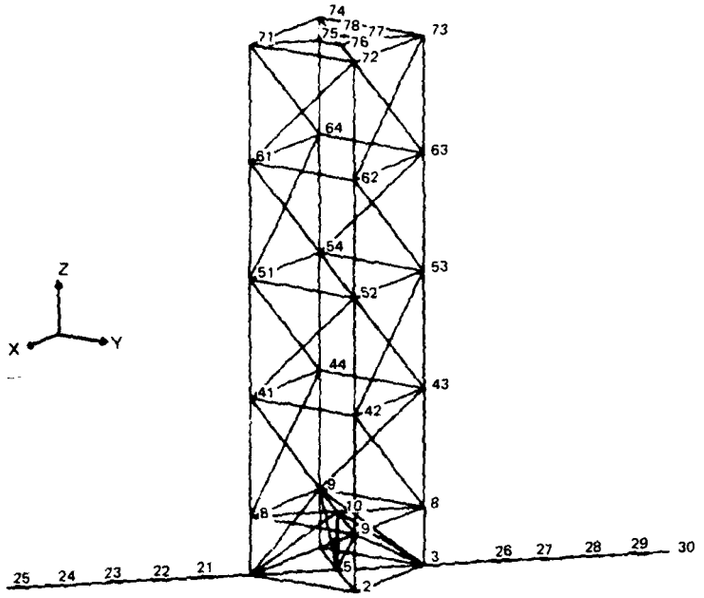

Figure F-3. Structural configuration and node-point numerical designation — side view.

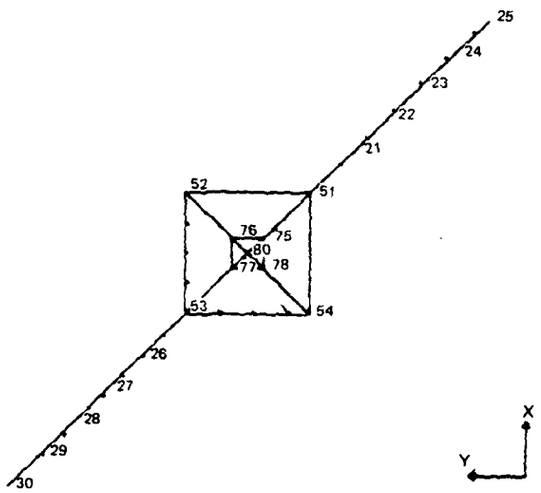

Figure F-4 Structural configuration and node-point numerical designation — top view.

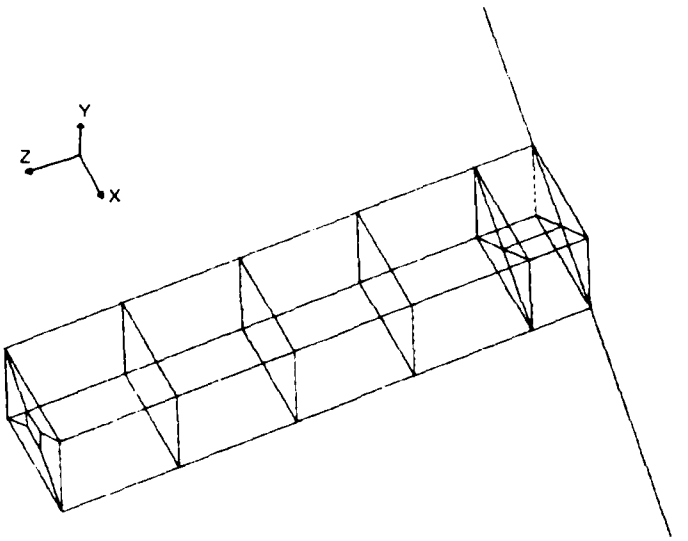

Figure F-5. Components of the structure of the basic box configuration.

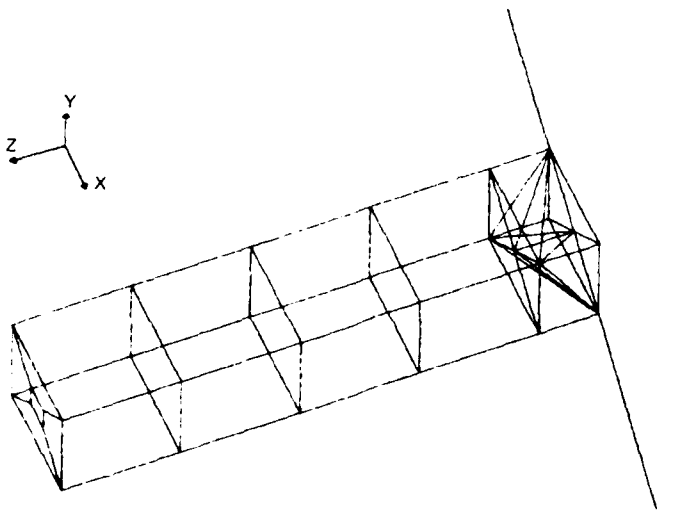

Figure F-6. Components of the structure of the basic box configuration, stiffened in the base area.

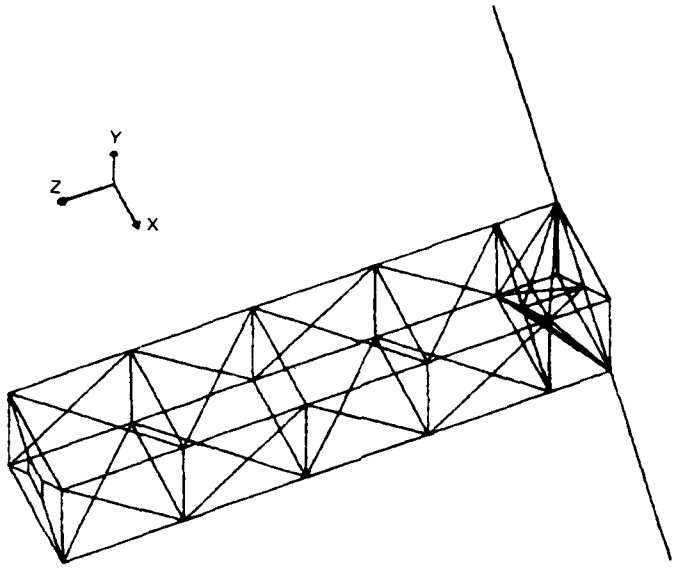

Figure F-7. Structural components of the basic-box configuration, stiffened in the base area and along the truss.

Table F-1. Satellite structural data.

Structural Material: Graphite Epoxy		
Density = 1720 kg/m^3		
Youngs modulus E = 1.24×10^{11} N/m^2		
Truss Member Sizing		
Type	**Area (m^2)**	**Use**
200	3.75×10^{-4}	basic truss members
300	5.97×10^{-3}	solar panels and base section stiffners
400	4.28×10^{-3}	support structure for secondary mirror

Spaceborne optical-grade mirrors[46] are typically composite-sandwich constructions of "glossy" low thermal-expansion materials. Tradenames of available materials include CERVIT from ITEK and ULE from Perkin-Elmer. Mirrors which are consistent with the spacecraft under discussion have masses of 100 kilograms (secondary) and 700 kilograms (primary), and have natural frequencies above 60 to 70 hertz.

F.9.2 Structural Modeling

The structure described previously was modeled with finite-element elements and analyzed using Nastran. The following assumptions were made.

(1) Small deformations.

(2) Leads below buckling limits.

(3) Member frequencies and mirror frequencies high compared to truss frequencies.

(4) The mirror mounting scheme prevents structural deformations from deforming the mirrors. This assumption implies that mirror masses are to be accounted for (but not mirror stiffness).

(5) Node connectors can support moment loads.

The finite-element model allowed for 240 degrees of freedom. One hundred response modes were derived from this model. The Nastran structural routines assume that there is no structural damping and that modes vibrate in phase. The vehicle mass properties are given in Table F-2.

Table F-2. Satellite mass and inertia properties.

- Total Mass 2.95655×10^4 kg

- cg

  x = 0

  y = 0

  z = 6.428 m

- Inertial Matrix (x, y, z)

$$\begin{bmatrix} 1.61277 \times 10^6 & -6.72754 \times 10^3 & 0 \\ -6.72754 \times 10^3 & 1.61277 \times 10^6 & 0 \\ 0 & 0 & 1.539709 \times 10^5 \end{bmatrix}$$

- Inertia Matrix (principle axes)

$$\begin{bmatrix} 1.61950 \times 10^6 & & \\ & 1.60604 \times 10^6 & \\ & & 1.539709 \times 10^5 \end{bmatrix}$$

- Component Massess

Secondary Mirror	100 kg	(25 kg/node: 75, 76, 77, 78)
Primary Mirror	700 kg	(160 kg/node: 6, 7, 8, 9, 10)
Support Equipment and CMG (Base)	100 kg	
Solar Panels	72 kg	(12 kg/node: 21, 23, 25, 26, 28, 30)

F.9.3 Vehicle Response Modes

Table F-3 gives the structural and rigid-body eigenfrequencies. Associated with each of these frequencies is a response mode. The modes can be categorized by the dominant motion.

(1) Translation, Modes 1, 2, 3 (Figures F8 through F-10)

(2) Rigid-Body Rotation, Modes 4, 5, 6 (Figure F-11 through F-13)

(3) Solar-Panel Deformation

Vertical

symmetric, Modes 9, 15, 34 (Figure F-14)

asymmetric, Modes 7, 18, 33 (Figure F-15)

Horizontal

symmetric, Modes 8, 17, 32 (Figure F-16)

asymmetric, Modes 10, 16, 31 (Figure F-17)

(4) Upper-Lens Vibration

Membrane, Mode 22 (Figure F-19)

Rotation, Mode 50 (Figure F-20)

(6) Pure Torsion, Modes 14, 28, 29, 41, 44 (Figure F-21)

(7) Pure Axial, Modes 24, 38, 47, 48 (Figure F-22)

(8) Bending

No Mirror Rotation, Modes 23, 30, 39, 40 (Figure F-23)

Top Mirror Rotation, Modes 20, 21, 25, 26, 42, 57 (Figure F-24)

(9) Coupled Axial, Torsion and Upper Lens Membrane, Modes 11, 36, 37 (Figure F-26)

(10) Coupled Axial and Symmetric Solar - Panel Vibration, Mode 19 (Figure F-27)

Table F-3. Rigid-body and structural vibration eigenfrequencies.

Mode	Freq (rad/s)	Freq (Hz)	Mode	Freq (rad/s)	Freq (Hz/s)
1 to 6	0	0	33	376.5	59.93
7	22.02	3.50	34	376.9	59.98
8	22.75	3.62	35	345.0	62.86
9	22.79	3.62	36	408.6	65.03
10	23.53	3.74	37	445.4	70.88
11	36.02	5.73	38	448.9	71.44
12	40.14	6.39	39	457.8	72.87
13	41.05	6.53	40	470.2	74.84
14	46.91	7.46	41	478.5	76.16
15	135.40	21.55	42	542.9	86.41
16	137.4	21.87	43	543.0	86.41
17	137.9	21.94	44	555.3	88.38
18	139.1	32.13	45	561.0	89.28
19	146.7	23.35	46	607.1	96.62
20	147.6	23.49	47	607.1	96.62
21	147.6	23.49	48	728.5	115.95
22	218.1	34.71	49	729.0	116.03
23	260.2	41.41	50	730.4	116.23
24	268.2	42.68	51	761.4	121.18
25	295.7	47.06	52	761.5	121.19
26	299.5	47.35	53	762.4	121.33
27	299.2	47.62	54	767.7	123.19
28	304.4	48.45	55	771.3	122.75
29	310.7	49.45	56	784.1	124.79
30	322.6	51.35	57	795.9	126.67
31	373.2	59.40	58	795.9	126.67
32	374.2	59.56	59	808.2	128.63
			60	810.8	129.03

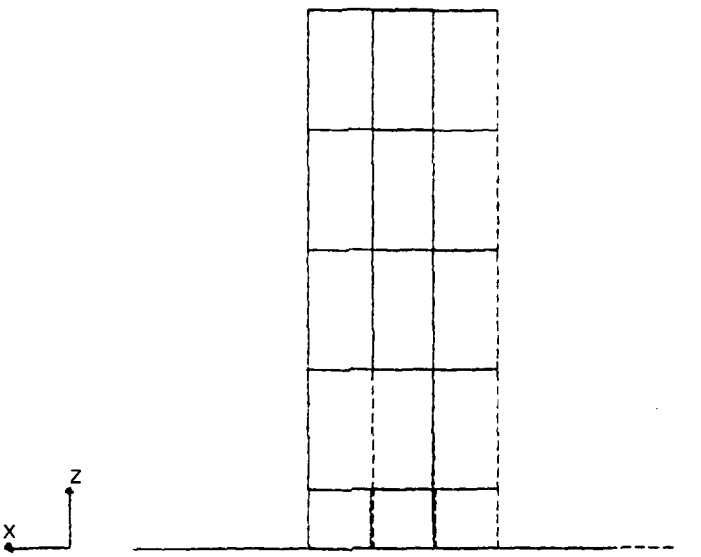

Figure F-8. Rigid-body translation: X.

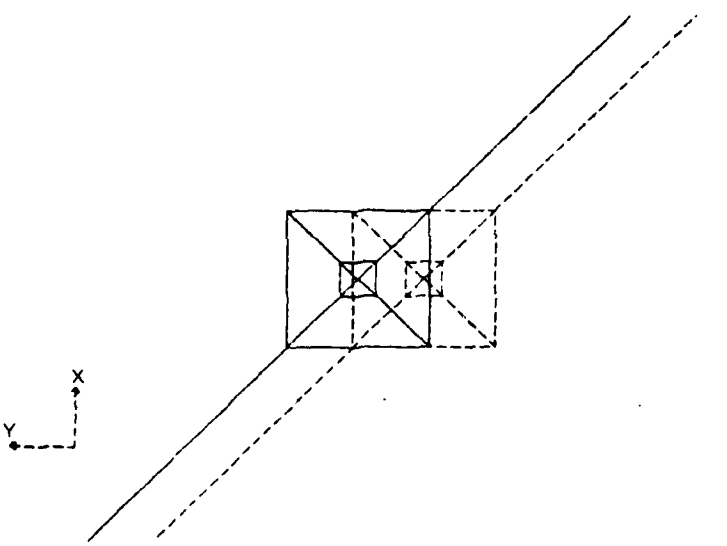

Figure F-9. Rigid-body translation: Y.

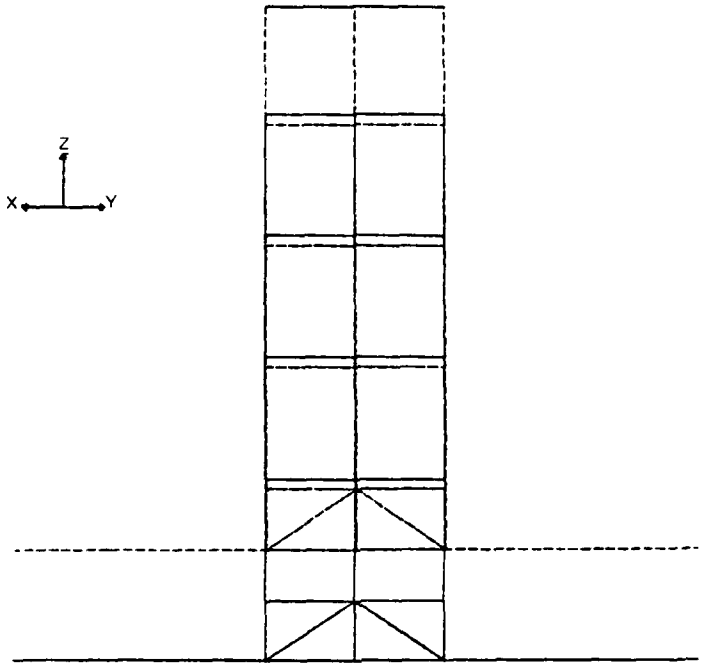

Figure F-10. Rigid-body translation: Z.

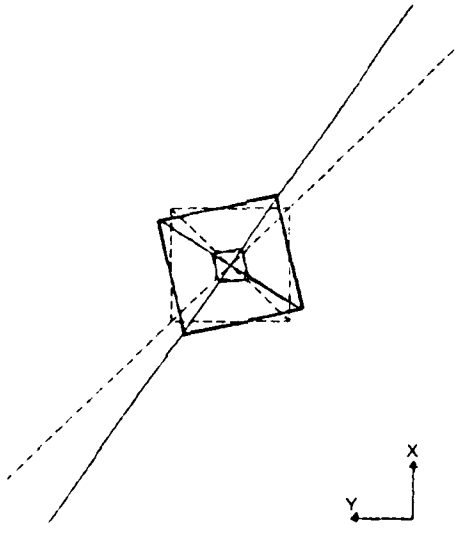

Figure F-11. Rigid-body rotation: X.

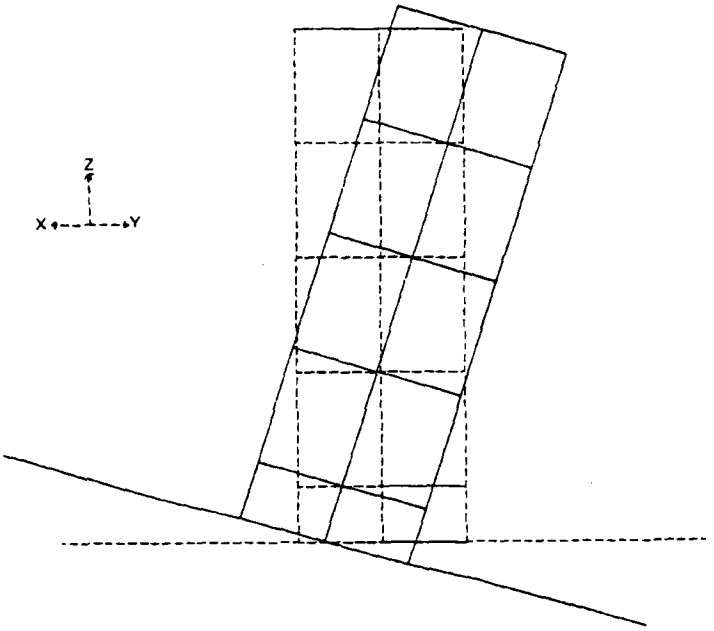

Figure 12. Rigid-body rotation: Y.

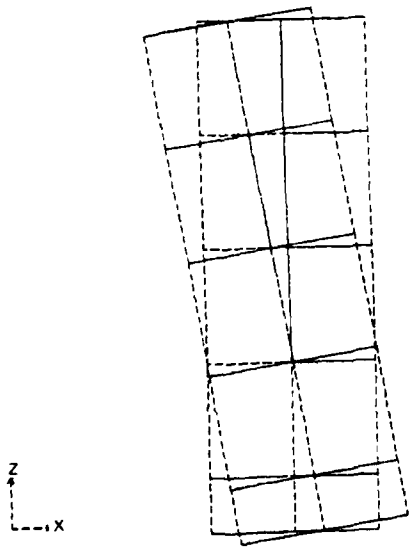

Figure 13. Rigid-body rotation: Z.

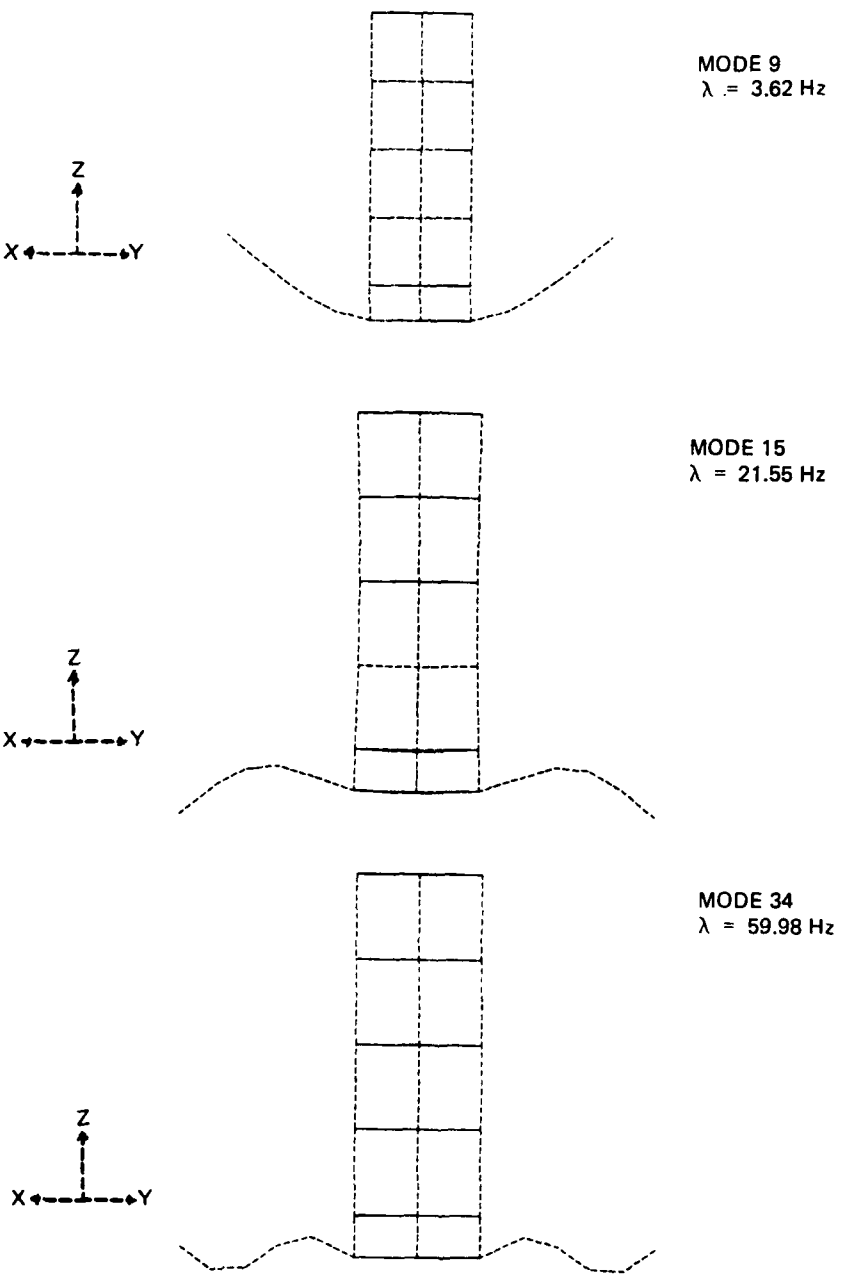

Figure F-14. Vertical symmetric solar-panel deformation modes.

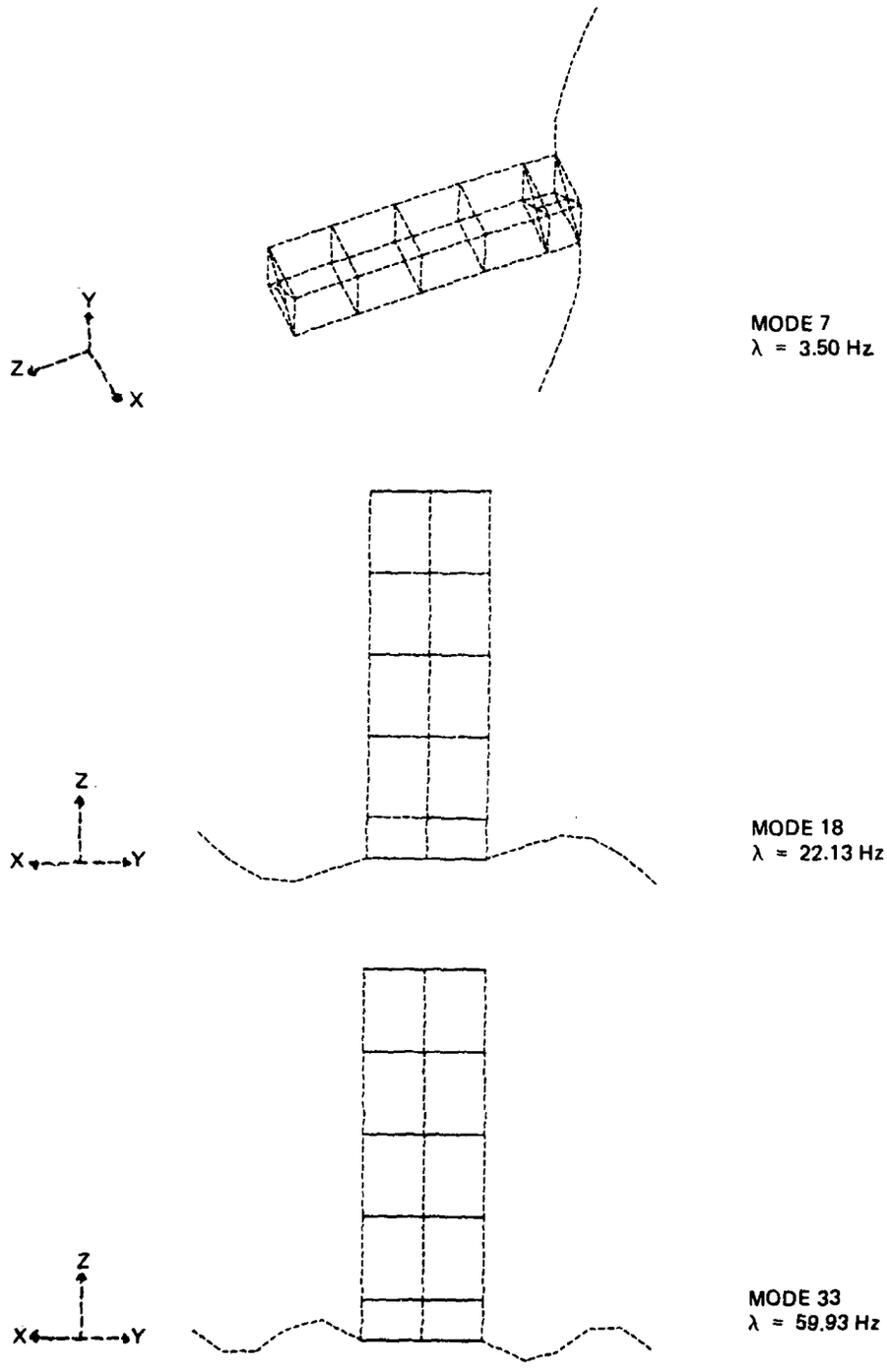

Figure F-15. Vertical asymmetric solar-panel deformation modes.

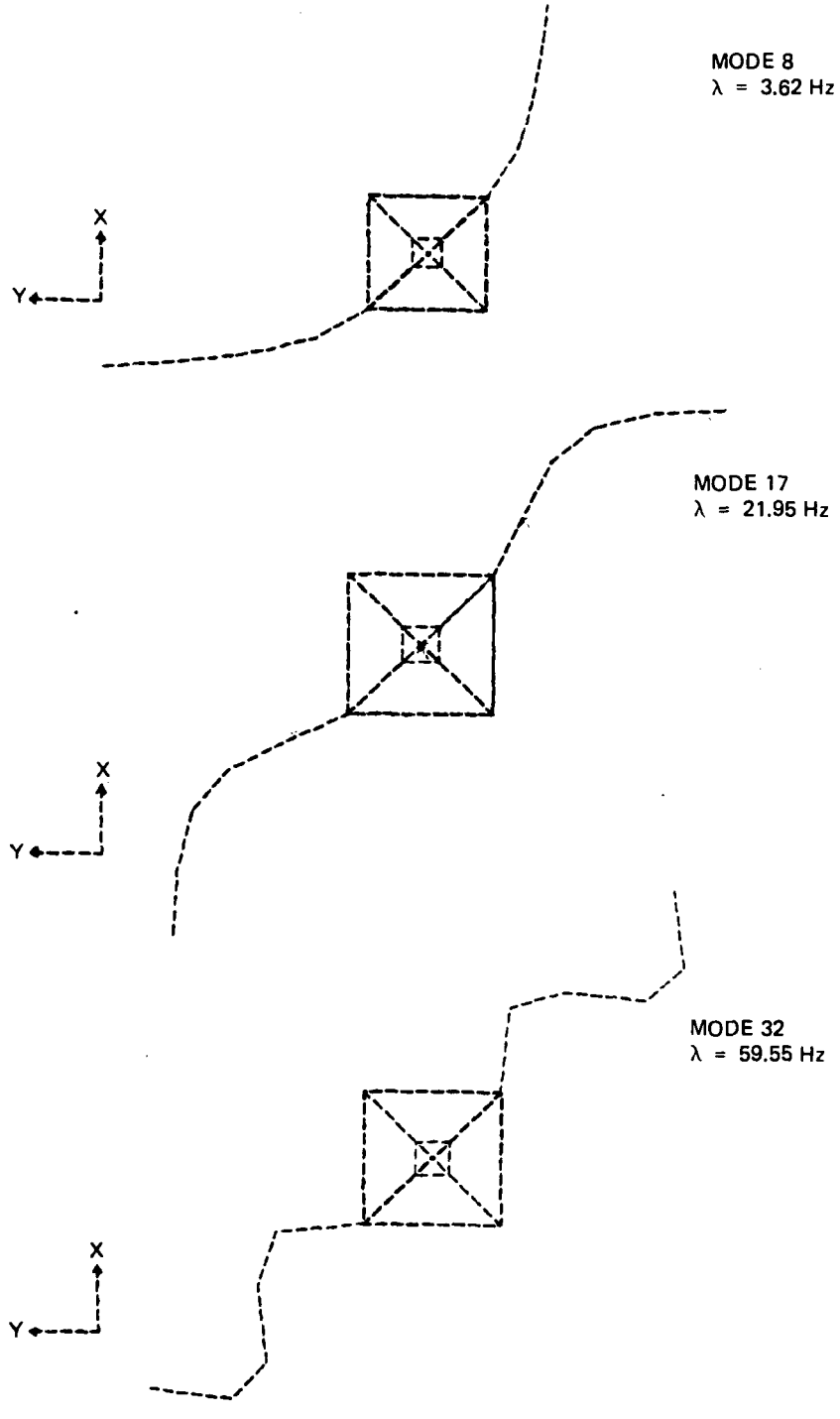

Figure F-16. Horizontal symmetric solar-panel deformation modes.

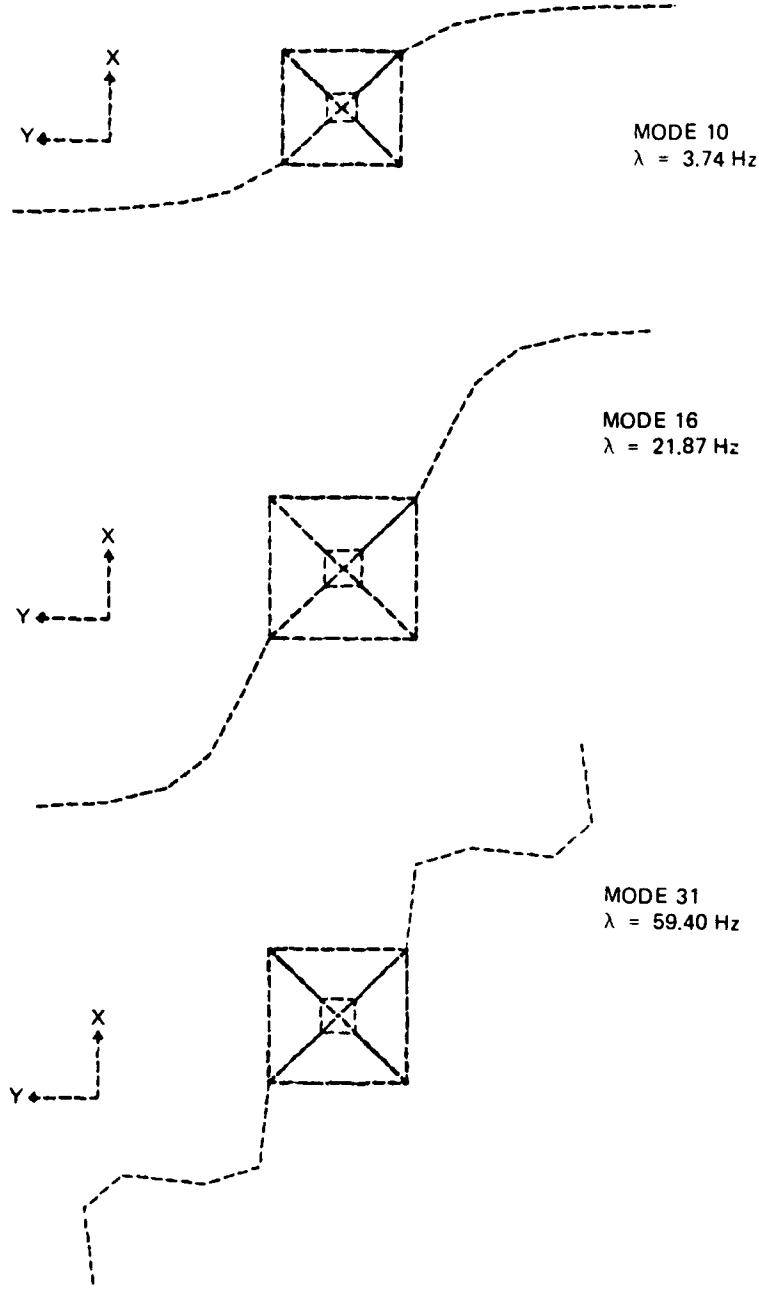

Figure F-17. Horizontal asymmetric solar-panel deformation modes.

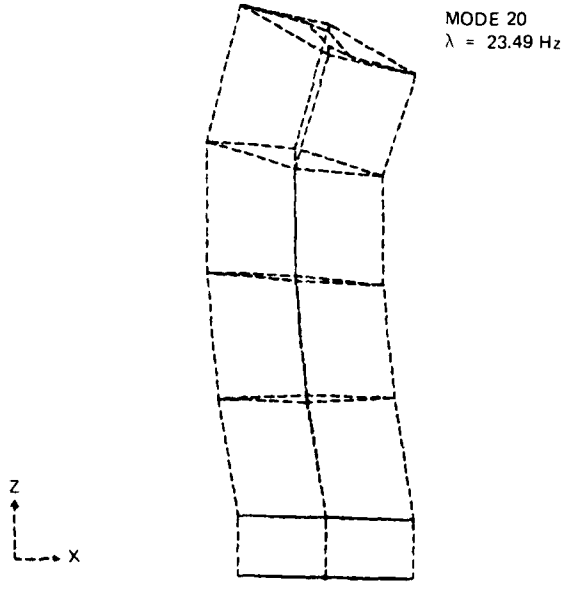

Figure F-18. Upper-mirror rotation.

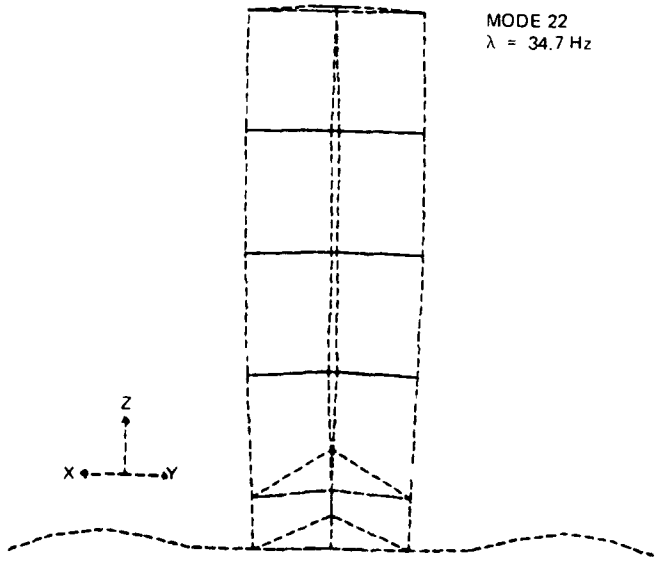

Figure F-19. Lower-mirror membrane vibration.

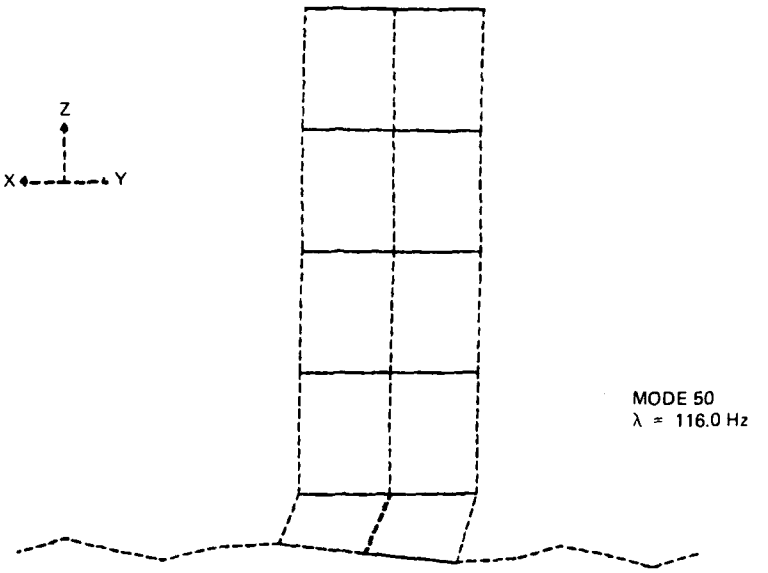

Figure F-20. Lower-mirror rotation.

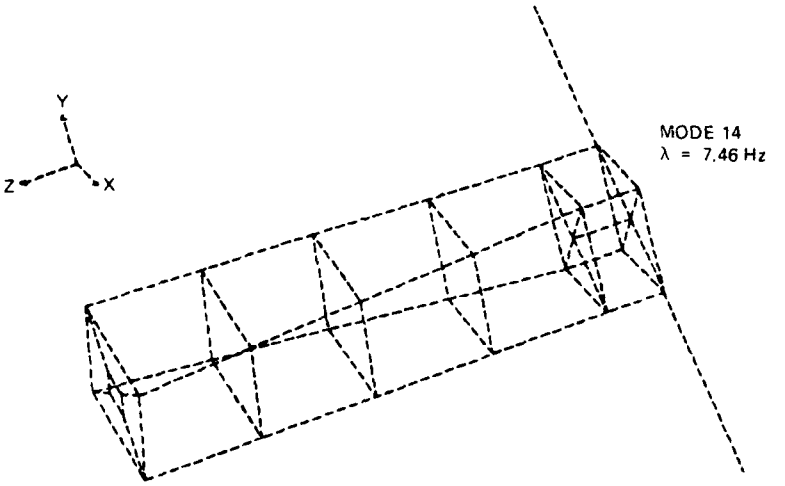

Figure F-21. Pure torsion.

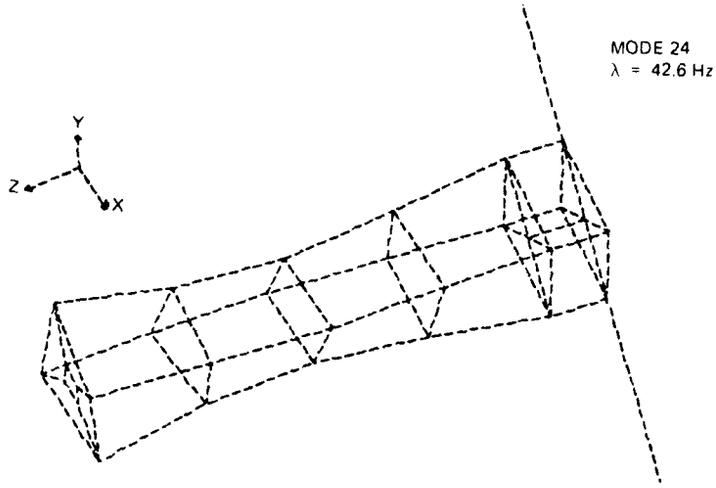

Figure F-22. Pure axial vibration.

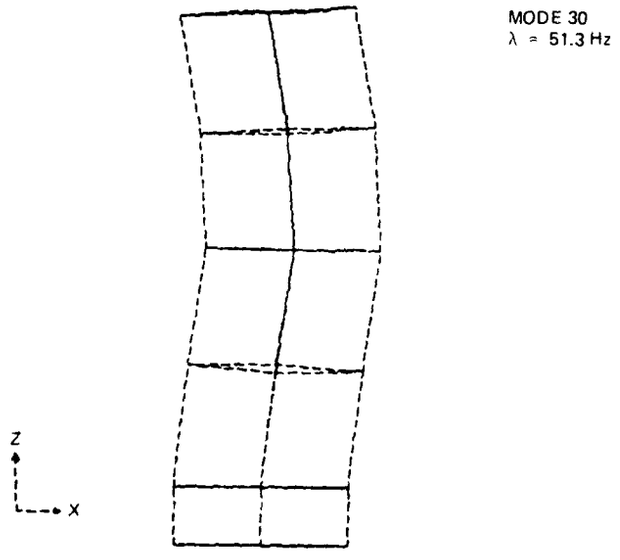

Figure F-23. Bending: no mirror rotation.

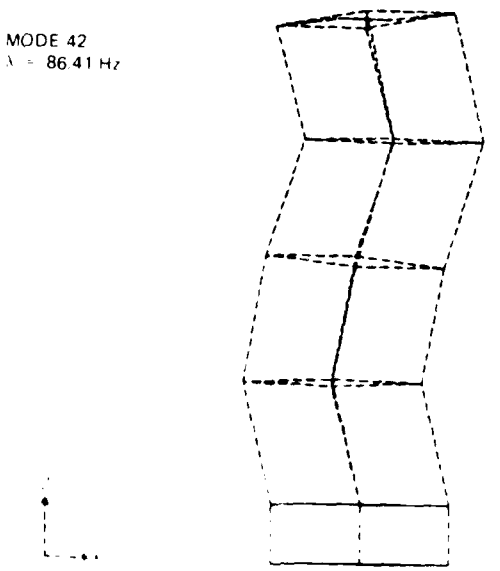

Figure F-24. [illegible] mode: top-mirror rotation.

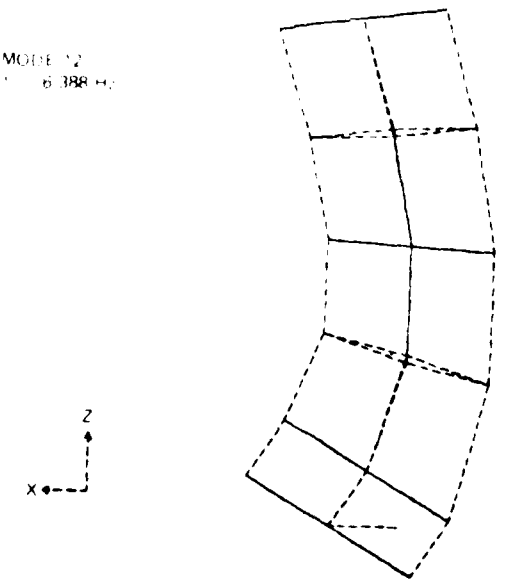

Figure F-25. Bending mode: rotation of both mirrors.

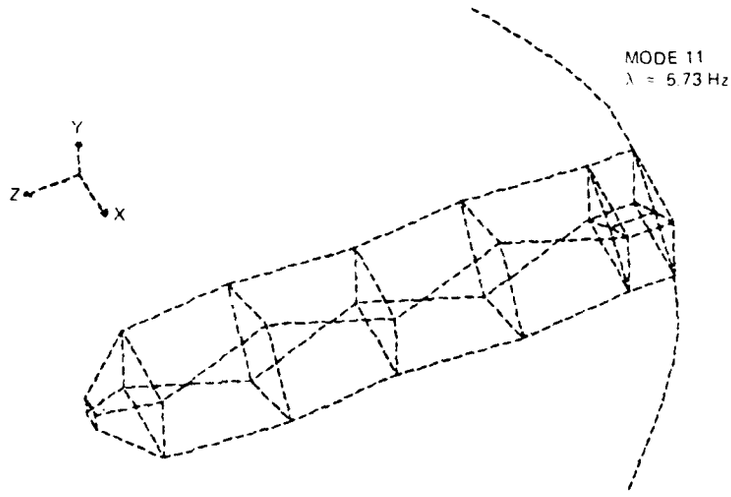

Figure F-26. Coupled axial, torsion, and upper-lens membrane.

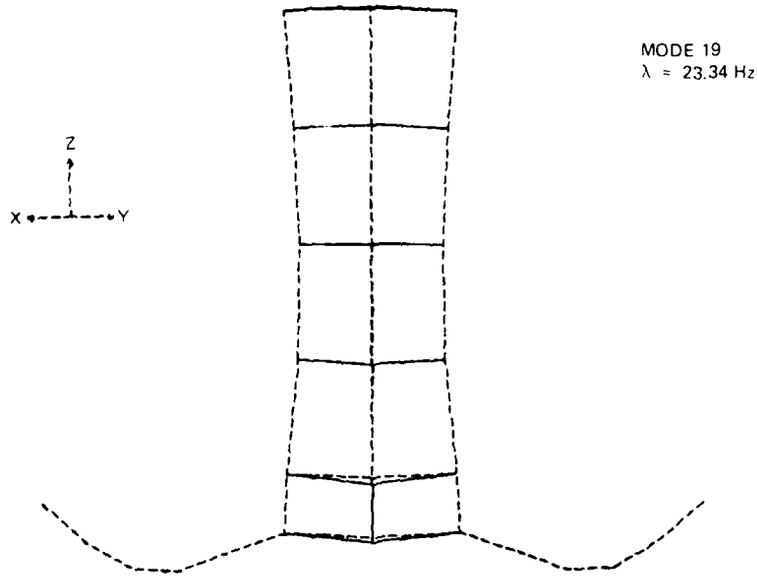

Figure F-27. Coupled axial and symmetric solar panel.

F.9.4 Actuators and Sensors

Sixteen control inputs are available for the structure under discussion. Control moment gyros located in base section (node 5) provide moments in the ω_x, ω_y, and ω_z directions. In addition, 13 member actuators are provided at the locations shown in Figure F-28. They are high-bandwidth piezoelectric devices deployed in series with the members. They provide axial force in the member direction. Devices of this kind have been demonstrated in the laboratory for small-scale structure.[47] The future development for space application is conjecture. Actuators were placed in locations that provided control authority to the $\underline{X}_1$ modes. No definative attempt was made to optimize these locations.

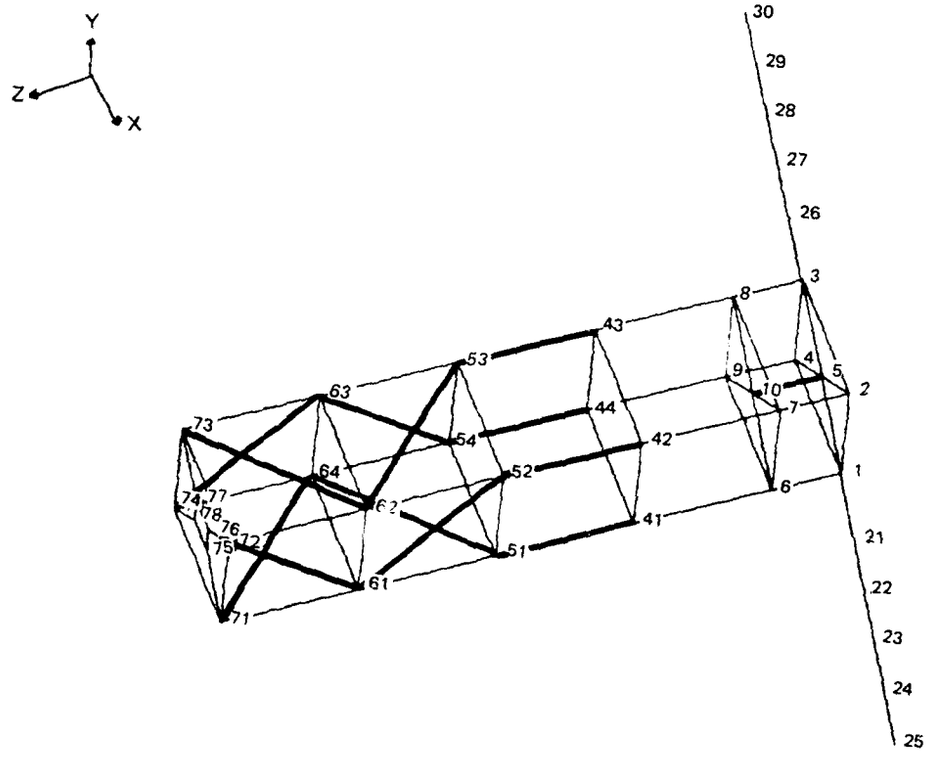

Figure F-28. Member actuator locations.

The output of 38 sensors is available to the control system. A platform located at node 5 provides the angular orientation of the vehicle with respect to inertial space. In addition, two other sets of sensors are deployed. Thirteen piezoelectric sensors are located with the member actuators and provide the relative elongation of the member in question. These sensors operate on the same principle as the actuators. Then, along the solar panels, x-y plane displacement measurements are made at 12 locations (nodes 1, 3, 21 to 30), and Z direction displacement measurements are made at 10 locations (nodes 21 to 30). Several mechanisms are available for making these measurements. Lockheed[48] has developed a high-bandwidth laser-ranging sensor which looks promising. Alternately, low-cost accelerometers could be used.

Significant actuator and sensor implementation issues must be addressed before the vibration control of spacecraft is feasible. There are very few space-qualified sensor/effector alternatives available, particularly electric-powered displacement actuators. The schemes, postulated previously are conceptually attractive, but undemonstrated. This thesis does not treat the actuator/sensor issues.

F.9.5 State Space Equations

The state space model used to describe the satellite dynamic response includes the three rotational rigid-body modes and the first 47 structural response modes. This model is used to evaluate pointing and tracking performance; it is assumed that there is no translation of the center of mass.

The state vector has 100 elements. The first 50 are modal displacements; the second 50 are the associated modal velocities. With the state vector defined, a state space model of the form

$$\dot{\underline{x}} = A\underline{x} + B\underline{u}$$
$$\underline{y} = C\underline{x}$$

can be constructed.

The dynamical matrix, A, can be partitioned into four 50 × 50 components.

$$A = \begin{bmatrix} O & I \\ \ddots & \ddots \\ -\omega_i^2 & 2\zeta\omega_i \end{bmatrix}$$

The frequencies, ω_i, i = 1 to 50, are the eigenfrequencies associated with modes 3 through 53 in Table F-3. Modal damping is assumed, and ζ is taken equal to 5 percent.

The input distribution matrix, B, has zero elements for its first 50 rows; the force inputs only effect states 51 to 100. Any element of B, $b_{i+50,j}$, represents the force input to the i^{th} mode from the j^{th} actuator. Numerically, $b_{i+50,j}$ is given by the displacement of the i^{th}-mode shape evaluated at the j^{th}-actuator location.

Similiarly, the output matrix C has nonzero elements only in columns 1 to 50, reflecting the fact that only displacements are measured. For the first 50 columns, any element of C, C_{ij} represents the displacement of the j^{th} mode as recorded at the i^{th} sensor.

The influence coefficient matrices from which B and C are derived are given in the following.

DRAPER MODEL #2

ACTUATOR LOCATIONS

NA = 16

ACTUATOR	NODE1	NODE2/DIRECTION
1	5	10
2	51	64
3	52	61
4	53	62
5	54	63
6	64	71
7	61	72
8	62	73
9	63	74
10	6	41
11	7	42
12	8	43
13	9	44
14	5	-4
15	5	-5
16	5	-6

SENSOR LOCATIONS

NS = 50

SENSOR	NODE1	NODE2/DIRECTION
1 - 16	SENSORS AND ACTUATORS COLLOCATED	
17	1	-1
18	1	-2
19	21	-1
20	21	-2
21	21	-3
22	22	-1
23	22	-2
24	22	-3
25	23	-1
26	23	-2
27	23	-3
28	24	-1
29	24	-2
30	24	-3
31	25	-1
32	25	-2
33	25	-3
34	3	-1
35	3	-2
36	26	-1
37	26	-2
38	26	-3
39	27	-1
40	27	-2
41	27	-3
42	28	-1
43	28	-2
44	28	-3
45	29	-1
46	29	-2
47	29	-3
48	30	-1
49	30	-2
50	30	-3

ACTUATOR INFLUENCE MATRIX

ACTUATOR

MODE	1	2	3	4	5	6	7	8
1	.7000D-19	.3168D-06	.7949D-08	.3181D-06	-.3109D-08	.3903D-06	-.1144D-07	.3890D-06
2	-.1300D-18	.9436D-08	.1005D-06	-.9537D-08	.1013D-06	-.9486D-08	.6066D-06	.9537D-08
3	-.6000D-13	.3507D-13	-.1262D-12	.3378D-14	.1199D-12	-.2288D-13	.1385D-12	.2510D-14
4	.7300D-17	-.5727D-03	-.5725D-03	-.5727D-03	.4917D-06	-.7308D-07	-.2154D-06	.7308D-07
5	-.9000D-19	.5812D-06	-.6429D-06	-.5227D-05	.5289D-05	.1540D-05	-.5588D-05	.9845D-06
6	.4900D-18	.3125D-05	.1952D-05	-.1745D-05	.1839D-03	.2417D-05	.2391D-05	-.5139D-05
7	-.4576D-12	.2741D-03	-.2736D-03	-.2741D-03	.2736D-03	-.2741D-03	.2739D-03	.2741D-03
8	.7675D-13	.5868D-04	.5301D-04	-.5868D-04	-.5301D-04	-.5892D-04	-.5898D-04	.5892D-04
9	-.1062D-04	.1082D-04	-.1099D-04	.1082D-04	-.1099D-04	-.1073D-04	.1102D-04	-.1073D-04
10	-.7234D-08	.6669D-04	.6705D-04	.6669D-04	.6705D-04	-.6352D-04	-.6390D-04	-.6352D-04
11	.2254D-04	.1640D-04	.1471D-04	.1640D-04	.1471D-04	-.1304D-04	-.1134D-04	-.1304D-04
12	-.9840D-14	.1571D-02	.1577D-02	-.1571D-02	-.1577D-02	-.1584D-02	-.1594D-02	.1584D-02
13	-.6155D-14	.1532D-02	-.1526D-02	-.1532D-02	.1526D-02	-.1549D-02	.1539D-02	.1549D-02
14	.3942D-06	-.3450D-02	-.3443D-02	-.3450D-02	-.3443D-02	.3321D-02	.3315D-02	.3321D-02
15	-.4539D-03	.7849D-03	-.8606D-03	.7849D-03	-.8606D-03	-.9890D-03	.1075D-02	-.9390D-03
16	-.3608D-07	.8698D-04	.7597D-04	.8698D-04	.7597D-04	-.8589D-04	-.7950D-04	-.9539D-04
17	-.3474D-13	-.5887D-04	-.4193D-04	.5887D-04	.4193D-04	.6575D-04	.6664D-04	-.6575D-04
18	-.8568D-12	.1575D-06	.1153D-04	-.1575D-06	-.1153D-04	-.1082D-03	.4867D-04	.1082D-03
19	-.8619D-03	.1415D-02	-.1576D-02	.1415D-02	-.1576D-02	-.1881D-02	.2056D-02	-.1881D-02
20	-.3814D-12	-.6191D-02	-.2389D-02	.6191D-02	.2389D-02	.4959D-02	.1260D-02	-.4959D-02
21	.1267D-12	.2390D-02	-.6194D-02	-.2390D-02	.6194D-02	-.1265D-02	.4963D-02	.1265D-02
22	-.2372D-02	-.2402D-03	.8009D-04	-.2402D-03	.8009D-04	.4118D-03	.6039D-05	.4118D-03
23	.3035D-13	-.1663D-02	.7538D-03	.1663D-02	-.7538D-03	.3434D-02	-.1605D-02	-.3434D-02
24	.2796D-03	.1972D-02	-.1789D-02	.1972D-02	-.1789D-02	-.1471D-01	.1437D-01	-.1471D-01
25	-.7879D-14	-.4654D-02	-.9002D-02	.4654D-02	.9002D-02	.1332D-01	.2771D-01	-.1332D-01
26	-.1411D-13	-.8941D-02	.4683D-02	.8941D-02	-.4683D-02	.2824D-01	-.1363D-01	-.2824D-01
27	-.7818D-04	.4071D-03	.1549D-03	.4071D-03	.1549D-03	.2445D-02	-.3775D-02	.2445D-02
28	.1308D-02	.9460D-02	.9528D-02	.9460D-02	.9528D-02	-.2366D-01	-.2453D-01	-.2366D-01
29	.3261D-02	-.4183D-02	-.4067D-02	-.4183D-02	-.4067D-02	.1217D-01	.1033D-01	.1217D-01
30	.2367D-13	-.8945D-03	-.1302D-02	.8945D-03	.1302D-02	.3404D-02	.6520D-02	-.3404D-02
31	.2595D-05	-.1868D-03	.2078D-03	-.1868D-03	.2078D-03	.1400D-03	.1067D-03	.1067D-03
32	-.1474D-13	-.3594D-04	-.3373D-04	.3594D-04	.3373D-04	.6476D-06	-.1760D-03	-.6476D-06
33	-.1699D-11	-.6649D-04	.7677D-04	.6649D-04	-.7677D-04	-.2031D-03	.2259D-04	.2031D-03
34	-.3313D-03	-.2261D-03	.2402D-03	-.2261D-03	.2402D-03	.1515D-03	.3850D-05	.1515D-03
35	-.2929D-04	.1208D-01	-.1208D-01	.1208D-01	-.1208D-01	-.1745D-01	.1745D-01	-.1743D-01
36	-.2731D-04	.6401D-03	.6242D-03	.6401D-03	.6242D-03	-.5341D-02	-.5280D-02	-.5341D-02
37	-.5345D-02	.2630D-02	.2450D-02	.2630D-02	.2459D-02	.1271D-02	.1410D-02	.1271D-02
38	.2836D-04	-.2813D-02	.2790D-02	-.2813D-02	.2790D-02	.2524D-03	-.2624D-03	.2524D-03
39	-.9560D-13	-.7024D-03	.1054D-02	.7024D-03	-.1054D-02	-.1083D-02	.2331D-02	.1083D-02
40	.4675D-13	.1187D-02	.6642D-03	-.1187D-02	-.6642D-03	.2366D-02	.5077D-03	-.2366D-02
41	.4170D-03	.3073D-01	.3075D-01	.3073D-01	.3075D-01	-.3261D-02	-.3268D-02	-.3261D-02
42	-.1482D-14	.4049D-01	.3920D-01	-.4049D-01	-.3920D-01	.1725D-01	.3458D-01	-.1725D-01
43	-.1542D-14	.3922D-01	-.4050D-01	-.3922D-01	.4050D-01	.3456D-01	-.1724D-01	-.3456D-01
44	-.1377D-03	-.2361D-01	-.2364D-01	-.2361D-01	-.2364D-01	-.4025D-01	-.4026D-01	-.4025D-01
45	-.4173D-04	.3707D-01	-.3705D-01	.3707D-01	-.3705D-01	.3387D-01	-.3395D-01	.3387D-01
46	.3054D-15	-.3112D-01	-.1339D-01	.3112D-01	.1339D-01	.6117D-01	.4966D-01	-.6117D-01
47	.7650D-15	.1337D-01	-.3111D-01	-.1337D-01	.3111D-01	-.4967D-01	.6117D-01	.4967D-01
48	-.5593D-05	-.1257D-01	.1258D-01	-.1257D-01	.1258D-01	.6213D-02	-.6211D-02	.6213D-02
49	-.2565D-04	-.5802D-01	.5804D-01	-.5802D-01	.5804D-01	.2595D-01	-.2595D-01	.2596D-01
50	-.7307D-15	.3235D-02	.3847D-02	-.3235D-02	-.3847D-02	.3352D-02	.9359D-03	-.3352D-02

ACTUATOR

ACTUATOR INFLUENCE MATRIX

MODE	9	10	11	12	13	14	15	16
1	.3109D-08	.8400D-18	-.1067D-16	-.1214D-16	-.3000D-19	.3809D-08	-.9261D-08	-.9227D-08
2	-.1013D-06	-.1707D-16	-.1270D-15	.1200D-18	-.4960D-15	-.1745D-08	.1941D-08	-.1975D-08
3	-.1035D-12	.5570D-11	.5160D-11	.5030D-11	.5410D-11	.4658D-05	-.6251D-06	-.2406D-05
4	.2154D-06	.7813D-16	.1005D-15	-.5672D-16	-.8485D-16	.1739D-06	-.4027D-08	.2549D 02
5	-.2264D-05	.3520D-11	-.2420D-17	-.3740D-11	.2180D-17	.5556D-03	-.5556D-03	-.1293D-08
6	.1368D-05	-.3160D-17	.4000D-11	.3139D-17	-.4000D-11	.5556D-03	.5556D-03	.9598D-08
7	-.2739D-03	.9605D-03	.1356D-03	-.9605D-03	-.1356D-03	-.2928D-03	-.2922D-03	.3534D-12
8	.5898D-04	-.2867D-04	.2064D-03	.2867D-04	-.2064D-03	.6554D-04	-.6560D-04	-.4645D-10
9	.1102D-04	.9641D-04	.3061D-04	.9641D-04	.3061D-04	.1392D-10	.1289D-10	-.6283D-07
10	-.6390D-04	-.3697D-04	-.3626D-04	-.3697D-04	-.3626D-04	.4247D-11	-.4667D-11	.8469D-03
11	-.1134D-04	-.2160D-02	-.2166D-02	-.2160D-02	-.2166D-02	.4128D-12	-.1070D-12	-.7810D-05
12	.1594D-02	-.7628D-03	.5522D-02	.7628D-03	-.5522D-02	.2613D-02	-.2613D-02	-.1956D-11
13	-.1539D-02	.5364D-02	.7401D-03	-.5364D-02	-.7401D-03	-.2608D-02	-.2608D-02	-.1616D-11
14	.3315D-02	.1745D-02	.1764D-02	.1745D-02	.1764D-02	.8363D-12	.4771D-11	.5776D-03
15	.1075D-02	.1971D-02	-.2023D-02	.1971D-02	-.2023D-02	.1215D-11	.1271D-11	-.2509D-06
16	-.7950D-04	-.1836D-04	-.3059D-04	-.1836D-04	-.3059D-04	-.1707D-11	.1745D-11	-.7308D-03
17	-.6664D-04	.1240D-04	-.2710D-03	-.1240D-04	.2710D-03	-.1181D-03	.1170D-03	.1060D-10
18	-.4867D-04	.6164D-03	-.8763D-04	-.6164D-03	.8763D-04	-.1014D-02	-.1015D-02	-.3162D-13
19	.2056D-02	.3465D-02	-.3411D-02	.3465D-02	-.3411D-02	.3708D-12	.3865D-12	.2718D-06
20	-.1260D-02	.2522D-02	-.2263D-02	-.2522D-02	.2263D-02	-.5602D-04	.2093D-03	.3083D-14
21	-.4963D-02	.2287D-02	.2529D-02	-.2287D-02	-.2529D-02	-.2414D-03	-.1202D-03	.2122D-14
22	.6039D-05	-.8818D-03	.2590D-03	-.8818D-03	.2590D-03	.1918D-15	-.5736D-13	.7659D-06
23	.1605D-02	.7580D-04	.1202D-02	-.7580D-04	-.1202D-02	.3545D-03	-.3972D-03	-.1004D-12
24	.1437D-01	-.1079D-01	.1091D-01	-.1079D-01	.1091D-01	.2739D-13	-.2133D-13	.4900D-03
25	-.2771D-01	-.1294D-01	.6298D-02	.1294D-01	-.6298D-02	.3473D-03	-.8539D-04	.1019D-12
26	.1363D-01	.6704D-02	.1333D-01	-.6704D-02	-.1333D-01	-.2539D-03	-.1409D-03	.6892D-12
27	-.3775D-02	.3193D-02	-.2558D-02	.3193D-02	-.2558D-02	.6504D-13	.5305D-13	.2729D-02
28	-.2453D-01	.1196D-01	.1183D-01	.1196D-01	.1183D-01	.5512D-14	.1796D-14	.4747D-04
29	.1033D-01	-.5913D-02	-.6020D-02	-.5913D-02	-.6020D-02	.5471D-14	.3978D-14	.8966D-06
30	-.6520D-02	-.3398D-02	.2421D-02	.3398D-02	-.2421D-02	-.4613D-03	-.5635D-03	-.3612D-13
31	.1400D-03	-.2408D-03	.6591D-04	-.2408D-03	.6591D-04	.5611D-12	-.3622D-12	-.1556D-02
32	.1760D-03	.1641D-03	-.2398D-03	-.1641D-03	.2398D-03	.1733D-03	-.1716D-03	.4143D-11
33	-.2259D-04	-.4404D-03	-.2247D-03	.4404D-03	.2247D-03	.1908D-02	.1906D-02	.6481D-13
34	.3350D-05	-.4927D-04	.5010D-03	-.4927D-04	.5010D-03	-.9755D-11	-.9744D-11	-.1993D-05
35	.1745D-01	-.3895D-02	.3949D-02	-.3895D-02	.3949D-02	.1176D-13	.1374D-13	-.9910D-04
36	-.5280D-02	-.2158D-01	-.2152D-01	-.2158D-01	-.2152D-01	.5918D-15	.2652D-14	.3231D-05
37	.1410D-02	-.2041D-03	-.1716D-02	-.2041D-03	-.1716D-02	.3229D-13	-.4993D-13	.3446D-05
38	-.2624D-03	.1685D-03	-.1587D-03	.1685D-03	-.1587D-03	.4189D-14	-.4890D-14	.1787D-04
39	-.2331D-02	-.1339D-02	.5430D-03	.1339D-02	-.5430D-03	-.2356D-02	.2371D-02	-.1208D 13
40	-.5077D-03	.3373D-03	.8950D-03	-.3373D-03	-.8950D-03	-.3734D-03	-.3662D-03	.1781D-13
41	-.3066D-02	.9874D-02	.9983D-02	.9874D-02	.9983D-02	-.4044D-14	.1016D-14	.5375D-04
42	-.3450D-01	.1230D-01	.2481D-02	-.1230D-01	-.2481D-02	.1173D-03	.1157D-03	-.3810D-14
43	.1724D-01	.2465D-02	-.1227D-01	-.2465D-02	.1227D-01	-.1337D-04	.1147D-03	-.4973D-14
44	-.4026D-01	-.1667D-01	-.1670D-01	-.1667D-01	-.1670D-01	-.4720D-15	-.1949D-14	-.5322D-04
45	-.3385D-01	.3718D-02	-.3708D-02	.3718D-02	-.3708D-02	.2717D-14	.1857D-14	-.1394D-03
46	-.4966D-01	.5044D-02	.1837D-01	-.5044D-02	-.1837D-01	.5953D-04	-.2057D-05	.1057D-15
47	-.6117D-01	-.1837D-01	.5040D-02	.1837D-01	-.5040D-02	.1053D-04	-.2262D-04	.7575D-16
48	-.6211D-02	.2240D-02	-.2239D-02	.2240D-02	-.2239D-02	.5843D-13	.5854D-13	-.2654D-04
49	-.2595D-01	.1027D-01	-.1026D-01	.1027D-01	-.1026D-01	.3637D-12	.3641D-12	-.1261D-03
50	-.9359D-03	-.5166D-04	-.1170D-02	.5166D-04	.1170D-02	-.8637D-02	-.8635D-02	.6695D-12

SENSOR INFLUENCE MATRIX

MODE

SENSOR	1	2	3	4	5	6	7	8	9	10
1	.7000D-19	.3168D-06	.7949D-08	.3191D-06	-.3109D-08	.3903D-06	-.1144D-07	.3890D-06	.3109D-08	.8400D-18
2	-.1300D-18	.9486D-08	.1005D-06	-.9537D-08	.1013D-06	-.9486D-08	.6066D-06	.9537D-08	-.1013D-06	-.1707D-16
3	-.6000D-13	.3507D-13	-.1262D-12	.3378D-14	.1199D-12	-.2288D-13	.1385D-12	.2510D-14	-.1035D-12	.5570D-11
4	.7300D-17	-.5727D-03	-.5725D-03	-.5727D-03	.4917D-06	-.7308D-07	-.2154D-06	.7309D-07	.2154D-06	.7813D-16
5	-.9000D-19	.5812D-06	-.6429D-06	-.5227D-05	.5289D-05	.1560D-05	-.5598D-05	.9045D-06	-.2264D-05	.3520D-11
6	.4900D-18	.3125D-05	.1852D-05	-.1745D-05	.1839D-03	.2417D-05	.2391D-05	-.5130D-05	.1368D-05	-.3160D-17
7	-.4576D-12	.2741D-03	-.2736D-03	-.2741D-03	.2736D-03	-.2741D-03	.2739D-03	.2741D-03	-.2739D-03	.9605D-03
8	.7675D-13	.5866D-04	.5881D-04	-.5868D-04	-.5881D-04	-.5830D-04	-.5898D-04	.5892D-04	.5898D-04	-.2867D-04
9	-.1062D-04	.1082D-04	-.1099D-04	.1082D-04	-.1099D-04	-.1073D-04	.1102D-04	-.1073D-04	.1102D-04	.9641D-04
10	-.7234D-08	.6669D-04	.6705D-04	.6669D-04	.6705D-04	-.6352D-04	-.6390D-04	-.6352D-04	-.6390D-04	-.3697D-04
11	.2254D-04	.1640D-04	.1471D-04	.1640D-04	.1471D-04	-.1304D-04	-.1134D-04	-.1304D-04	-.1134D-04	-.2160D-02
12	-.9640D-14	.1571D-02	.1577D-02	-.1571D-02	-.1577D-02	-.1584D-02	-.1594D-02	.1584D-02	.1594D-02	-.7628D-03
13	-.6155D-14	.1532D-02	-.1526D-02	-.1532D-02	.1526D-02	-.1549D-02	.1539D-02	.1549D-02	-.1539D-02	.5364D-02
14	.3942D-06	-.3450D-02	-.3443D-02	-.3450D-02	-.3443D-02	.3321D-02	.3315D-02	.3321D-02	.3315D-02	.1745D-02
15	-.4538D-03	.7849D-03	-.8606D-03	.7849D-03	-.8606D-03	-.9890D-03	.1075D-02	-.9890D-03	.1075D-02	.1971D-02
16	-.3608D-07	.8693D-04	.7597D-04	.8693D-04	.7597D-04	-.9589D-04	-.7950D-04	-.9589D-04	-.7950D-04	-.1836D-04
17	-.3474D-13	-.5887D-04	-.4193D-04	.5887D-04	.4193D-04	.6575D-04	.6664D-04	-.6575D-04	-.6664D-04	.1240D-04
18	-.8568D-12	.1575D-06	.1153D-04	-.1575D-06	-.1153D-04	-.1082D-03	.4867D-04	.1082D-03	-.4867D-04	.6164D-03
19	-.8619D-03	.1415D-02	-.1576D-02	.1415D-02	-.1576D-02	-.1881D-02	.2056D-02	-.1881D-02	.2056D-02	.3465D-02
20	-.3914D-12	-.6191D-02	-.2388D-02	.6191D-02	.2388D-02	.4959D-02	.1260D-02	-.4959D-02	-.1260D-02	.2522D-02
21	.1267D-12	.2390D-02	-.6194D-02	-.2390D-02	.6194D-02	-.1265D-02	.4963D-02	.1265D-02	-.4963D-02	.2287D-02
22	-.2372D-02	-.2402D-03	.8009D-04	-.2402D-03	.8009D-04	.4118D-03	.6039D-05	.4118D-03	.6039D-05	-.8818D-03
23	.3035D-13	-.1663D-02	.7538D-03	.1663D-02	-.7538D-03	.3434D-02	-.1605D-02	-.3434D-02	.1605D-02	.7580D-04
24	.2796D-03	.1972D-02	-.1788D-02	.1972D-02	-.1788D-02	-.1471D-01	.1437D-01	.1471D-01	-.1437D-01	-.1079D-01
25	-.7879D-14	-.4654D-02	-.9002D-02	.4654D-02	.9002D-02	.1332D-01	.2771D-01	-.1332D-01	-.2771D-01	-.1294D-01
26	-.1411D-13	-.8941D-02	.4683D-02	.8941D-02	-.4683D-02	.2824D-01	-.1363D-01	-.2824D-01	.1363D-01	.6704D-02
27	-.7818D-04	.4071D-03	.1549D-03	.4071D-03	.1549D-03	.2445D-02	-.3775D-02	.2445D-02	-.3775D-02	.3193D-02
28	.1303D-02	.9460D-02	.9528D-02	.9460D-02	.9528D-02	-.2366D-01	-.2453D-01	.2366D-01	.2453D-01	.1196D-01
29	.3261D-02	-.4183D-02	-.4067D-02	-.4183D-02	-.4067D-02	.1217D-01	.1033D-01	.1217D-01	.1033D-01	-.5913D-02
30	.2867D-13	-.8945D-03	-.1302D-02	.8945D-03	.1302D-02	.3404D-02	.6520D-02	-.3404D-02	-.6520D-02	-.3398D-02
31	.2595D-05	-.1868D-03	.2078D-03	-.1868D-03	.2078D-03	.1067D-03	.1400D-03	.1067D-03	.1400D-03	-.2406D-03
32	-.1474D-13	-.3594D-04	-.3373D-04	.3594D-04	.3373D-04	.6476D-06	-.1760D-03	-.6476D-06	.1760D-03	.1641D-03
33	-.1699D-11	-.6649D-04	.7677D-04	.6649D-04	-.7677D-04	-.2031D-03	.2259D-04	.2031D-03	-.2259D-04	-.4404D-03
34	-.3313D-03	-.2261D-03	.2402D-03	-.2261D-03	.2402D-03	.1515D-03	.3850D-05	.1515D-03	.3950D-05	-.4927D-04
35	-.2929D-04	.1208D-01	-.1208D-01	.1208D-01	-.1208D-01	-.1743D-01	.1745D-01	-.1743D-01	.1745D-01	-.3885D-02
36	-.2731D-04	.6491D-03	.6242D-03	.6491D-03	.6242D-03	-.5341D-02	-.5280D-02	.5341D-02	-.5280D-02	-.2150D-01
37	-.5345D-02	.2630D-02	.2450D-02	.2630D-02	.2450D-02	.1271D-02	.1410D-02	.1271D-02	.1410D-02	-.2041D-03
38	.2836D-04	-.2813D-02	.2790D-02	-.2813D-02	.2790D-02	.2524D-03	-.2624D-03	.2524D-03	-.2624D-03	.1685D-03
39	-.9560D-13	-.7024D-03	.1054D-02	.7024D-03	-.1054D-02	-.1083D-02	.2331D-02	.1083D-02	-.2331D-02	-.1339D-02
40	.4675D-13	.1187D-02	.6642D-03	-.1187D-02	-.6642D-03	.2366D-02	.5077D-03	-.2366D-02	-.5077D-03	.3373D-03
41	.4170D-03	.3073D-01	.3075D-01	.3073D-01	.3075D-01	-.3261D-02	-.3268D-02	.3261D-02	.3268D-02	.9874D-02
42	-.1482D-14	.4049D-01	.3920D-01	-.4049D-01	-.3920D-01	.1725D-01	.3458D-01	-.1725D-01	-.3458D-01	.1230D-01
43	-.1542D-14	.3922D-01	-.4050D-01	-.3922D-01	.4050D-01	.3456D-01	-.1724D-01	-.3456D-01	.1724D-01	.2465D-02
44	-.1377D-03	-.2361D-01	-.2364D-01	-.2361D-01	-.2364D-01	-.4025D-01	-.4026D-01	-.4025D-01	-.4026D-01	-.1667D-01
45	-.4173D-04	.3707D-01	-.3705D-01	.3707D-01	-.3705D-01	.3387D-01	-.3385D-01	.3387D-01	-.3385D-01	.3718D-02
46	.3054D-15	-.3111D-01	-.1333D-01	.3111D-01	.1333D-01	.6117D-01	.4966D-01	-.6117D-01	-.4966D-01	.5044D-02
47	.7650D-15	.1337D-01	-.3111D-01	-.1337D-01	.3111D-01	-.4967D-01	.6117D-01	.4967D-01	-.6117D-01	-.1837D-01
48	-.5593D-05	-.1257D-01	.1258D-01	-.1257D-01	.1258D-01	.6213D-02	-.6211D-02	.6213D-02	-.6211D-02	.2246D-02
49	-.2565D-04	-.5800D-01	.5804D-01	-.5800D-01	.5804D-01	.2596D-01	-.2595D-01	-.2596D-01	.2595D-01	.1027D-01
50	-.7307D-15	.3235D-02	.3847D-02	-.3235D-02	-.3847D-02	.3352D-02	.9359D-03	-.3352D-02	-.9359D-03	-.5166D-04

MODE

SENSOR INFLUENCE MATRIX

SENSOR	11	12	13	14	15	16	17	18	19	20
1	-.1067D-16	-.1214D-16	-.3000D-19	.3809D-08	-.9261D-08	-.9027D-08	.5807D-02	.1000D-08	.5807D-02	.3753D-08
2	-.1270D-15	.1200D-18	-.4960D-15	-.1745D-08	.1941D-08	-.1975D-08	-.3835D-08	.5306D-02	-.3177D-08	.5807D-02
3	.5160D-11	.5030D-11	.5410D-11	.4653D-05	-.6251D-06	-.2406D-05	.2902D-05	.1141D-08	-.4998D-06	.1107D-08
4	.1005D-15	-.5672D-16	-.8485D-16	.1730D-06	-.4007D-08	.2548D-02	.5096D-02	.5094D-02	.7893D-02	.7896D-02
5	-.2420D-17	-.3740D-11	.2180D-17	.5556D-03	-.5556D-03	-.1293D-08	.3598D-02	-.3598D-02	.3585D-02	-.3585D-02
6	.4000D-11	.3130D-17	-.4000D-11	.5556D-03	.5556D-03	.9503D-08	.3587D-02	.3586D-02	.3582D-02	.3580D-02
7	.1356D-03	-.9605D-03	-.1356D-03	-.2920D-03	-.2922D-03	.3534D-12	.4991D-03	-.5018D-03	.4990D-03	-.5012D-03
8	.2064D-03	.2857D-04	-.2064D-03	.6554D-04	-.6560D-04	-.4445D-10	-.3223D-03	-.3220D-03	.8367D-02	.8367D-02
9	.3061D-04	.9641D-04	.3061D-04	.1392D-10	.1289D-10	-.6283D-07	.2556D-04	-.2570D-04	.2745D-04	-.2381D-04
10	-.3626D-04	-.3597D-04	-.3626D-04	.4247D-11	-.4667D-11	.8469D-03	.1411D-02	.1411D-02	-.6627D-02	-.6627D-02
11	-.2166D-02	-.2160D-02	-.2166D-02	.4189D-12	-.1070D-12	-.7810D-05	-.7068D-06	-.2945D-04	-.1450D-06	-.2890D-04
12	.5522D-02	.7622D-03	-.5522D-02	.2615D-02	-.2613D-02	-.1956D-11	.4578D-02	.4591D-02	.3740D-02	.3753D-02
13	.7401D-03	-.5364D-02	-.7401D-03	-.2602D-02	-.2603D-02	-.1616D-11	.4429D-02	-.4438D-02	.4433D-02	-.4438D-02
14	.1764D-02	.1745D-02	.1764D-02	.8363D-12	.4771D-11	.5776D-03	.1138D-02	.1137D-02	.1325D-02	.1324D-02
15	-.2023D-02	.1971D-02	-.2023D-02	.1215D-11	.1271D-11	-.2509D-06	.8573D-03	-.8593D-03	.8484D-03	-.8775D-03
16	-.3059D-04	-.1836D-04	-.3059D-04	-.1707D-11	.1745D-11	-.7308D-03	.1332D-03	.1329D-03	.3618D-01	.3618D-01
17	-.2710D-03	-.1240D-04	.2710D-03	-.1181D-03	.1170D-03	.1060D-10	-.1879D-03	-.1890D-03	.3591D-01	.3591D-01
18	-.8763D-04	-.6164D-03	.8763D-04	-.1014D-02	-.1015D-02	-.3162D-13	.4637D-03	-.4638D-03	.4319D-03	-.5059D-03
19	-.3411D-02	.3465D-02	-.3411D-02	.3703D-12	.3865D-12	.2718D-06	.1233D-02	-.1232D-02	.1237D-02	-.1243D-02
20	-.2263D-02	-.2522D-02	.2263D-02	-.5602D-04	.2093D-03	.3083D-14	-.1100D-03	-.2644D-04	.1060D-03	.1900D-03
21	.2529D-02	-.2287D-02	-.2529D-02	-.2414D-03	-.1202D-03	.2122D-14	.1765D-04	-.2060D-03	.2608D-03	.3576D-04
22	.2590D-03	-.8818D-03	.2590D-03	.1918D-15	-.5736D-13	.7650D-06	-.2247D-02	.2250D-02	-.2280D-02	.2281D-02
23	.1202D-02	-.7590D-04	-.1202D-02	.3545D-03	-.3972D-03	-.1004D-12	-.2813D-02	-.2836D-02	-.1660D-02	-.1684D-02
24	.1091D-01	-.1079D-01	.1091D-01	.2739D-13	-.2138D-13	.4900D-03	.7445D-03	.1272D-02	.7073D-03	.1246D-02
25	.6298D-02	.1294D-01	-.6298D-02	.3473D-03	-.8589D-04	.1019D-12	.1520D-03	.4446D-03	.1671D-03	.4675D-03
26	.1333D-01	-.6704D-02	-.1333D-01	-.2539D-03	-.1409D-03	.6892D-12	.5300D-03	.1986D-03	.4629D-03	.1225D-03
27	-.2553D-02	.3193D-02	-.2559D-02	.6504D-13	.5305D-13	.2729D-02	.5819D-02	.5720D-02	.7947D-02	.7845D-02
28	.1183D-01	.1196D-01	.1183D-01	.5512D-14	.1796D-14	.4747D-04	.4223D-04	.1414D-03	.1049D-03	.2069D-03
29	-.6020D-02	-.5913D-02	-.6020D-02	.5471D-14	.3978D-14	.8966D-06	-.1575D-03	.1696D-03	-.1694D-03	.1673D-03
30	.2421D-02	.3398D-02	-.2421D-02	-.4613D-03	-.5635D-03	-.3612D-13	.5465D-03	-.3889D-03	.6058D-03	-.3596D-03
31	.6591D-04	-.2408D-03	.6591D-04	.5511D-12	-.3622D-12	-.1556D-02	.1226D-02	.1229D-02	.6639D-01	.6639D-01
32	-.2398D-03	-.1641D-03	.2398D-03	.1733D-03	-.1716D-03	.4143D-11	.1268D-02	.1266D-02	.6677D-01	.6676D-01
33	-.2247D-03	.4404D-03	.2247D-03	.1908D-02	.1906D-02	.6481D-13	.5278D-03	-.5282D-03	.5221D-03	-.5309D-03
34	.5010D-03	-.4927D-04	.5010D-03	-.9755D-11	-.9744D-11	-.1973D-05	.1704D-03	-.1722D-03	.2246D-03	-.1333D-03
35	.3949D-02	-.3895D-02	.3949D-02	.1176D-13	.1374D-13	-.9910D-04	-.1886D-03	-.1094D-03	.6217D-03	.7051D-03
36	-.2152D-01	-.2159D-01	-.2152D-01	.5918D-15	.2652D-14	.3231D-05	-.7800D-04	.9197D-04	-.1074D-03	.7166D-04
37	-.1716D-02	-.2041D-03	-.1716D-02	.3229D-13	-.4993D-13	.3948D-05	.1135D-02	-.1123D-02	.1195D-02	-.1208D-02
38	-.1587D-03	.1685D-03	-.1587D-03	.4157D-14	-.4890D-14	.1784D-04	.3381D-04	.3101D-04	-.3197D-04	-.3495D-04
39	.5430D-03	.1339D-02	-.5430D-03	-.2356D-02	.2371D-02	-.1200D-13	-.5028D-02	-.5772D-02	.4386D-02	.4445D-02
40	.8950D-03	-.3373D-03	-.8950D-03	-.3734D-03	-.3662D-03	.1781D-13	.6533D-02	-.6554D-02	.7026D-02	-.7012D-02
41	.9983D-02	.9874D-02	.9983D-02	-.4044D-14	.1016D-14	.5375D-04	-.6143D-05	.1954D-03	-.1754D-03	.4134D-04
42	.2481D-02	-.1230D-01	-.2481D-02	.1173D-03	.1157D-03	-.3251D-14	-.3475D-03	.4839D-03	-.4794D-03	.4410D-03
43	-.1227D-01	-.2465D-02	.1227D-01	-.1337D-04	.1147D-03	-.4973D-14	-.4281D-03	-.1328D-03	-.1013D-03	.2240D-03
44	-.1670D-01	-.1667D-01	-.1670D-01	-.4720D-15	-.1949D-14	-.5320D-04	-.6903D-04	-.1232D-03	.5436D-04	-.5643D-05
45	-.3703D-02	.3718D-02	-.3703D-02	.2717D-14	.1857D-14	-.1396D-03	-.3068D-03	-.2299D-03	.1510D-04	.1004D-03
46	.1837D-01	-.5044D-02	-.1837D-01	.5953D-04	-.2057D-05	.1857D-15	.4776D-04	.2407D-03	-.1168D-03	.1017D-03
47	.5040D-02	.1837D-01	-.5040D-02	.1053D-04	-.2262D-04	.7575D-16	.1168D-03	-.1281D-05	.6451D-04	-.6929D-04
48	-.2238D-02	.2240D-02	-.2238D-02	.5843D-13	.5854D-13	-.2694D-04	-.5624D-04	-.5492D-04	-.2059D-04	-.1878D-04
49	-.1026D-01	.1027D-01	-.1026D-01	.3637D-12	.3641D-12	-.1261D-03	-.2637D-03	-.2568D-03	-.9779D-04	-.8937D-04
50	-.1170D-02	.5166D-04	.1170D-02	-.8637D-02	-.8635D-02	.6695D-12	.1963D-01	-.1965D-01	.2387D-01	-.2386D-01

MODE

SENSOR INFLUENCE MATRIX

SENSOR	21	22	23	24	25	26	27	28	29	30
1	-.1072D-08	.5807D-02	.2775D-08	-.1378D-08	.5806D-02	.1796D-08	-.1684D-08	.5807D-02	.8173D-08	-.1990D-08
2	.1291D-08	-.5272D-08	.5807D-02	.1692D-08	-.7367D-08	.5806D-02	.2073D-08	-.9462D-08	.5807D-02	.2464D-08
3	.5801D-02	-.3051D-05	.1081D-08	.5797D-02	-.5603D-05	.1056D-08	.5793D-02	-.8154D-05	.1030D-03	.5788D-02
4	.1372D-08	.1053D-01	.1054D-01	.1799D-08	.1330D-01	.1330D-01	.2226D-08	.1598D-01	.1597D-01	.2653D-08
5	.3430D-02	.3583D-02	-.3599D-02	.4647D-02	.3584D-02	-.3593D-02	.5824D-02	.3585D-02	-.3597D-02	.7007D-02
6	-.2117D-08	.3584D-02	.3589D-02	-.2775D-08	.3586D-02	.3587D-02	-.3433D-08	.3587D-02	.3586D-02	-.4091D-08
7	.1401D-01	.5006D-03	-.5006D-03	.3315D-01	.5014D-03	-.4998D-03	.5768D-01	.5023D-03	-.4989D-03	.8517D-01
8	-.1796D-06	.2245D-01	.2245D-01	-.7547D-06	.4068D-01	.4068D-01	-.1487D-05	.6119D-01	.6119D-01	-.2306D-05
9	.1196D-01	.3052D-04	-.2075D-04	.3186D-01	.3450D-04	-.1677D-04	.5766D-01	.3898D-04	-.1229D-04	.8672D-01
10	.1826D-05	-.2047D-01	-.2047D-01	.6835D-05	-.3861D-01	-.3861D-01	.1349D-04	-.5913D-01	-.5913D-01	.2092D-04
11	-.2835D-02	.1078D-04	-.1793D-04	-.1438D-02	.2798D-04	-.7894D-06	.4705D-03	.4889D-04	.2012D-04	.2697D-02
12	-.2851D-05	.2194D-02	.2206D-02	-.4876D-06	.2092D-04	.3358D-04	.4191D-05	-.2555D-02	-.2543D 02	.1024D-04
13	.1103D-01	.4435D-02	-.4439D-02	.5433D-02	.4436D-02	-.4439D-02	-.4052D-02	.4437D-02	-.4440D-02	-.1591D-01
14	-.3265D-04	.8352D-03	.8347D-03	-.2194D-04	-.6977D-04	-.7030D-04	-.7386D-05	-.1239D-02	-.1239D-02	.9932D-05
15	.4648D-01	.8418D-03	-.8892D-03	.7564D-01	.8470D-03	-.8879D-03	.6530D-01	.8659D-03	-.8714D-03	.8826D-02
16	.1550D-04	.6109D-01	.6109D-01	.2609D-04	.5358D-01	.5358D-01	.2283D-04	.7748D-02	.7748D-02	.3314D-05
17	-.4605D-04	.6115D-01	.6114D-01	-.7814D-04	.5384D-01	.5384D-01	-.6877D-04	.7919D-02	.7918D-02	-.1014D-04
18	-.4951D-01	.4054D-03	-.5352D-03	-.8535D-01	.4138D-03	-.5292D-03	-.7626D-01	.4634D-03	-.4809D-03	-.1165D-01
19	-.2065D-01	.1039D-02	-.1253D-02	-.4193D-01	.1242D-02	-.1253D-02	-.3969D-01	.1249D-02	-.1251D-02	-.7462D-02
20	.7523D-03	.2789D-03	.3531D-03	.1585D-02	.2651D-03	.3497D-03	.1512D-02	.1594D-04	.1007D-03	.2891D-03
S 21	-.1804D-02	.4471D-03	.2213D-03	-.3777D-02	.4349D-03	.2083D-03	-.3602D-02	.1738D-03	-.5301D-04	-.6901D-03
E 22	-.1780D-02	-.2299D-02	.2297D-02	.2011D-02	-.2313D-02	.2311D-02	.4167D-02	-.2320D-02	.2319D 02	.1870D-02
N 23	.7599D-04	.6184D-04	.3752D-04	-.8312D-05	.1345D-02	.1321D-02	-.7612D-04	.8063D-03	.7817D-03	-.4502D-04
S 24	-.1044D-02	-.3094D-03	.2357D-03	.4991D-04	-.1176D-02	-.6257D-03	.9928D-03	-.8344D-03	-.2815D-03	.6144D-03
O 25	-.4340D-03	-.1057D-03	.1989D-03	-.5197D-04	-.3868D-03	-.7090D-04	.3812D-03	-.3230D-03	-.1304D-04	.2727D-03
R 26	.1063D-02	.2219D-03	-.1234D-03	.1584D-03	-.1875D-04	-.3679D-03	-.8169D-03	.3405D-04	-.3173D-03	-.5935D-03
27	.2417D-03	.1309D-02	.1206D-02	.3826D-04	-.5925D-02	-.6030D-02	-.1843D-03	-.4331D-02	-.4435D-02	-.1351D-03
28	.8426D-03	-.2301D-04	.8053D-04	.1423D-03	-.1703D-03	-.6551D-04	-.7357D-03	-.1415D-03	-.3598D-04	-.5496D-03
29	.1916D-02	-.1711D-03	.1709D-03	.3991D-03	-.1712D-03	.1751D-03	-.1592D-02	-.1729D-03	.1758D-03	-.1229D-02
30	.1848D-02	.5250D-03	-.4568D-03	.5097D-03	.4157D-03	-.5793D-03	-.1428D-02	.4335D-03	-.5689D-03	-.1172D-02
31	-.9061D-04	.3412D-01	.3412D-01	-.4649D-04	-.4004D-01	-.4004D-01	.5443D-04	-.4259D-01	-.4258D-01	.5791D-04
32	.3639D-04	.3460D-01	.3460D-01	.1882D-04	-.4012D-01	-.4012D-01	-.2177D-04	-.4289D-01	-.4289D-01	-.2328D-04
33	.9445D-01	.5498D-03	-.5890D-03	.4997D-01	.5924D-03	-.5572D-03	.5997D-03	-.5616D-03	.5956D-03	-.6105D-01
34	.9451D-01	.2074D-03	-.1589D-03	.5016D-01	.1592D-03	-.2139D-03	-.5641D-01	.1588D-03	-.2131D-03	-.6113D-01
35	.1127D-02	.3714D-03	.4569D-03	.6991D-03	-.4327D-03	-.3454D-03	-.6532D-03	-.5060D-03	-.4177D-03	-.7760D-03
36	.1106D-02	-.1045D-03	.7952D-04	.7683D-03	-.8367D-04	.1044D-03	-.6338D-03	-.8197D-04	.1034D-03	-.8076D-03
37	-.1193D-02	.1235D-02	-.1248D-02	-.9770D-03	.1278D-02	-.1270D-02	.5555D-03	.1298D-02	-.1286D 02	.8772D-03
38	-.3719D-04	-.3098D-04	-.3398D-04	-.3576D-04	.2088D-04	.1772D-04	.2119D-04	.3217D-04	.2696D-04	.3358D-04
39	.2675D-04	.4660D-02	.4722D-02	.2702D-04	-.2654D-02	-.2591D-02	-.1438D-04	-.4397D-02	-.4333D-02	-.2476D-04
40	-.2588D-02	.7288D-02	-.7274D-02	-.2712D-02	.7490D-02	-.7498D-02	.1319D-02	.7607D-02	-.7602D-02	.2391D-02
41	.8514D-04	-.1951D-03	.3011D-04	.8263D-04	-.7701D-04	.1550D-03	-.3920D-04	-.4423D-04	.1916D-03	-.7549D-04
42	.1183D-03	-.5296D-03	.4387D-03	.2479D-03	-.4903D-03	.5162D-03	-.6900D-04	-.4752D-03	.5530D-03	-.2093D-03
43	.7100D-04	-.1373D-04	.3282D-03	.1552D-03	-.2229D-03	.1325D-03	-.4353D-04	-.3171D-03	.4599D-04	-.1317D-03
44	-.3388D-05	.9833D-04	.3510D-04	.4485D-05	.1597D-04	-.4997D-04	-.1633D-05	-.2332D-04	-.9065D-04	-.4819D-05
45	.5908D-04	.1305D-03	.2205D-03	.1641D-03	-.8934D-04	.4481D-05	-.3920D-04	-.1983D-03	-.1023D-03	-.1395D-03
46	.6033D-05	-.1965D-03	.3635D-04	.3131D-04	-.1107D-03	.1338D-03	-.4309D-05	-.5511D-04	.1360D 03	-.2700D-04
47	-.6571D-05	.4151D-04	-.1011D-03	-.2766D-04	.7915D-04	-.7054D-04	.3728D-05	.1031D-03	-.5041D-04	.2363D-04
48	-.4199D-05	.5511D-04	.5689D-04	.1243D-04	.5543D-05	.7444D-05	.1442D-05	-.6114D-04	-.5917D-04	-.1332D-04
49	-.2009D-04	.2587D-03	.2673D-03	.5904D-04	.2590D-04	.3595D-04	.6928D-05	-.2885D-03	-.2731D-03	-.6337D-04
50	.5209D-02	.2628D-01	-.2627D-01	-.1516D-01	.2824D-01	-.2824D-01	-.1828D-02	.2936D-01	-.2937D-01	.1633D-01

MODE

SENSOR INFLUENCE MATRIX

SENSOR	31	32	33	34	35	36	37	38	39	40
1	.5007D-02	-.1614D-08	-.2295D-08	.5907D-02	.8749D-08	.5906D-02	.1005D-08	.8963D-08	.5906D-02	.1103D-08
2	-.1156D-08	.5306D-02	.2855D-08	.7917D-08	.5804D-02	.1031D-08	.5807D-02	-.1226D-08	.1241D-08	.5907D-02
3	-.1071D-04	.1005D-08	.5734D-02	.1252D-04	.1237D-08	.1593D-04	.1271D-08	.5829D-02	.1340D-04	.1297D-08
4	.1866D-01	.1866D-01	.3080D-08	-.5095D-02	-.5095D-02	-.7899D-02	-.7899D-02	-.1376D-08	-.1053D-01	-.1053D-01
5	.3587D-02	-.3560D-02	.8196D-02	.3577D-02	-.3590D-02	.3594D-02	-.3587D-02	-.3457D-02	.3586D-02	-.3583D-02
6	.3595D-02	.3584D-02	-.4749D-08	.3590D-02	.3590D-02	.3593D-02	.3592D-02	.2119D-08	.3534D-02	.3581D-02
7	.5032D-03	-.4980D-03	.1139	.4991D-03	-.5018D-03	.4998D-03	-.5012D-03	-.1401D-01	.5006D-03	.5006D-03
8	.8264D-01	.8264D-01	-.3160D-05	-.3223D-03	-.3220D-03	.8367D-02	.8367D-02	.1794D-06	.2245D-01	.2245D-01
9	.4366D-04	-.7610D-05	.1171	-.2556D-04	.2570D-04	-.2745D-04	.2391D-04	.1196D-01	-.3052D-04	.2075D-04
10	-.8062D-01	-.8062D-01	.2871D-04	-.1411D-02	-.1411D-02	.6627D-02	.6627D-02	.1876D-05	.2047D-01	.2047D-01
11	.7130D-04	.4261D-04	.5064D-02	.7068D-06	.2945D-04	.1450D-06	.2890D-04	-.2835D-02	-.1078D-04	.1798D-04
12	-.5312D-02	-.5299D-02	.1687D-04	.4573D-02	.4591D-02	.3740D-02	.3753D-02	.2851D-05	.2194D-02	.2206D-02
13	.4437D-02	-.4440D-02	-.2801D-01	.4429D-02	-.4436D-02	.4433D-02	-.4438D-02	-.1103D-01	.4435D-02	-.4438D-02
14	-.2525D-02	-.2525D-02	.2855D-04	-.1138D-02	-.1137D-02	-.1325D-02	-.1324D-02	-.3265D-04	-.8352D-03	-.8347D-03
15	.8925D-03	-.8460D-03	-.7430D-01	-.8573D-03	.8593D-03	-.8464D-03	.8775D-03	.4643D-01	-.8418D-03	.8892D-03
16	-.6034D-01	-.6034D-01	-.2574D-04	-.1332D-03	-.1329D-03	-.3618D-01	-.3613D-01	.1550D-04	-.6109D-01	-.6109D-01
17	-.6045D-01	-.6045D-01	.7714D-04	-.1879D-03	-.1890D-03	.3591D-01	.3591D-01	.4605D-04	.6115D-01	.6114D-01
18	.5371D-03	-.4080D-03	.8502D-01	.4687D-03	-.4638D-03	.4318D-03	-.5059D-03	.4951D-01	.4054D-03	-.5352D-03
19	.1256D-02	-.1245D-02	.4254D-01	-.1233D-02	.1232D-02	-.1237D-02	.1243D-02	-.2065D-01	-.1239D-02	.1250D-02
20	-.3729D-03	-.2882D-03	-.1618D-02	-.1100D-03	-.2644D-04	.1040D-03	.1900D-03	-.7923D-03	.2784D-03	.3631D-03
21	-.2345D-03	-.4615D-03	.3849D-02	.1765D-04	-.2060D-03	.2608D-03	.3576D-04	.1804D-02	.4471D-03	.2213D-03
22	-.2323D-02	.2325D-02	-.3570D-02	.2247D-02	-.2253D-02	.2288D-02	-.2281D-02	-.1780D-02	.2239D-02	-.2397D-02
23	-.1130D-02	-.1155D-02	.6320D-04	-.2813D-02	-.2836D-02	-.1660D-02	-.1684D-02	-.7599D-04	.6184D-04	.3751D-04
24	.4677D-03	.1022D-02	-.8178D-03	-.7445D-03	-.1272D-02	-.7073D-03	-.1246D-02	-.1044D-02	.3094D-03	-.2357D-03
25	.3628D-04	.3473D-03	-.3067D-03	.1520D-03	.4446D-03	.1671D-03	.4675D-03	.4340D-03	-.1057D-03	.1934D-03
26	.3378D-03	-.1494D-04	.6676D-03	.5300D-03	.1986D-03	.4629D-03	.1225D-03	-.1063D-02	.2219D-03	-.1234D-03
27	.4942D-02	.4837D-02	.1506D-03	-.5819D-02	-.5720D-02	-.7947D-02	-.7845D-02	.2417D-03	-.1309D-02	-.1204D-02
28	.4319D-04	.1491D-03	.5892D-03	-.4223D-04	-.1414D-03	-.1049D-03	-.2069D-03	.8426D-03	.2301D-04	-.8054D-04
29	-.1765D-03	.1735D-03	.1279D-02	.1575D-03	-.1696D-03	.1694D-03	-.1673D-03	.1916D-02	.1711D-03	-.1704D-03
30	.5707D-03	-.4359D-03	.1154D-02	.5465D-03	-.3889D-03	.6053D-03	-.3596D-03	.1818D-02	.5250D-03	-.4568D-03
31	.3423D-01	.3423D-01	-.4655D-04	-.1206D-02	-.1229D-02	-.6639D-01	-.6639D-01	-.9061D-04	-.3412D-01	.3412D-01
32	.3435D-01	.3435D-01	.1865D-04	.1268D-02	.1266D-02	.6677D-01	.6676D-01	-.3639D-04	.3460D-01	.3460D-01
33	.5689D-03	-.5991D-03	.4848D-01	.5278D-03	-.5282D-03	.5221D-03	-.5909D-03	-.9445D-01	.5490D-03	-.6000D-03
34	.2130D-03	-.1660D-03	.4849D-01	-.1704D-03	.1722D-03	-.2246D-03	.1333D-03	.9451D-01	-.2074D-03	.1589D-03
35	.2991D-03	.3379D-03	.5775D-03	.1893D-03	.1094D-03	-.6217D-03	-.7051D-03	.1127D-02	-.3714D-03	-.4569D-03
36	-.1052D-03	.8643D-04	.5744D-03	.7508D-04	-.9197D-04	.1074D-03	-.7166D-04	.1106D-02	.1049D-03	-.7952D-04
37	.1293D-02	-.1306D-02	-.5610D-03	-.1135D-02	.1123D-02	-.1195D-02	.1208D-02	-.1193D-02	-.1235D-02	.1245D-02
38	-.1763D-04	-.2086D-04	-.2115D-04	-.3391D-04	-.3101D-04	.3197D-04	.3495D-04	-.3719D-04	.3078D-04	.3339D-04
39	.2647D-02	.2712D-02	.1502D-04	-.5828D-02	-.5772D-02	.4386D-02	.4445D-02	-.2675D-04	.4660D-02	.4722D-02
40	.7605D-02	-.7678D-02	-.1424D-02	.6533D-02	-.6554D-02	.7026D-02	-.7012D-02	.2595D-02	.7285D-02	-.7274D-02
41	-.1619D-03	.7615D-04	.4412D-04	.6143D-05	-.1954D-03	.1754D-03	-.4134D-04	.8614D-04	.1951D-03	-.3011D-04
42	-.5397D-03	.5007D-03	.1049D-03	-.3479D-03	.4889D-03	-.4794D-03	.4418D-03	-.1183D-03	-.5296D-03	.4387D-03
43	-.1159D-03	.2515D-03	.6597D-04	-.4291D-03	-.1328D-03	-.1013D-03	.2240D-03	-.7100D-04	-.1378D-04	.3282D-03
44	.6189D-04	-.6287D-05	.2312D-05	.6903D-04	.1232D-03	-.5436D-04	.5648D-05	-.3308D-05	-.9337D-04	-.3510D-04
45	.2386D-04	.1211D-03	.6733D-04	.3068D-03	.2299D-03	-.1910D-04	-.1004D-03	.5908D-04	-.1304D-03	-.2204D-03
46	-.1585D-03	.9633D-04	.1194D-04	.4778D-04	.2407D-03	-.1166D-03	.1017D-03	-.6037D-05	-.1965D-03	.3639D-04
47	.6643D-04	-.8854D-04	-.1045D-04	.1168D-03	-.1281D-05	.6451D-04	-.6929D-04	.6571D-05	.4151D-04	-.1011D-03
48	.2094D-04	.2296D-04	.4859D-05	.5624D-04	.5492D-04	.2059D-04	.1899D-04	-.4199D-05	-.5511D-04	-.5686D-04
49	.9800D-04	.1084D-03	.2311D-04	.2437D-03	.2568D-03	.9779D-04	.8937D-04	-.2008D-04	-.2557D-03	-.2673D-03
50	.3001D-01	-.3000D-01	-.5942D-02	.1963D-01	-.1965D-01	.2387D-01	-.2388D-01	-.5209D-02	.2659D-01	-.2627D-01

SENSOR INFLUENCE MATRIX

MODE

SENSOR	41	42	43	44	45	46	47	48	49	50
1	.1202D-08	.5907D-02	.1201D-08	.1508D-08	.5806D-02	.1299D-08	.1814D-08	.5806D-02	.1397D-08	.2119D-08
2	-.1617D-08	.1450D-08	.5807D-02	-.2003D-08	.1660D-08	.5807D-02	-.2399D-08	.1869D-08	.5807D-02	-.2790D-08
3	.5833D-02	.2103D-04	.1322D-08	.5837D-02	.2358D-04	.1348D-08	.5842D-02	.2613D-04	.1373D-08	.5846D-02
4	-.1803D-08	-.1330D-01	-.1329D-01	-.2233D-08	-.1598D-01	-.1598D-01	-.2657D-08	-.1866D-01	-.1867D-01	-.3084D-08
5	-.4673D-02	.3556D-02	-.3590D-02	-.5823D-02	.3588D-02	-.3586D-02	-.7008D-02	.3585D-02	-.3583D-02	-.8194D-02
6	.2777D-08	.3585D-02	.3589D-02	.3435D-08	.3586D-02	.3588D-03	.4093D-08	.3587D-02	.3586D-03	.4751D-08
7	-.3315D-01	.5014D-03	-.4998D-03	-.5768D-01	.5023D-03	-.4988D-03	-.8517D-01	.5032D-03	-.4980D-03	-.113
8	.7543D-06	.4058D-01	.4068D-01	.1486D-05	.6119D-01	.6119D-01	.2304D-05	.8264D-01	.8264D-01	.3153D-05
9	.3186D-01	-.3458D-04	.1677D-04	.5764D-01	-.3998D-04	.1229D-04	.8572D-01	-.4366D-04	.7611D-05	.1171
10	.6885D-05	.3861D-01	.3861D-01	.1349D-04	.5913D-01	.5913D-01	.2092D-04	.8062D-01	.8062D-01	.2871D-04
11	-.1438D-02	-.2798D-04	.7894D-06	.4705D-03	-.4889D-04	-.2012D-04	.2697D-02	-.7133D-04	-.4261D-04	.5064D-02
12	.4876D-06	.2092D-04	.3358D-04	-.4191D-05	-.2555D-02	-.2543D-02	-.1024D-04	-.5312D-02	-.5299D-02	-.1687D-04
13	-.5433D-02	.4436D-02	-.4439D-02	.4052D-02	.4437D-02	-.4440D-02	.1591D-01	.4437D-02	-.4440D-02	.2881D-01
14	-.2194D-04	.6977D-04	.7030D-04	-.7386D-05	.1239D-02	.1239D-02	.9932D-05	.2525D-02	.2525D-02	.2855D-04
15	.7564D-01	-.8470D-03	.8879D-03	.6530D-01	-.8659D-03	.8714D-03	.8826D-02	-.8925D-03	.8460D-03	-.7430D-01
16	.2609D-04	-.5358D-01	-.5358D-01	.2288D-04	-.7748D-02	-.7748D-02	.3314D-05	.6034D-01	.6034D-01	-.2574D-04
17	.7814D-04	.5384D-01	.5384D-01	.6877D-04	.7919D-02	.7918D-02	.1014D-04	-.6045D-01	-.6045D-01	-.7714D-04
18	.8585D-01	.4138D-03	-.5292D-03	.7626D-01	.4634D-03	-.4896D-03	.1165D-01	.5371D-03	-.4030D-03	-.8502D-01
19	-.4199D-01	-.1242D-02	.1253D-02	-.3969D-01	-.1249D-02	.1251D-02	-.7462D-02	-.1256D-02	.1245D-02	.4254D-01
20	-.1565D-02	.2651D-03	.3497D-03	-.1512D-02	.1594D-04	.1007D-03	-.2891D-03	-.3729D-03	-.2892D-03	.1618D-02
21	.3777D-02	.4348D-03	.2083D-03	.3602D-02	.1738D-03	-.5301D-04	.6901D-03	-.2345D-03	-.4615D-03	-.3949D-02
22	.2011D-02	.2313D-02	-.2311D-02	.4167D-02	.2320D-02	-.2319D-02	.1870D-02	.2323D-02	-.2325D-02	-.3570D-02
23	.8312D-05	.1345D-02	.1321D-02	.7612D-04	.8063D-03	.7817D-03	.4502D-04	-.1130D-02	-.1155D-02	-.6320D-04
24	.4991D-04	.1176D-02	.6257D-03	.9928D-03	.8344D-03	.2815D-03	.6144D-03	-.4677D-03	-.1022D-02	-.8172D-03
25	.5197D-04	-.3868D-03	-.7880D-04	-.3812D-03	-.3230D-03	-.1304D-04	-.2727D-03	.3628D-04	.3473D-03	.3067D-03
26	-.1584D-03	-.1875D-04	-.3679D-03	.8169D-03	.3405D-04	-.3173D-03	.5935D-03	.3378D-03	-.1484D-04	-.6576D-03
27	.3826D-04	.5925D-02	.6030D-02	-.1843D-03	.4331D-02	.4435D-02	-.1351D-03	-.4942D-02	-.4837D-02	.1506D-03
28	.1423D-03	.1703D-03	.6551D-04	-.7357D-03	.1415D-03	.3598D-04	-.5496D-03	-.4518D-04	-.1491D-03	.5892D-03
29	.3991D-03	.1711D-03	-.1751D-03	-.1592D-02	.1729D-03	-.1758D-03	-.1229D-02	.1765D-03	-.1735D-03	.1279D-02
30	-.5097D-03	.4157D-03	-.5793D-03	.1423D-02	.4335D-03	-.5689D-03	.1172D-02	.5707D-03	-.4359D-03	-.1154D-02
31	-.4649D-04	.4004D-01	.4004D-01	.5443D-04	.4259D-01	.4258D-01	.5791D-04	-.3423D-01	-.3423D 01	-.4655D-04
32	-.1832D-04	-.4012D-01	-.4012D-01	.2177D-04	-.4288D-01	-.4288D-01	.2328D-04	.3435D-01	.3435D-01	-.1865D-04
33	-.4997D-01	.5924D-03	-.5572D-03	.5644D-01	.5997D-03	-.5616D-03	.6105D-01	.5683D-03	-.5991D-03	-.4848D-01
34	.5016D-01	-.1592D-03	.2139D-03	-.5641D-01	-.1588D-03	.2181D-03	-.6113D-01	-.2130D-03	.1660D-03	.4849D-01
35	.6991D-03	.4327D-03	.3454D-03	-.6532D-03	.5060D-03	.4177D-03	-.7760D-03	-.2991D-03	.3875D-03	.5775D-03
36	.7683D-03	.8367D-04	-.1044D-03	-.6338D-03	.8197D-04	-.1054D-03	-.8076D-03	.1052D-03	-.8643D-04	.5744D-03
37	-.9770D-03	-.1278D-02	.1270D-02	.5555D-03	-.1298D-02	.1286D-02	.8772D-03	-.1299D-02	.1306D-02	-.5610D-03
38	-.3576D-04	-.2088D-04	-.1772D-04	.2119D-04	-.3217D-04	-.2898D-04	.3359D-04	.1763D-04	.2086D-04	-.2115D-04
39	-.2702D-04	-.2654D-02	-.2591D-02	.1480D-04	-.4397D-02	-.4333D-02	.2476D-04	.2647D-02	.2712D-02	-.1522D-04
40	.2712D-02	.7490D-02	-.7498D-02	-.1319D-02	.7607D-02	-.7622D-02	-.2391D-02	.7686D-02	-.7670D-02	.1424D-02
41	.8863D-04	.7701D-04	-.1550D-03	-.3920D-04	.4423D-04	-.1916D-03	-.7549D-04	.1619D-03	-.7615D-04	.4412D-04
42	-.2479D-03	-.4903D-03	.5162D-03	.6900D-04	-.4752D-03	.5530D-03	.2093D-03	-.5397D-03	.5007D-03	-.1049D-03
43	-.1552D-03	-.2229D-03	.1325D-03	.4353D-04	-.3171D-03	.4599D-04	.1317D-03	-.1159D-03	.2515D-03	-.6597D-04
44	.4485D-05	-.1597D-04	.4987D-04	-.1633D-05	.2332D-04	.9865D-04	-.4819D-05	.6189D-04	.6039D-05	.2312D-05
45	.1641D-03	.8934D-04	-.4491D-05	-.3920D-04	.1983D-03	.1003D-03	-.1395D-03	-.2386D-04	-.1211D-03	.6733D-04
46	-.3131D-04	-.1107D-03	.1332D-03	.4303D-05	-.5511D-04	.1960D-03	.2700D-04	-.1505D-03	.9633D-04	-.1194D-04
47	.2766D-04	.7915D-04	-.7054D-04	-.3728D-05	.1031D-03	-.5061D-04	-.2363D-04	.6643D-04	-.8952D-04	.1045D-04
48	.1243D-04	-.5543D-05	-.7444D-05	.1442D-05	.6114D-04	.5917D-04	-.1332D-04	-.2094D-04	-.2298D-04	.4859D-05
49	.5904D-04	-.2590D-04	-.3585D-04	.6922D-05	.2805D-03	.2781D-03	-.6337D-04	-.9800D-04	-.1086D-03	.2311D-04
50	.1516D-01	.2824D-01	-.2824D-01	.1028D-02	.2936D-01	-.2937D-01	-.1633D-01	.3001D-01	-.3000D-01	.5942D-02

APPENDIX G

EIGENSYSTEM PERTURBATION THEORY

Given the linear, time-invariant system Σ_0, described by

$$\dot{\underline{x}} = A\underline{x} + B\underline{u} \tag{G-1}$$

where

λ_n = the eigenvalues of A.

R_N and L_n = the right and left eigenvectors of A associated with λ_n.

That is

$$A\,\underline{R}_n = \lambda_n\,\underline{R}_n \tag{G-2}$$

$$\underline{L}_n^T A = \lambda_n\,\underline{L}_n \tag{G-3}$$

This appendix derives expressions for the incremental changes in λ_n and R_n as a result of known perturbations in the A matrix.

Define a perturbed matrix

$$A^* = A + \delta A \tag{G-4}$$

then

$$[A + \delta A]\,[\underline{R}_N + \delta\underline{R}_N] = [\lambda_n + \delta\lambda_n]\,[\underline{R}_N + \delta\underline{R}_N] \tag{G-5}$$

Using Eq. (G-2), Eq. (G-5) becomes

$$A\,\delta\underline{R}_N + \delta A[\underline{R}_N + \delta\underline{R}_N] = \lambda_n\delta\underline{R}_N + \delta\lambda_n[\underline{R}_N + \delta\underline{R}_N] \qquad \text{(G-6)}$$

If Eq. (G-6) is multiplied by $\underline{L}_n^T$, and Eq. (G-3) is used, then

$$d\lambda_n = \frac{\underline{L}_n^T\,\delta A\,[\underline{R}_n + \delta\underline{R}_N]}{\underline{L}_n^T[\underline{R}_N + \delta\underline{R}_N]} \qquad \text{(G-7)}$$

To first order

$$d\lambda_n = \frac{\underline{L}_n^T\,\delta A\,\underline{R}_N}{\underline{L}_n^T\,\underline{R}_N} \qquad \text{(G-8)}$$

This expression was first derived by Jacobi. Aubrun[44] extended Jacobi's work by developing a relation for δR. Specifically, if a normalization matrix G_n is defined, such that

$$\underline{R}_n^T\,G_n\,\underline{R}_n = 1 \qquad \text{(G-9)}$$

then, for sufficiently small δR_N, denoted dR_n

$$\underline{R}_n^T\,G_n\,d\underline{R}_n \approx 0 \qquad \text{(G-10)}$$

Using Eq. (G-9) and (G-10), Eq. (G-6) can be expanded and premultiplied by $R_n^T\,G_n$, giving

$$d\lambda_n = \underline{R}_n^T\,G_n\,\delta A\underline{R}_n + \underline{R}_n^T\,G_n\,A\,d\underline{R}_n \qquad \text{(G-11)}$$

If Eq. (G-7) is used to eliminate $d\lambda_n$ from Eq. (G-11),

$$d\underline{R}_N = [A - \underline{R}_n \underline{R}_n^T G_n A - \lambda_n I]^{-1} [\underline{R}_n \underline{R}_n^T G_n - I] \delta A \underline{R}_n \qquad \text{(G-12)}$$

Equations (G-7) and (G-12) give the incremental change in λ_n and R_n resulting from a perturbation in the A matrix. Equation (G-7) implies that

$$d\lambda \sim \delta A \qquad \text{(G-13)}$$

Equation (G-12) implies that

$$d\underline{R}_N \sim A^{-1} \delta A \underline{R}_n \text{ for } \lambda_n \text{ small} \qquad \text{(G-14)}$$

Additionally, for the special case where Σ_0 is a self-adjoint system, orthonormal modes can be chosen, and $G_N = I$. Then Eq. (G-12) can be rewritten

$$d\underline{R}_N = [A - \lambda_n \underline{R}_N \underline{R}_n^T - \lambda_n I]^{-1} [\underline{R}_N \underline{R}_N^T - I] \delta A \underline{R}_n \qquad \text{(G-15)}$$

if λ_n is large enough, then

$$d\underline{R}_N \simeq \frac{1}{\lambda_n} [I + \underline{R}_N \underline{R}_N^T]^{-1} [I - \underline{R}_N \underline{R}_N^T] \delta A \underline{R}_N \qquad \text{(G-16)}$$

Note that $\underline{R}_N \underline{R}_N^T$ is a positive definite quantity so

$$d\underline{R}_N < \frac{1}{\lambda_n} \delta A \underline{R}_N \qquad \text{(G-17)}$$

APPENDIX H

IMPLEMENTATION ISSUES

Chapter 3 exhibits specific controller designs which include up to four distinct components.

(1) Regulator gain matrix

(2) Asymptotic observer

(3) Input transform

(4) Output transform

This appendix deals with the designs of Chapter 3 at the component level. This intent is to discuss the component design algorithms, and to exhibit the algorithm input data.

H.1 Regulator Gains

Regulators are designed for two systems $[A_1\ B_1]$ and $[A_1,\ B_1T_2]$. Given a dynamical matrix A, an input distribution matrix B, and a quadratic expression for cost, the optimal feedback gain matrix is

$$K = R_2^{-1}B^TP \qquad (H\text{-}1)$$

where P satisfies the algebraic Riccati equation

$$0 = R_1 - PBR_2^{-1}B^TP + A^TP + PA$$

AD-A092 547 AIR FORCE INST OF TECH WRIGHT-PATTERSON AFB OH F/G 22/2
OPTIMAL REGULATION WITHIN SPATIAL CONSTRAINTS. AN APPLICATION T--ETC(U)
AUG 80 E G TAYLOR
UNCLASSIFIED AFIT-CI-80-46D NL

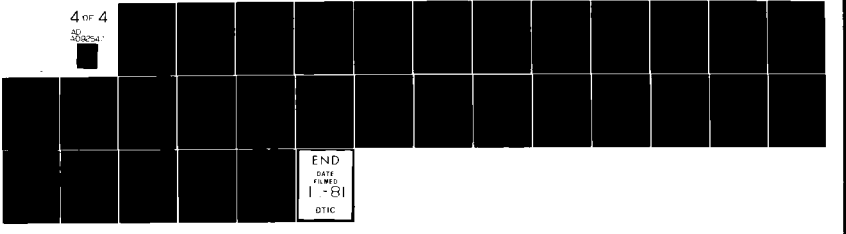

and where R_1 and R_2 are state-deviation and control-effort weighting matrices in the cost function

$$J = \int_{t_1}^{\infty} \underline{x}_1^T R_1 \underline{x}_1 + \underline{u}^T R_2 \underline{u} \, dt \qquad \text{(H-3)}$$

In this thesis, Eq. (H-2) is solved using Potter's noniterative method,[6] which constructs the matrix P from the eigenvectors of Z

$$Z = \begin{bmatrix} A & -BR_2^{-1}B^T \\ -R_1 & -A^T \end{bmatrix} \qquad \text{(H-4)}$$

This method is efficient, but has numerical difficulties when R_1 and R_2 choices lead to multiplicity of eigenvalues in Z.

For the $[A_1 B_1]$ design, the weighting matrices R_1 and R_2 are given in Table H-1 (note, $R_1 = \overline{Q}$ and $R_2 = \overline{R}$). The cost matrix and poles of [A + BK] are given in Chapter 3. The gain matrix is given in Table H-2.

For the design $[A_1, B_1 T_2]$, the weighting matrices R_1 and R_2 are given in Table H-3. The weighting matrix on state deviations R_1, is the same as above ($R_1 = \overline{Q}$). The weighting matrix for control effort is given by

$$R_2 = T_2^T \overline{R} T_2 \qquad \text{(H-5)}$$

In this way, both designs have the same cost functions. The cost matrix P for the second design is exhibited in Table H-4, and the gains K are given in Table H-5.

Table H-1. State and control weightings for regulator $[A_1, B_1]$.

```
    POTTER    INPUT DATA                TIME:  8:50:03.5    DATE: 07/08/80  (80/190)
    ----+----+----+----+----+----+----+----+----+----+----+----+----+----+----+----+

  1 * CONTROL GAINS
  2 * X1 TRANS  MODEL  X1 WEIGHTS
  3 /GET=S206
  4 /PUT=Q411 X1  GAINS NO TRANS
  5 /STATES ARE WEIGHTED
  6 Q      1 1  1.666666666E+00  2 2  1.666666666E+00  3 3  1.666666666E+00
  7 Q      4 4  1.000000000E+00
  8 Q      5 5  0.000000000E+00
  9 Q      6 6  1.000000000E+00  7 7  1.000000000E+00  8 8  1.000000000E+00
 10 Q      9 9  1.666666666E+00 1010  1.666666666E+00 1111  1.666666666E+00
 11 Q     1212  1.666666666E+00 1313  1.666666666E+00 1414  1.666666666E+00
 12 Q     1515  1.000000000E+01
 13 Q     1616  0.000000000E+00 1717  1.000000000E+00 1818  1.000000000E+00
 14 Q     1919  1.000000000E+00
 15 Q     2020  1.666666666E+00
 16 Q     2121  1.666666666E+00 2222  1.000000000E+01
 17 R      1 1  1.000000000E-07  2 2  1.000000000E-07  3 3  1.000000000E-07
 18 R      4 4  1.000000000E-07  5 5  1.000000000E-07  6 6  1.000000000E-07
 19 R      7 7  1.000000000E-07  8 8  1.000000000E-07  9 9  1.000000000E-07
 20 R     1010  1.000000000E-07 1111  1.000000000E-07 1212  1.000000000E-07
 21 R     1313  1.000000000E-07 1414  1.000000000E-08 1515  1.000000000E-08
 22 R     1616  1.000000000E-08
 23 /COMPUTE
 24 /END
    ----+----+----+----+----+----+----+----+----+----+----+----+----+----+----+----+
    END OF INPUT DATA
```

Notes: (1) States 1 to 11 correspond to displacements of modes 4, 5, 6, 7, 10, 11, 12, 13, 20, 21, and 22. States 12 to 22 correspond to modal displacements.

(2) $R_1 = Q$, $R_2 = R$

(3) Only nonzero elements are given.

Table H-2. Optimal gain matrix for $[A_1 B_1]$ regulator (sheet 1 of 2).

OPTIMAL GAIN MATRIX K

	1	2	3	4	5
1	-3.657003607D-01	-3.955847971D-03	-2.158158961D-02	2.280209186D-02	2.219972651D-10
2	2.883143772D+02	1.186799060D+02	-1.268889412D+02	8.578248218D+03	8.661539560D-10
3	2.809792790D+02	9.955998307D+01	1.362767450D+02	-8.836682430D+03	2.249179546D-09
4	2.875720175D+02	-1.115134170D+02	1.224276828D+02	-8.448886577D+03	-7.696019324D-10
5	6.976831500D+00	-1.084885639D+02	-5.002302545D+02	1.165846895D+04	-2.246570167D-09
6	1.227958636D-01	-1.168129343D+02	1.079525473D+02	-8.394287134D+03	-8.561553223D-10
7	6.013206393D+00	-8.214028138D+01	-1.384849160D+02	8.870710982D+03	-1.633964152D-09
8	1.763895640D-02	1.120651661D+02	-1.026346359D+02	8.353827114D+03	7.792896797D-10
9	-5.999226323D+00	9.689626217D+01	1.311123260D+02	-8.814610398D+03	1.632632834D-09
10	9.254946957D+00	-5.522031324D+01	-3.606536595D+02	2.901333925D+04	-1.232435450D-09
11	-1.103776970D-01	3.034170919D+02	-6.799637526D+01	4.276403364D+03	-2.020920773D-10
12	-6.185691021D+00	5.520916130D+01	3.605536264D+02	-2.901376099D+04	1.412767915D-09
13	3.523412089D+00	-3.034244194D+02	6.791730226D+01	-4.276846009D+03	1.688440643D-10
14	-2.294162674D+01	-9.045190145D+03	-8.940401276D+03	-5.204048953D+04	4.486887898D-10
15	-2.796435991D+00	9.057721474D+03	-8.969775075D+03	-5.178905346D+04	-2.224947148D-10
16	-1.281467273D+04	3.475846222D+01	3.863829378D+01	-2.417720915D+03	-1.153423841D-09

	6	7	8	9	10
1	-1.687924177D+02	-2.908175937D-03	6.691273068D-03	5.932822071D-02	1.445832971D-01
2	-3.447732441D+01	1.927201864D+03	-3.752910675D+03	5.382622980D+03	-7.364673445D+03
3	-1.112634478D+01	9.219406171D+02	2.548212642D+03	5.180940663D+03	7.705148349D+03
4	-3.403806376D+01	-1.932985066D+03	3.783134239D+03	-5.223620469D+03	7.784739727D+03
5	4.727497955D+00	-9.668810992D+02	-1.021687475D+03	-5.209979610D+03	-7.833921253D+03
6	2.953293484D+01	-1.629001667D+03	4.231465117D+03	-5.428470815D+03	7.727163282D+03
7	1.330185262D-01	-5.599260433D+02	-2.936648949D+03	-5.211469028D+03	-7.665977785D+03
8	2.915644933D+01	1.606231890D+03	-4.253692562D+03	5.426974293D+03	-7.721556110D+03
9	8.028928709D-01	6.302393216D+02	2.967564139D+03	5.218611721D+03	7.657034239D+03
10	-5.532717206D+01	-8.340771505D+02	-1.594340699D+04	-1.700868015D+03	-2.773832141D+04
11	2.664718792D+01	1.356148156D+03	-1.398835514D+03	1.903123969D+04	-3.097843849D+03
12	-5.362956175D+01	8.339276298D+02	1.594369985D+04	1.701647253D+03	2.774109261D+04
13	2.672152712D+01	-1.356294526D+03	1.399121373D+03	-1.903031976D+04	3.100469675D+03
14	-1.491700650D+01	-4.529265852D+04	8.909121261D+04	7.700319629D+04	1.080267102D+05
15	-1.294543141D+01	4.594938377D+04	8.962364777D+04	-9.025275933D+04	1.000548164D+05
16	7.622315015D+02	1.052399891D+03	-4.180757099D+02	-3.433282955D+03	-9.428896785D+03

	11	12	13	14	15
1	-6.161968643D+01	-3.654584984D-01	-3.982776029D-03	-2.176517677D-02	4.176037878D-04
2	7.979301160D+01	2.968618168D+02	1.244309970D+02	-1.274372462D+02	-1.138080488D+03
3	8.665370890D+01	2.895194103D+02	1.026844793D+02	1.393800502D+02	1.031236660D+03
4	8.445373801D+01	2.961468733D+02	-1.165767806D+02	1.225480271D+02	1.135154043D+03
5	-4.730046176D+01	7.012326037D+00	-1.124569725D+02	-5.388701773D+02	-1.001517850D+03
6	3.667681221D+01	1.392216765D-01	-1.220845133D+02	1.062229832D+02	1.163983347D+03
7	2.927736967D+01	6.027748585D+00	-8.331205302D+01	-1.413061016D+02	-1.063571574D+03
8	3.247012376D+01	1.020909421D-03	1.168816899D+02	-1.003862915D+02	-1.164442449D+03
9	2.980129318D+01	-6.013927390D+00	9.948169182D+01	1.332132421D+02	1.064210143D+03
10	5.629034370D+03	9.238476179D+00	-5.768413740D+01	-3.525935844D+02	-4.192117346D+03
11	5.649049692D+03	-1.030160707D-01	3.089637619D+02	-6.910534015D+01	-5.297059090D+02
12	5.638763226D+03	-6.163213734D+00	5.767259820D+01	3.524931123D+02	4.192088316D+03
13	5.650943862D+03	3.521810375D+00	-3.089714499D+02	6.902600510D+01	5.296765919D+02
14	-2.839027725D+02	-2.186578600D+01	-1.002459858D+04	-9.961806959D+03	9.618358162D+03
15	-1.892750425D+02	-2.682708384D+00	1.003875316D+04	-9.997009493D+03	9.598947906D+03
16	-5.367773355D+03	-1.319561955D+04	3.806302271D+01	4.224328955D+01	7.037395290D+01

Note: Columns 1 to 11 correspond to displacements of modes 4, 5, 6, 7, 10, 11, 12, 13, 20, 21, and 22. Columns 12 to 22 correspond to modal velocities.

Table H-2. Optimal gain matrix for $[A_1 B_1]$ regulator (sheet 2 of 2).

	16	17	18	19	20
1	6.297368784D-11	-1.472522894D+01	-1.414909512D-04	-8.419811350D-05	5.305049553D-04
2	3.354201401D-13	-9.007058898D+00	-2.668180116D+02	-2.466301161D+02	1.492170511D+03
3	-3.374796825D-11	-7.793227373D+00	-2.975191236D+02	2.193555851D+02	5.683879109D+02
4	1.242262265D-11	-9.012070295D+00	2.673019299D+02	2.459700935D+02	-1.492432065D+03
5	2.950106707D-11	-8.208700375D+00	2.980947716D+02	-2.368454100D+02	-5.684475841D+02
6	-3.486275563D-12	7.702051600D+00	2.799755652D+02	2.586878752D+02	-1.192604637D+03
7	2.417498569D-11	6.412147842D+00	3.107031312D+02	-2.317603463D+02	-2.939724484D+02
8	-1.838421681D-11	7.706433323D+00	-2.798406154D+02	-2.584354027D+02	1.192585043D+03
9	-2.449984318D-11	6.389365679D+00	-3.111215896D+02	2.314088548D+02	2.940297782D+02
10	4.152495125D-11	1.217098820D+03	1.325494444D+02	-9.115772382D+02	-6.099290345D+02
11	-8.094735020D-12	1.221221951D+03	-1.100599023D+03	-1.084288679D+02	5.040151064D+02
12	4.495753547D-12	1.217050894D+03	-1.325396688D+02	9.115651758D+02	6.099289479D+02
13	-6.458381793D-12	1.221240321D+03	1.100608912D+03	1.084169127D+02	-5.040157006D+02
14	-5.233974673D-11	-3.461505216D-02	-4.996978673D+03	4.732199199D+03	-1.069150684D+02
15	1.142063992D-11	6.456898264D-02	4.983512525D+03	4.744751258D+03	-2.372211777D+02
16	-2.175585785D-13	2.436848320D+01	-1.627456310D+01	1.179192765D+01	6.564355682D+00

	21	22
1	1.320816023D-03	4.145083841D+03
2	-5.633483467D+02	4.196390068D+02
3	1.488107621D+03	-1.400262219D+02
4	5.626234375D+02	4.196385904D+02
5	-1.489988857D+03	-1.399483377D+02
6	2.891773456D+02	-7.196819139D+02
7	-1.188741681D+03	-1.056651540D+01
8	-2.891563818D+02	-7.196809083D+02
9	1.188713569D+03	-1.056040129D+01
10	-4.896263697D+02	1.539187422D+03
11	-6.077554735D+02	-4.544298123D+02
12	4.896261825D+02	1.539190689D+03
13	6.077540178D+02	-4.544284967D+02
14	2.599932068D+02	6.286629736D-02
15	-1.784768678D+01	4.048904507D-02
16	1.591469342D+01	-9.695808297D+00

Note: Columns 1 to 11 correspond to displacements of modes 4, 5, 6, 7, 10, 11, 12, 13, 20, 21, and 22. Columns 12 to 22 correspond to modal velocities.

Table H-3. State and control weightings for regulator $[A_1, B_1T_2]$.

```
    POTTER    INPUT DATA                TIME: 17:50:11.6    DATE: 07/07/80  (80/189)
    ----+----+----+----+----+----+----+----+----+----+----+----+----+----+----+----+

  1 * CONTROL GAINS
  2 * X1 TRANS  MODEL  X1 WEIGHTS
  3 /GET=S306
  4 /PUT=Q409 X1  GAINS
  5 /STATES ARE WEIGHTED
  6 Q      1 1  1.666666666E+00  2 2  1.666666666E+00  3 3  1.666666666E+00
  7 Q      4 4  1.000000000E+00
  8 Q      5 5  0.000000000E-05
  9 Q      6 6  1.000000000E+00  7 7  1.000000000E+00  8 8  1.000000000E+00
 10 Q      9 9  1.666666666E+00 1010  1.666666666E+00 1111  1.666666666E+00
 11 Q     1212  1.666666666E+00 1313  1.666666666E+00 1414  1.666666666E+00
 12 Q     1515  1.000000000E+01
 13 Q     1616  0.000000000E-05 1717  1.000000000E+00 1818  1.000000000E+00
 14 Q     1919  1.000000000E+00
 15 Q     2020  1.666666666E+00
 16 Q     2121  1.666666666E+00 2222  1.666666666E+01
 17 R      1 1  1.800000000E-09  1 3 -9.000000000E-10  2 3  7.000000000E-10
 18 R      1 5 -6.000000000E-10  1 9 -3.000000000E-10  2 2  1.120000000E-08
 19 R      2 4  6.800000000E-09  2 6  6.900000000E-09  2 7  3.700000000E-09
 20 R      2 8 -2.100000000E-09  2 9  1.000000000E-10  210  4.900000000E-09
 21 R      3 1 -9.000000000E-10  3 2  7.000000000E-10  3 3  9.500000000E-09
 22 R      3 4 -2.200000000E-09  3 5  5.000000000E-10  3 6 -3.300000000E-09
 23 R      3 7 -2.400000000E-09  3 8  5.800000000E-09  3 9  5.000000000E-10
 24 R      310  6.800000000E-09  4 2  6.800000000E-09  4 3 -2.200000000E-09
 25 R      4 4  6.410000000E-08  4 6 -3.350000000E-08  4 7  3.640000000E-08
 26 R      4 8  6.890000000E-08  410  2.140000000E-08  5 1 -6.000000000E-10
 27 R      5 3  5.000000000E-10  5 5  1.490000000E-08  5 9  1.500000000E-09
 28 R      610 -1.450000000E-08  8 4  6.890000000E-08  6 2  6.900000000E-09
 29 R      6 3 -3.300000000E-09  6 4 -3.350000000E-08  6 6  7.440000000E-08
 30 R      6 7 -1.880000000E-08  6 8 -7.390000000E-08  7 2  3.700000000E-09
 31 R      7 3 -2.400000000E-09  7 8  3.860000000E-08  7 6 -1.880000000E-08
 32 R      7 7  2.090000000E-08  710  1.190000000E-08  8 2 -2.100000000E-09
 33 R      8 3  5.800000000E-09  7 4  3.640000000E-08  8 6 -7.390000000E-08
 34 R      8 7  3.860000000E-08  8 8  1.082000000E-07 1010  3.570000000E-08
 35 R      810  3.800000000E-08  9 1 -3.000000000E-10  9 2  1.000000000E-10
 36 R      9 3  5.000000000E-10  9 5  1.500000000E-09  9 9  5.600000000E-09
 37 R     10 2  4.900000000E-09 10 3  6.800000000E-09 10 4  2.140000000E-08
 38 R     10 6 -1.450000000E-08 10 8  3.800000000E-08 10 7  1.190000000E-08
 39 /COMPUTE
 40 /END
    ----+----+----+----+----+----+----+----+----+----+----+----+----+----+----+----+
    END OF INPUT DATA
```

Notes: (1) States 1 to 11 correspond to displacements of modes 4, 5, 6, 7, 10, 11, 12, 13, 20, 21 and 22. States 12 to 22 correspond to the modal velocities.

(2) $R_1 = Q$, $R_2 = R$

(3) Only nonzero elements are given.

Table H-4. Cost matrix for $[A_1, T_2B_1]$ Regulator (sheet 1 of 3).

SOLUTION MATRIX "P" OF ALGEBRAIC RICCATI EQUATION

	1	2	3	4	5
1	1.729608672D+00	-2.2834191110-03	-8.122002672D-05	-8.435001156D-03	0.0
2	-2.2834191110-03	1.949722975D+00	-1.9251041330-02	1.992956908D+00	0.0
3	-8.122002672D-05	-1.9251041330-02	1.8626699910+00	-1.8616999530+00	0.0
4	-8.4350011560-03	1.9929569080+00	-1.8616999530+00	3.425145457D+02	0.0
5	0.0	0.0	0.0	0.0	0.0
6	-1.5179884540-02	2.9521546600-03	7.0588859970-03	-7.3164814340-02	6.2979147810-13
7	-1.9486495710-03	7.6813520010-01	5.5572447510-02	-1.9832011030+00	6.7970647970-13
8	-1.9237908270-03	3.4861824790-01	-8.0669105700-01	-2.8061066430+01	3.1653316880-13
9	2.8369281150-02	-3.1937485200-01	2.1223856730-01	-5.1282478270+00	-3.6796694560-12
10	3.0824000040-02	8.1060602010-01	2.0388858770-01	-3.9383843030+00	1.1593051880-12
11	6.0118051240-02	1.6249744650-03	1.6417825140-02	-1.8376799690-01	1.2281327500-12
12	6.4132092460-02	-2.5338819680-03	-6.7529732180-05	-1.1114175570-02	-5.2799567530-18
13	-2.5063829470-03	3.0726543990-01	-2.2548865440-02	2.3643950010+00	2.1340136960-14
14	-8.1393950820-05	-2.1557897880-02	2.0777059850-01	-2.1276888720+00	-3.2086069000-15
15	-2.9779836070-04	4.7067095810-03	-8.7744122840-03	-7.8311962030-02	3.1810376990-14
16	0.0	0.0	0.0	0.0	0.0
17	3.2567596670-04	-1.4435736420-05	-4.5372017390-05	-4.6332773830-04	-9.5194608690-15
18	-8.9884742650-05	-3.1559733300-03	2.6352132130-05	-6.5274104550-02	7.8890002240-15
19	1.9054520880-05	-5.8166248200-03	9.7922387460-03	-5.7495917980-01	8.0574751760-16
20	-3.0841244210-05	9.6921921320-04	1.4886223070-04	-8.8597503080-03	1.8497250450-14
21	-4.6939411470-05	-1.2503749710-03	5.2703085150-04	-1.9088429440-02	3.4207722590-14
22	-3.2278626480-05	-5.7896780330-07	-1.5688745120-06	5.7133602110-06	1.3702341370-14

	6	7	8	9	10
1	-1.5179884540-02	-1.9486495710-03	-1.9237908270-03	2.8369281150-02	3.0824000040-02
2	2.9521546600-03	7.6813520010-01	3.4861824790-01	-3.1937485200-01	8.1060602010-01
3	7.0588859970-03	5.5572447510-02	-8.0669105700-01	2.1223856730-01	2.0388858770-01
4	-7.3164814340-02	-1.9832011030+00	-2.8061066430+01	-5.1282478270+00	-3.9383843030+00
5	6.2979147810-13	6.7970647970-13	3.1653316880-13	-3.6796694560-12	1.1593051880-12
6	7.8539010860+01	-2.0634949920-02	-7.7537006170-03	6.9800627480-04	5.6210452030-03
7	-2.0634949920-02	3.9798632940+01	-1.0764406830+00	3.3594609330+00	1.2442946100+00
8	-7.7537006170-03	-1.0764406830+00	5.6656433350+01	-2.4299500400-01	2.6867259690+00
9	6.9800627480-04	3.3594609330+00	-2.4299500400-01	6.2459463960+02	-5.5782889490+01
10	5.6210452030-03	1.2442946100+00	2.6867259690+00	-5.5782889490+01	6.9642801900+02
11	-3.1023519440-01	2.3727263790-02	-6.3215236870-02	-9.2672664200-03	2.9814061260-01
12	-1.6233797030-02	-3.0182794150-03	-2.4530596050-03	2.9943839730-02	3.0953237700-02
13	3.4802118110-03	9.0592425630-01	4.2522221310-01	-3.7602919030-01	9.4882291520-01
14	7.8743060250-03	6.0560270070-02	-9.2276218110-01	2.2813093800-01	2.1497339340-01
15	1.1079601550-03	2.5992251380-01	2.1995240060+00	5.3554703210-01	1.0242774290+00
16	0.0	0.0	0.0	0.0	0.0
17	3.4246173260-04	1.5469308170-04	-3.6799146080-05	3.2368043090-04	1.4772535340-03
18	-1.4134406180-04	-5.5891671140-03	-1.4459833570-02	-6.3968169640-01	3.2708803540-01
19	2.9220185510-04	-9.9240769840-03	-7.3842566570-02	1.0502625180-01	1.7977971860-01
20	1.0076555840-06	4.8970509010-02	-6.9218763600-03	-1.5054883470-02	1.2953323660-02
21	-7.0634625350-05	-2.7938008300-02	-2.6690439370-02	6.7328793190-03	-1.3385614670-02
22	-5.6847944390-03	-1.8751818150-05	-8.9544096320-05	-3.6577392360-04	1.4011705390-03

Note: States 1 to 11 are $\underline{x}_1$ modal displacements. States 12 to 22 are corresponding modal velocities.

Table H-4. Cost matrix for $[A_1, T_2B_1]$ regulator (sheet 2 of 3).

	11	12	13	14	15
1	6.0118051240-02	6.4132092460-02	-2.5063829470-03	-8.1393990220-05	-2.9779836070-04
2	1.6249744650-03	-2.5338919630-03	3.0726543990-01	-2.1557897880-02	4.7037095810-03
3	1.6417825140-02	-6.7529732180-05	-2.2548865440-02	2.0777059850-01	-8.7744122840-03
4	-1.8376799690-01	-1.1114175570-02	2.3643950010+00	-2.1276888720+00	-7.8311962030-02
5	1.2281327500-12	-5.2799567530-18	2.1340136960-14	-3.2086069000-15	3.1810376990-14
6	-3.1023519440-01	-1.6233797030-02	3.4802118110-03	7.8743060250-03	1.1079601550-03
7	2.3727263790-02	-3.0182794150-03	9.0592425630-01	6.0560270070-02	2.5992251380-01
8	-6.3215236870-02	-2.4530596050-03	4.2522221310-01	-9.2276218110-01	2.1995240060+00
9	-9.2672664200-03	2.9943839730-02	-3.7602919030-01	2.2813093800-01	5.3554703210-01
10	2.9814061260-01	3.0953237700-02	9.4682291520-01	2.1497339340-01	1.0242774290+00
11	1.3287458800+04	6.2424569700-02	1.8372923080-03	1.8049700650-02	-3.4571109560-04
12	6.2424569700-02	6.6557069970-02	-3.0012430910-03	-8.0359944670-05	-3.3233994840-04
13	1.8372923080-03	-3.0012430910-03	3.5314003010-01	-2.4693723520-02	9.8265316320-03
14	1.8049700650-02	-8.0359944670-05	-2.4693723520-02	2.2661862520-01	-1.3959454320-02
15	-3.4571109560-04	-3.3233994840-04	9.8265316320-03	-1.3959454320-02	7.4580953950-01
16	0.0	0.0	0.0	0.0	0.0
17	2.0873881920-01	3.2629837910-04	-1.4529372890-05	-4.5068738760-05	-3.1287498380-05
18	3.8070713060-04	-9.0188400770-05	-3.2188188090-03	1.1887163340-04	-7.0412054860-03
19	2.7569946030-03	2.6095721630-05	-6.7277910020-03	1.0583494590-02	-4.1952267600-02
20	7.7694443270-04	-3.2099984640-05	1.1440676750-03	1.7518566650-04	-2.0688379940-04
21	-3.1085624140-03	-4.5596177040-05	-1.4351471980-03	6.1292436600-04	-2.3777994400-03
22	-6.7801417340-05	-3.2225266560-05	-5.8885358540-07	-1.3692809050-06	-3.7173208230-06

	16	17	18	19	20
1	0.0	3.2567596670-04	-8.9884742650-05	1.9054520880-05	-3.0841244210-05
2	0.0	-1.4435736420-05	-3.1559733300-03	-5.8166248200-03	9.8921921320-04
3	0.0	-4.5372017390-05	2.6352132130-05	9.7922387460-03	1.4886223070-04
4	0.0	-4.6332773830-04	-6.5274104550-02	-5.7495917980-01	-8.8597503080-03
5	0.0	-9.5194608690-15	7.8890002240-15	8.0574751760-16	1.8497250450-14
6	0.0	3.4246173260-04	-1.4134406180-04	2.9220185510-04	1.0076555840-06
7	0.0	1.5469308170-04	-5.5891671140-03	-9.9240769840-03	4.8970509010-02
8	0.0	-3.6799146080-05	-1.4459833570-02	-7.3842566570-02	-6.9218763600-03
9	0.0	3.2368043090-04	-6.3968169640-01	1.0502625160-01	-1.5054883470-02
10	0.0	1.4772535340-03	3.2709803540-01	1.7977971880-01	1.2953323660-02
11	0.0	2.0873881920-01	3.8070713060-04	2.7569946030-03	7.7694443270-04
12	0.0	3.2629837910-04	-9.0188400770-05	2.6095721630-05	-3.2099984640-05
13	0.0	-1.4529372890-05	-3.2188188090-03	-6.7277910020-03	1.1440676750-03
14	0.0	-4.5068738760-05	1.1887163340-04	1.0583494590-02	1.7518566650-04
15	0.0	-3.1287498380-05	-7.0412054860-03	-4.1952267600-02	-2.0688379940-04
16	0.0	7.6394652940-16	2.6713916830-16	3.0619755810-16	4.7160586840-16
17	7.6394652940-16	6.0524992830-02	-2.1870159470-05	1.1576987370-05	5.2451235420-07
18	2.6713916830-16	-2.1870159470-05	2.3818087950-02	-1.7590000820-03	1.3192129900-03
19	3.0619755810-16	1.1576987370-05	-1.7590000820-03	2.6435511750-02	-1.1487095430-04
20	4.7160586840-16	5.2451235420-07	1.3192129900-03	-1.1487095430-04	2.7839579100-02
21	7.6696996010-16	-1.3647381730-06	-7.4029515970-04	-4.5837511440-04	-2.1766632030-03
22	6.2786211200-16	-6.2882505130-05	3.9361635630-07	-1.2303746640-06	-1.2914465630-06

Note: States 1 to 11 are $\underline{x}_1$ modal displacements. States 12 to 22 are corresponding modal velocities.

Table H-4. Cost matrix for $[A_1, T_2B_1]$ regulator (sheet 3 of 3).

	21	22
1	-4.693941147D-05	-3.227862648D-05
2	-1.250374971D-03	-5.789676033D-07
3	5.270308515D-04	-1.568874512D-06
4	-1.908842944D-02	5.713360211D-06
5	3.420772259D-14	1.370234137D-14
6	-7.063462535D-05	-5.684794439D-03
7	-2.793800830D-02	-1.875181815D-05
8	-2.669043937D-02	-8.954409632D-05
9	6.732879319D-03	-3.657739236D-04
10	-1.338561467D-02	1.401170539D-03
11	-3.108562414D-03	-6.780141734D-05
12	-4.559617704D-05	-3.222526656D-05
13	-1.435147198D-03	-5.888535854D-07
14	6.129243660D-04	-1.389280905D-06
15	-2.377799440D-03	-3.717320823D-06
16	7.669699601D-16	6.278621120D-16
17	-1.364738173D-06	-6.288250513D-05
18	-7.402951597D-04	3.936163583D-07
19	-4.583751144D-04	-1.230374664D-06
20	-2.176663203D-03	-1.291446563D-06
21	3.139656606D-02	6.532726911D-06
22	6.532726911D-06	2.792730786D-01

Note: States 1 to 11 are $\underline{x}_1$ modal displacements. States 12 to 22 are corresponding modal velocities.

Table H-5. Gain matrix for [A_1, T_2B_1] regulator.

OPTIMAL GAIN MATRIX K

	1	2	3	4	5
1	-3.649506084D+04	-1.137696446D+02	1.945403637D+02	-4.754360032D+03	-1.755672733D-10
2	1.021778829D+04	-9.131781779D+03	-8.899883678D+03	-1.363622700D+04	-6.673895542D-09
3	-2.008753309D+04	-2.167183764D+03	-1.897525455D+03	3.531778157D+03	-2.553631199D-10
4	2.059804479D+04	-1.858472799D+03	-1.091330799D+04	-7.357218419D+04	5.992687621D-10
5	-6.193664291D+02	2.974358171D+01	-1.349810824D+01	2.915909464D+02	8.503095407D-10
6	9.555607453D+03	3.422425421D+03	-9.042316190D+03	-4.542751793D+02	3.147614402D-10
7	-6.413872565D+04	-4.744112815D+03	4.055231811D+04	2.000711527D+05	-4.652787914D-09
8	1.948377269D+04	6.206147892D+03	-1.717167656D+04	-9.300894327D+03	3.401616274D-10
9	-2.603227973D+02	3.503452821D+02	2.440533167D+02	5.759212259D+02	-1.477684706D-09
10	-5.769111877D+03	-2.494259659D+03	8.386608521D+03	9.917996168D+03	-4.413952479D-09

	6	7	8	9	10
1	9.254892957D+03	-3.000883201D+03	-9.525005085D+02	-3.316954403D+03	-2.893566534D+04
2	-3.032821497D+03	-2.484713294D+04	3.159500032D+04	1.212969531D+05	-7.176613753D+04
3	5.022760536D+03	-9.362808460D+03	5.882625316D+03	1.683645614D+04	-3.544400946D+04
4	-5.633259389D+03	-5.450781075D+03	1.226744618D+05	7.223095320D+04	9.034068870D+04
5	1.604382475D+02	3.027398288D+01	1.139315515D+02	-3.344376280D+02	-4.143162645D+02
6	-2.712942191D+03	1.249659713D+04	9.316256066D+04	5.707024651D+04	6.071758707D+04
7	1.768551467D+04	-2.629884295D+04	-4.740794715D+05	-1.218393750D+05	-4.355062158D+05
8	-5.519176985D+03	1.910360200D+04	1.750157387D+05	-1.578062177D+04	1.801503770D+05
9	6.471615847D+02	1.070828063D+03	-7.280326963D+02	-3.861953763D+03	2.706109188D+03
10	1.755437138D+03	-7.257947412D+03	-8.236626776D+04	3.736318056D+03	-8.097580095D+04

	11	12	13	14	15
1	-3.486414174D+04	-3.787301534D+04	-8.779534809D+01	2.158983104D+02	2.580688601D+02
2	9.549962183D+03	1.061660178D+04	-1.058680757D+04	-9.825008326D+03	-2.203742580D+03
3	-2.038460968D+04	-2.084290259D+04	-2.479998346D+03	-2.089493438D+03	3.761309141D+02
4	2.121703072D+04	2.137861511D+04	-2.020179730D+03	-1.225489353D+04	1.547259296D+04
5	-2.205598689D+04	-6.415984244D+02	3.476841623D+01	-1.533123208D+01	-2.749789968D-01
6	9.066303759D+03	9.912504402D+03	3.999845636D+03	-1.011190774D+04	1.006891687D+04
7	-6.444696675D+04	-6.655566881D+04	-5.994953708D+03	4.552730777D+04	-5.938545986D+04
8	1.855335416D+04	2.021209030D+04	7.336185216D+03	-1.918571451D+04	1.774255094D+04
9	5.795667508D+03	-2.711058511D+02	4.055479996D+02	2.696547438D+02	2.690765502D+01
10	-4.994956544D+03	-5.984275406D+03	-2.968642647D+03	9.367284619D+03	-8.472930795D+03

	16	17	18	19	20
1	-1.581879684D-12	1.908570740D+01	-3.724794812D+02	2.413024339D+01	5.941250093D+00
2	-1.200811315D-10	1.847453789D+01	-3.876644109D+03	2.617278643D+03	2.033414669D+03
3	-1.038069707D-11	-2.603156023D+02	-8.604072825D+02	-2.912899298D+01	-8.364532533D+00
4	8.737533992D-11	5.722283161D+02	-1.707370402D+03	7.310054770D+03	-2.993334126D+03
5	-8.420393975D-11	-6.232524720D+03	3.797252908D+00	2.143102972D+00	3.279063892D+00
6	4.663430979D-11	3.961587946D+01	-1.769450284D+03	4.878236135D+03	-1.707051094D+02
7	-3.705239602D-10	-1.157963520D+03	1.475870750D+03	-2.626684584D+04	5.431694753D+03
8	9.412484177D-11	8.188110453D+01	1.180796672D+03	8.898422631D+03	-2.838841901D+03
9	-3.675832743D-11	1.754744793D+03	1.251423466D+02	-4.822269336D+01	-3.605621896D+01
10	-1.433427524D-10	1.677000607D+01	-3.907562631D+02	-4.333724674D+03	2.277372632D+02

	21	22
1	1.926322384D+02	-1.275150691D+03
2	-5.774943796D+03	1.342416693D+03
3	3.180411873D+02	-2.247828749D+03
4	7.662546771D+02	1.707205645D+03
5	-1.460688958D+01	-2.349696464D+03
6	-8.748308685D+02	1.247695952D+03
7	1.022699190D+03	-6.580757252D+03
8	-1.591025762D+03	2.531008716D+03
9	8.809975149D+01	-2.728450283D+04
10	-2.286383819D+03	-7.735829181D+02

Note: Columns 1 to 11 correspond to displacements of modes 4, 5, 6, 7, 10, 11, 12, 13, 20, 21, and 22. Columns 12 to 22 correspond to modal velocities.

H.2 Observer Gains

Three observer designs are discussed in Section 3.3. All are asymptotic observers and, when evaluated against their own design model, they exhibit similar error dynamics. They are different, however, in dimension and measurement processing.

Observer 1 is based on $[A_1, C_1]$ and has the form

$$\dot{\hat{\underline{x}}}_1 = A_1\hat{\underline{x}}_1 + B_1\underline{u} + G[\underline{y} - C_1\hat{\underline{x}}_1] \qquad \text{(H-6)}$$

The elements of the gain matrix G are chosen using the alpha-shift technique (see Section 3.2), and duality is exploited to allow the use of Potter's noniterative method. The relative weightings between model dynamics and measurement incorporation are governed by matrices V_1 and V_2 (see Table H-6), and alpha equals six.

Observer 2 is based on $[A_1, A_2, C_1, C_2]$. The gain matrix G, which is 38×38, is chosen using the same methodology as above. Weighting matrices V_1 and V_2 are given in Table H-7. The poles of

$$\left[\begin{bmatrix} A_1 & 0 \\ 0 & A_2 \end{bmatrix} - G[C_1 \; C_2]\right]$$

are given in Chapter 3. Again, alpha equals six.

Observer 3 is based on $[A_1, T_3C_2]$ and has the form

$$\dot{\hat{x}}_1 = A_1\hat{x}_1 + B_1\underline{u} + GT_3[y - C_1\hat{x}_1]$$

The elements of the 22×4 gain matrix G are chosen using the Potter algorithm. V_1 and V_2 are given in Table H-8, and alpha equals six.

Table H-6. Observer 1 weighting matrices.

```
OBSERVER  INPUT DATA                TIME: 16:29:25.3    DATE: 07/07/80  (80/189)
----+----+----+----+----+----+----+----+----+----+----+----+----+----+----+----+

 1  * OBSERVER FOR X1/X2
 2  /GET=S206
 3  /PUT=Q412   OBSR X1
 4  /SIGMA=  6.000000000E+00
 5  /STATES ARE WEIGHTED
 6  Q      1 1  1.000000000E-05  2 2  1.000000000E-05  3 3  1.000000000E-05
 7  Q      4 4  1.000000000E-04  5 5  1.000000000E-04  6 6  6.000000000E-03
 8  Q      7 7  1.000000000E-03  8 8  1.000000000E-03  9 9  1.000000000E-02
 9  Q     1010  1.000000000E-02 1111  1.000000030E-01 1212  1.000000000E-05
10  Q     1313  1.000000000E-04 1414  1.000000000E-04 1515  1.000000000E-04
11  Q     1616  1.000000000E-01 1717  1.000000000E-01 1818  1.000000000E-01
12  Q     1919  1.000000000E-01 2020  1.000000000E+00 2121  1.000000000E+00
13  Q     2222  1.000000000E+01
14  R      1 1  1.000000000E-08  2 2  1.000000000E-08  3 3  1.000000000E-08
15  R      4 4  1.000000000E-08  5 5  1.000000000E-08  6 6  1.000000000E-08
16  R      7 7  1.000000000E-08  8 8  1.000000000E-08  9 9  1.000000000E-08
17  R     1010  1.000000000E-08 1111  1.000000000E-08 1212  1.000000000E-08
18  R     1313  1.000000000E-08 1414  1.000000000E-08 1515  1.000000000E-08
19  R     1616  1.000000000E-08 1717  1.000000000E-08 1818  1.000000000E-08
20  R     1919  1.000000000E-08 2020  1.000000000E-08 2121  1.000000000E-08
21  R     2222  1.000000000E-08 2323  1.000000000E-08 2424  1.000000000E-08
22  R     2525  1.000000000E-08 2626  1.000000000E-08 2727  1.000000000E-08
23  R     2828  1.000000000E-08 2929  1.000000000E-08 3030  1.000000000E-08
24  R     3131  1.000000000E-08 3232  1.000000000E-08 3333  1.000000000E-08
25  R     3434  1.000000000E-08 3535  1.000000000E-08 3636  1.000000000E-08
26  R     3737  1.000000000E-08 3838  1.000000000E-08
27  /COMPUTE
28  /END
----+----+----+----+----+----+----+----+----+----+----+----+----+----+----+----+
END OF INPUT DATA
```

Note: $V_1 = Q$, $V_2 = R$

Table H-7. Observer 2 weighting matrices.

```
OBSERVER  INPUT DATA                TIME: 17:54:41.2    DATE: 07/07/80  (80/189)
----+----+----+----+----+----+----+----+----+----+----+----+----+----+----+----+

 1  * OBSERVER FOR X1/X2
 2  /GET=S202
 3  /PUT=S604   OBSR X1-X2
 4  /SIGMA=  6.000000000E+00
 5  /STATES ARE WEIGHTED
 6  Q      1 1  1.000000000E-05  2 2  1.000000000E-05  3 3  1.000000000E-05
 7  Q      4 4  3.000000000E-03  5 5  1.000000000E-03  6 6  1.000000000E-03
 8  Q      7 7  1.000000000E-03  8 8  8.000000000E-02  9 9  8.000000000E-02
 9  Q     1010  8.000000000E-02 1111  8.000000000E-02 1212  1.000000000E-02
10  Q     1313  1.000000000E-02 1414  1.000000000E-02 1515  1.000000000E-02
11  Q     1616  1.000000000E-02 1717  1.000000000E-02 1818  1.000000000E-02
12  Q     1919  2.000000000E-01 2020  1.000000000E-05 2121  1.000000000E-05
13  Q     2222  1.000000000E-05 2323  3.000000000E-01 2424  1.000000000E-01
14  Q     2525  1.000000000E-01 2626  1.000000000E-01 2727  3.000000000E-01
15  Q     2828  3.000000000E-01 2929  3.000000000E-01 3030  1.000000000E-01
16  Q     3131  1.000000000E-01 3232  6.000000000E-01 3333  8.000000000E-01
17  Q     3434  9.000000000E-01 3535  1.000000000E+00 3636  1.000000000E+01
18  Q     3737  1.000000000E+01 3838  2.000000000E+01
19  R      1 1  1.000000000E-07  2 2  1.000000000E-07  3 3  1.000000000E-07
20  R      4 4  1.000000000E-07  5 5  1.000000000E-07  6 6  1.000000000E-07
21  R      7 7  1.000000000E-07  8 8  1.000000000E-07  9 9  1.000000000E-07
22  R     1010  1.000000000E-07 1111  1.000000000E-07 1212  1.000000000E-07
23  R     1313  1.000000000E-07 1414  1.000000000E-07 1515  1.000000000E-07
24  R     1616  1.000000000E-07 1717  1.000000000E-07 1818  1.000000000E-07
25  R     1919  1.000000000E-07 2020  1.000000000E-07 2121  1.000000000E-07
26  R     2222  1.000000000E-07 2323  1.000000000E-07 2424  1.000000000E-07
27  R     2525  1.000000000E-07 2626  1.000000000E-07 2727  1.000000000E-07
28  R     2828  1.000000000E-07 2929  1.000000000E-07 3030  1.000000000E-07
29  R     3131  1.000000000E-07 3232  1.000000000E-07 3333  1.000000000E-07
30  R     3434  1.000000000E-07 3535  1.000000000E-07 3636  1.000000000E-07
31  R     3737  1.000000000E-07 3838  1.000000000E-07
32  /COMPUTE
33  /END
----+----+----+----+----+----+----+----+----+----+----+----+----+----+----+----+
END OF INPUT DATA
```

Note: $V_1 = Q$, $V_2 = R$

Table H-8. Observer 3 weighting matrices.

```
OBSERVER  INPUT DATA                TIME: 17:08:23.0    DATE: 07/07/80  (80/189)
----+----+----+----+----+----+----+----+----+----+----+----+----+----+----+----+

 1  * CONTROL GAINS
 2  * X1 TRANS  11
 3  /GET=S306
 4  /PUT=Q607 X1  OBSR
 5  /SIGMA=6.0
 6  /STATES ARE WEIGHTED
 7  Q      1 1  1.000000000E-04  2 2  5.000000000E-04  3 3  5.000000000E-04
 8  Q      4 4  1.000000000E-01
 9  Q      5 5  1.000000000E-01
10  Q      6 6  6.000000000E+01  7 7  5.000000000E-02  8 8  5.000000000E-02
11  Q      9 9  1.000000000E+00 1010  1.000000000E+00 1111  2.000000000E+03
12  Q     1212  1.000000000E-04 1313  5.000000000E-04 1414  5.000000000E-04
13  Q     1515  1.000000000E-01
14  Q     1616  5.000000000E+00 1717  3.000000000E+01 1818  1.000000000E+00
15  Q     1919  1.000000000E+00
16  Q     2020  1.000000000E+00
17  Q     2121  1.000000000E+02 2222  2.000000000E+03
18  R      1 1  7.000000000E-07  2 2  7.000000000E-07  3 3  7.000000000E-07
19  R      4 4  7.000000000E-07
20  /COMPUTE
21  /END
----+----+----+----+----+----+----+----+----+----+----+----+----+----+----+----+
END OF INPUT DATA
```

Note: $V_1 = Q$, $V_2 = R$

H.3 Input and Output Transforms

The input transform T_2 is chosen to satisfy two conditions

$$B_1 T_2 \neq 0 \tag{H-7}$$

$$B^* T_2 = 0 \tag{H-8}$$

The rows of B* are the rows of B_3, which correspond to modes 23, 26, 28, 29, and 30. B* is a 10×16 matrix, but only 5 rows are nonzero. B_1 is a 22×16 matrix with 11 rows nonzero.

Equation (H-7) demands that control authority be provided to the $\underline{x}_1$ modes; Eq. (H-8) prevents control spillover into the set of B* modes.

If the columns of T_2 are viewed as 16 element vectors, then Eq. (H-7) and (H-8) can be satisfied by picking T_2 outside the space scanned by the rows of B*. There is not a unique solution, however, unless the row dimension of B* is one less than its column dimension, and the rows are independent. The algorithm used in this thesis chose the columns of T_2 to be the transposes of the rows of B_1. This ensures that maximum control authority is supplied to $\underline{x}_1$. Then, Eq. (H-8) was satisfied by using a Gram-Schmidt scheme to subtract off from these columns, any component that was not orthogonal to the B* row space. This is a computationally simple algorithm. The resulting transform is given in Table H-9, and the matrix product B T_2 is given in Table H-10. Rows 1 to 36 of BT_2 correspond to displacements of modes 4 to 39, and are all zero. Rows 37 to 72 are nonzero, and correspond to the modal velocities of modes 4 to 39. Of specific interest are rows 56, 59, 61, 62, and 63, which correspond to modes 20, 23, 26, 27, and 28. Note that for the most part, the elements of these rows are orders of magnitude less than elements in rows associated with $\underline{x}_1$.

Appendix A discusses equations of the form of (H-7) and (H-8), and indicates when solutions will exist. Geometric arguments are made which indicate that the control inputs should span the $\underline{x}_1$ space, but be spatially orthogonal to the modes which must not be excited by control. A practical consideration that influences transform construction is spatial aliasing. Mode shapes are evaluated at a discrete number of points (the actuator locations), and within this constraint certain modes may not be distinct. As an example, consider the 36 nonzero rows of the B matrix. These row vectors span R^{16}, but because there are 36 vectors, a large degree of dependence can be expected. To demonstrate this dependence, it is useful to construct the matrix of normalized inner products of each row vector with the other 37 row vectors (see Table H-11). The results are presented row by row. Looking at the first row, one sees that mode 1 looks very similar to mode 10, 16, and 31. This similarity means that it is very difficult to

Table H-9. Input transform T_2.

	1	2	3	4	5
1	1.279000000D-02	-2.300000000D-03	-1.250000000D-02	0.0	-6.077000000D-02
2	-5.025000000D-02	1.074000000D-01	-1.460000000D-02	-2.715000000D-01	2.698000000D-02
3	-4.974000000D-02	-4.530000000D-02	-2.500000000D-03	-8.150000000D-02	2.446000000D-02
4	-5.025000000D-02	-1.131000000D-01	4.300000000D-03	2.715000000D-01	2.698000000D-02
5	-4.975000000D-02	4.870000000D-02	1.756000000D-01	8.150000000D-02	2.466000000D-02
6	-1.231000000D-02	-2.400000000D-03	2.790000000D-02	-3.580000000D-02	-9.419000000D-02
7	-1.980000000D-02	3.080000000D-02	2.500000000D-02	1.926000000D-01	-5.784000000D-02
8	-1.231000000D-02	5.600000000D-03	-1.180000000D-02	3.560000000D-02	-9.419000000D-02
9	-1.979000000D-02	-3.500000000D-02	1.210000000D-02	-1.926000000D-01	-5.784000000D-02
10	6.940000000D-03	1.118000000D-01	-1.750000000D-02	4.181000000D-01	-1.731500000D-01
11	6.350000000D-03	7.800000000D-02	-1.100000000D-03	-9.400000000D-02	-1.712100000D-01
12	6.950000000D-03	-1.124000000D-01	6.600000000D-03	-4.181000000D-01	-1.731500000D-01
13	6.340000000D-03	-7.800000000D-02	-8.600000000D-03	9.400000000D-02	-1.712100000D-01
14	0.0	4.831000000D-01	5.595000000D-01	2.010000000D-02	0.0
15	0.0	-4.490000000D-01	5.499000000D-01	-6.030000000D-01	0.0
16	2.549400000D-01	0.0	-1.000000000D-04	0.0	1.030000000D-03

	6	7	8	9	10
1	0.0	0.0	0.0	-2.354700000D-01	0.0
2	1.194800000D-01	-1.521000000D-01	-3.771300000D-01	-1.168000000D-02	-1.286900000D-01
3	1.619700000D-01	-4.394000000D-02	-3.109800000D-01	1.434000000D-02	-3.818300000D-01
4	-1.194800000D-01	1.521000000D-01	3.771300000D-01	-1.168000000D-02	1.286700000D-01
5	-1.619700000D-01	4.394000000D-02	3.109800000D-01	1.434000000D-02	3.818300000D-01
6	-2.244200000D-01	-2.221000000D-02	8.832000000D-02	-5.470000000D-03	-2.457000000D-02
7	-1.062600000D-01	1.034100000D-01	1.689000000D-01	7.000000000D-05	-3.481000000D-02
8	2.224200000D-01	2.221000000D-02	-8.832000000D-02	-5.470000000D-03	2.457000000D-02
9	1.062600000D-01	-1.034100000D-01	-1.689200000D-01	7.000000000D-05	3.481000000D-02
10	-1.757300000D-01	2.354700000D-01	3.783800000D-01	0.0	1.004000000D-01
11	4.798600000D-01	-5.532000000D-02	-3.486600000D-01	0.0	1.480000000D-02
12	1.757300000D-01	-2.354700000D-01	-3.783800000D-01	0.0	-1.004000000D-01
13	-4.798600000D-01	5.532000000D-02	3.486600000D-01	0.0	-1.480000000D-02
14	3.006500000D-01	-8.540000000D-02	-7.208000000D-02	0.0	2.186700000D-01
15	-3.009200000D-01	-4.343600000D-01	1.092900000D-01	0.0	-1.920000000D-01
16	0.0	0.0	0.0	9.100000000D-04	0.0

Control Inputs	Member Actuators
1	Base-section axial.
2-5	Top-section diagonal.
6-9	Second-section diagonal.
10-13	Third-section axial.
	CMG torques
14,15	x, y rotati-
16	z rotation.

Table H-10. Matrix product of BT_2 (sheet 1 of 2).

	1	2	3	4	
1	0.0	0.0	0.0	0.0	0.0
2	0.0	0.0	0.0	0.0	0.0
3	0.0	0.0	0.0	0.0	0.0
4	0.0	0.0	0.0	0.0	0.0
5	0.0	0.0	0.0	0.0	0.0
6	0.0	0.0	0.0	0.0	0.0
7	0.0	0.0	0.0	0.0	0.0
8	0.0	0.0	0.0	0.0	0.0
9	0.0	0.0	0.0	0.0	0.0
10	0.0	0.0	0.0	0.0	0.0
11	0.0	0.0	0.0	0.0	0.0
12	0.0	0.0	0.0	0.0	0.0
13	0.0	0.0	0.0	0.0	0.0
14	0.0	0.0	0.0	0.0	0.0
15	0.0	0.0	0.0	0.0	0.0
16	0.0	0.0	0.0	0.0	0.0
17	0.0	0.0	0.0	0.0	0.0
18	0.0	0.0	0.0	0.0	0.0
19	0.0	0.0	0.0	0.0	0.0
20	0.0	0.0	0.0	0.0	0.0
21	0.0	0.0	0.0	0.0	0.0
22	0.0	0.0	0.0	0.0	0.0
23	0.0	0.0	0.0	0.0	0.0
24	0.0	0.0	0.0	0.0	0.0
25	0.0	0.0	0.0	0.0	0.0
26	0.0	0.0	0.0	0.0	0.0
27	0.0	0.0	0.0	0.0	0.0
28	0.0	0.0	0.0	0.0	0.0
29	0.0	0.0	0.0	0.0	0.0
30	0.0	0.0	0.0	0.0	0.0
31	0.0	0.0	0.0	0.0	0.0
32	0.0	0.0	0.0	0.0	0.0
33	0.0	0.0	0.0	0.0	0.0
34	0.0	0.0	0.0	0.0	0.0
35	0.0	0.0	0.0	0.0	0.0
36	0.0	0.0	0.0	0.0	0.0
37	7.3568676340-04	2.930164926D-05	7.2506701940-06	4.661810347D-05	-4.227064428D-05
38	1.2635326410-07	5.187017027D-04	6.119073086D-06	3.444138541D-04	2.057100657D-07
39	-9.3489775000-06	2.834044085D-05	6.487728074D-04	-3.103922098D-04	4.655566091D-06
40	-1.3723163090-08	3.3260156580-04	-3.1041425370-04	9.688220339D-04	5.471528602D-08
41	3.5169156060-09	9.088319974D-05	-1.184999347D-05	-8.1844698590-05	-1.176458025D-08
42	1.4097445900-06	-2.1304516160-07	-2.992134045D-06	-4.402613991D-11	-4.243150775D-05
43	2.0566422510-04	-6.4832177120-08	8.197182932D-06	-4.493432959D-12	5.234470845D-05
44	-6.1533174260-05	1.206687668D-06	4.601944387D-05	-5.2171397860-13	1.493685576D-03
45	9.4548375070-08	3.2329596590-03	-3.0807870320-04	-1.658091604D-03	-3.153744101D-07
46	-7.6887738680-08	1.823919294D-03	-2.8156286370-03	5.986828641D-03	3.051530721D-07
47	6.7014241500-04	3.6139256940-06	-4.2023877600-04	-5.2340947010-12	-2.571822733D-03
48	-1.5639428320-05	-1.5219015500-05	-1.2928011060-04	-1.5321117140-12	9.971955469D-05
49	-1.9775300250-04	-1.9935476130-07	8.3317117330-06	6.9102778540-13	5.176956453D-05
50	-3.9172610440-09	-1.5425895690-04	7.9536326640-06	4.8187265210-05	8.384966612D-09
51	-7.4114410230-09	9.3156672490-05	-1.1469492940-03	1.1480332270-03	-2.306117932D-09
52	-2.6657950470-05	-2.8171835560-05	-2.3520276070-04	-2.7362893010-12	1.359156376D-04
53	-8.4329587840-08	-1.0059649810-03	7.6138132040-04	6.2882181850-03	4.775251655D-07
54	-1.0914920670-07	2.2904030650-03	8.3442142440-04	3.2189500700-03	1.238786572D-06
55	-3.3311902300-05	8.9179758870-06	5.9938316330-05	3.3218060740-14	2.735266150D-04
56	3.4853570690-08	-1.6484768630-05	-9.6205516840-08	-1.4870110430-07	-1.507585207D-07
57	-1.1015598030-04	-1.1892384690-04	-2.5091653720-05	-4.4372611510-14	1.112709024D-03
58	-1.7471433600-07	-1.7564075440-04	3.0835477850-03	1.7684086770-03	1.800440393D-06
59	2.4937676530-07	-1.2150709470-05	-6.5400643460-07	-1.3624387940-06	-9.365660489D-07
60	7.3962502940-04	2.0151398170-05	-8.7365672590-05	-9.8451936950-14	-2.167615972D-04
61	-3.5247041140-08	-4.4087004430-06	-5.2415620130-07	1.7990363330-14	2.253829717D-06
62	3.3676502870-08	1.6209952920-06	2.0850503700-07	2.0983127770-14	-9.429745002D-07
63	-2.0032929250-08	-2.6905414730-05	1.0079075420-07	-3.8589311910-09	2.604112062D-07
64	-4.0931163570-04	1.6632187860-06	4.6916136790-05	5.8557607690-13	2.290219216D-05
65	-2.6154630150-09	1.4383093410-04	1.2592434550-06	2.4648481940-04	6.744967339D-09
66	2.6992219060-09	-8.6593893350-05	2.1045186620-03	-1.3902364640-03	-1.535515914D-08
67	-4.1210409510-06	3.3653811700-06	4.6299951180-05	7.1030968940-12	-1.637286692D-04
68	-3.0382614640-04	-2.3664883910-04	-1.8446103860-03	1.1322611260-14	1.321579300D-03
69	-3.5831044450-04	1.6569573770-05	2.6392236010-04	-7.3589780510-14	1.652730191D-02
70	-6.8730240310-04	3.8965718850-06	5.5548275910-04	2.0261327000-14	8.430039256D-04
71	1.4549769040-05	2.7264097010-05	5.0560157850-04	2.1805621470-15	-3.762565247D-05
72	6.0475718050-09	-2.5101453230-03	-1.6514132890-04	-1.5138786480-03	-2.107866953D-07

Table H-10. Matrix product of BT_2 (sheet 2 of 2).

	6	7	8	9	10
1	0.0	0.0	0.0	0.0	0.0
2	0.0	0.0	0.0	0.0	0.0
3	0.0	0.0	0.0	0.0	0.0
4	0.0	0.0	0.0	0.0	0.0
5	0.0	0.0	0.0	0.0	0.0
6	0.0	0.0	0.0	0.0	0.0
7	0.0	0.0	0.0	0.0	0.0
8	0.0	0.0	0.0	0.0	0.0
9	0.0	0.0	0.0	0.0	0.0
10	0.0	0.0	0.0	0.0	0.0
11	0.0	0.0	0.0	0.0	0.0
12	0.0	0.0	0.0	0.0	0.0
13	0.0	0.0	0.0	0.0	0.0
14	0.0	0.0	0.0	0.0	0.0
15	0.0	0.0	0.0	0.0	0.0
16	0.0	0.0	0.0	0.0	0.0
17	0.0	0.0	0.0	0.0	0.0
18	0.0	0.0	0.0	0.0	0.0
19	0.0	0.0	0.0	0.0	0.0
20	0.0	0.0	0.0	0.0	0.0
21	0.0	0.0	0.0	0.0	0.0
22	0.0	0.0	0.0	0.0	0.0
23	0.0	0.0	0.0	0.0	0.0
24	0.0	0.0	0.0	0.0	0.0
25	0.0	0.0	0.0	0.0	0.0
26	0.0	0.0	0.0	0.0	0.0
27	0.0	0.0	0.0	0.0	0.0
28	0.0	0.0	0.0	0.0	0.0
29	0.0	0.0	0.0	0.0	0.0
30	0.0	0.0	0.0	0.0	0.0
31	0.0	0.0	0.0	0.0	0.0
32	0.0	0.0	0.0	0.0	0.0
33	0.0	0.0	0.0	0.0	0.0
34	0.0	0.0	0.0	0.0	0.0
35	0.0	0.0	0.0	0.0	0.0
36	0.0	0.0	0.0	0.0	0.0
37	-9.2676811250-05	2.5117797970-05	1.7808606930-04	7.4942203450-06	2.1886412620-04
38	3.3417726360-04	1.9288441440-04	-1.0162214440-04	1.0652626400-07	2.2977822750-04
39	-3.0846407840-05	-2.8155924240-04	7.6287700670-05	2.6626411250-06	8.3479618530-05
40	-1.6639488080-04	5.9870962850-04	6.2897649570-04	8.9926477210-14	3.2172802470-04
41	3.1951085900-04	-4.6035885170-05	-2.8866254120-04	-1.1085213160-13	-2.5734441670-05
42	2.1230721940-08	-2.7230936490-11	-2.5055769560-10	2.0508118940-06	-2.3084222740-10
43	1.2567226750-07	-2.4893764330-12	1.2596373910-09	1.8237826720-06	-1.3350660090-09
44	2.5801403300-08	-3.2298614060-13	2.2590467410-10	-5.1340367480-06	-3.2817902300-10
45	9.0725338320-03	-9.3408149310-04	-7.8854483570-03	-4.1082255140-14	-3.3586947550-04
46	-9.3720342480-04	3.8547818040-03	3.4858434950-03	-5.9717309850-14	1.7692699110-03
47	-6.5689369830-06	-3.4674457590-12	-6.6288957300-08	-5.3604517260-05	6.8989469140-08
48	1.9562247750-06	-1.0996546070-12	-2.1503106790-08	7.4812175190-05	-1.5698548280-08
49	1.8967342830-07	3.8991711090-13	1.5947556290-09	5.2837443110-07	-1.7398037120-09
50	-4.0638688800-04	2.7566522580-05	3.2429554540-04	-1.7504825860-15	-1.4516024390-05
51	-2.5853965790-04	8.4126636440-04	4.7979266720-04	1.4206285430-13	8.7289218090-05
52	3.7200215660-06	-1.6076432080-12	-4.1123702570-08	1.4556947380-04	-2.8299140720-08
53	-7.8748507500-03	3.4854159640-03	1.0969782160-02	6.4341336010-14	3.4721952890-03
54	-3.3776030810-04	1.7701112420-03	3.4744977780-03	-1.9926415810-14	4.3360837040-03
55	-8.1454846970-07	2.4360282970-14	-1.2083910650-10	5.6190453900-04	4.8032561860-09
56	6.7985967520-06	-7.4383634910-10	-2.8861717050-07	-1.1415589640-14	-1.1639902750-07
57	2.9095877210-05	-2.9298761180-14	-2.8746130360-07	2.1618334330-07	-3.9438353120-08
58	-5.1461140860-03	5.6276733750-04	6.6038949590-03	-1.7244167220-15	3.1696756260-03
59	5.5913081120-05	-7.7186118300-08	-1.4136185230-06	1.9407796330-15	-1.7355876410-06
60	-4.8367554690-06	-4.2531396220-14	7.5507516770-08	-1.1454560960-05	-8.1431077930-09
61	4.6800424170-05	9.3582654420-15	4.9054881990-07	-2.8858726620-07	-1.8919690160-07
62	-2.4065041110-05	1.1645238640-14	-2.0655272830-07	-9.1836824220-04	8.3664101400-08
63	6.7244295690-06	7.9490424870-09	3.2492978060-07	-7.5657319910-15	6.4353048120-08
64	-2.1097943380-07	3.1761863500-13	-2.7993899610-09	7.1493385700-06	3.7366499500-09
65	-1.6647083920-04	1.4105088310-04	2.4891855630-04	-1.4430644980-14	1.4393345490-04
66	3.4193040890-05	-1.1462734630-03	-1.3167226180-04	4.5608462030-13	-7.6917604180-05
67	-2.9965508930-07	5.8576785080-12	-7.6334340330-11	8.8524334550-05	4.5220706960-09
68	3.4480485560-05	3.1128373710-15	-3.4908041870-07	-4.2887738110-04	-2.4169139130-07
69	1.0565111590-05	-3.8548617940-14	1.0559692370-07	6.7075905370-05	-1.2801739510-08
70	-2.5131034730-06	1.3211349900-14	-2.8204477870-08	1.2536597240-03	-5.2603430070-08
71	-4.9915403240-07	1.2258026410-15	5.2486345170-09	1.3627174150-04	5.6261763370-08
72	-2.6774286760-04	-8.6818360900-04	-4.9265828930-04	2.2391508580-14	-1.9563880540-03

Table H-11. Normalized inner products of $\bar{B}$-matrix row vectors with transposes of other 37 rows (sheet 1 of 3).

MODE	4	5	6	7	8	9	10	11	12	13	14	15	16	17	18
	1														
	1.000000	0.000044	-0.047485	-0.000037	0.000068	0.000080	0.824975	-0.004595	0.000064	-0.000041	0.328452	0.006395	-0.951292	-0.000055	-0.000037
4	0.007758	-0.000056	-0.000085	0.023776	0.000018	0.010179	-0.000112	0.000015	0.249800	-0.135759	0.125166	-0.000108	-0.858869	0.000065	0.000045
	-0.008052	-0.002124	-0.011603	-0.252940	0.004590	-0.000070									
	2														
	0.000044	1.000000	0.001555	0.001391	0.264809	-0.001864	0.000501	0.000014	0.378201	0.001575	-0.002196	-0.004917	0.000548	-0.369815	-0.000052
5	-0.005198	-0.016988	-0.003371	0.001131	0.084143	-0.005840	0.004632	-0.002027	0.004875	0.002973	-0.002347	0.004127	0.000769	0.450234	0.000067
	0.003416	-0.008650	0.000000	-0.001347	0.006487	-0.597138									
	3														
	-0.047485	0.001555	1.000000	-0.209695	-0.038710	-0.016516	0.017789	0.000787	-0.036967	-0.340438	-0.077810	-0.039174	0.022802	0.020012	-0.827860
6	-0.040433	0.051222	0.090381	0.005975	-0.028882	-0.007996	0.046758	-0.022196	0.001170	0.038141	-0.034636	-0.030943	0.028741	0.015299	0.929244
	0.057991	-0.060725	0.003110	0.069428	0.112723	-0.042318									
	4														
	-0.000037	0.001391	-0.209695	1.000000	0.001518	-0.000000	0.000000	0.000000	0.001501	0.990220	-0.000000	-0.000000	0.000000	-0.079293	0.665294
7	-0.000000	0.003410	0.637521	0.000000	-0.355937	-0.000000	-0.159001	-0.165695	0.000000	0.000000	0.000000	-0.183493	0.000000	0.171378	-0.432787
	0.000000	0.000000	0.000000	0.000000	0.000000	-0.165447									
	5														
	0.000068	0.264809	-0.038710	0.001518	1.000000	0.000000	0.000000	0.000000	0.992823	-0.000178	-0.000000	0.000000	0.000000	-0.983615	-0.106164
8	0.000000	-0.632331	0.004529	-0.000000	0.100649	0.000000	-0.174812	0.161023	0.000000	-0.000000	0.000000	-0.053165	0.000000	-0.384324	-0.045693
	-0.000000	0.000000	0.000000	0.000000	0.000000	-0.058055									
	6														
	0.000080	-0.001864	-0.016516	-0.000000	0.000000	1.000000	-0.074263	-0.865418	0.000000	-0.000000	0.298596	0.484316	-0.042869	0.000000	-0.000000
9	0.495680	0.000000	-0.000000	-0.353421	0.000000	-0.131133	0.000000	-0.000000	0.248376	0.356066	-0.397955	0.000000	-0.205524	0.000000	0.000000
	0.082483	0.122646	-0.841117	-0.067003	-0.134096	0.000000									
	7														
	0.824975	0.000501	0.017789	0.000000	0.000000	-0.074263	1.000000	0.884355	0.000000	0.000000	-0.172875	-0.005187	-0.851763	0.000000	-0.000000
10	-0.007416	0.000000	0.000000	-0.011247	0.000000	0.015036	0.000000	0.000000	0.318773	0.140682	-0.131598	0.000000	-0.921903	-0.000000	-0.000000
	-0.063774	-0.002843	0.121186	0.067152	0.002982	0.000000									
	8														
	-0.004595	0.000014	0.000787	0.000000	0.000000	-0.865418	0.884355	1.000000	0.000000	0.000000	-0.352322	0.011470	0.868043	-0.000000	0.000000
11	-0.005724	0.000000	0.000000	0.216922	0.000000	-0.003490	0.000000	0.000000	-0.069014	-0.409883	0.435231	0.000000	0.105805	0.000000	-0.000000
	-0.485138	-0.000957	0.972054	0.233058	-0.002078	0.000000									
	9														
	0.000064	0.378201	-0.036967	0.001501	0.992823	0.000000	0.000000	0.000000	1.000000	-0.000132	-0.000000	0.000000	0.000000	-0.990016	-0.101691
12	0.000000	-0.609274	0.002279	-0.000000	0.107163	-0.000000	-0.169451	0.154371	0.000000	-0.000000	0.000000	-0.052744	0.000000	-0.311609	-0.043552
	-0.000000	-0.000000	-0.000000	0.000000	0.000000	-0.130459									
	10														
	-0.000041	0.001575	-0.340438	0.990220	-0.000178	-0.000000	0.000000	0.000000	-0.000132	1.000000	-0.000000	0.000000	0.000000	-0.073547	0.756886
13	0.000000	0.001143	0.610686	0.000000	-0.341883	0.000000	-0.152491	-0.160790	0.000000	-0.000000	0.000000	-0.167032	0.000000	0.163989	-0.550610
	0.000000	0.000000	0.000000	0.000000	0.000000	-0.156761									
	11														
	0.328452	-0.002196	-0.077810	-0.000000	-0.000000	0.298596	-0.172875	-0.352322	-0.000000	-0.000000	1.000000	0.016523	-0.366157	0.000000	-0.000000
14	0.026269	0.000000	-0.000000	0.060292	0.000000	-0.007015	0.000000	0.000000	-0.097126	-0.630876	0.595463	0.000000	-0.000733	0.000000	0.000000
	0.264387	0.000087	-0.508289	-0.285976	0.002942	0.000000									
	12														
	0.006395	-0.004917	-0.039174	-0.000000	0.000000	0.484316	-0.005187	0.011470	0.000000	0.000000	0.016523	1.000000	0.020520	-0.000000	-0.000000
15	0.998974	0.000000	0.000000	-0.354967	0.000000	-0.117492	-0.000000	0.000000	0.238741	-0.032078	-0.014289	0.000000	-0.222229	0.000000	0.000000
	-0.693645	0.367605	0.005354	0.227470	-0.331539	0.000000									

Table H-11. Normalized inner products of $\bar{B}$-matrix row vectors with transposes of other 37 rows (sheet 2 of 3).

13

-0.951292 0.000548 0.022802 0.000000 0.000000 -0.042869 -0.851763 0.068043 0.000000 0.000000 -0.366157 0.020520 1.000000 0.000000 0.000000
0.018559 0.000000 0.000000 -0.043467 0.000000 -0.000780 0.000000 0.000000 -0.248105 0.235080 -0.227306 0.000000 0.856962 -0.000000 0.000000
-0.082815 0.024293 0.121997 0.074486 -0.018786 0.000000

14

-0.000055 -0.369815 0.020012 -0.079293 -0.983615 0.000000 0.000000 -0.000000 -0.990016 -0.073547 0.000000 -0.000000 0.000000 1.000000 0.072395
-0.000000 0.533146 -0.098268 0.000000 -0.131525 0.000000 0.131236 -0.194786 -0.000000 0.000000 -0.000000 0.022377 0.000000 0.315520 0.068187
0.000000 0.000000 -0.000000 -0.000000 -0.000000 0.153840

15

-0.000037 -0.000052 -0.827860 0.665294 -0.106164 -0.000000 -0.000000 0.000000 -0.101691 0.756886 -0.000000 -0.000000 0.000000 0.072395 1.000000
-0.000000 0.108318 0.154985 0.000000 -0.090969 0.000000 -0.208972 -0.011606 -0.000000 -0.000000 0.000000 -0.179672 0.000000 0.244444 -0.911533
0.000000 0.000000 0.000000 0.000000 -0.000000 -0.133924

16

0.007750 -0.005198 -0.040433 -0.000000 0.000000 0.495680 -0.007416 -0.005724 0.000000 0.000000 0.026269 0.998974 0.018559 -0.000000 -0.000000
1.000000 -0.000000 0.000000 -0.348931 0.000000 -0.076671 0.000000 0.000000 0.202443 -0.028963 -0.021873 0.000000 -0.221044 -0.000000 0.000000
-0.678950 0.423596 -0.011894 0.223448 -0.344861 0.000000

17

-0.000056 -0.016988 0.051222 0.003410 -0.632331 0.000000 0.000000 0.000000 -0.609274 0.001143 0.000000 0.000000 0.000000 0.533146 0.108318
-0.000000 1.000000 0.000156 -0.000000 0.526866 0.000000 0.325897 0.470465 0.000000 0.000000 -0.000000 0.252174 0.000000 0.293238 -0.067311
0.000000 0.000000 0.000000 0.000000 0.000000 -0.135897

18

-0.000085 -0.003371 0.090381 0.637521 0.004529 -0.000000 0.000000 0.000000 0.002279 0.610686 -0.000000 0.000000 0.000000 -0.098268 0.154985
0.000000 0.000156 1.000000 0.000000 -0.446575 -0.000000 0.472667 -0.319736 0.000000 0.000000 0.000000 0.415577 0.000000 -0.285485 -0.121709
0.000000 0.000000 0.000000 0.000000 0.000000 0.088345

19

0.023776 0.001131 0.005975 0.000000 -0.000000 -0.353421 -0.011247 0.216922 -0.000000 0.000000 0.060292 -0.354967 -0.043467 0.000000 0.000000
-0.348931 -0.000000 0.000000 1.000000 -0.000000 0.106563 -0.000000 -0.000000 -0.197053 -0.256927 0.146946 -0.000000 0.143152 0.000000 -0.000000
0.536513 -0.107160 0.180084 0.538067 0.098967 -0.000000

20

0.000018 0.004143 -0.028882 -0.355937 0.100649 0.000000 0.000000 0.000000 0.107163 -0.341883 0.000000 0.000000 0.000000 -0.131525 -0.090969
0.000000 0.526866 -0.446575 -0.000000 1.000000 -0.000000 0.057093 0.968008 0.000000 -0.000000 0.000000 0.116513 -0.000000 0.064017 -0.104349
-0.000000 0.000000 0.000000 0.000000 -0.000000 -0.333409

21

0.010179 -0.005840 -0.007996 -0.000000 0.000000 -0.131133 0.015036 -0.003490 -0.000000 0.000000 -0.007015 -0.117492 -0.000780 0.000000 0.000000
-0.076671 0.000000 -0.000000 0.106563 -0.000000 1.000000 0.000000 0.000000 -0.917764 -0.002612 -0.066715 0.000000 0.087040 0.000000 -0.000000
0.169535 0.810036 0.001242 -0.099214 -0.209676 -0.000000

22

-0.000112 0.004632 0.046758 -0.159801 -0.174812 0.000000 0.000000 0.000000 -0.169451 -0.152491 0.000000 -0.000000 0.000000 0.131236 -0.208972
0.000000 0.325897 0.472667 -0.000000 0.057093 0.000000 1.000000 -0.003809 0.000000 0.000000 -0.000000 0.986068 0.000000 -0.587346 0.029490
-0.000000 0.000000 0.000000 0.000000 0.000000 0.454532

23

0.000015 -0.002027 -0.022196 -0.165695 0.161023 -0.000000 0.000000 0.000000 0.154371 -0.160790 0.000000 0.000000 0.000000 -0.194786 -0.01160
0.000000 0.470465 -0.319736 -0.000000 0.968008 0.000000 -0.003809 1.000000 0.000000 0.000000 0.000000 0.060127 0.000000 0.034233 -0.15911
-0.000000 0.000000 0.000000 0.000000 -0.000000 -0.366088

24

0.249800 0.004875 0.001170 0.000000 0.000000 0.248376 0.318773 -0.069014 0.000000 0.000000 -0.097126 0.238741 -0.248105 -0.000000 -0.000000
0.202443 0.000000 0.000000 -0.197053 0.000000 -0.917764 0.000000 0.000000 1.000000 0.186258 -0.124253 0.000000 -0.448636 -0.000000 0.000000
-0.265771 -0.656682 -0.033066 0.085682 0.073063 0.000000

Table H-11. Normalized inner products of $\bar{B}$-matrix row vectors with transposes of other 37 rows (sheet 3 of 3).

25

-0.135759	0.002973	0.038141	0.000000	-0.000000	0.356066	0.140682	-0.409883	-0.000000	-0.000000	-0.630876	-0.032078	0.235080	0.000000	-0.0000
-0.028963	0.000000	0.000000	-0.256927	-0.000000	-0.002612	0.000000	0.000000	0.186258	1.000000	-0.985427	0.000000	-0.166237	-0.000000	0.0000
0.059447	-0.013285	-0.193336	-0.182030	0.003693	0.000000									

26

0.125166	-0.002347	-0.034636	0.000000	0.000000	-0.397955	-0.131598	0.435231	0.000000	0.000000	0.595463	-0.014289	-0.227306	-0.000000	0.0000
-0.021873	-0.000000	0.000000	0.146946	0.000000	-0.066715	-0.000000	0.000000	-0.124253	-0.985427	1.000000	0.000000	0.165131	0.000000	0.0000
-0.111440	-0.058340	0.220638	0.106939	0.010320	0.000000									

27

-0.000108	0.004127	-0.030943	-0.183493	-0.053165	0.000000	0.000000	0.000000	-0.052744	-0.167032	0.000000	0.000000	0.000000	0.022377	-0.179
0.000000	0.252174	0.415577	-0.000000	0.116513	0.000000	0.986068	0.060127	0.000000	0.000000	0.000000	1.000000	-0.000000	-0.664267	-0.035
-0.000000	-0.000000	0.000000	0.000000	0.000000	0.480626									

28

-0.858869	0.000769	0.028741	0.000000	0.000000	-0.205524	-0.921903	0.105805	0.000000	0.000000	-0.000733	-0.222229	0.856962	0.000000	0.0000
-0.221044	0.000000	0.000000	0.143152	-0.000000	0.087040	0.000000	0.000000	-0.448636	-0.166237	0.165131	-0.000000	1.000000	0.000000	-0.0000
0.198512	-0.081068	0.067103	0.040550	0.219929	-0.000000									

29

0.000065	0.450234	0.015299	0.171378	-0.384324	0.000000	-0.000000	0.000000	-0.311609	0.163989	0.000000	0.000000	-0.000000	0.315520	0.24
-0.000000	0.293238	-0.285485	0.000000	0.064017	0.000000	-0.587346	0.034233	-0.000000	-0.000000	0.000000	-0.664267	0.000000	1.000000	-0.027528
0.000000	0.000000	0.000000	0.000000	-0.000000	-0.769899									

30

0.000045	0.000067	0.929244	-0.432787	-0.045693	0.000000	-0.000000	-0.000000	-0.043552	-0.550610	0.000000	0.000000	0.000000	0.068187	-0.91153
0.000000	-0.067311	-0.121709	-0.000000	-0.104349	-0.000000	0.029490	-0.159110	0.000000	0.000000	0.000000	-0.035648	-0.000000	-0.027528	1.0
0.000000	-0.000000	-0.000000	0.000000	0.000000	0.111377									

31

-0.008052	0.003416	0.057991	0.000000	-0.000000	0.082483	-0.063774	-0.485138	-0.000000	0.000000	0.264387	-0.693645	-0.082815	0.000000	0.0
-0.678950	0.000000	0.000000	0.536513	-0.000000	0.169535	-0.000000	-0.000000	-0.265771	0.059447	-0.111440	-0.000000	0.198512	0.000000	0.0
1.000000	-0.297981	-0.505841	0.058937	0.473075	0.800000									

32

-0.002124	-0.008650	-0.060725	0.000000	0.000000	0.122646	-0.002843	-0.000957	-0.000000	0.000000	0.000087	0.387605	0.824293	0.000000	0.0
0.423596	0.000000	0.000000	-0.107160	0.000000	0.810036	0.000000	0.000000	-0.656682	-0.013285	-0.058340	-0.000000	-0.081068	0.000000	-0.0
-0.297981	1.000000	0.000235	-0.007098	-0.641054	0.000000									

33

-0.011603	0.000800	0.903110	0.000000	0.000000	-0.841117	0.121186	0.972054	-0.000000	0.000000	-0.508289	0.005354	0.121997	-0.000000	0.0
-0.011894	0.000000	0.000000	0.180084	0.000000	0.001242	0.000000	0.000000	-0.033066	-0.193336	0.220638	0.000000	0.067103	0.000000	-0.0
-0.505841	0.000235	0.000000	0.166504	-0.001934	-0.000000									

34

-0.252940	-0.001347	0.069428	0.000000	0.000000	-0.067003	0.067152	0.233058	0.000000	0.000000	-0.285976	0.227470	0.074486	-0.000000	0.0
0.223448	0.000000	0.000000	0.538067	0.000000	-0.099214	0.000000	0.000000	0.085682	-0.182030	0.106939	0.000000	0.040550	0.000000	0.0
0.058937	-0.007098	0.166504	1.000000	-0.019430	0.000000									

35

0.004590	0.006487	0.112723	0.000000	0.000000	-0.134096	0.002982	-0.002078	0.000000	0.000000	0.002942	-0.331539	-0.018786	-0.000000	-0.0
-0.344861	0.000000	0.000000	0.098967	-0.000000	-0.209676	0.000000	-0.000000	0.073063	0.003693	0.010320	0.000000	0.219929	-0.000000	0.0
0.473075	-0.641054	-0.001934	-0.019430	1.000000	0.000000									

36

-0.000878	-0.597138	-0.042318	-0.165447	-0.058055	0.000000	0.000000	0.000000	-0.130459	-0.156761	0.000000	0.000000	0.000000	0.153840	-0.1
0.000000	-0.135897	0.008345	-0.000000	-0.333409	-0.000000	0.454532	-0.366088	0.000000	0.000000	0.000000	0.480626	-0.000000	-0.769899	0.1
0.000000	0.000000	-0.000000	0.000000	0.000000	1.000000									

Table H-12. Output transform (sheet 1 of 2).

	1	2	3	4	5
1	6.4800000000D-03	1.9576000000D-02	4.9300000000D-02	8.1432000000D-02	1.1241000000D-01
2	3.5380000000D-01	9.0000000000D-03	-2.3400000000D-02	2.9700000000D-02	-1.7000000000D-02
3	0.0	0.0	0.0	0.0	0.0
4	-1.0300000000D-02	-2.1500000000D-02	-3.8700000000D-02	-6.8400000000D-02	-1.0100000000D-01
5	-3.3600000000D-02	-2.6010000000D-01	2.2000000000D-01	8.3300000000D-02	-2.3990000000D-01
6	-1.8227000000D-01	-1.3890000000D-02	1.5480000000D-02	-3.4900000000D-03	-8.3100000000D-03

	6	7	8	9	10
1	1.4817000000D-01	-6.4800000000D-03	-1.9593000000D-02	-4.9300000000D-02	-8.1432000000D-02
2	6.0000000000D-03	3.2440000000D-01	-1.5230000000D-01	-4.9200000000D-02	4.6520000000D-01
3	0.0	0.0	0.0	0.0	0.0
4	-1.2560000000D-01	1.0300000000D-02	2.1500000000D-02	3.8700000000D-02	6.8400000000D-02
5	9.4300000000D-02	-3.3600000000D-02	-2.6010000000D-01	2.2000000000D-01	8.3300000000D-02
6	2.8200000000D-03	-1.8227000000D-01	-1.3890000000D-02	1.5480000000D-02	-3.4900000000D-03

	11	12	13	14	15
1	-1.1240000000D-01	-1.4817000000D-01	3.1800000000D-03	-3.4700000000D-03	-9.9000000000D-03
2	-5.4290000000D-01	2.0220000000D-01	2.7000000000D-03	-1.8500000000D-02	-1.8000000000D-03
3	0.0	0.0	1.5620000000D-02	3.5950000000D-02	6.0170000000D-02
4	1.0100000000D-01	1.2560000000D-01	-4.0560000000D-01	3.7970000000D-01	-6.8000000000D-03
5	-2.3990000000D-01	9.4300000000D-02	-7.2430000000D-01	7.0710000000D-01	1.9410000000D-01
6	-8.3000000000D-03	2.8200000000D-03	1.3680000000D-02	-1.1940000000D-02	-3.5300000000D-03

	16	17	18	19	20
1	9.4200000000D-04	-2.3970000000D-03	3.1790000000D-03	-3.4650000000D-03	-9.9500000000D-04
2	8.4000000000D-03	-8.2000000000D-03	-3.6000000000D-03	1.8600000000D-02	3.1000000000D-03
3	8.5550000000D-02	1.1109000000D-01	-1.5625600000D-02	-3.5950000000D-02	-6.0170000000D-02
4	-2.2490000000D-01	1.0800000000D-01	-4.0560000000D-01	3.7970000000D-01	-6.8000000000D-03
5	-2.9070000000D-01	4.5750000000D-01	7.2430000000D-01	-7.0700000000D-01	-1.9410000000D-01
6	2.2400000000D-03	-9.6700000000D-03	-1.3680000000D-02	1.1940000000D-02	3.5300000000D-03

	21	22	23	24	25
1	9.4200000000D-04	-2.3970000000D-03	3.0200000000D-02	-9.3300000000D-02	-9.4800000000D-02
2	-7.3000000000D-03	7.9000000000D-03	-7.0000000000D-04	-5.7150000000D-01	5.5740000000D-01
3	-8.5550000000D-02	-1.1109000000D-01	0.0	2.7410000000D-04	-2.7400000000D-04
4	-2.2490000000D-01	1.0800000000D-01	2.1590000000D-01	-4.4400000000D-02	2.0890000000D-01
5	2.9070000000D-01	-4.5750000000D-01	0.0	-4.4340000000D-01	-8.2300000000D-01
6	-2.2400000000D-03	9.6900000000D-03	0.0	1.7997000000D-01	-4.8280000000D-01

Table H-12. Output transform (sheet 2 of 2).

	26	27	28	29	30
1	-9.3300000000D-02	-9.4850000000D-02	-3.3200000000D-02	-3.4500000000D-02	-3.3200000000D-02
2	5.6370000000D-01	-3.8060000000D-01	-9.8800000000D-02	-1.1350000000D-01	1.2140000000D-01
3	-2.7410000000D-04	2.7400000000D-04	-2.7050000000D-04	2.7230000000D-04	2.7050000000D-04
4	-4.4400000000D-02	2.0890000000D-01	-8.9800000000D-02	1.5030000000D-01	-8.9800000000D-02
5	4.4340000000D-01	8.2300000000D-01	-1.4732000000D+00	-4.6280000000D-01	1.4752000000D+00
6	-1.7997000000D-01	4.8280000000D-01	-4.4880000000D-02	2.2870000000D-02	4.4880000000D-02

	31	32	33	34	35
1	-3.4500000000D-02	4.6300000000D-03	6.5000000000D-03	4.6000000000D-03	6.5000000000D-03
2	1.4370000000D-01	-5.3280000000D-01	-1.6180000000D-01	5.6810000000D-01	1.4750000000D-01
3	-2.7230000000D-04	9.4000000000D-04	1.3850000000D-04	-9.4000000000D-04	-1.3850000000D-04
4	1.5030000000D-01	1.4680000000D-01	-1.5290000000D-01	1.4680000000D-01	-1.5290000000D-01
5	4.6280000000D-01	-3.2520000000D-01	2.8764000000D+00	3.2520000000D-01	-2.8764000000D+00
6	-2.2870000000D-02	3.7912000000D-02	2.2279000000D-01	-3.7912000000D-01	-2.2279000000D-01

	36	37	38
1	0.0	0.0	5.0900000000D-03
2	4.2950000000D-01	6.0030000000D-01	4.8000000000D-03
3	-2.5970000000D-04	-2.5910000000D-04	0.0
4	0.0	0.0	-2.2000000000D-03
5	3.6143000000D+00	9.4910000000D-01	0.0
6	6.7980000000D-02	-1.0225000000D-01	0.0

Sensors

1-12	Horizontal solar sensors.
13-22	Vertical solar sensors
23	Base-section member sensor.
24-27	Top-section diagonal.
28-31	Second-section diagonal.
32-35	Third-section axial.
36,37	Rotation x, y.
38	Rotation z.

Table H-13. Matrix product $T_3\ C_1C_2C_3$ (sheet 1 of 2).

	1	2	3	4	5
1	1.2876031220-02	-5.1590736880-05	4.0252426520-04	-5.1378069050-04	4.8741424880-07
2	3.4282561100-04	-3.0256080710-04	3.2211586180-03	-3.8996763380-03	6.7142818430-07
3	1.5848122820-07	4.1630127600-03	-2.4120448880-07	4.9636316470-02	-1.3321040410-06
4	-1.1068610530-02	8.1326735280-07	-3.2598416140-04	5.8795504930-11	-2.0553946850-09
5	4.7469149190-04	8.7700959570-03	1.9321905850-03	1.0322832120-01	6.7044698710-06
6	2.7670491430-04	-8.7022877390-05	-1.2815732880-03	-1.7670189940-03	-1.9601898550-04

	6	7	8	9	10
1	-1.1598961340-03	-4.5743553820-02	-5.8284298920-05	-7.0529274620-08	3.6150836310-05
2	1.2872645100-04	-8.4343492780-06	-4.0870665150-05	1.8895727750-03	-1.1945244670-02
3	-6.9103164140-08	-8.4849515120-11	1.5871364450-08	5.9582973570-06	-8.8604566780-03
4	9.6280334670-06	3.9329842790-02	1.0960883910-03	-8.7468772870-12	-5.5250873830-12
5	3.1605691920-06	-1.2649889580-07	-1.6989143170-07	4.0341033500-02	-3.3807937750-02
6	-3.0552920210-05	1.3207448790-05	7.3716796610-04	3.8102166870-06	5.5788189900-03

	11	12	13	14	15
1	1.1511467130-07	-5.8113460520-04	5.4892821770-06	7.9662465480-08	6.7948426070-04
2	-2.2447307690-04	3.3148213790-05	-2.2883627680-06	3.5536989010-07	2.1851181130-05
3	1.9198797530-10	-2.6031261580-07	-8.6850012810-11	1.0396869440-08	3.5821017720-07
4	1.0989588530-07	2.0903518370-07	-1.0553328960-06	3.9306989320-13	-2.2337156460-14
5	6.6393052990-06	5.5864876140-06	-1.8918013990-07	-7.9811678440-06	9.8874367950-06
6	-5.9527829440-04	-6.7390385150-04	6.1872305270-06	-3.8409158060-06	-2.1171104850-04

	16	17	18	19	20
1	3.5366291170-04	-1.3518796310-05	3.1850501900-05	-1.2456383040-04	7.5432697280-07
2	-1.5638068120-04	1.3257513460-03	-1.2978900880-02	2.8924393090-06	6.9372967570-06
3	1.1565291760-07	9.4601402000-06	-1.1209090780-05	9.9702486240-09	-4.6146003630-06
4	2.7292101020-07	1.4736470680-14	2.5579357650-14	4.3446860220-04	-1.2193116720-14
5	-7.9599870180-06	-2.0911687000-02	1.9119140510-02	1.0246586630-06	6.0445279340-06
6	-1.1815021590-03	-2.6160442430-04	9.2819975010-03	3.0080424730-04	-2.5877225450-05

	21	22	23	24	25
1	-7.1879212480-06	-4.2396735030-06	7.7031845380-06	8.4688882980-07	3.1945806110-06
2	-6.2263329360-04	-6.4655938920-04	3.3752671510-04	9.4183230830-04	5.9949277250-04
3	5.8444227390-09	-5.3110852340-06	-2.0691274050-05	-1.3535522410-09	-4.7184653710-09
4	1.7431262740-06	-4.6147833390-14	8.5473937970-15	-6.6309372760-07	1.4389512360-06
5	-2.9414500590-05	2.7470273950-05	5.2490527070-05	4.8943772280-06	-4.7306728730-05
6	3.6826890010-03	4.4149283010-03	-2.2873189480-03	-1.0895004800-03	-4.0801998260-03

	26	27	28	29	30
1	1.5637100970-05	1.2542719410-05	-1.4254454280-06	-1.3667789800-06	5.0246705380-04
2	-2.2977644750-04	-1.6959880830-04	-2.1077722290-05	6.8041409710-06	-1.6634720540-05
3	-1.0730501970-08	-2.5038250890-05	5.0739998500-10	1.7468477390-07	7.6594635360-05
4	-3.5031329360-07	1.8057377220-14	1.0199613350-06	-5.5596572810-14	1.0487290440-13
5	2.4372611320-05	6.8559232790-06	2.0867685570-07	-3.9215250540-08	-7.2802565870-06
6	2.0177170890-03	6.0811572150-04	8.2591619960-05	-5.6697826600-05	1.4941379890-04

	31	32	33	34	35
1	5.0253404390-04	8.3973995410-06	5.7349496490-06	-1.3251990250-03	-2.2472359070-06
2	-1.9641291250-04	-2.3221178600-03	-6.3044477520-04	5.0905769710-04	5.2754465820-04
3	-5.2927504130-07	-6.3107390810-09	-6.1929481610-09	6.6829292690-09	2.0826051090-10
4	1.3754734960-05	8.4234744130-07	-3.3629260450-06	-4.1818072720-07	1.3777050820-03
5	5.3189183600-06	-3.4794077640-05	-1.0605793600-05	2.4433594070-06	5.0112963370-07
6	1.7782944740-05	1.3290560850-03	7.3643602200-03	6.9626157670-05	-5.7490186510-05

Table H-13. Matrix product T3 $C_1C_2C_3$ (sheet 2 of 2).

	36	37	38	39	40
1	2.5485074520-08	0.0	0.0	0.0	0.0
2	-6.1308306040-05	0.0	0.0	0.0	0.0
3	-1.3333611110-06	0.0	0.0	0.0	0.0
4	-9.1378294230-15	0.0	0.0	0.0	0.0
5	-2.7493586030-06	0.0	0.0	0.0	0.0
6	4.5684029640-04	0.0	0.0	0.0	0.0

	41	42	43	44	45
1	0.0	0.0	0.0	0.0	0.0
2	0.0	0.0	0.0	0.0	0.0
3	0.0	0.0	0.0	0.0	0.0
4	0.0	0.0	0.0	0.0	0.0
5	0.0	0.0	0.0	0.0	0.0
6	0.0	0.0	0.0	0.0	0.0

	46	47	48	49	50
1	0.0	0.0	0.0	0.0	0.0
2	0.0	0.0	0.0	0.0	0.0
3	0.0	0.0	0.0	0.0	0.0
4	0.0	0.0	0.0	0.0	0.0
5	0.0	0.0	0.0	0.0	0.0
6	0.0	0.0	0.0	0.0	0.0

	51	52	53	54	55
1	0.0	0.0	0.0	0.0	0.0
2	0.0	0.0	0.0	0.0	0.0
3	0.0	0.0	0.0	0.0	0.0
4	0.0	0.0	0.0	0.0	0.0
5	0.0	0.0	0.0	0.0	0.0
6	0.0	0.0	0.0	0.0	0.0

	56	57	58	59	60
1	0.0	0.0	0.0	0.0	0.0
2	0.0	0.0	0.0	0.0	0.0
3	0.0	0.0	0.0	0.0	0.0
4	0.0	0.0	0.0	0.0	0.0
5	0.0	0.0	0.0	0.0	0.0
6	0.0	0.0	0.0	0.0	0.0

	61	62	63	64	65
1	0.0	0.0	0.0	0.0	0.0
2	0.0	0.0	0.0	0.0	0.0
3	0.0	0.0	0.0	0.0	0.0
4	0.0	0.0	0.0	0.0	0.0
5	0.0	0.0	0.0	0.0	0.0
6	0.0	0.0	0.0	0.0	0.0

	66	67	68	69	70
1	0.0	0.0	0.0	0.0	0.0
2	0.0	0.0	0.0	0.0	0.0
3	0.0	0.0	0.0	0.0	0.0
4	0.0	0.0	0.0	0.0	0.0
5	0.0	0.0	0.0	0.0	0.0
6	0.0	0.0	0.0	0.0	0.0

	71	72
1	0.0	0.0
2	0.0	0.0
3	0.0	0.0
4	0.0	0.0
5	0.0	0.0
6	0.0	0.0

construct a control input that would spatially differentiate between these modes.

For the design of the M2V2 controller, the major concern is that mode 22 (row 19 in Table H-11) is spatially similar to modes 28 and 29. Given the actuator configuration described in Appendix E, there are only two effective axial actuators: the base-section member actuator, and the four section-3 member actuators used in combination. There is no way to combine these actuators to isolate modes 28 and 29 (which are both axial modes), and to continue to control mode 22 (also axial). The orthogonalization algorithm produced a null vector for this case. The best solution is to reconfigure the actuators. For the results of Chapter 3, spillover of mode 22 commands into mode 29 was permitted.

Another practical comment can be made regarding the requirement that the columns of T_2 be orthogonal to the rows of matrix B*. Orthogonalization is a geometrically attractive idea, but it is too restrictive. All that is required is that the inner products of T_2 columns and B* rows must be small. In other words, both direction and magnitude are important.

The output transform T_3 is required to satisfy

$$T_3 C_1 \neq 0 \qquad \text{(H-9)}$$

$$T_3 C_2 = 0$$
$$T_3 C_3 = 0 \qquad \text{(H-10)}$$

The columns if C_1 were chosen to be the initial rows of T_3. Then, as before, the components of these rows which were contained in the column space of C_2 or C_3 were subtracted off. The final transform is shown in Table H-12 and the matrix of C column dot products is shown in Table H-13. The orthogonalization scheme started out with 11 rows which

were transposes of the C columns. These rows were made orthogonal to the 28 C_2 and C_3 columns. Of the 11 original rows, 5 became null vectors; an indication that these starting vectors were in C_2, C_3 space. The six remaining vectors make up the T_3 given in Table H-12. The matrix product $T_3 \lfloor C_1\ C_2\ C_3 \rfloor$ (see Table H-13) allows T_3 to be evaluated. Only rows 1, 3, 4, and 5 meet the criteria of being nonzero for $\underline{x}_1$ states and very small for $\underline{x}_2$ and $\underline{x}_3$ states. Spatial aliasing, as dictated by the sensor placement, is responsible for the degraded character of rows 2 and 6. However, the remaining four measurements span $\underline{x}_1$ space.

The computations associated with T_2 and T_3 are straightforward, and easy checks are available. Stronger designs could have been achieved if the sensor/actuator locations had been iterated. In particular, more axial actuators, and more sensors near the solar panel tips would have eased the T_2/T_3 design process.

LIST OF REFERENCES

1. Roberson, R.E., "Two Decades of Spacecraft Attitude Control", Journal of Guidance and Control, Vol. 2, No. 1, Jan./Feb. 1979.

2. Croopnick, S.R., Y.H. Lin, and R.R. Strunce, A Survey of Automatic Control Techniques for Large Space Structures, Presented at VIII IFAC Symposium on Automatic Control in Space, Oxford, U.K., July 1979.

3. Harris, R.S., A Parametric Study into Structural Flexibility-Satellite Attitude Interaction for a Three Axis Stabilized Satellite, European Space Agency SP-128, Nov. 1977.

4. Ginter, S.D., Attitude Control of Large Flexible Spacecraft, M.S. Thesis, CSDL Report T-666, Sept. 1978.

5. Strunce, R.R., and T. Henderson, "Application of Modern Modal Controller Design to a Large Space Structure", CSDL Report P-870, Second Symposium on the Dynamics and Control of Large Flexible Spacecraft (VPI and SU/AIAA), June 21-23, 1979.

6. Kwakernaak, H., and R. Sivan, Linear Optimal Control Systems, John Wiley and Sons, Inc., New York, 1972.

7. Safonov, M.D., and M. Athans, "Gain and Phase Margin for Multiloop LQG Regulators" IEEE Transactions on Automatic Control, Vol. AC-22, No. 2, April 1977, pp. 173-179.

8. Doyle, J.C., and G. Stein, "Robustness with Observers", Honeywell Memo MR12486, Minneapolis (also presented at IEEE Conference on Decision and Control, Jan. 1979).

LIST OF REFERENCES (Cont.)

9. Suzuki, M., and M. Miura, "Stabilizing Feedback Controllers for Singularly Perturbed Linear Constant Systems", IEEE Transactions on Automatic Control, Feb. 1976, p. 123.

10. Balas, M.J., "Observer Stabilization of Singularly Perturbed Systems", Journal Guidance and Control, Vol. 1, No. 1, Jan./Feb. 1978, p. 93.

11. Sesak, J.R., "Control of Large Space Structures Via Singular Perturbation Optimal Control", presented at AIAA Conf. on Large Space Platforms, Los Angeles, CA, Sept. 27-29, 1978.

12. Benhabib, R.J. and R.P. Owens, Control of Large Space Structures Using Equilibrium Enforcing Optimal Control, TRW, Space Park, Ca., 1979 (to be published).

13. Coradetti, T., Orthogonal Subspace Reduction of Optimal Regulator Order, General Dynamics, San Diego, 1979 (to be published).

14. Balas, M.J., "Modal Control of Certain Flexible Dynamic Systems", SIAM Journal Control and Optimization, Vol. 16, No. 3, May 1978, p. 450.

15. Gupta, N.K., "Frequency-Shaping Techniques in Modern Control Design Methods", Systems Control, Palo Alto, June 1978 (to be published).

16. Skelton, R.E., and P.W. Likins, "Orthogonal Filters for Model Error Compensation in the Control of Nonrigid Spacecraft", Journal of Guidance and Control, Vol. 1, Jan./Feb. 1978, pp. 41-49

17. Joshi, S.M., and N.J. Groom, "Controller Design Approaches for Large Space Structures using LQG Control Theory", presented at Second VPI and SU/AIAA Symposium on Dynamics and Control of Large Flexible Spacecraft, June 21-23 1979.

18. Moore, B.L., "On the Flexibility Offered by State Feedback in Multivariable Systems Beyond Closed Loop Eigenvalue Assignment", IEEE Transactions in Automatic Control, Vol. AC-21, pp. 689-692 Oct. 1976.

19. Canavin, J.R., "The Control of Spacecraft Vibrations Using Multivariable Output Feedback", AIAA/AAS Astrodynamics Conference, Paper No. 78-1419, Palo Alto, CA, August 1979.

20. Kipt, E.H., T. Brown, and Marsh, "Flexible Stator Control on the Galileo Spacecraft", AIAA/AAS Astrodynamics Conference, Provincetown, MA, 1979.

21. Rammath, R. V., "Minimal and Subminimal Simplification", Journal of Guidance and Control, Vol. 3, No. 1, Jan./Feb. 1980, pp. 86-89.

22. Private Communication with T. Henderson, CSDL, March 1979.

23. Meirovitch, L., and H. Öz, "Computational Aspects of the Control of Large Flexible Structures", Proceedings of the IEEE, CH1486-0/79/0000-0820.

24. Bryson, A. and Y. Ho., Applied Optimal Control, John Wiley and Sons, Inc., New York, 1975.

25. Kontakos, T., PhD Dissertation, University of Manchester, 1973.

26. Whitaker, H.P., Development of a Parameter Optimization Technique for the Design of Automatic Control Systems, NASA CR-143844..

27. Blakelock, J.H., Automatic Control of Aircraft and Missiles, John Wiley and Sons, Inc., New York, 1965.

28. Konigsberg, W.D., Spectral Analysis of Random Signals—Techniques and Interpretation. CSDL Report E-2771, June 1973.

29. Kay, Steven M., Noise Compensation for Autoregressive Spectral Estimates," IEEE Transactions on Acoustics, Speech, and Signal Processing, Vol. ASSP-28, No. 3, June 1980, pp. 292-303.

30. MacFarlane, A.J., and N. Karcanias, "Poles and Zeroes of Linear Multivariable Systems: A Survey of the Algebraic, Geometric, and Complex Variable Theory". International Journal of Control, 1976, Vol. 24, No. 1, pp. 33-74.

31. Rosenbrock, H.H., State Space and Multivariable Theory, London: Nelson, 1970.

32. Rosenbrock, H.H., International Journal of Control, Vol. 18, p. 297, 1973.

33. Rosenbrock, H.H, International Journal of Control, Vol. 20, p. 525, 1974.

34. Desoer, C.A., and J.D. Schulman, IEEE Transactions on Circuits and Systems, Vol. 21, No. 3, 1974.

35. Sannuti, P., and P.V. Kokotovic, "Near-Optimum Design of Linear Systems by a Singular Perturbation Method", IEEE Transactions on Automatic Control, AC-14, pp. 15-22, 1969.

36. Kokotovic, P.V., and P. Sannuti, "Singular Perturbation Method for Reducing the Model Order in Optimal Control Design", IEEE Transactions on Automatic Control, AC-13, pp. 377-384, 1968.

37. Kokotovic, P.V., R.E., O'Malley, and P. Sannuti, "Singular Perturbations and Order Reduction in Control Theory—An Overview" Automatica, Vol. 12, pp. 123-132, 1976.

38. Desoer, C.A., and M.J. Shensa, "Networks with Very Small and Very Large Parasitics: Natural Frequencies and Stability", Proceedings of the IEEE, Vol. 58, No. 12, Dec. 1970, pp. 1933-1938.

39. Klimushehev, A.I., and N.N. Krasovskii, "Uniform Asymptotic Stability of Systems of Differential Equations with a Small Parameter in the Derivative Terms", Journal of Applied Mathematics and Mechanics, Vol. 25, 1961, pp. 1011-1025.

40. Kokotovic, P.V., and R.A. Yachel, "Singular Perturbation of Linear Regulators: Basic Theorems", IEEE Transactions on Automatic Control, Vol. AC-17, No. 1, Feb. 1972, pp. 29-37.

41. Singh, G., and R.A. Yackel, "Optimal Regulation with Order Reduction of a Power System", Computers and Electrical Engineering, Vol. 1, pp. 425-452, 1973.

42. Mahapatra, G.B., "A Further Note on Selecting a Low Order System Using the Dominant Eigenvalue Concept", IEEE Transactions on Automatic Control, Vol. AC-24, No. 1, Feb. 1979, pp. 135-136.

43. Bisplinghoff, R.L., and H. Ashley, Principles of Aeroelasticity, John Wiley and Sons, New York, 1962.

44. Aubrun, J.N., "Theory of the Control of Structures by Low Authority Controllers", Proceedings of AIAA, paper 78-1689.

45. D'azzo, J.J., and C.H. Houpis, Linear Control Analysis and Design, McGraw Hill, 1975.

46. Soosar, K., et al., Structural Evaluation of Candidate Designs for the Large Space Telescope Primary Mirror, CSDL Report R-874, April 1975.

47. Forward, R.L., "Electronic damping of Vibrations in Optical Structures", Applied Optics, Vol. 18, No. 5, 1 March 1979.

48. Anderson, R.H., et al., "A Family of Sensors for the Sensing of the Position and Vibration of Spacecraft Structures", AIAA Paper 79-1741.